

1995

Pressure Event Detection Based on the Dyadic Wavelet Transform

Lynn T. Antonelli
University of Rhode Island

Follow this and additional works at: https://digitalcommons.uri.edu/oa_diss

Terms of Use

All rights reserved under copyright.

Recommended Citation

Antonelli, Lynn T., "Pressure Event Detection Based on the Dyadic Wavelet Transform" (1995). *Open Access Dissertations*. Paper 778.
https://digitalcommons.uri.edu/oa_diss/778

This Dissertation is brought to you by the University of Rhode Island. It has been accepted for inclusion in Open Access Dissertations by an authorized administrator of DigitalCommons@URI. For more information, please contact digitalcommons-group@uri.edu. For permission to reuse copyrighted content, contact the author directly.

PRESSURE EVENT DETECTION
BASED ON THE DYADIC WAVELET TRANSFORM

BY
LYNN T. ANTONELLI

A DISSERTATION SUBMITTED IN PARTIAL FULFILLMENT OF THE
REQUIREMENTS FOR THE DEGREE OF
DOCTOR OF PHILOSOPHY
IN
ELECTRICAL ENGINEERING

UNIVERSITY OF RHODE ISLAND

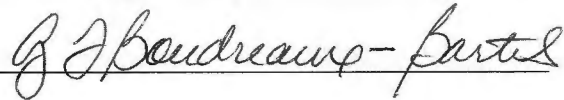
1995

DOCTOR OF PHILOSOPHY DISSERTATION
OF
LYNN T. ANTONELLI

Approved:

Dissertation Committee
Major Professor





Gerasimos Ladas



DEAN OF THE GRADUATE SCHOOL

UNIVERSITY OF RHODE ISLAND
1995

Abstract

The physiological condition of the human cardiovascular system is primarily determined from the electrocardiogram (ECG) and blood pressure signals. Diagnostic and therapeutic medical procedures and the operation of various medical devices often rely on the temporal location of various events observed in these signals. The QRS complex (R wave) is one distinguishing characteristic of the ECG waveform; whereas the systolic peak, upstroke and the dicrotic notch are the most prominent events in the arterial blood pressure signal. Detection of these waveform characteristics may be used for calculating heart rate and the systolic time intervals including the pre-ejection period (PEP), left ventricular ejection time (LVET) and electromechanical systole (QS2).

This report describes an algorithm which accurately and consistently locates the dicrotic notch in the arterial blood pressure waveform for a range of heart rates, arrhythmias and irregular pressure waveforms (including baseline drift, catheter artifact, signal damping and noise) using the dyadic wavelet transform (DyWT). Simultaneous occurrences of minima in the DyWT across several successive dyadic scales indicates a transient in the pressure waveform, from which the corresponding temporal location of the dicrotic notch is determined for each cardiac cycle.

The dyadic wavelet transform scheme for dicrotic notch detection has been tested on arterial blood pressure waveforms (radial, femoral, and axillary) with various heart rates, ranging from 40 to 140 beats per minute (bpm). Algorithm performance was evaluated using 71 patient data files from the Massachusetts General Hospital (MGH) database which includes simultaneous ECG and arterial pressure recordings. Four criteria were

used to indicate detection performance: sensitivity, positive productivity, false positive rate and false negative rate. The accuracy of the proposed DyWT based dicrotic notch detection algorithm outperformed five previously published detection algorithms in terms of each of the four performance criteria. The DyWT based detection algorithm achieved a sensitivity of 84%, a positive productivity of 85%, a false positive rate of 15 % and a false negative rate of 16% when tested 72 patient arterial blood pressure files of various waveform types, illustrative of a clinical environment. The next highest performers achieved a sensitivity as high as 66%, positive productivity of 72%, a false positive rate as low as 25 %, and a false negative rate of 34%.

Acknowledgments

Any accomplishment of this magnitude cannot be achieved alone. It is with my deepest appreciation that I thank my major Professor, William Ohley for his expert guidance, encouragement and support. It was a pleasure learning from someone who is tops in his field. In this same light, I would like to express my sincerest gratitude to my advisory committee, Professor G. Faye Boudreaux-Bartels, Professor Gerry Ladas, Professor Harish Sunak and Professor Ed Grove. A substantial research project relies on a good support team, and I am grateful that I had such an accomplished and expert assembly.

This entire venture would not have been possible without the full support of my entire family. I especially thank my husband, Tony, who has encouraged me in ways he may not even realize, and whose presence has been my strength. I also thank my daughter, Christine, who keeps me smiling and reminds me what life is all about. I also thank my parents, whose pride and support I have cherished throughout. I especially thank my mother, who gave me time to do this research; without her, this would never have been possible. Thanks also to Ma B., Peter, Marc, Chris and Amy for allowing me a life outside of books. A special thanks to my extended family, especially Anthony and Irene for being such nice people and encouraging me every step of the way. I also would like to thank my pal, Maureen O'Gorman, for setting up the extremely time saving programs which automated the statistical data calculations.

Contents

Abstract	ii
Acknowledgements	iv
Table of Contents	v
List of Tables	viii
List of Figures	x
Glossary	xiv
1 Introduction	1
1.1 Justification of Study	1
1.2 Physiological Background	4
1.3 Clinical Implications	9
1.3.1 Systolic Time Intervals	9
1.3.2 Intraaortic Balloon Pump Timing	11
1.4 Rationale for Selecting the DyWT	14
1.4.1 Signal Processing Requirements	14
1.4.2 Feasibility Study	15
2 Introduction to the Dyadic Wavelet Transform	19
2.1 Motivation	19
2.2 Time Varying Signal Analysis	20
2.3 The Wavelet Transform	24
2.3.1 Historical Background	24
2.3.2 Applications of the Wavelet Transform	25
2.3.3 Definition and Significance	26
2.3.4 Discrete Wavelet Transform	28
2.4 The Dyadic Wavelet Transform	30

2.4.1	Definition and Significance	30
2.4.2	Properties	33
3	Methodology	37
3.1	Motivation.	37
3.2	Application of the DyWT to Dicrotic Notch Detection	40
3.3	Rationale	47
3.3.1	Selection of the Wavelet Function	47
3.3.2	Selection of Algorithm Procedures	52
3.4	Previously Developed Dicrotic Notch Detection Algorithms	59
3.4.1	Introduction	59
3.4.2	Lee Algorithm.	62
3.4.3	Jundanian Algorithm	63
3.4.4	Martino Algorithm	64
3.4.5	Kinias Algorithm	66
3.4.6	Elghazzawi Algorithm.	68
4	Simulations	69
4.1	Introduction	69
4.2	MGH Database of Clinical Recordings	69
4.3	Performance Criteria	74
4.4	Illustrative Examples of DyWT Dicrotic Notch Detection	76
4.5	Statistical and Comparative Results of Simulation	102
4.6	Observations	106
5	Conclusion	108
A	Source Code (Matlab v.4.2)	
A.1	Dyadic Wavelet Transform Algorithm	111
A.2	Lee Algorithm.	119

A.3	Jundanian Algorithm	123
A.4	Martino Algorithm	126
A.5	Kinias Algorithm	129
A.6	Elghazzawi Algorithm.	138
B	Tabular Performance Results of the Dicrotic Notch Detection Algorithms	
	for each of the test sets (A) 30 files; (B) 50 files; (C) 72 files	143
C	Graphical Results of Detection Algorithm Performance	147
	List of References	177
	Bibliography	197

List of Tables

1.1. Events of the Cardiac Cycle [37]	5
2.1 Applications of the Wavelet Transform	25
2.2 Properties of the DyWT	33
3.1. Previously Published Dicrotic Notch Detection Algorithms	60
4.1. Column Vector Designation for the Physiological Signals in each MGH File	70
4.2a. List of 30 MGH Database Files used to Test Performance of Dicrotic Notch Detection Algorithms (Test set A)	71
4.2b. List of 50 MGH Database Files used to Test Performance of Dicrotic Notch Detection Algorithms (Test set B)	71
4.2c. List of 72 MGH Database Files used to Test Performance of Dicrotic Notch Detection Algorithms (Test set C)	72
4.2d. List of MGH Database Files used to Test Performance of Dicrotic Notch Detection Algorithms (Test sets A, B and C) According to Waveform Pathology	73
4.3. Performance of Detection Algorithms on a Damped Pressure Signal (MGH file 009)	78
4.4. Performance of Detection Algorithms on a Pressure Signal with Pulsus Alternans (MGH file 019)	82
4.5. Performance of Detection Algorithms on a Damped, Non Stationary Pressure Signal with Baseline Drift (MGH file 077)	86

4.6. Performance of Detection Algorithms on a Pressure Signal with an Irregular Heart Rate (MGH file 023)	90
4.7. Performance of Detection Algorithms on a Femoral Pressure Signal Containing Noise (MGH file 060)	94
4.8. Performance of Detection Algorithms on a Pressure Signal with a Notch Artifact (MGH file 021)	98
4.9. Simulation Performance Results for each of the Dicrotic Notch Detection Algorithms for test sets (A) 30 files; (B) 50 files; and (C) 72 files.	105
4.10 Illustrative MGH Patient Files Whose Detection Results are Contained in Appendix B	105
5.1 Performance Results of the DyWT Based Dicrotic Notch Detection Algorithm: Test Set C	109

List of Figures

1.1.	Structure of the human heart, depicting the four cardiac chambers and the four valves and the direction of blood flow [36].	5
1.2.	Events during a cardiac cycle. Temporal coordination of aortic, left ventricular and left atrial pressures with the heart sounds, left ventricular volume and the ECG [37].	6
1.3.	MGH database files illustrating typical pressure waveform contours at various points along the circulatory track. (a) aortic , (b) radial, (c) brachial, (d) femoral, (e) pedal and (f) axillary pressures, [22] showing the locations of the systolic peak and the dicrotic notch.	8
1.4.	Schematic of the left ventricular events which comprise the STI, including the PEP, LVET and the QS2 from the combination of the ECG, LVP, aortic pressure and phonocardiogram signals [1]	11
1.5.	Results of DyWT algorithm feasibility study on radial blood pressure waveform containing a (a) premature ventricular contraction; (b) with added white gaussian noise.	18
2.1.	Lack of time resolution of the FT magnitude spectrum.	23
2.2.	Coverage of the time-frequency plane for the (a) STFT; (b) for WT.	23
2.3.	Block diagram of the algorithmic approach for digital computation of the DyWT using low pass (H) and high pass (G) filters [67].	29
2.4.	(a) Cubic spline wavelet function at dyadic scales $m = 1, 2, 3$; (b) FT magnitude of each of the scaled versions of the cubic spline wavelet in (a)	31

3.1. MGH database blood pressure waveforms illustrating four difficult cases for dicrotic notch detection algorithms. (a) pulsus alternans, (b) catheter artifact, (c) damped signal, (d) signal shape irregularity, (e) classic arterial blood pressure waveform	39
3.2. Block diagram of the DyWT dicrotic notch detection algorithm.	43
3.3. Flow chart of the DyWT discrete convolution calculation procedure.	44
3.4. Flow chart of the R wave detection algorithm.	45
3.5. Flow chart of the dyadic wavelet transform based dicrotic notch detection algorithm.	46
3.6. Graphical representation of the wavelet functions: (a) Haar; (b) Shannon; (c) Morlet; (d) Mexican Hat; (e) Meyer; and (f) the cubic spline.	50
3.7. Three dyadic scales of the Mexican Hat wavelet function, generated with a sample rate of 360 Hz	51
3.8. Pole/zero plot of the 4th order Butterworth prefilter with $f_c=20$ Hz.	53
3.9. (a) Magnitude response; (b) Phase response of the 4th order Butterworth prefilter with cutoff frequency of 20 Hz.	53
3.10. (a) Radial pressure waveform MGH file038; (b-d) results of the discrete convolution calculation of the dyadic wavelet transform for scales 1, 2 and 3, respectively.	56
3.11. Dicrotic notch detection algorithm by Burratini displaying an arterial flow waveform superimposed with the double threshold detection method. [186].	61
3.12. Dicrotic notch detection algorithm by Jundanian et al [183] displaying arterial pressure signal superimposed with proposed 40 msec slope bar detection method.	63

3.13. Dicrotic notch detection algorithm by Martino et al (a) Comparison of original and filtered waveforms; (b) blood pressure and ECG signals with estimated locations of systolic peaks and dicrotic notches [184]	65
3.14. Dicrotic notch detection algorithm by Kinias et al displaying the dicrotic notch portion of an arterial pressure signal superimposed with proposed minima 'bent point' selection detection method [185]	67
4.1. (a) MGH file 009 damped radial artery pressure signal; (b-d) DyWT decompositions for dyadic scales 1, 2 and 3, respectively.	79
4.1. (e) Enlarged view of the MGH file 009 damped radial artery pressure signal; (f-h) DyWT decompositions for dyadic scales 1, 2 and 3, respectively.	80
4.2. Comparison between the calculation of QS2 using dicrotic notch information the regression equation based on HR, for MGH file 009.	81
4.3. (a) MGH file 019 radial artery pressure signal containing pulsus alternans; (b-d) DyWT decompositions for dyadic scales 1, 2 and 3, respectively.	83
4.3. (e) Enlarged view of the MGH file 019 radial artery pressure signal containing pulsus alternans; (f-h) DyWT decompositions for dyadic scales 1, 2 and 3, respectively.	84
4.4. Comparison between the calculation of QS2 using dicrotic notch information to the regression equation, based on HR, for MGH file 019.	85
4.5. (a) MGH file 077 damped radial artery pressure signal exhibiting an increased HR; (b-d) DyWT decompositions for dyadic scales 1, 2 and 3, respectively.	87
4.5. (e) Enlarged view of the MGH file 077 damped radial artery pressure signal exhibiting an increased HR; (f-h) DyWT decompositions for dyadic scales 1, 2 and 3, respectively.	88

4.6. Comparison between the calculation of QS2 using dicrotic notch information to the regression equation based on HR for a damped signal exhibiting an increased HR, MGH file 077.	89
4.7. (a) MGH file 023 radial artery pressure signal exhibiting an irregular HR; (b-d) DyWT decompositions for dyadic scales 1, 2 and 3, respectively.	91
4.7. (e) MGH file 023 radial artery pressure signal exhibiting an irregular HR; (f-g) DyWT decompositions for dyadic scales 1, 2 and 3, respectively.	92
4.8. Comparison between the calculation of QS2 using dicrotic notch information to the regression equation based on HR for a pressure signal exhibiting an irregular HR, MGH file 023.	93
4.9. (a) MGH file 060 femoral artery pressure signal containing noise; (b-d) DyWT decompositions for dyadic scales 1, 2 and 3, respectively.	95
4.9. (e) Enlarged view of the MGH file 060 femoral artery pressure signal containing noise; (f-g) DyWT decompositions for dyadic scales 1, 2 and 3, respectively.	96
4.10. Comparison between the calculation of QS2 using dicrotic notch information to the regression equation based on HR, for a femoral artery pressure signal containing noise, MGH file 060.	97
4.11. (a) MGH file 021 radial artery pressure signal containing a notch artifact; (b-d) DyWT decompositions for dyadic scales 1, 2 and 3, respectively.	99
4.11. (e) Enlarged view of the MGH file 021 radial artery pressure signal containing a notch artifact; (f-g) DyWT decompositions for dyadic scales 1, 2 and 3, respectively.	100

4.12. Comparison between the calculation of QS2 using dicrotic notch information to the regression equation based on HR for a pressure signal containing a notch artifact, MGH file 021.	101
4.13. Histogram of the statistical results for all of the dicrotic notch detection algorithms.	104

Glossary

AP	aortic pressure
AV	atrioventricular
BP	blood pressure
bpm	beats per minute
CWT	continuous wavelet transform
DN	dicrotic notch
DyWT	dyadic wavelet transform
ECG	electrocardiogram
EDP	end diastolic pressure
f_c	cutoff frequency
FFT	fast Fourier transform
FN	false negative
FP	false positive
FT	Fourier transform
HR	heart rate
IABP	intraaortic balloon pump
LV	left ventricle
LVET	left ventricular ejection time
LVP	left ventricular pressure
MGH	Massachusetts General Hospital
msec	millisecond
PCG	phonocardiogram

PEP	pre-ejection period
PSD	power spectral density
PSP	peak systolic pressure
PVC	preventricular contraction
QS2	electromechanical systole (duration of Q wave to second heart sound)
STFT	short time Fourier transform
STI	systolic time interval
TP	true positive
WT	wavelet transform

Chapter 1

Introduction

1.1 Justification of Study

The blood pressure waveform reflects the mechanical function of the myocardium as well as of the arteries and veins and represents the hemodynamic pressures generated by the heart muscle throughout the systolic and diastolic cycles. The most commonly used features in the arterial waveform are systolic upstroke, systolic peak and the dicrotic notch. The dicrotic notch is observed in arterial pressure waveforms as a consequence of the closing of the aortic valve, after left ventricular ejection, indicating the start of the diastolic cycle. Locating the dicrotic notch is critical for analyzing systolic time interval (STI) [1-10], for determining the heart rate relative to the beginning of the diastolic cycle and for determining the proper inflation time of an intraaortic balloon [11-21].

The detection of the dicrotic notch is non-trivial in that the blood pressure signal may be corrupted by noise, contain motion artifacts, respiratory modulation, or change abruptly with arrhythmias; and in sick patients, the pressure curve may deviate greatly from the norm. The blood pressure waveform also varies depending on which part of the circulatory system is being monitored, (aortic, radial, brachial, femoral, pedal or axillary pressures) and is dependent upon the fidelity of the pressure sensor. Previously developed dicrotic notch detection algorithms have accommodated some but not all of these waveform irregularities.

One signal processing technique, the dyadic wavelet transform, has been applied to detect the dicrotic notch in a variety of pressure signals available in the Massachusetts General Hospital (MGH) clinical waveform database [22]. Physiological signals such as the blood pressure, are classified as time varying or non-stationary. The wavelet transform provides local frequency information of a signal and is used for analyzing a waveform according to its changing spectral position by altering the filter function according to the local spectral information in the signal [23-30]. The wavelet transform is well suited to process non-stationary signals that exhibit transient behavior and for time-frequency analysis where linear time invariant systems fail. Application of the wavelet transform allows high frequency components of a signal to be studied with sharper time resolution than low frequency components [31].

The dyadic wavelet transform uses scaled and translated versions of the mother wavelet. This scaling produces variable length windows, providing variable resolution in the time or frequency domain. Thus, varying the scale of the wavelet allows for a multiresolution view of a signal. Application of the wavelet transform therefore provides a means of analyzing a range of time varying signals, such as slow, fast and arrhythmic heart rhythms, to observe both high frequency transient information from lower frequency signal behavior [25-28]. Signal transients or discontinuities, such as the dicrotic notch, can be isolated from background noise by comparing the DyWT across successive dyadic scales, thus making the DyWT an appropriate method for dicrotic notch detection. Band limited noise whose spectra lies outside of the frequency resolution of any of the dyadic wavelet scales will not correlate between scales of the dyadic wavelet transform. For such cases, actual events such as the dicrotic notch can be detected in relatively noisy signals. The ability of the dyadic wavelet based algorithm to detect the dicrotic notch in non-stationary and noisy signals enhances its performance over the preexisting detection algorithms.

The dyadic wavelet transform detection method provides non-stationary temporal information on the dirotic notch by applying three time dilated scales of the mother wavelet to the pressure signal. Simultaneous occurrences of minima in the wavelet transform across the three successive dyadic scales indicates a transient in the pressure waveform. This idea is based on the work by Mallat [32-35] who developed an algorithm to detect rapidly varying signal components such as edges in images and an algorithm for efficient coding using a smoothing wavelet function. The algorithm has since been modified and applied to a range of signal analysis tasks. Various scientific disciplines have applied the wavelet transform to analyze an assortment of signals, including image processing and coding, analysis of acoustic signals, physiological signals, and astronomical data, as discussed in section 2.3.

1.2 Physiological Background

The human heart is a hollow muscle whose contractile motion controls blood flow through the circulatory system. The heart contains four muscular chambers: the left and right atria and the left and right ventricles, which are each separated from the remaining cardiac system by one way valves as shown in figure 1.1 [36]. The mitral valve separates the left atrium from the left ventricle; the tricuspid valve separates the right atrium from the right ventricle; the aortic valve enables blood flow out from the left ventricle into the aorta; and the pulmonary valve controls the blood flow out of the right ventricle into the vena cava.

The function of the heart muscle is governed by electrical impulses that contract the muscle fibers. Each of the four chambers of the heart contains a certain blood volume. When a cardiac chamber receives an electrical signal, the muscle contracts and blood is forced out of the chamber. The left ventricle (LV) is responsible for forcing blood into the aorta (through the aortic valve) with enough pressure to allow circulation of blood throughout the body. The arterial pressure waveform is the pressure of the blood flow out of the LV into the aorta and through the arterial system over time.

The complete series of cardiac events which occur in a single heartbeat is referred to as a cardiac cycle. An outline of the events in the cardiac cycle are listed in table 1.1 [37] including the 8 phases of each cycle, the events at the onset, during and at the end of each phase. Also provided are the durations (in seconds) of each of the 8 phases for both man and dog. Figure 1.2 [37] shows the coordination of the electrocardiogram, left ventricular, left atrial and aortic pressure curves, the heart sounds and the left ventricular volume curve, according to the phases of the cardiac cycle listed in table 1.1. The approximate duration of the various events in both the systolic and diastolic portions of the cardiac cycle in man are labeled accordingly for a heart rate of 75 bpm. Typical heart rates for adult humans can range from 40 to 200 bpm.

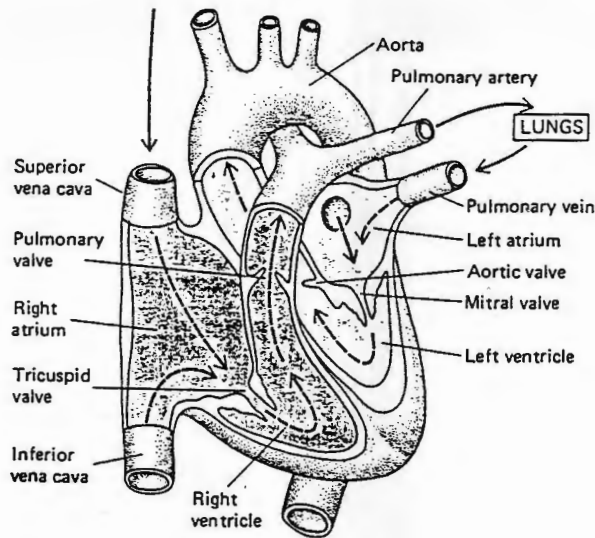


Figure 1.1 Structure of the human heart, depicting the four cardiac chambers and the four valves and the direction of blood flow. [36]

Table 1.1
Events of the Cardiac Cycle [37]

Phase	Event at Onset of Phase	Main Event During Phase	Event at End of Phase	Phase Duration sec	
				Man	Dog
1 Isovolumic contraction ^{L/}	Onset of left ventricular contraction	Rapid rise of left ventricular pressure with no volume change	Opening of aortic valve	0.06	0.05
2 Maximum ejection	Opening of aortic valve	Rapid outflow of blood from left ventricle	Peak left ventricular pressure	0.12	0.10
3 Reduced ejection	Peak left ventricular pressure	Decreasing outflow of blood from left ventricle	End of left ventricular ejection	0.14	0.12
4 Protodiastole	End of left ventricular ejection	Rapid decrease in left ventricular pressure	Closure of aortic valve	0.03	0.02
5 Isovolumic relaxation ^{L/}	Closure of aortic valve	Continued relaxation of left ventricle, with no volume change	Opening of mitral valve	0.09	0.05
6 Rapid inflow	Opening of mitral valve	Rapid flow of blood from left atrium to left ventricle	Slowing of inflow from left atrium to left ventricle	0.09	0.06
7 Diastasis	Slowing of inflow from left atrium to left ventricle	Continued slower flow from left atrium to left ventricle	Onset of left atrial contraction	0.16	0.29
8 Atrial systole	Onset of left atrial contraction	Increased flow from left atrium to left ventricle	End of left atrial contraction and onset of left ventricular contraction	0.11	0.11

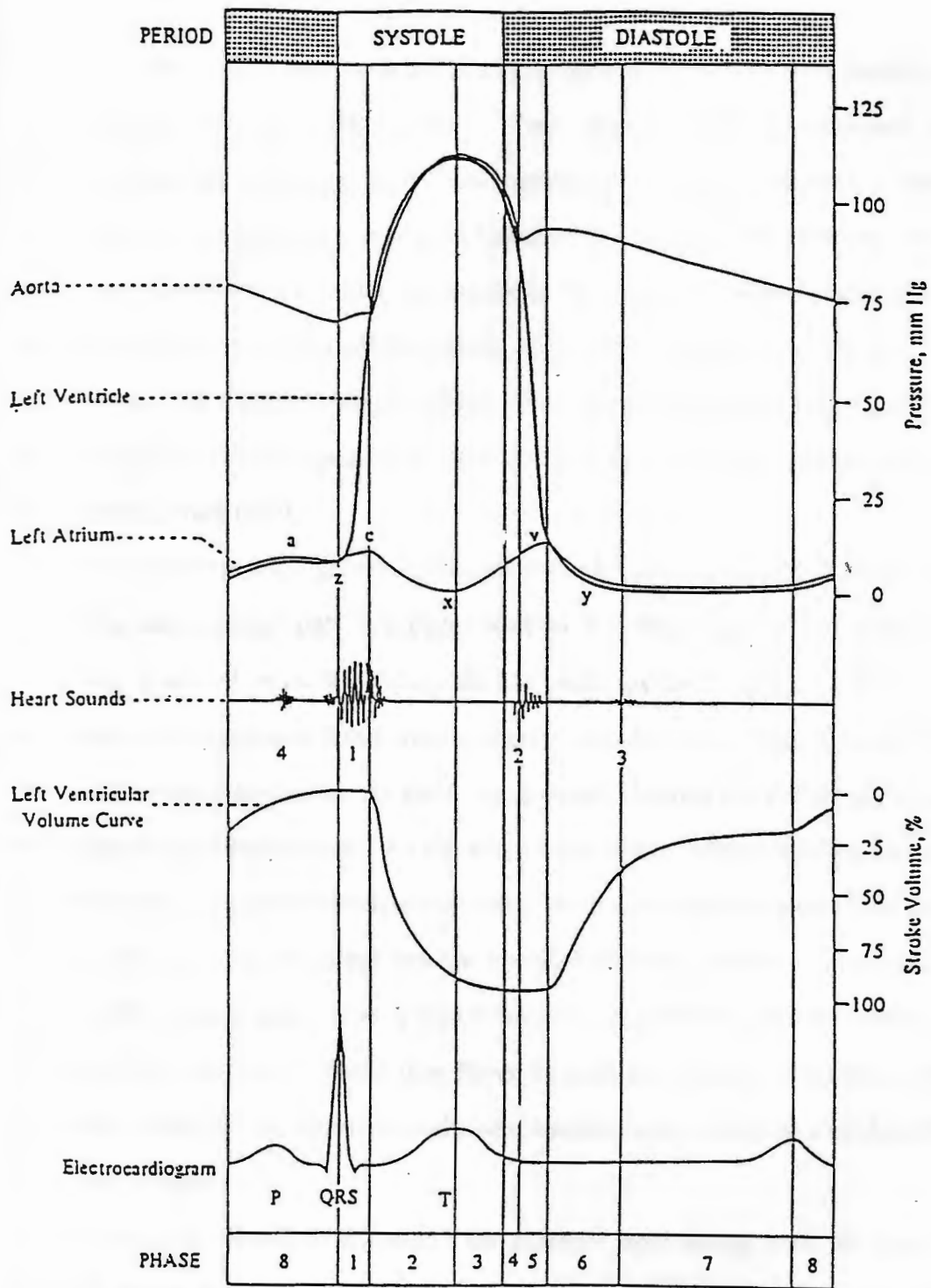


Figure 1.2 Events during a cardiac cycle. Temporal coordination of aortic, left ventricular and left atrial pressures with the heart sounds, left ventricular volume and the ECG. [37]

The cardiac cycle begins with an electrical signal generated by the Sino-Atrial (SA) node, located in the right atrium. This signal, which is recorded on the electrocardiogram, propagates to the atrioventricular (AV) node where it is delayed so the left atrium can adequately empty its blood volume into the left ventricle. The signal then travels along the AV bundle (or Bundle of His) which stimulates contraction of the ventricle, defining the onset of the systolic cycle [38]. Contraction of the left ventricle corresponds with the QRS complex observed in the ECG waveform. The time between the generated electrical impulse and actual contraction of the left ventricle is called the pre-ejection period (PEP).

Once the left ventricle generates enough pressure relative to the aortic root pressure, the aortic valve opens. Left ventricular ejection into the arterial system increases to a maximum, observed on the left ventricular and aortic pressures as the systolic peak, then decreases as the remaining blood volume empties into the aorta. Once the aortic and left ventricular pressures equalize, the aortic valve closes, defining the end of systole and the beginning of the diastolic cycle. As the aortic valve closes, there is a slight retraction of blood flow and a dip in the pressure waveform. After valve closure, blood flow continues forward into the arterial system and the pressure increases slightly. The result of the aortic valve closure appears as a notch (*dicrotic notch* (DN)) in the arterial blood pressure (BP) waveform. Blood then flows through the systemic circulation while the left atrium refills the left ventricle for the next cardiac cycle, shown as a gradual decay in the aortic pressure.

The pressure waveform represents the pressure state during both the systolic and diastolic phases of the cardiac cycle. A peak systolic pressure (PSP) of 120 mmHg and a diastolic pressure of 60 mmHg is typical for a healthy adult human. The contour of the pressure waveform varies depending on which part of the circulatory system is being monitored. Figure 1.3 a-f [22] show the typical waveform shape at various points along

the circulatory track, with the locations of the systolic peak and the diastolic notch labeled.

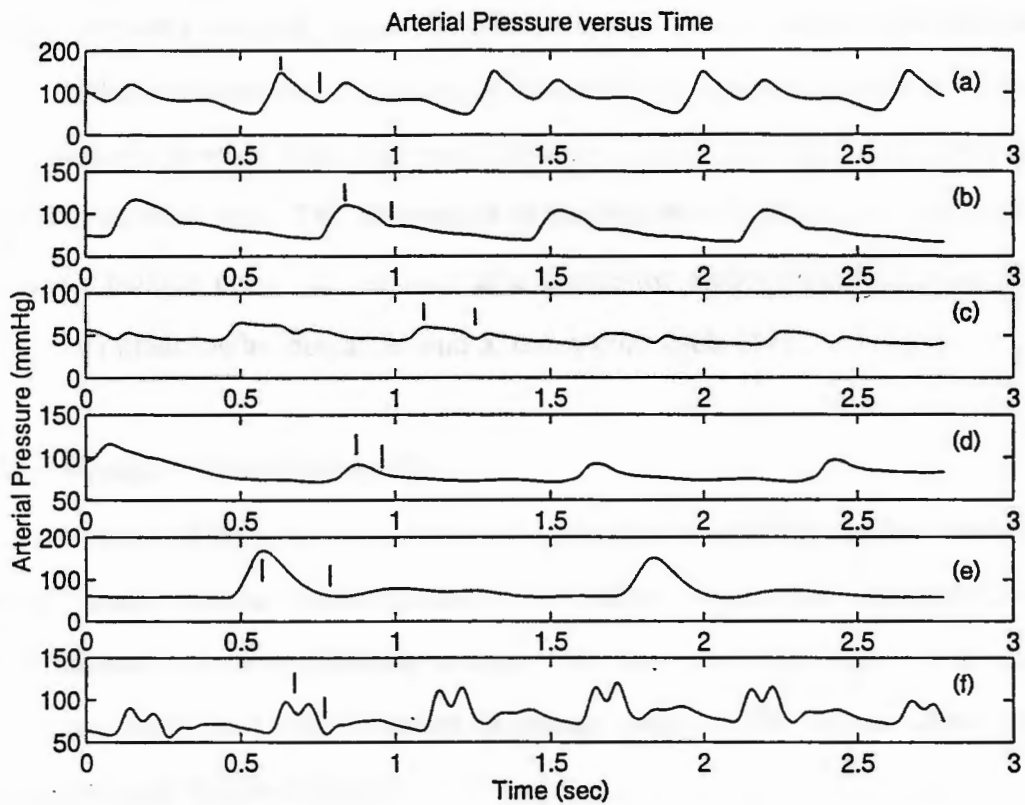


Figure 1.3 MGH database files illustrating typical pressure waveform contours at various points along the circulatory track. (a) aortic, (b) radial, (c) brachial, (d) femoral, (e) pedal and (f) axillary pressures, [22] depicting the locations of the systolic peak and the DN.

1.3 Clinical Implications

Locating the dicrotic notch in arterial blood pressure signals has several clinically important applications. The location of the dicrotic notch indicates the closure of the aortic valve which occurs at the end of left ventricular ejection. Thus, the dicrotic notch represents the end of the systolic phase and the start of diastole and left ventricular relaxation. The duration of the systolic phases, including pre-ejection and left ventricular ejection, provides valuable diagnostic information of the condition of the myocardium and of cardiac performance. Locating the dicrotic notch is also important for evaluating the accuracy of a set of linear regression equations used to predict systolic time interval according to heart rate. The information of the regression equation is also used in the intraaortic balloon pump cardiac assistance device for determining the proper inflation time of an intraaortic balloon at the end of the systolic cycle [14].

1.3.1 Systolic Time Intervals

Information of the systolic time intervals are useful in assessing cardiac condition and various cardiac disease states (including LV failure, myocardial infarction, coronary artery disease, and valve disorders) in man. The time intervals of the various stages of the cardiac cycle have been observed to change under cardiac disease conditions and pharmacological influence [1-10].

The three basic systolic time intervals are the pre-ejection period (PEP), left ventricular ejection time (LVET) and total electromechanical systole (QS2). The first stage of the systolic cycle, referred to as the pre-ejection period, involves an electromechanical delay (30 to 40 msec) followed by initial isovolumetric contraction of the left ventricle (60 to 80 msec). The PEP is immediately followed by left ventricular ejection which lasts throughout the remaining systolic cycle. The entire systolic cycle time is defined from the Q wave of the ECG to the occurrence of the second heart sound

in the phonocardiogram signal or the dicrotic notch in the arterial blood pressure signal. Thus, the duration of QS2 includes both the PEP and the LVET as shown in figure 1.4 [1].

The PEP is effected by a change in the rise of left ventricular pressure (LVP). The PEP is shortened by lower LV isovolumetric pressure and more forceful ventricular contraction; and becomes longer in duration during LV failure, LV conduction delay, diminished preload and reduced LV contractile intensity. Left ventricular ejection time is shortened by nearly all deviations from a normal cardiac state, including LV failure, a decrease in stroke volume relative to end diastolic volume, or by a more rapid rate of ejection. The QS2 provides information on the increased contractile motion (inotropic stimulation) since both the PEP and the LVET are shortened.

Linear relationships between heart rate and the duration of the systolic phases of the left ventricle have been derived from patient observations [1, 2, 4, 6]. These regression equations predict the durations of the systolic time intervals according to the heart rate, as shown in equations (1.1) to (1.3) for normal patient conditions. Thus, the existence and extent of cardiac dysfunction can be observed through the systolic time intervals. Information of the temporal location of the dicrotic notch, in relation to the QRS complex of the electrocardiogram, is critical for evaluating the STI if the phonocardiogram is unavailable and determining the accuracy of the linear regression equations.

$$\text{PEP} = -0.0004 * \text{HR} + 0.126 \quad (1.1)$$

$$\text{LVET} = -0.0016 * \text{HR} + 0.394 \quad (1.2)$$

$$\text{QS 2} = -0.020 * \text{HR} + 0.522 \quad (1.3)$$

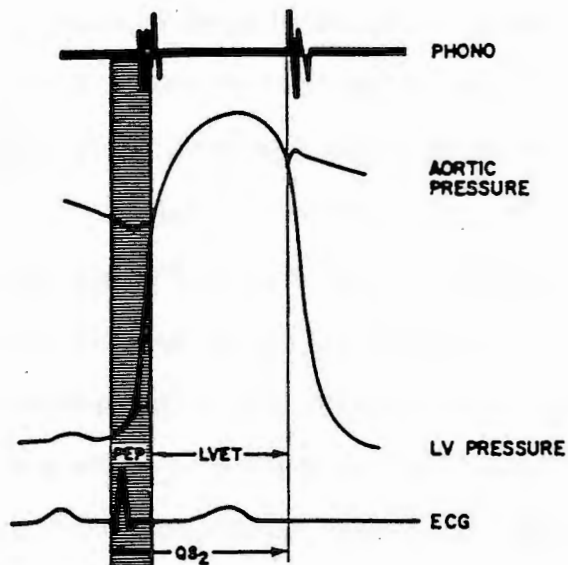


Figure 1.4 Schematic of the left ventricular events which comprise the STI, including the PEP, LVET and the QS2 from the combination of the ECG, LVP, aortic pressure and phonocardiogram signals [1]

1.3.2 Intraaortic Balloon Pump Timing

Hemodynamic benefit from the intraaortic balloon pump (IABP) is achieved by allowing inflation and deflation of the balloon to occur relative to the function of the left ventricle. Since the IABP is used for life saving circulatory assistance, it is vital that the device correctly time balloon inflation and deflation. The intraaortic balloon should be inflated at the closing of the aortic valve, thus, knowledge of the temporal location of the dicrotic notch in the pressure signal is crucial.

IABP is most extensively applied in cases of cardiac pump failure which includes cardiogenic shock, myocardial infarction, weaning from bypass and low output syndrome. With an estimated 800,000 myocardial infarctions occurring annually in the

United States, [39] the potential use of IABP therapy for this and related symptoms is quite large and increasing. Since the first clinical use of the IABP in 1967 for the treatment of cardiogenic shock, the complication rate has been reduced and its clinical usage has broadened. Clinical experience with IABP has grown from more than 50,000 insertions between 1968 and 1980, [40] to more than 300,000 by 1989, [41] with an estimated 70,000 IABP procedures performed annually [11].

The intraaortic balloon pump's counterpulsating action is used to manipulate arterial blood flow to augment systemic and coronary circulation while attempting to balance the myocardial oxygen supply/demand ratio by decreasing oxygen demand and increasing oxygen supply to the myocardium. Potential benefits from IABP, which have been experimentally verified, include decreased systolic and left ventricular end diastolic pressures, increased diastolic arterial pressure and cardiac output and changes in coronary flow and cardiac work. Increasing diastolic arterial pressure may increase coronary perfusion and improve the oxygen supply to the myocardium, whereas reducing left ventricular end diastolic pressure decreases afterload, cardiac work and myocardial oxygen consumption, and increases cardiac output. The likelihood and magnitude of hemodynamic benefit, especially coronary perfusion, depends upon a patient's cardiac condition prior to IABP and a partially functional LV. If, however, over 40% of the cardiac muscle is necrotic, then IABP alone will not be effective.

Current IABP systems initiate balloon inflation at aortic valve closure (dicrotic notch), and final balloon deflation occurs just prior to left ventricular ejection. Once the IABP console generates a signal to trigger balloon inflation or deflation, there is a fixed time delay of approximately 40 msec before the balloon is actually activated. It is this pneumatic delay which forces the controlling electronics to predict the start of the next cardiac cycle based on the previous R waves and the systolic time interval, QS2.

Once the left ventricle has emptied its blood volume into the aorta and the aortic valve closes, the balloon is inflated. This action, occurring at the beginning of diastole, displaces blood both back towards the ascending aorta, into the coronary arteries, to enhance coronary artery perfusion, and outward along the descending aorta to enhance the systemic circulation. If inflation occurs much before this, the balloon would present a resistance to the blood flow out of the LV and make the LV work harder to empty, with the added risk of pushing blood up into the brachiocephalic, subclavian or carotid arteries. Early inflation would also cause a reduction in stroke volume, and an increase in end systolic volume, effecting ventricular preload.

The IAB is deflated for left ventricular ejection. The effect of reduced afterload is a decrease in cardiac work and myocardial oxygen consumption and an increase in cardiac output. Balloon deflation occurring much beyond this point imposes a resistance to the ensuing ventricular ejection, create intraventricular wall stress and effects the amount of stroke volume; (slightly late deflation has been shown to be acceptable).

1.4 Rationale for Selecting the DyWT

1.4.1 Signal Processing Requirements

The dyadic wavelet transform dicrotic notch detection scheme has been designed to accommodate various types of arterial blood pressure waveforms, with various heart rates, arrhythmias and signal irregularities, encountered in a clinical setting. No assumptions of catheter type or signal acquisition method were made since prerecorded MGH patient clinical data was used to verify the performance of the detection algorithm.

Originally, it was hypothesized that since the aortic valve resonates upon closure at a characteristic frequency, that this frequency, once detected, would provide the temporal location of the dicrotic notch. Also, the algorithm used in this regard would therefore have to be robust for nonstationary signals. The Fourier transform (FT), short time Fourier transform (STFT) and eventually the wavelet transform methods were considered. Research into the FT and STFT led to the discovery of the wavelet transform as a possible method of detecting the dicrotic notch frequency. However, it was also observed at this time that there was no distinctive frequency content of the dicrotic notch in the arterial pressure waveform, except for the possibility of defining dicrotic notch frequency related to the velocity of valve closure. Otherwise, the desired notch frequency, referred to as the second heart sound, may be found with the FT and STFT if applied to a patient's phonocardiogram rather than the blood pressure signal [42-50]. Rather than locating the time in which the resonant frequency occurs, the task of detecting the event of notch closure focused on observing the change in the contour of the pressure waveform that corresponded to the dicrotic notch.

Since the arterial pressure is a time varying or non stationary signal, and changes with patient condition and sensor drifting, a detection scheme that could accommodate both time varying and noisy signals would be the most advantageous. The wavelet

transform technique for waveform analysis does accommodate nonstationary signal behavior and is able to locate rapidly changing signals, such as with pre-ventricular contractions (PVCs) or arrhythmias. For example, if the frequency of the dicrotic notch changes in a patient for any reason, the wavelet method would still be able to track that frequency.

This is accomplished by evaluating and comparing the DyWT calculated with several dyadically time scaled versions of the wavelet function. Scaling the mother wavelet is the means by which the DyWT accommodates various signal transients, according to the transient duration. As the scale is increased, the width of the wavelet is expanded in time allowing the DyWT to focus in on increasingly longer duration transients (having lower frequency spectral content) providing information on the overall signal behavior. Smaller scale wavelets are compressed in time and the resulting DyWT would therefore accentuate higher frequency transients of shorter duration, such as edges in images or sudden signal discontinuities. The dyadic wavelet transform detection method can therefore provide a multiresolution (or multi spectral) view of a signal and be used to isolate a portion of the actual signal from background noise [23-35]. It is these two aspects of the wavelet transform method, (time varying signal analysis and noise reduction capabilities), that prompted a feasibility study for the dyadic wavelet transform dicrotic notch detection scheme.

1.4.2 Feasibility Study

Several signal processing methods for time varying signals were found from a search of the current literature, including the wavelet transform, Fourier transform and short time Fourier transform analysis techniques [29,31, 51-70]. Although other signal processing techniques were explored [71], it appeared that the dyadic wavelet transform

method would provide the best detection scheme for normal, arrhythmic and noisy time varying signals. Thus, the dyadic wavelet transform approach was taken to detect the dicrotic notch in the pressure signal. Initial feasibility tests indicated successful dicrotic notch detection with the dyadic wavelet technique for a radial pressure signal containing pre-ventricular contractions (PVC), and with added broad band white noise, as shown in figure 1.5 a and 1.5 b, respectively, where the solid vertical lines indicate the estimated locations of the dicrotic notches and the dotted vertical lines indicate the locations of the systolic peaks for each cardiac cycle.

The feasibility study [72] demonstrated that it was possible to distinguish signal transients, such as the dicrotic notch, systolic peak and the upstroke following end diastole, from background noise by comparing the DyWT across several successive dyadic scales. The cubic spline, Mexican Hat, Morlet, Harr and Shannon wavelet functions were tried in early feasibility tests of the wavelet analysis method, of which the cubic spline and the Mexican Hat wavelets showed the best results. Since the specific frequency bandwidth of the dicrotic notch does not overlap with any of the other characteristics of the arterial blood pressure signal, such as the systolic peak or end diastole, the DyWT was found to be applicable for dicrotic notch detection.

The dicrotic notch detection algorithm based on the dyadic wavelet transform is able to detect the dicrotic notch in cases of non-stationary circumstances of changing patient condition which is reflected in changing pressure waveform characteristics. This is accomplished by calculating the DyWT with several time dilated scales of the wavelet function. Also, since the clinical environment is sensitive to its surroundings and the fidelity of its sensor equipment, noise is always a factor in the recorded signals. Since band limited noise does not correlate between scales, this method of dicrotic notch detection is appropriate for the clinical environment.

Various methods of signal analysis were initially applied to evaluate the pressure signal [71], including the fast Fourier transform (FFT), power spectral density (PSD), auto and cross covariance and the first and second derivatives of the pressure signal [52-53]. These signal analysis tools were applied to pig blood pressure data. The results provided information on the waveform's FFT, power spectral density and derivatives and on the catheter effects on signal measurement. No algorithms for dicrotic notch detection were devised from these results. This information led to the testing of several methods (including Butterworth filtering, inverse FFT, signal damping, Jackson's Poles method [73], and Prony's method) to clean the pressure signal of unwanted oscillations from IABP for future for dicrotic notch detection.

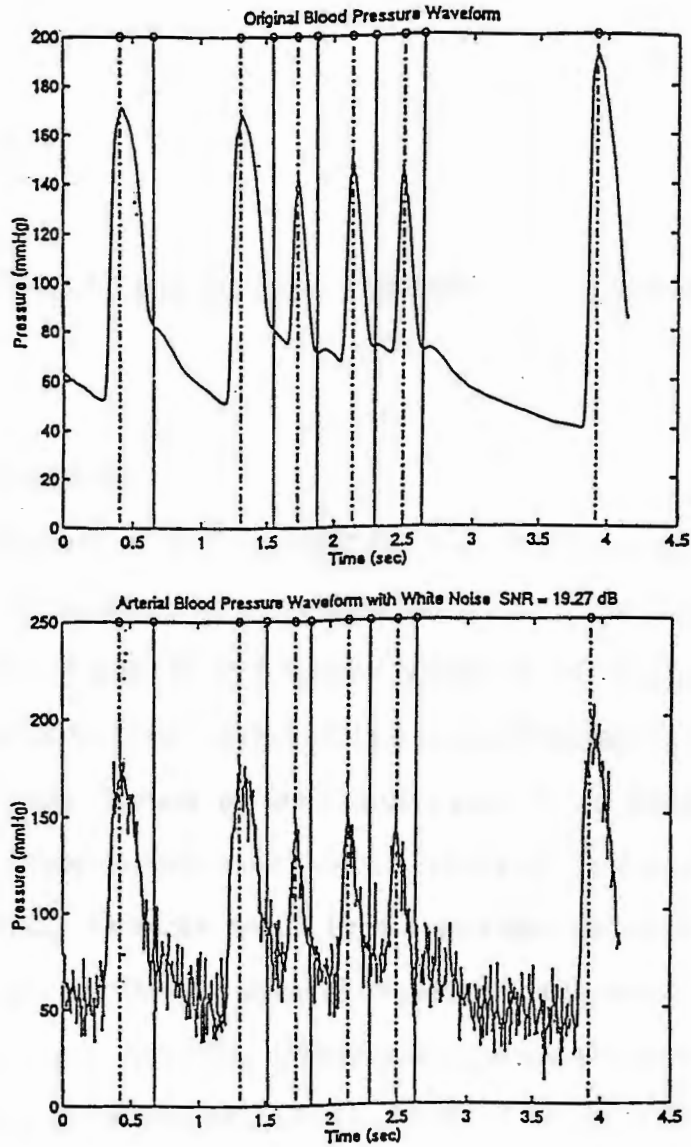


Figure 1.5 Results of DyWT algorithm feasibility study on radial blood pressure waveform containing a (a) premature ventricular contraction; (b) with added white Gaussian noise. The solid vertical lines indicate the estimated locations of the diastolic notches, and the dotted vertical lines indicate the locations of the systolic peaks for each cardiac cycle.

Chapter 2

Introduction to the Dyadic Wavelet Transform

2.1 Motivation

Typical methods of dicrotic notch detection rely on slope characteristics of the arterial pressure waveform. An alternative observation of the signal can be made on the signal analyzed in terms of its frequency content. It was originally hypothesized that aortic valve closure would correspond to a unique frequency; and once the frequency was detected, the location of the dicrotic notch would be found. Dicrotic notch frequency is defined as either valve closure vibrations or the velocity of valvular closure, (not heart rate), whichever would be characteristic of the dicrotic notch and be observable in the physiological signal of interest, (arterial pressure or phonocardiogram) [42-50]. Thus, signal processing techniques, such as the Fourier transform [51-52, 74], the short time Fourier transform [30-31, 54-57, 67, 76-78] and eventually the dyadic wavelet transform were explored for the purpose of dicrotic notch detection [29-35, 59-71, 79-81]. This section describes the mathematics of the time domain to frequency domain transformations according to their relative applicability to dicrotic notch detection.

2.2 Time Varying Signal Analysis

The Fourier transform, $FT_x(f)$, of a signal $x(t)$, shown in equation (2.1) [51] is typically used for frequency analysis of stationary signals, whose characteristics do not change with time [51-52]. The magnitude of the FT provides information on the frequency content of the original signal. Since the FT represents a signal as the decomposition of a basis of complex sinusoidal functions of infinite extent, $(e^{-j2\pi ft})$, any temporal variation in the waveform is spread out over the entire frequency plane. Thus, although the frequency corresponding to the diastolic notch may be discerned, the actual temporal location of the diastolic notch is not available. Therefore, the FT method does not provide any information regarding the time of notch closure, but rather the existence of it in terms of acknowledgment that its frequency was present in the analyzed signal. Figure 2.1 [82] pictorially describes the lack of temporal resolution in the resulting FT magnitude spectrum for a signal containing three different frequencies.

$$FT_x(f) = \int_{-\infty}^{+\infty} x(t) e^{-j2\pi ft} dt \quad (2.1)$$

By applying the Fourier transform to a portion of the signal $x(t)$, isolated using a sliding temporal window function, $h(t)$, frequency information can be located as a function of the time in which these frequencies occurred [29-30, 54-58]. For example, a change in the pattern of the waveform's slope, such as with the diastolic notch, the systolic peak or the upstroke following end diastole, would indicate a change in the waveform's frequency pattern. The time of this frequency change would be recorded at the time in which it occurred. This method, known as the windowed Fourier transform [29, 31] or the short time Fourier transform, $STFT_x(\tau, f)$, shown in equation (2.2) [30], is a two dimensional, (time versus frequency) representation of a signal.

$$STFT \quad x(\tau, f) = \int_{-\infty}^{+\infty} x(t) h(t - \tau) e^{-j2\pi ft} dt \quad (2.2)$$

The frequency information is obtained for the portion of the waveform which overlaps the time duration of the window function, where τ is the center time of the window function. In this time window, time varying signals are approximated as stationary (the signal is assumed to be quasi-stationary where the spectral properties of the signal do not vary within the analysis window length) [57]. The STFT is computed each time the window is shifted. *Translation* of the window in time provides a frequency analysis of the entire data string localized within each time frame. Thus, temporal resolution of each frequency contained in the analyzed signal depends upon the duration of the window function. Good time resolution is obtained with small windows at the cost of reduced frequency resolution, due to the Heisenberg uncertainty principle [30, 75, 83-84] which establishes a lower bound on the time-bandwidth product, shown in equation (2.3) [30]. Higher frequencies are resolved using windows of shorter duration; and as the window duration is increased, lower signal frequencies are resolved with the STFT method. The STFT calculated using a Gaussian window function provides a good compromise for both frequency and temporal resolution, and is referred to as the Gabor transform [29, 31, 67, 75, 85]. Along with expressing a local FT, the STFT can be interpreted as the time-frequency filtered output (low or band pass) of the signal with the window function or as an inner product of the signal with the window function.

$$\text{Time|Bandwidth Product} = \Delta t \Delta f \geq \frac{1}{4\pi} \quad (2.3)$$

The STFT however, is limited by the constant duration of the window $h(t)$, resulting in the same signal time-frequency resolution (filter pass band) for all signal frequencies at

all times. Thus, the STFT would not be an adequate analysis tool for accommodating changing patient conditions. It is desirable to have a window function which can be altered to accommodate a variety of possible frequencies, (varying filter band). In this regard, the wavelet transform is an extension of the STFT incorporating various window durations for a multiresolution view of the signal and its frequency content. Figure 2.2 [30] window durations corresponding to the various frequencies for both the STFT and the wavelet transform (WT). Notice that the STFT windows have the same duration regardless of the signal frequency being analyzed. Whereas, the wavelet transform uses modified window durations for different frequencies. By having smaller window widths for higher frequencies and longer window durations for lower frequencies, the WT has improved frequency resolution over a larger spectral range than the STFT.

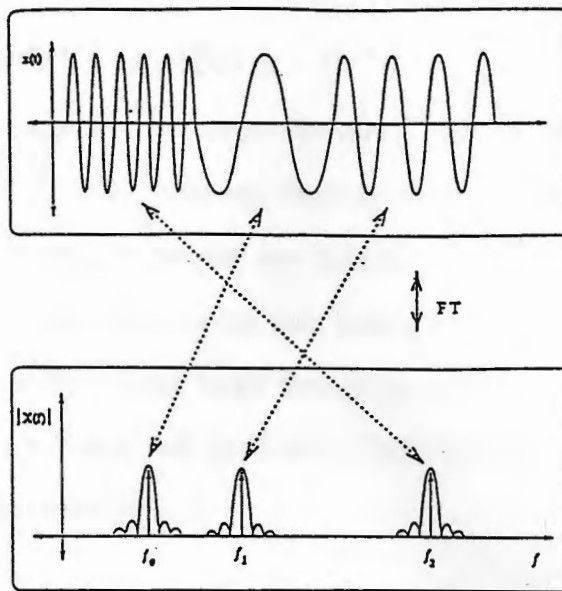


Figure 2.1. Lack of time resolution of the FT magnitude spectrum [82].

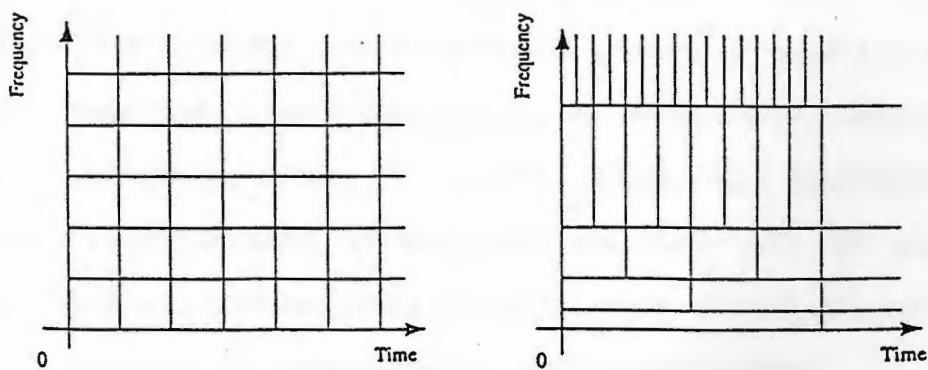


Figure 2.2. Coverage of the time-frequency plane for the (a) STFT; (b) for WT [30].

2.3 The Wavelet Transform

The wavelet transform overcomes the limitations of the fixed time-frequency resolution of the STFT, for analyzing non-stationary signals. The multiresolution capabilities of the wavelet transform are realized through the use of various size windows, obtained by first time-scaling then time-translating a wavelet function. The wavelet transform provides better (high frequency) time resolution with smaller scale wavelets (narrower wavelets), and good (low frequency) spectral resolution at larger scales, with dilated wavelets [30-31].

2.3.1 Historical Background

The concept of looking at a signal at various scales and analyzing it with various resolutions has emerged independently in different scientific fields. Mathematical constructs of what is now referred to as wavelet theory had been presented mathematically in the early twentieth century [86-87], with application to harmonic analysis [87]. Wavelet transform mathematics were introduced by Calderon [88] in 1964 and have been developed under various names, including scale-space transforms [89]. The mathematical formulation and terminology of a wavelet as a decomposition of a signal into dilated and translated basis functions was introduced as a signal processing tool by Grossmann and Morlet [79] in 1984. Mathematical development of the continuous wavelet transform by Grossmann and Morlet [79, 90] and major contributions from Daubechies [31, 63, 91-96] and Mallat [26-29] have increased the utility and application of the wavelet transform in numerous disciplines.

2.3.2 Applications of the Wavelet Transform

Various scientific disciplines have applied the wavelet transform to analyze an assortment of signals, including image processing and coding, analysis of acoustic signals, physiological signals, and astronomical data. Mallat demonstrated the utility of the multiresolution wavelet transform for edge detection, represented as high frequency signal transients, and outlined fast algorithms for analyzing 1 and 2 dimensional signals [33]. Mallat showed that high frequency signal components produce local maxima in the dyadic wavelet transform which occur simultaneously across several consecutive scales using a smoothing wavelet function [33]. Applications of similar algorithms using the wavelet transform are presented in table 2.1.

Table 2.1

Applications of the Wavelet Transform

- Edge detection [33-35]
- Pitch detection in speech [81, 97-100]
- Analysis of acoustical signals [101-105]
- Medical applications include detection of the onset of the QRS complex in the electrocardiogram signal [82, 106-108], ventricular late potentials [109-110] and analysis of other biomedical signals [111-117].
- Seismic data interpretation [118-119]
- Astronomical data [120-123]
- Image processing [124-132]; and image coding [133-139];
- Radar applications [140-143]
- Detection of various transients signals [144-149].
- Random processes, fractional Brownian motion [150-151]; and fractals [152-157]
- Electromagnetics applications [158-159]
- Applications to fluid dynamics and turbulence [160-162]

2.3.3 Definition and Significance

Physiological signals, such as the blood pressure and the electrocardiogram are classified as time-varying or nonstationary. Since physiological signals, in general can exhibit erratic behavior due to changing patient condition, the wavelet transform is more appropriate than the FT and the STFT for analyzing these time-varying signals. The wavelet transform technique for waveform analysis accommodates nonstationary signals and is able to resolve low and high frequency information by incorporating windows of various widths (scaled wavelet functions) in the signal analysis. Also, in general, band limited noise does not correlate between the various transform scales and thus, frequency content as a function of the wavelet transform scale is obtained. The wavelet transform provides time-scale information. The time-scale representation of a signal implicitly depends on frequency through the scale parameter. The frequency content of the wavelet transform can be obtained by substituting $a = \frac{f_0}{f}$, where f_0 is the center frequency of the magnitude of the Fourier transform of the mother wavelet [30, 98,111]. The mother wavelet, however, must have a unimodal spectrum, such as the Mexican Hat wavelet function.

The continuous wavelet transform (CWT), shown in equation (2.4), gives local frequency information, like the STFT, but differs in that it utilizes scaled and translated versions of the "mother" wavelet function $g(t/a)$ as basis functions [30-33, 60-71]. The $g^*(\frac{t-b}{a})$ in equation (2.3) indicates the complex conjugate of the wavelet $g(\frac{t-b}{a})$. Scaling of the mother wavelet produces multiple length windows, providing variable resolution in the time or frequency domain. Scaling and subsequent translation of the mother wavelet is the means by which the wavelet transform accommodates various durations of the transient being analyzed or various frequency ranges of interest. Variations, transients or changes in the slope pattern in the time domain signal, (or changes in the signal's frequency content) can thus be detected by comparing the results from the

wavelet transform calculated using progressively dilated wavelets obtained by increasing the scale of the wavelet function. The combination of WT results from various scales allows for a multiresolution view of the signal. Thus, signal transients can be isolated from background noise by comparing the wavelet transform across several scales.

$$WT_x(b,a) = \frac{1}{\sqrt{|a|}} \int_{-\infty}^{+\infty} x(t) g^* \left(\frac{t-b}{a} \right) dt \quad (2.4)$$

where: $a \in \mathbb{R}^+$ time scale of wavelet function
 $b \in \mathbb{R}$ time shift of wavelet function

The *scale* parameter, a , allows expansion or contraction of the wavelet function in time. The WT has good spectral resolution at large scale values with dilated wavelets (larger window durations for lower frequency resolution), and good temporal resolution at smaller scales with compressed wavelets (smaller window durations for higher frequency resolution). Like the STFT, the temporal location of the window (wavelet function) is controlled by the time *shift* parameter, b which gives the position of the wavelet (in time) [31].

The integral expression in (2.4) is equivalent to the convolution in time of the two signals, shown in equation (2.5), where the factor $\left(\frac{1}{\sqrt{|a|}}\right)$ is included for energy normalization, and $*$ refers to the convolution operation between $x(t)$ and the wavelet function. Thus, by application of Fourier transform properties, the WT convolution operation can also be calculated by taking the inverse Fourier transform of {the Fourier transform of the signal multiplied by the Fourier transform of the scaled version of the mother wavelet}[51].

$$= \frac{1}{\sqrt{|a|}} \left(x(t) * g^* \left(\frac{-t-b}{a} \right) \right) \quad (2.5)$$

2.3.4 Discrete Wavelet Transform

The continuous time wavelet transform is a function of both a continuous translation parameter and a continuous scale parameter, making the CWT computationally intensive. A discrete wavelet transform (DWT) of a continuous signal is obtained by discretizing both the scale and shift parameters [26, 29, 30, 31, 33, 35, 69, 163-167]. The development of the DWT led to the development of compactly supported wavelets with orthonormal bases [91-96]. The scale and shift parameters are discretized as [30]:

$$a = a_o^l \qquad b = ka_o^l T$$

where l and k are integers. The a_o and T determine the sampling density in the time-scale plane [82]. The DWT is shown in equation (2.6) in relation to the continuous wavelet transform, in equation (2.4).

$$DWT_x[k, l] = CWT(a_o^l, ka_o^l T) \qquad (2.6)$$

The wavelet become discretized as shown in equation (2.7) [82].

$$g_{[k, l]}(\tau) = a_o^{-\frac{l}{2}} g(a_o^{-l} \tau - kT) \qquad (2.7)$$

An alternative approach to describing and implementing the discrete time wavelet transform is through the use of filter banks [28, 30, 67, 168-172]. The wavelet can be interpreted as "the impulse response of a band-pass filter and the wavelet transform as a convolution with a band-pass filter which is dilated", [35]. The wavelet transform decomposition uses a cascade of constant Q , low pass and high pass quadrature mirror filters as shown in figure 2.3 [67]. The dyadic wavelet transform corresponds to an

octave band filter scheme (as in music where increasing a tone by an octave involves doubling the frequency). The data decimation process corresponds to the dyadic scaling and the output of the high pass filters corresponds to the wavelet transform output.

Although the DWT is more computationally efficient than the CWT, it is both scale and shift variant. However, by discretizing only the scale parameter, the complexity of the CWT computations can be reduced while maintaining the properties of scale and shift invariance, as outlined in section 2.4.2.

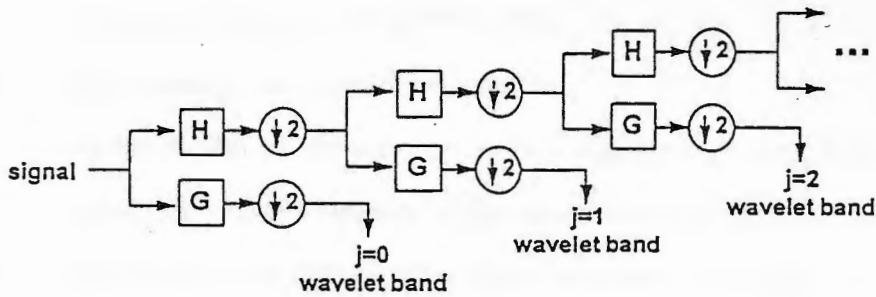


Figure 2.3 Block diagram of the algorithmic approach for digital computation of the DyWT using low pass (H) and high pass (G) filters [67].

2.4 The Dyadic Wavelet Transform

2.4.1 Definition and Significance

A reduction in computation is achieved by discretizing the scale parameter [173]. The dyadic wavelet transform (DyWT) [33,35, 81, 98] of a signal $x(t)$, shown in equation (2.8) is mathematically equivalent to the wavelet transform with a dyadic time scale, $a=2^m$, where m is an integer.

$$\text{DyWT}_x(b, 2^m) = \frac{1}{\sqrt{|2^m|}} \int_{-\infty}^{+\infty} x(t) g^* \left(\frac{t-b}{2^m} \right) dt \quad (2.8)$$

Since the spectral resolution of the WT depends on the time duration and bandwidth of the wavelet, scaling the mother wavelet has the effect of changing the center frequency and bandwidth of the wavelet, as observed in its Fourier transform. As the scale is increased, the center frequency of the equivalent band pass filter is reduced and the bandwidth becomes narrower. The effect of dyadically scaling the cubic spline wavelet function is shown in figure 2.4a for the dyadic scales, $m = 1, 2, 3$. The width of the wavelet function is doubled in time as the scale is dyadically increased. The magnitude of the FT of these three scaled versions of the mother wavelet is shown in figure 2.4b. As the scale is dyadically increased, the FT magnitude becomes narrower and has a lower center frequency which is half of the center frequency of the previous scaled version. Thus, as the scale is increased dyadically, the wavelet is expanded in time (doubled) and compressed in frequency, (halved).

Cubic Spline Wavelet Function $\varphi\left(\frac{t}{a}\right)$

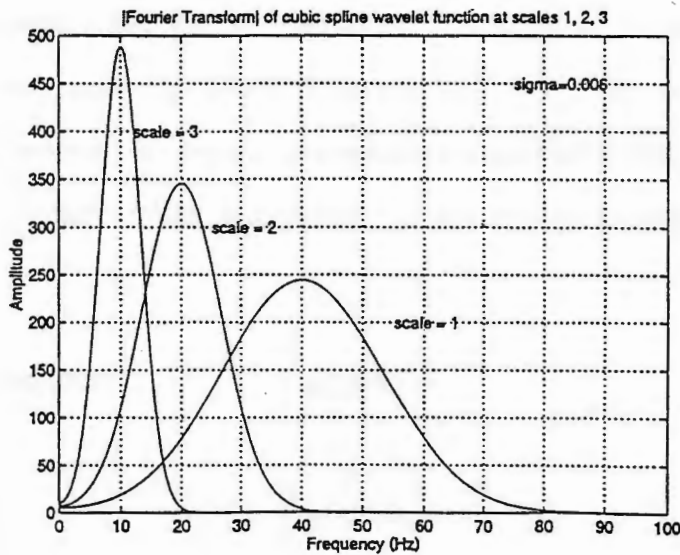
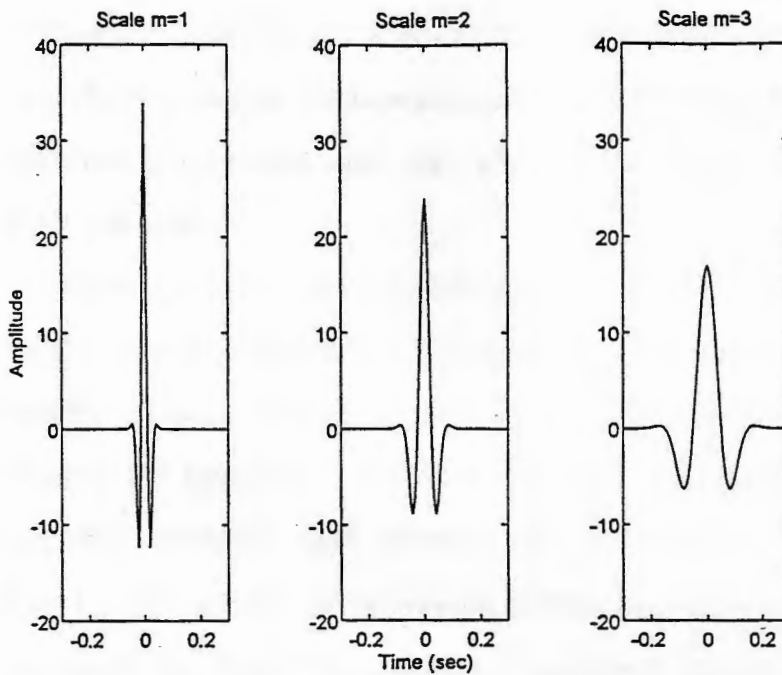


Figure 2.4(a) Cubic spline wavelet function at dyadic scales $m = 1, 2, 3$; (b) FT magnitude of each of the scaled versions of the cubic spline wavelet in (a).

Each of the scaled versions of the mother wavelet are convolved with the signal $x(t)$ to achieve the dyadic wavelet decompositions of the signal at various levels of frequency resolution. Therefore, successful implementation of the dyadic wavelet transform for a particular application is dependent upon the choice of the wavelet function and the magnitude of the time scaling.

The term 'wavelet' refers to a portion of an oscillating wave. The wavelet function, in general, follows several constraints. The mother wavelet must be a zero mean function, therefore, it must oscillate in time. The wavelet function must also be absolutely integrable and have finite energy as in equations (2.9a) and (2.9b) [81]. For signal reconstruction purposes, (not necessary for dirotic notch detection) the magnitude of the Fourier transform of the wavelet function must not contain any dc ($\omega = 2\pi f = 0$), according to the admissibility condition in equation (2.9c) [30, 35, 79, 81], by virtue of energy conservation, where $G(2^m \omega)$ is the FT of the wavelet function. This constraint also ensures that the WT represents the signal as a complete set of basis functions that encompass the entire frequency axis [35]. As with the FT, where sinusoidal basis functions to expand nonperiodic signals, time shifted and time scaled versions of the mother wavelet incorporate the set of basis functions for the wavelet transform.

$$\text{Absolutely Integrable:} \quad \int_{-\infty}^{+\infty} |g(\frac{t}{a})| dt < \infty \quad (2.9a)$$

$$\text{Finite Energy:} \quad \int_{-\infty}^{+\infty} |g(\frac{t}{a})|^2 dt < \infty \quad (2.9b)$$

$$\text{Admissibility Condition:} \quad \int_{-\infty}^{+\infty} \frac{|G(af')|^2}{|af'|} df' < \infty \quad (2.9c)$$

2.4.2 Properties

The wavelet transform and therefore the dyadic wavelet transform possess several desirable properties consistent with the properties of the continuous wavelet transform (CWT) as listed in table 2.2. The proofs for the properties are found in references [26, 34, 79, 81-82, 103].

Table 2.2

Properties of the DyWT

- | | |
|--|---------------------------------------|
| i) Linearity | v) Convolution to Multiplication (FT) |
| ii) Scale Invariant | vi) Transient Localization |
| iii) Time Shift Invariant | vii) Signal Reconstruction |
| iv) Conservation of Energy (Isometric) | viii) Real Input/Real Output |

i) *Linearity* allows a signal $x(t)$ which is composed of several weighted signals to have a DyWT equal to the sum of each individual weighted DyWT (of weight α_i), as shown in equation 2.10.

$$DyWT_{x(t)}(b, 2^m) = \sum_{i=1}^n \alpha_i DyWT_{x_i(t)}(b, 2^m) \quad (2.10)$$

ii) The DyWT is *scale invariant*. A scale change in the input corresponds to a change in both the scale and shift parameters of the DyWT, to within a magnitude factor ($\sqrt{|\alpha|}$) as shown in equation (2.11). Scaling the wavelet function changes the center frequency and bandwidth of its Fourier transform. The wavelet is compressed in time for small scales and expanded in time for larger scales. Thus, varying the scale parameter allows for low or high frequency analysis for a multi resolution characterization of a signal. Analysis of

the DyWT at several dyadic scales is the mechanism by which the DyWT adjusts to the specific time and frequency characteristics of a particular signal. Transient detection based on the DyWT is based on calculating the DyWT across several dyadic scales and comparing the DyWT outputs for simultaneous peaks across consecutive dyadic scales. The property is also useful for wideband Doppler analysis where moving targets produce scale changes in reflected signals. This property is also useful for fractal analysis (where certain properties exist regardless of scale) and for analyzing the cochlea and other such octave band systems [174].

$$DyWT_{x(\alpha t)} = DyWT_{x(t)}(\alpha b, \alpha 2^m) \quad (2.11)$$

iii) The DyWT is *time shift invariant*. Thus, the DyWT preserves a shift in the original signal $x(t-t_0)$ as translations of the wavelet function by the shift parameter of the DyWT by an equivalent "delay" $(b - t_0)$ as shown in equation (2.12). The shifted wavelets act as a sliding window for different values of t_0 . This property is useful for transient detection in a signal or for edge detection in image analysis. The translation parameter, b , along with the scale parameter, 2^m , defines a set (basis) of wavelet functions from the mother wavelet. Morlet proposed the use of scaled and translated versions of a single function to analyze seismic data [68, 163].

$$DyWT_{x(t-t_0)}(b, 2^m) = DyWT_{x(t)}(b-t_0, 2^m) \quad (2.12)$$

iv) The DyWT operation *preserves the energy*, (E) of a signal. Thus, the transform operator is isometric in that the energy in the time domain is equal to the energy in the wavelet domain as shown in equation (2.13). Since the DyWT is an alternate

representation of a signal, it should maintain the energy characteristics of the signal. For signal reconstruction, it is important that the signal and its DyWT are of finite energy and that the DyWT operation does not alter the energy of the signal.

$$E_{x(t)} = \int_t |x(t)|^2 dt = \sum_{m=-\infty}^{\infty} \int \left| \text{DyWT}_{x(t)}(b, 2^m) \right|^2 \frac{db}{(2^m)^2} \quad (2.13)$$

v) The Fourier transform property in which the *convolution of two signals in the time domain is equivalent to multiplication in the frequency domain* is applicable to the DyWT operation as shown in equation (2.14). The DyWT is the inverse FFT of the product between the FFT of the signal, $(X(f))$ and the FFT of the wavelet function, $(G(f))$. This property allows more efficient computation of the DyWT, especially when the scale parameter is large and the wavelet function is compressed in frequency. Thus, there are fewer multiplications involved in computing the DyWT in terms of the frequency representation than with the convolution procedure in the time domain.

$$\text{DyWT}_{x(t)}(b, 2^m) = x(t) * g^*\left(\frac{-t}{2^m}\right) = \text{IFFT} \left\{ X(f) \left(G^*(2^m f) \sqrt{|2^m|} \right) \right\} \quad (2.14)$$

vi) Use of the Dirac delta function $(\delta(t))$ highlights the *transient localization* ability of the DyWT in that the DyWT can focus in on short time fluctuations (transients) or slowly varying spectral components. Time resolution then depends upon the bandwidth of the mother wavelet and the inverse of the scale parameter. The DyWT of a signal $x(t)=\delta(t-t_0)$ is a modified wavelet function with translation replacing the time parameter as shown in equation (2.15). Transient localization is achieved since the modulus of the DyWT of a signal $x(t)$ exhibits local maxima around transients or points of discontinuity

that are contained in the signal. "Lines of constant phase of the DyWT converge toward the points of discontinuity" at, $t-t_0$ [81, 90].

$$\frac{1}{\sqrt{|2^m|}} \int_{-\infty}^{+\infty} \delta(\tau - t_0) g^* \left(\frac{\tau - b}{2^m} \right) d\tau = \frac{1}{\sqrt{|2^m|}} g^* \left(\frac{t_0 - b}{2^m} \right) \quad (2.15)$$

vii) Under certain constraints on the signal $x(t)$ and the mother wavelet $g(t/2^m)$, the original signal can be reconstructed from its DyWT as shown in equation (2.16) where $\tilde{g}(t) = g(-t)$. The Fourier transform of the wavelet function $G(2^m f)$ must be zero at dc and the signal $x(t)$ must be of finite energy. Thus, the DyWT is a one to one transform which is critical for most mathematical analysis and synthesis.

$$x(t) = \sum_{m=-\infty}^{\infty} \int_{-\infty}^{\infty} DyWT_{x(t)}(b, 2^m) \frac{1}{2^m} \tilde{g} \left(\frac{t-b}{2^m} \right) db \quad (2.16)$$

ix) If a signal $x(t)$ and the wavelet function are real valued, then the DyWT is real.

Chapter 3

Methodology

3.1 Motivation

A reliable dicrotic notch detection algorithm provides physiological information useful in the diagnosis of cardiac condition as patient condition changes, through such tools as the systolic time interval. The development of intelligent cardiovascular monitoring devices with robust signal processing algorithms is increasingly important. Monitors that can detect pathological condition and differentiate true signal events and fluctuations from artifacts are necessary for this task.

The dicrotic notch is observed in arterial pressure waveforms as a change in slope, as a consequence of the closing of the aortic valve, following left ventricular ejection, indicating the end of systole and the start of the diastolic cycle. Detection of the dicrotic notch is non-trivial in that the blood pressure signal may be damped, corrupted by noise, contain motion artifacts, respiratory modulation, or change abruptly due to pre-ventricular contractions (PVCs) or arrhythmias. Figures 3.1a-d [22] demonstrates four cases in which dicrotic notch detection is problematic compared to a classic arterial blood pressure waveform shown in figure 3.1e. Figure 3.1a indicates a pulsus alternans condition, where a weak pulse alternates with a strong one. Algorithms based on a threshold of the signal amplitude usually fail on signals containing alternating pressure amplitudes, arrhythmias and baseline drifts. The pressure waveform is subject to physiological variations due to patient condition and may be corruption by noise

(especially noise which resembles the dicrotic notch) possibly from the sensing catheter as in figure 3.1b. Damping of the pressure signal, shown in figure 3.1c, makes it is visually difficult to locate any notch inflection; and in sick patients, the pressure curve may deviate greatly from the classical shape shown in figure 1.3. Figure 3.1d involves a slight inflection of the curve prior to the actual dicrotic notch. Although the waveform in figure 3.1d has a well defined notch, it is difficult for a program to distinguish a damped notch inflection from the real notch. The application of the DyWT attempts to overcome the majority of these and other signal irregularities, (which are mainly due to signal non-stationarity and superimposed noise), to consistently and accurately detect the temporal location of the dicrotic notch.

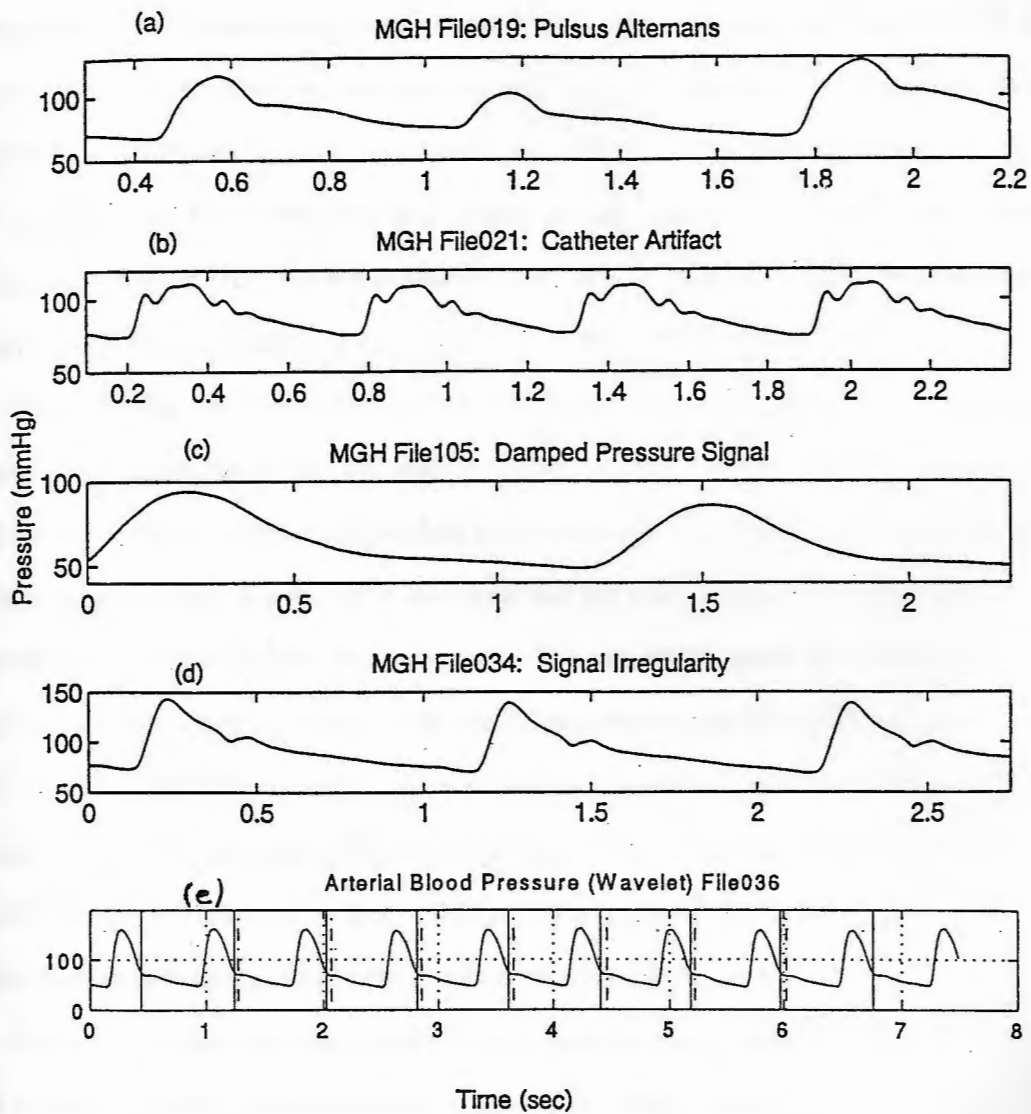


Figure 3.1 MGH database blood pressure waveforms illustrating four difficult cases for dirotic notch detection algorithms. (a) pulsus alternans, (b) catheter artifact, (c) damped signal, (d) signal shape irregularity, (e) classic arterial blood pressure waveform.

3.2 Application of the DyWT to Dicrotic Notch Detection

The dyadic wavelet transform algorithm has been developed using the Matlab programming environment version 4.2 on both a personal computer and a UNIX based Sparc station. The proposed detection algorithm, outlined in the block diagram in figure 3.2 finds the temporal locations of the dicrotic notch in the blood pressure signal using the dyadic wavelet transform method. Three dyadic scales of the DyWT were computed using the Mexican Hat wavelet function. The dicrotic notch locations are estimated by nearly simultaneous minima across consecutive dyadic scales of the DyWT.

The Mexican Hat wavelet function is precalculated for each of the three dyadic scales. The quantity of wavelet sample points, generated with the same sample rate as the recorded MGH blood pressure data to be analyzed (180 Hz or 360 Hz depending on which database file), are stored in memory and are subsequently accessed by the dyadic wavelet dicrotic notch detection program. The algorithm starts by loading the wavelet function samples and a portion of an MGH blood pressure file [22] (approximately 30 seconds of data) into memory. The pressure waveform is immediately preprocessed using a 4th order low pass Butterworth filter, with cutoff frequency of 20 Hz. The dyadic wavelet transform is then calculated for each of the three dyadic scales using discrete convolution as outlined in the flow chart in figure 3.3.

Since the convolution operation contains the number of points equal to the (length of the pressure signal plus the quantity of wavelet sample points minus one), In order to achieve correct sample number placement of the resulting DyWT points, relative to the original blood pressure signal, each resulting DyWT is truncated in relation to the length of the wavelet function. This process is outlined in the flow chart in figure 3.3 and described further in section 3.3.2. This manipulation of the sample points is the method used to keep track of the sample number placement of the DyWT results and is a consequence of the form of the generated wavelet points (which include zero entries)

and the application of the discrete convolution between the blood pressure and wavelet data arrays.

A global search for all R waves in the ECG within the 30 seconds of patient data is performed using a simple threshold algorithm, adapted from Elghazzawi et al [175] as outlined in figure 3.4. Once all of the R waves have been determined, each cardiac cycle of the DyWT (defined between R waves) is individually searched for the temporal location of the dicrotic notch. Simultaneous occurrences of minima in the DyWT across several dyadic scales indicates a transient in the pressure waveform from which the corresponding temporal location of the dicrotic notch is determined.

The dicrotic notch in each cardiac cycle is represented by a local minimum in the DyWT. The algorithm therefore examines the three scaled versions of the DyWT for minima which exist within a neighborhood of ± 50 milliseconds (msec) across dyadic scales and selects the appropriate minimum as the dicrotic notch for each cardiac cycle. The dicrotic notch detection algorithm contains three major sections as outlined in figure 3.5, (A, B and C, respectively). The first section (A) locates the sample numbers of all minima in each cardiac cycle for each scale of the DyWT. The second section (B) compares minima between scales, and saves those minima which occur within ± 50 msec across consecutive dyadic scales. The last portion of the algorithm selects which valid minimum point is the dicrotic notch for each cardiac cycle. If there are no minima found for any given cardiac cycle, in any of the DyWT scales, the algorithm defines this cardiac cycle to have no dicrotic notch then continues the minima search on the next cardiac cycle.

A portion of each cardiac cycle, between the time of the systolic peak in the BP waveform and the time of the ensuing R wave in the ECG signal, is defined as the search window for possible dicrotic notch (minima) points. A simple algorithm, which locates the maximum in the amplitude of the blood pressure signal contained between the two

consecutive R waves of the ECG, is used to approximate the systolic peak location. All minima in the search window are found by locating all zero crossings of the DyWT then determining the minimum between consecutive zero crossings. Once all of the cardiac cycles of one DyWT scale have been found, the cardiac cycles in the next DyWT scale are examined for minima.

Once all of the available minima have been found for all cardiac cycles in all of the DyWT scales, the sample locations of the minima are compared between dyadic scales. For a given cardiac cycle, the algorithm will locate all minima which occur within a neighborhood of ± 50 milliseconds (msec) across consecutive dyadic scales. This neighborhood is evaluated in terms of sample numbers and for a sample rate of 180 Hz, ± 50 msec becomes ± 9 data samples and for a sample rate of 360 Hz, ± 50 msec becomes ± 18 data samples. If there are minima that exist across dyadic scales within the given neighborhood, the sample number of the minima *of the higher scale* is retained. All minima which do not exist within ± 50 msec between consecutive dyadic scales are eliminated. The surviving minima are the sample locations of all *possible* dicrotic notches for all of the cardiac cycles in the data file stored in computer memory.

The dicrotic notch is defined as the first minima in each cardiac cycle which exceeds a threshold. The threshold is equal to 65% of the local minimum amplitude of the DyWT (of the highest scale) defined within the search window for that particular cardiac cycle. Once the dicrotic notch is found for a given cardiac cycle, then the next cycle is evaluated. The *temporal* locations of the dicrotic notches are obtained directly from the sample numbers in terms of the sample rate in which the data was recorded.

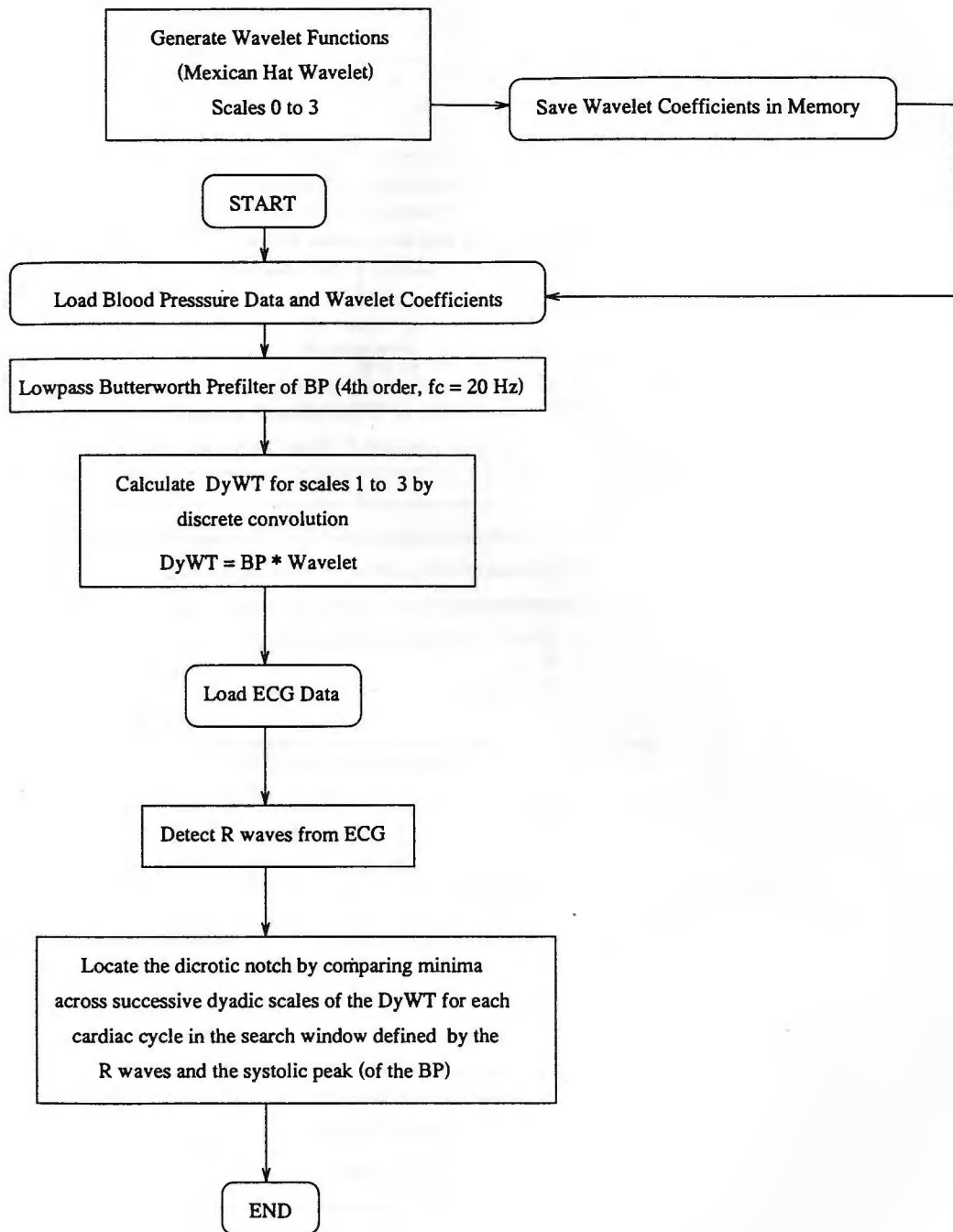


Figure 3.2 Block diagram of the DyWT dicrotic notch detection algorithm.

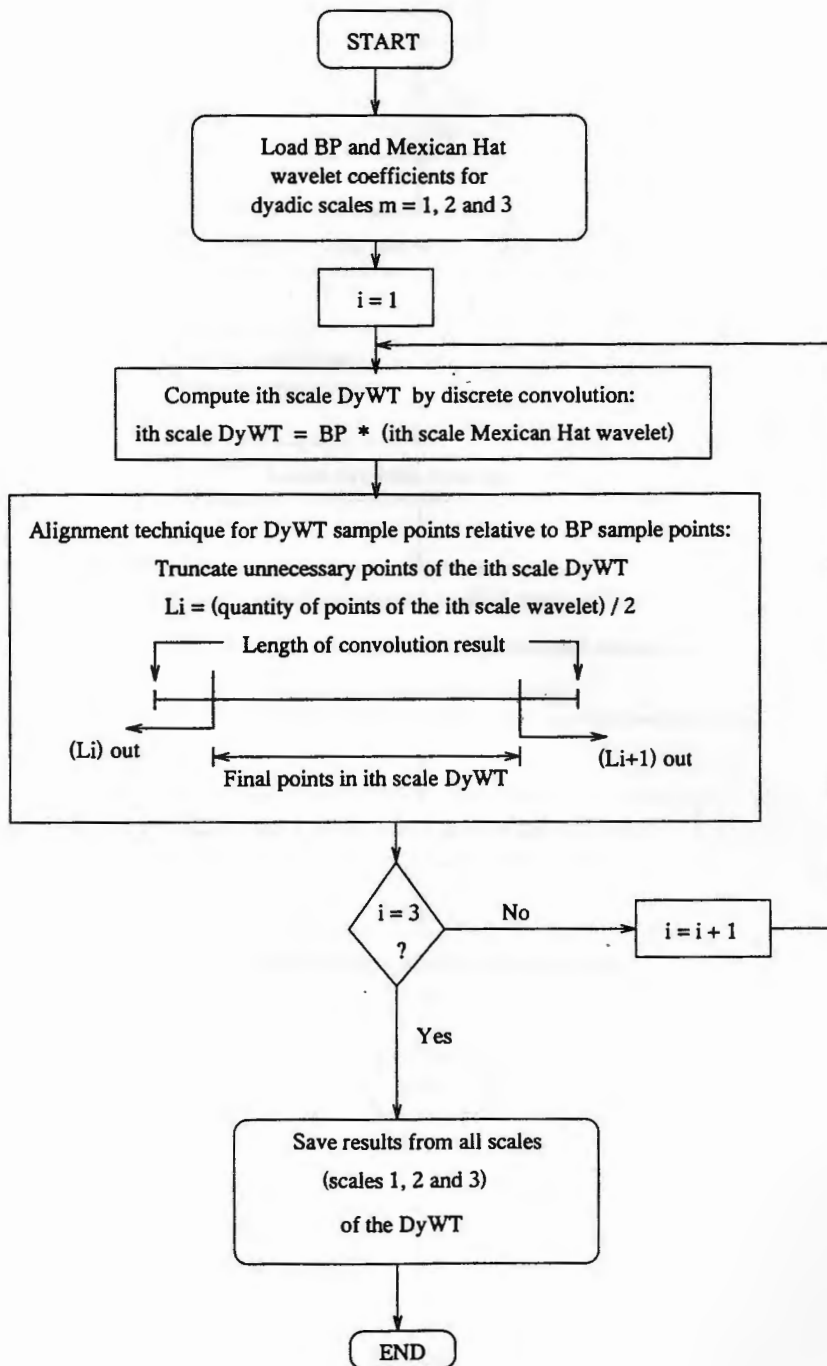


Figure 3.3 Flow chart of the DyWT discrete convolution calculation procedure.

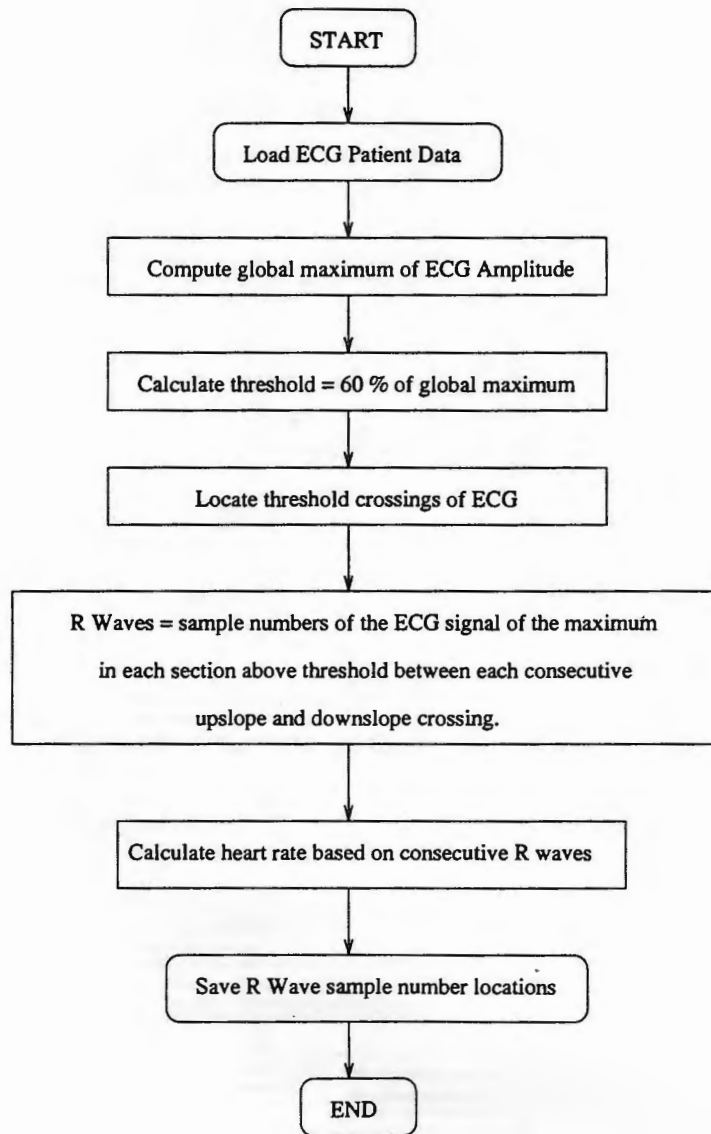


Figure 3.4 Flow chart of the R wave detection algorithm.

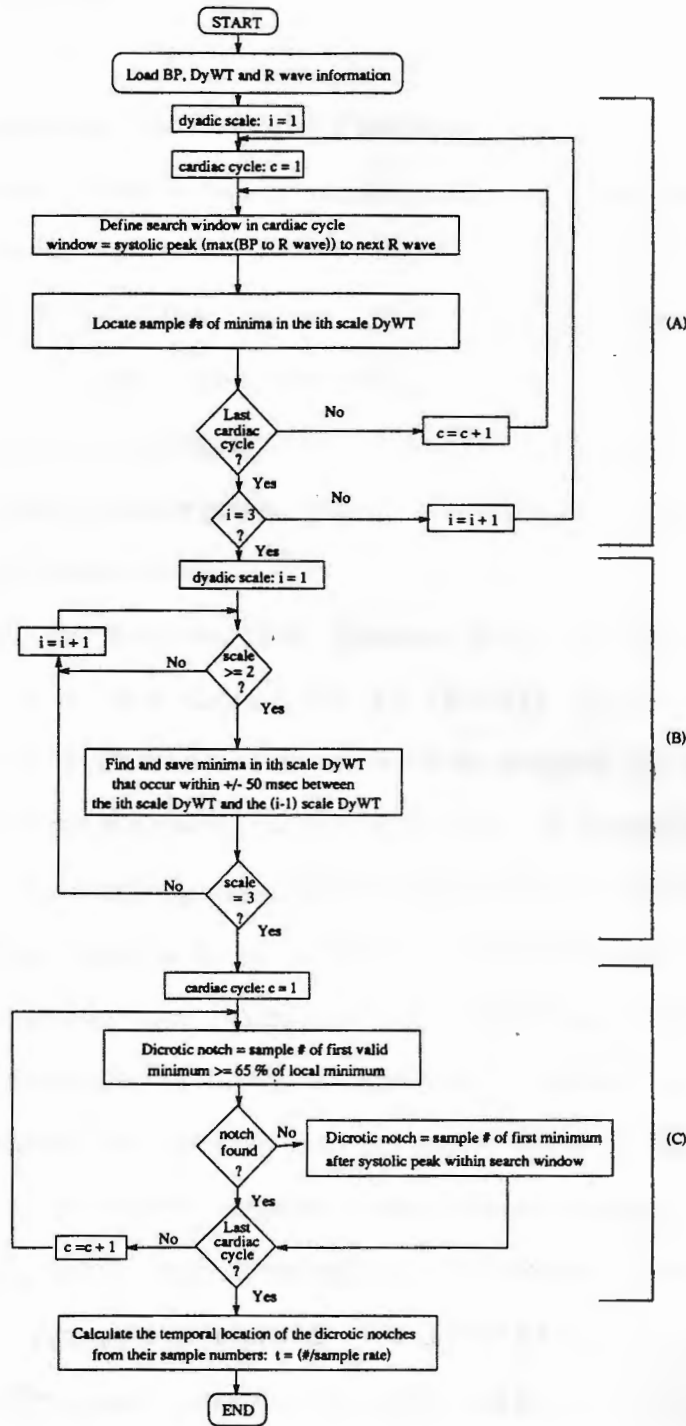


Figure 3.5 Flow chart of the DyWT based dicotic notch detection algorithm.

3.3 Rationale

3.3.1 Selection of the Wavelet Function

Multiresolution analysis can be obtained using the dyadic wavelet transform from scaled and translated versions of a variety of mother wavelet functions $g(\frac{t-b}{a})$. The issue of wavelet function selection depends upon the particular application of the wavelet transform [61, 176-180]. This section discusses the rationale for selecting the Mexican Hat, the parameters defining the wavelet function equation and the process used to generate the wavelet sample points. The wavelet parameters include the shift and scaling factors, b and a , respectively.

Several wavelet functions, Haar, Shannon, Morlet, Mexican Hat, Meyer and the cubic spline are shown in figure 3.6a-f [31, 180-181]. Each of the wavelet functions oscillates in time and has no dc content. Both the temporal and spectral characteristics were considered when selecting the wavelet function. A wavelet function acts as both a time window and a filtering device when implemented into the wavelet transform. The wavelet function (referred to as 'wavelet') is of finite duration, thus, it is *part* of a continuous oscillating wave. In this regard, the wavelet acts as a finite duration window.

The continuous wavelet transform, equation (2.3), rewritten in equation (3.1), is the *correlation* between the signal $x(t)$ and the scaled version of the mother wavelet [30]. The correlation provides a measure of the similarity between two signals. Thus, wavelets having similar shape to the analysis signal correlate better and effectively slope changes in the signal are accentuated. The DyWT dirotic notch detection algorithm, presented in this research correlates the scaled versions of the mother wavelet with the filtered pressure signal. Since the dirotic notch can be a rather subtle slope change in the pressure signal, a higher correlation between the signal and the wavelet helps to

emphasize the notch area. Therefore, the Mexican Hat [31] was selected as the mother wavelet since it best approximated the shape of the pressure signal.

$$WT_x(b, a) = \frac{1}{\sqrt{|a|}} \int_{-\infty}^{+\infty} x(t) g^* \left(\frac{t-b}{a} \right) dt \quad (3.1)$$

The scale (a) parameter is used to control the temporal and spectral resolution of the mother wavelet as well as the dyadically scaled ($a = 2^m$) versions of the Mexican Hat wavelet chosen such that the main lobe of the scaled wavelets are narrower (in time) than the dicrotic notch. If the width of oscillation is larger, the wavelet will effectively pass right over the notch area; the correlation will be small and the notch frequency will not be resolved.

The corresponding spectral resolution of each of the scaled versions of the wavelet is observed in its Fourier transform. The magnitude of a wavelet's FT indicates its center frequency and bandwidth. Thus, the DyWT operation, from each dyadically scaled version of the wavelet, acts as a band pass filter on the data. The scaling operation is the mechanism by which the DyWT is adjusted to the duration of the transient being analyzed, which in this case is the dicrotic notch. As scale is increased the magnitude of the FT has a narrower bandwidth and a lower center frequency, as demonstrated in figure 2.3 for the cubic spline wavelet.

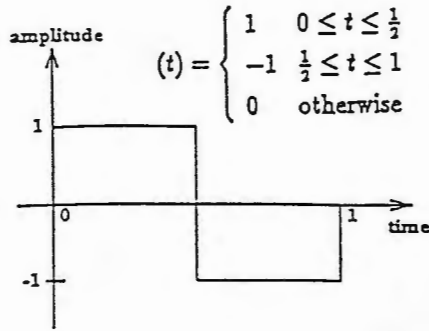
The center frequency (and bandwidth) of the scaled wavelets were chosen in coordination with the desired frequency filtering necessary to resolve the dicrotic notch from the pressure waveform. These three scales provided a wide and narrow enough spectral range for the appearance of the dicrotic notch for the MGH database arterial pressure signals tested. Dyadic scales were chosen to span the range of possible

frequencies in the blood pressure signal and to reduce the mathematical complexity of calculating a continuous range of scales.

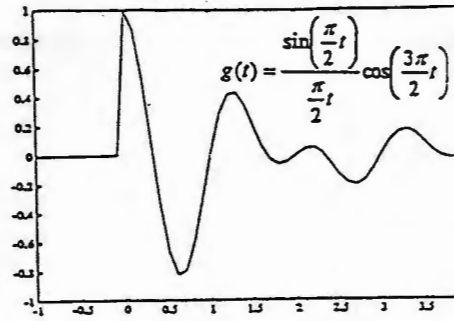
The FT magnitude of the scaled versions of the Mexican Hat wavelet showed no dc components. The presence of a dc component would not affect the performance of the wavelet for diastolic notch detection. However, it would affect signal reconstruction, which is not important for diastolic notch detection. The constraint on the choice of wavelet regarding dc content can therefore be relaxed with the tradeoff that the DyWT is no longer a one to one representation, rather the wavelet decomposition does not form a complete and independent basis set for reconstructing the original signal from the transform domain.

The number of non-zero sample points for each scaled wavelet, generated with a 180 Hz sample frequency, are 21, 43, and 85 for the first, second and third scales, respectively. For a sample rate of 360 Hz, there are 43, 87, and 171 non zero wavelet sample points for the first, second and third scales, respectively. A zero value implemented on the computer has been defined as less than 10^{-10} . The relatively small scales produces somewhat sharp (impulsive) wavelet shape, symmetric about the origin, which quickly tends to zero. As the scale is increased dyadically, the wavelet is expanded in time (by 2), with twice as many non-zero points and the frequency, observed in the FT magnitude, is compressed by $\frac{1}{2}$. Figure 3.7 shows the three scales of the Mexican Hat wavelet function, generated with a sample rate of 360 Hz.

Haar Wavelet

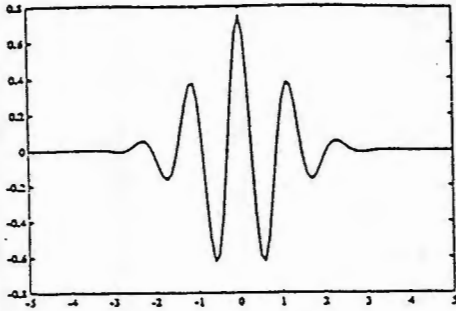


Shannon Wavelet

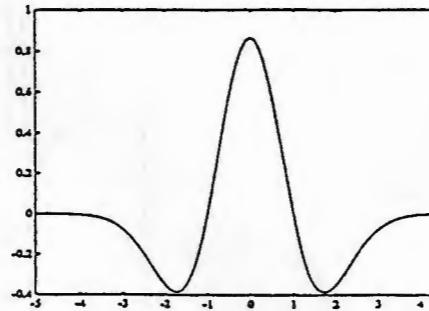


Morlet Wavelet

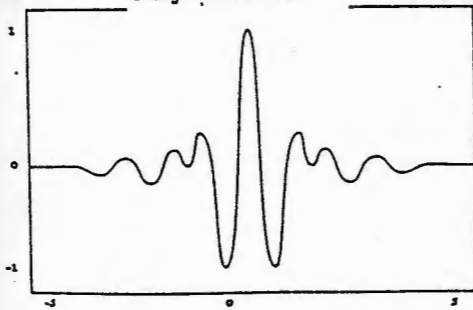
$$g(t) = \pi^{1/4} \left(e^{-i\pi t^2} - e^{-i\pi/4} \right) e^{-\pi/2 t^2}$$



Mexican Hat Wavelet



Meyer Wavelet



Spline Wavelet

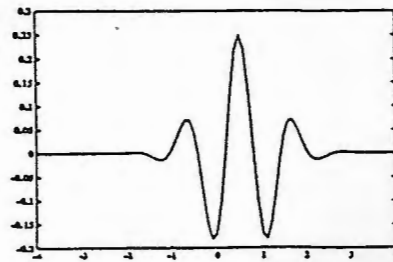


Figure 3.6 Graphical representation of the wavelet functions: (a) Haar; (b) Shannon; (c) Morlet; (d) Mexican Hat; (e) Meyer; and (f) the cubic spline.

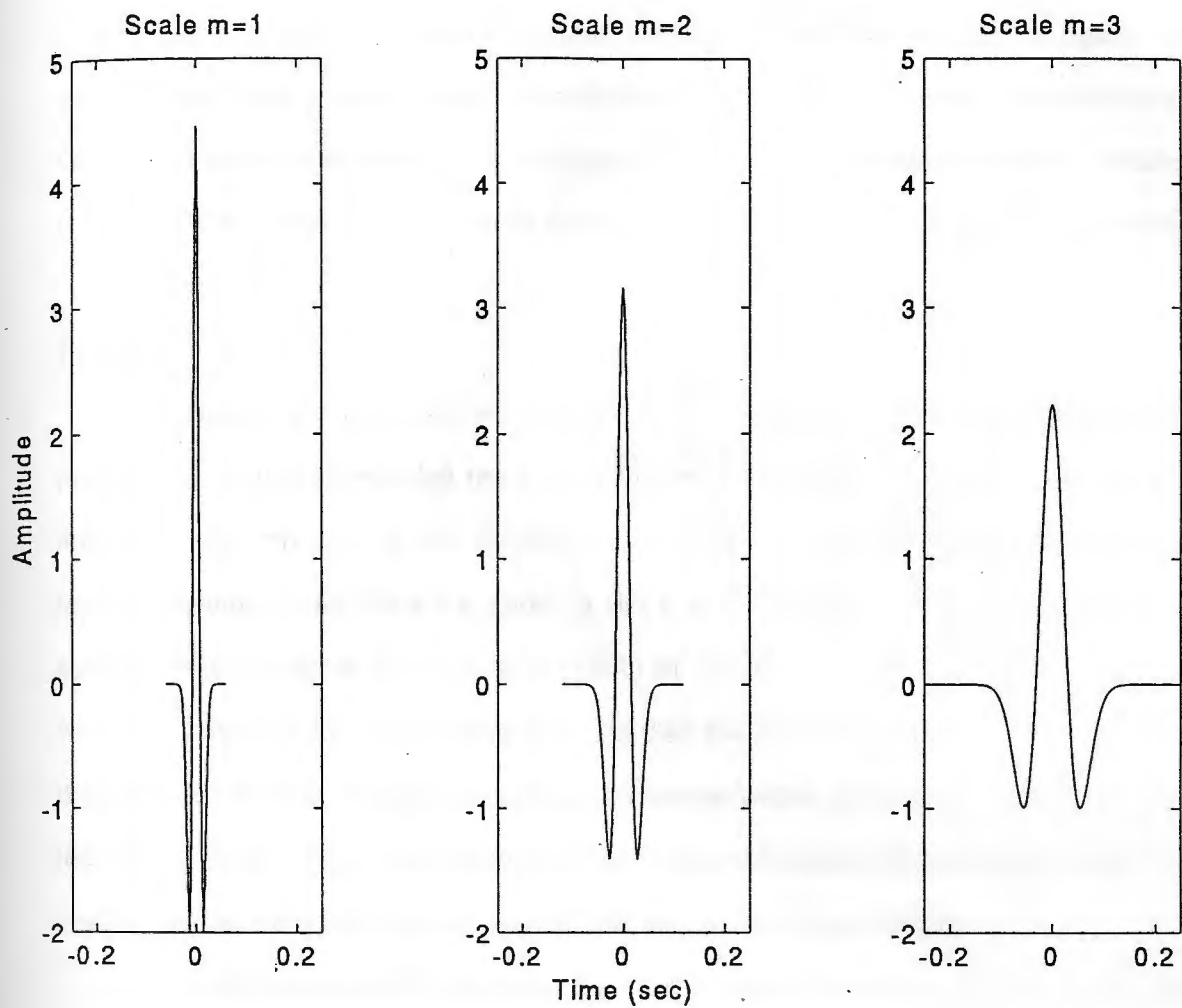


Figure 3.7 Three dyadic scales of the Mexican Hat wavelet function, generated with a sample rate of 360 Hz.

3.3.2 Selection of Algorithm Procedures

The dicrotic notch detection algorithm, outlined in the block diagram in figure 3.2, prefilters the input pressure signal. The filtered signal is then convolved with the scaled versions of the mother wavelet and the algorithm proceeds to locate the dicrotic notches from the DyWT results. The rationale for each of the steps in this procedure is presented.

Prefilter

The original work of the wavelet feasibility test were performed without any prefiltering. It was shown that the dyadic wavelet could be used to resolve the dicrotic notch for relatively normal and noiseless waveforms. Further testing of the algorithm involved adding white Gaussian noise to the pressure signal. The algorithm was not accurate below a signal to noise ratio (SNR) of 30 dB. The DyWT detection scheme with the prefiltered signal was more accurate than the notch detection algorithm without the prefilter for noisy signals containing oscillations within the same frequency band of the dicrotic notch. Also, the detection of the temporal location of the dicrotic notch was nearly identical on highly damped signals with and without the prefilter.

A 4th order Butterworth low pass filter with a cutoff frequency (f_c) of 20 Hz was added from which the algorithm attained better noise performance. A Butterworth filter was selected because it has a magnitude response that is maximally flat in the pass band and has a smooth but not exceedingly steep roll off [67]. The pole zero plot of this Butterworth filter is shown in figure 3.8. The filter's frequency response, magnitude and phase are shown in figure 3.9a and b, respectively, generated with a sample rate of 180 Hz. The zero phase Butterworth filter was implemented in the detection algorithm using a digital filtering process.

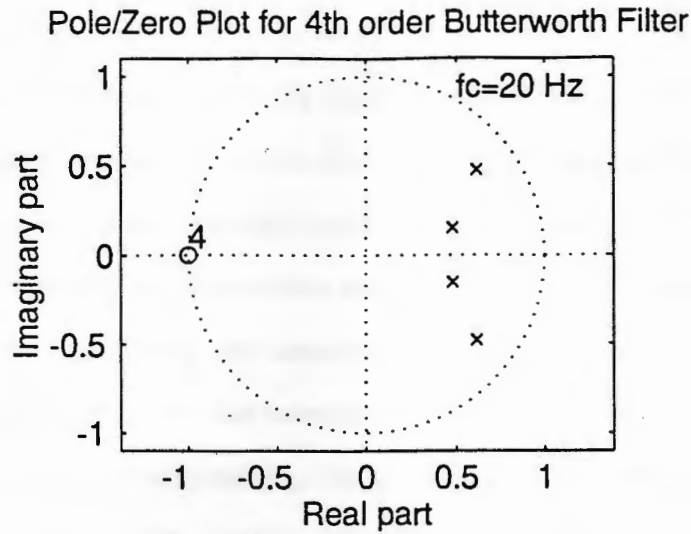


Figure 3.8 Pole/zero plot of the 4th order Butterworth prefilter with $f_c=20$ Hz.

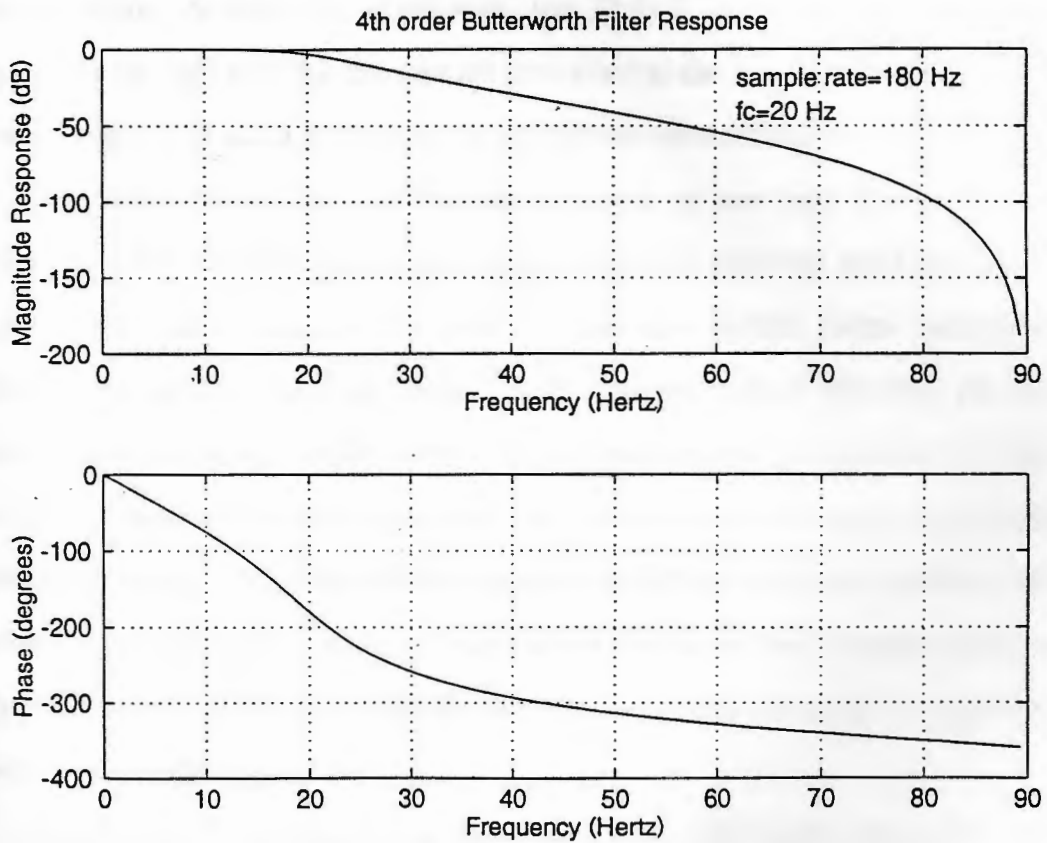


Figure 3.9 (a) Magnitude response; (b) Phase response of the 4th order Butterworth prefilter with cutoff frequency of 20 Hz, generated with a sample rate of 180 Hz.

Calculation of the DyWT

The DyWT can be evaluated either by discrete convolution or with the use of the FFT. The convolution technique involves the complex discrete convolution of the BP and the wavelet function. Thus, the total number of calculations involves additions and multiplies for a total number of output points equal to the sum of the number of points in the BP and the wavelet. Using the convolution property of the FT, the temporal convolution of the BP signal with the wavelet can be evaluated in the spectral domain with an equivalent spectral multiplication. In general, the FFT method would allow a more efficient computation of the DyWT, especially when the scale parameter is large and the wavelet function is compressed in frequency. Thus, there are fewer multiplications involved in computing the DyWT in terms of the frequency representation than with the convolution procedure in the time domain. Either method would benefit from the fact that both the BP and the wavelet function are real valued.

Each scaled wavelet has an increasing number of non-zero sample points with increasing scale. Since the number of wavelet samples is relatively small for each of the three dyadic scales calculated (at most 171 non-zero sample points comprising the Mexican Hat wavelet at dyadic scale 3 with a sample rate of 360 Hz), the discrete convolution method was implemented. The discrete convolution operation between the wavelet function and the BP signal results in a data string containing a total number of data points equal to the number of data points in the BP signal plus the number of sample points (L) of the wavelet function. Thus, the result is longer than necessary as shown in figure 3.10 for MGH file003, where the number of points in the signal is larger than the number of wavelet function samples.

To access the correct portion of the output of ($L + \text{BP signal}$) data points for each dyadic scale, the first and last ($L/4$) data points of the DyWT are removed and the remaining points correspond to the actual DyWT result at the proper time. L is the

number of wavelet sample points generated at a particular dyadic scale; and L is increasingly larger as the dyadic scale is increased. The number of data points which should be discarded in the wavelet transform results after the convolution has been calculated and is equal to the (number of points of the wavelet function -1), (the -1 is due to the Matlab convolution process). These points are eliminated from the result symmetrically on each end of the convolution result (half on each side) as indicated in the flow chart in figure 3.3.

The end effects of the discrete convolution are observed in several DyWT results due to the abrupt cessation of data and the non-causal wavelet, as observed in figure 3.10. The results show spikes at the ends of the DyWT, especially for scales 1 and 2. Detection of the dicrotic notch is not affected by these spikes since the algorithm does not take a *global* minimum of the data for threshold purposes but rather a *local* minimum between consecutive R waves. These spikes have been discarded in the plots of the DyWT algorithm performance.

ECG R wave Detection Algorithm

The R wave is used by the dicrotic notch detection algorithm to locate the start and end of each cardiac cycle. The cardiac cycle is used as reference in determining the search window for minima in the DyWT as possible dicrotic notch locations which will be used for comparison across dyadic scales. The R wave detection algorithm has been modified from that proposed by Elghazzawi et al [175] finding peaks above 60% of a global maximum threshold. Where this algorithm fails, the ECG has been manually observed and the locations of the R waves predetermined for a patient file. Although there exists a robust method of detecting the R wave using the wavelet transform [82], it was not necessary to involve a more developed detection algorithm.

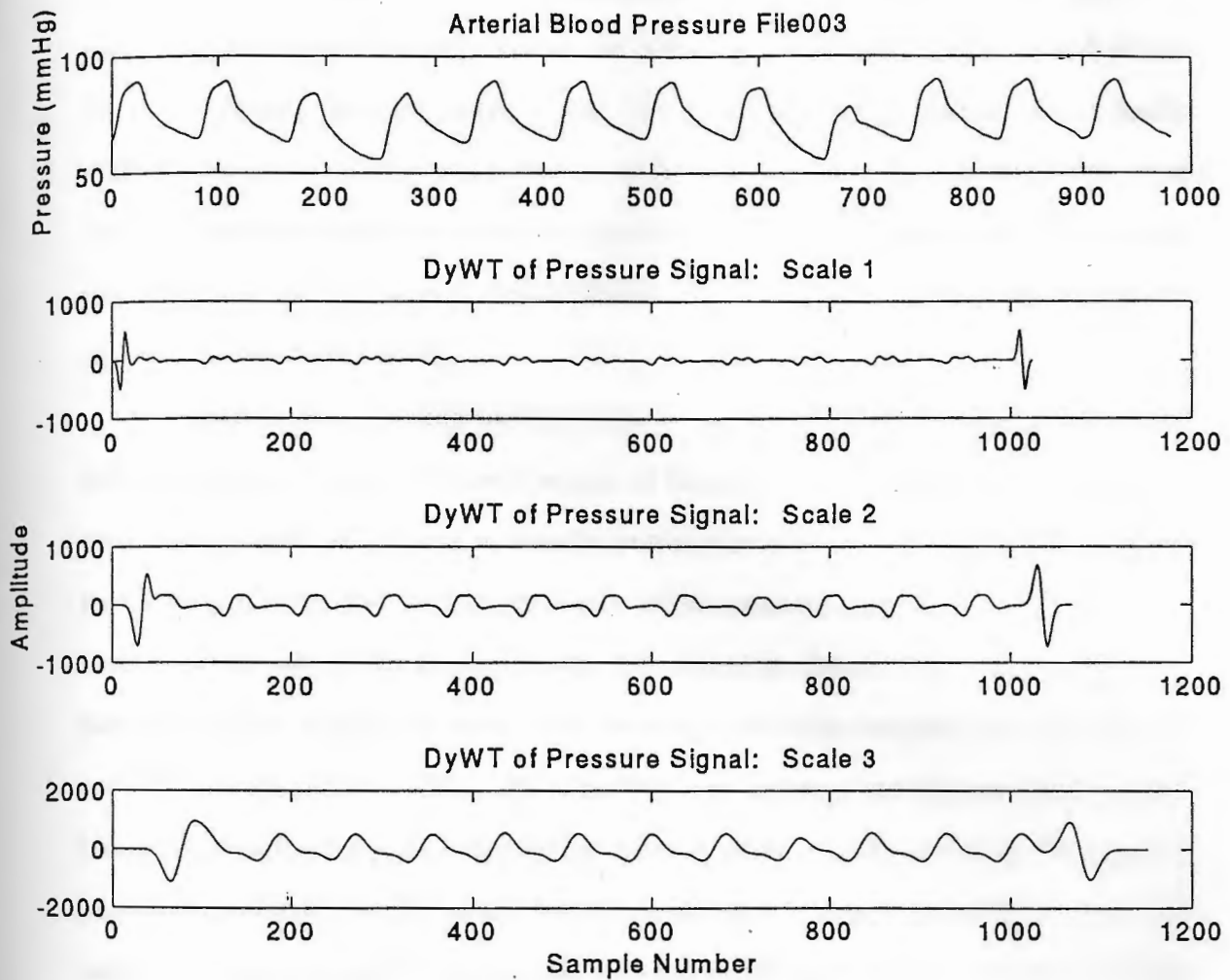


Figure 3.10 (a) Radial pressure waveform MGH file003, plotted as pressure (mmHg) versus sample number; (b-d) results of the discrete convolution calculation of the dyadic wavelet transform for scales 1, 2 and 3, respectively, plotted as amplitude versus sample number.

Search Windows

Two types of search windows are discussed. The first partitions a time segment of each cardiac cycle to focus the search for minima in the DyWT. The second search "window" defines the time range of data for comparison of the minima across dyadic scales of the DyWT. The eventual location of the dicrotic notch for a given cardiac cycle will be a minimum which lies within the search window of the cardiac cycle (first search window), and exists within a neighborhood of ± 50 msec samples (second search window) across dyadic scales.

A limited portion of each cardiac cycle is searched for the dicrotic notch. The dicrotic notch will occur between the time of maximum left ventricle pressure (systolic peak) and the start of the next ventricular contraction (the next R wave). This window length was chosen also to accommodate blood pressure waveforms recorded from various points along the arterial system (as shown in figure 1.3). The further the pressure reading is from the aortic root, the longer the delay between the systolic peak and the dicrotic notch. Thus, the algorithm can examine waveforms from various locations including the aorta, radial artery, femoral artery or pedal locations. The systolic peak is relatively easy to detect and R wave information is readily available. A relatively simple algorithm is used to estimate the location of the peak systolic pressure for each cardiac cycle. The systolic peak algorithm locates a maximum in the blood pressure waveform between the times of consecutive R waves in the ECG signal.

Minima which occur in the DyWT within the search window for each cardiac cycle are compared across dyadic scales. Minima which exist within ± 50 msec between dyadic scales (± 9 data samples for sample frequency = 180 Hz and ± 18 data samples for sample frequency = 360 Hz) is retained while all other minima are discarded from the total set of minima found in the cardiac cycle search window. A first estimate of ± 5 data samples was used for the detection algorithm based on the algorithm for pitch

detection [98]. This range, tested on files recorded at a rate of 180 Hz, was found to be too small. Inspection of the resulting DyWT coefficients for several files indicated that ± 9 samples, (± 50 msec), would suffice. If increased much beyond this point, minima in the DyWT representing different transients would be compared across dyadic scales, and this is to be avoided.

Threshold Level

The dicrotic notch location for each cardiac cycle is defined as the first minima, that survived the DyWT comparison across dyadic scales, which has a magnitude greater than 65 % of the local minimum amplitude of the DyWT. The local amplitude of the DyWT is defined within the confines of the search window for that cardiac cycle. The threshold method was used such that the detection algorithm did not falsely select the minimum due to minor inflections in the curve located between the systolic peak and the actual dicrotic notch, (as was the case in figure 3.1d). The actual dicrotic notch is more transient and is represented in the DyWT as a minimum with a higher absolute amplitude. The threshold is set relatively low such that minima due to oscillatory noise in roughly the same frequency band as the dicrotic notch are not detected. A range of threshold levels were tested between 40 and 90 % and the threshold of 65 % seemed to provide the best results. If there are no minima which exist above the threshold, then the first minimum in the search window is selected. This occurs if the blood pressure waveform is very damped or the dicrotic notch is a very subtle inflection in the signal.

3.4 Previously Published Dicrotic Notch Detection Algorithms

3.4.1 Introduction

Various methods of dicrotic notch detection have been found in the literature [175, 182-185] and a summary of these detection techniques is presented. Predominantly, dicrotic notch detection techniques rely on slope characteristics of the pressure waveform [175, 183-184, 186]. Analysis using the derivative of the pressure signal is prone to error with noisy signals in which minor changes in slope are accentuated. Various computational methods were devised to obtain the signal's relative minimum and reduce the effects of oscillatory disturbances around the dicrotic notch detection area using amplitude threshold and slope bar curve fitting techniques [183, 185]. Also, the use of the ECG in defining a search window for locating the dicrotic notch in the arterial blood pressure signal has been published [175]. After the detection of the R-wave, a search for a zero crossing in the derivative waveform is initiated to find the location of the dicrotic notch. Although these methods may accommodate somewhat noisy signals, they are primarily not designed to characterize a wider range of irregular waveforms.

The five leading dicrotic notch detection algorithms [175, 182-185] which operate on the arterial pressure waveform were reprogrammed (in the Matlab environment). These algorithms, identified in table 3.1 by reference number, author and a brief description of the detection method, were tested on the MGH patient database files and their performance has been compared to the proposed dyadic wavelet based dicrotic notch detection algorithm.

Table 3.1**Previously Published Dicrotic Notch Detection Algorithms**

<u>Ref #</u>	<u>Author</u>	<u>Algorithm Description</u>
175	Elghazzawi	Slope analysis with ECG windowing of dicrotic notch search
182	Lee	Threshold peak then analysis of global (11 data samples) and local
(3		data samples) operators locate notch as "slope changes"
183	Jundanian	Iterative use of slope bars to detect systolic peak and dicrotic notch
184	Martino	Identify negative slope after intersection of pressure wave with delayed filtered wave
185	Kinias	Identify curvature zones of bent points using slope bar iteration

Several algorithms localize the systolic peak [182-183], ECG R wave [175] or other characteristics in the pressure signal derivative [185] to define the beginning of a search range for the dicrotic notch. Once a reference point in a cardiac cycle is defined, the algorithm selectively searches a given region of time in the signal for the slope changes corresponding to the dicrotic notch. A windowed search for the dicrotic notch is important because the dicrotic notch is a rather subtle point in the blood pressure waveform compared to the upstroke between end diastole and peak systole or the minimum (end diastole) or maximum (systolic peak) of the waveform which are more easily detected.

Dicrotic notch detection has also been applied to the derivative of the left ventricular pressure waveform [42], and to arterial flow [186], and valve closure resonance has been rendered from the second heart sound detected from non invasive phonocardiograms (PCGs) [43-47].

Attempting to define the mean cardiac cycle of aortic flow and pressure during steady state conditions, Burattini et al [186] designed an algorithm to single out the

dicrotic notch from aortic flow. This was used to separate consecutive cardiac cycles during steady state conditions. The algorithm is based on a double threshold method applied to previously digitized recordings of aortic flow and pressure. The location of the dicrotic notch is determined using a technique to find the minimum of the curve between two maxima defined above a certain threshold value, as outlined in the flow diagram in figure 3.11. The dicrotic notch follows a rapid flow declination from its maximum and precedes a relatively long period of virtually zero flow. Aortic flow assumes its minimal value at the tip of the dicrotic notch and thus the minima of the data sequence corresponds to the dicrotic notch.

Among other dicrotic notch detection schemes found in the literature, Smith and Craige [42] compared canine aortic pressure, left ventricular dP/dt and aortic surface vibrations. The comparison showed that the maximal negative spike of LV dP/dt seems to consistently occur just after the notch. Also, a US patented circuit design for detecting the dicrotic notch has been devised by Gebber and Welch in 1974 [187].

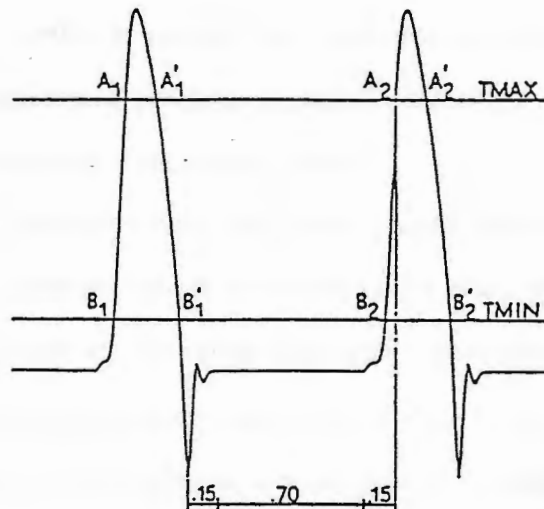


Figure 3.11 Dicrotic notch detection algorithm by Burratini displaying an arterial flow waveform superimposed with the double threshold detection method. [186].

3.4.2 Lee Algorithm

Lee et al [182] first locate a negative to positive change in the pressure derivative which is declared as the "foot" (end diastolic pressure (EDP)). After each foot, a maxima above a threshold equal to 85% of maximum pressure amplitude is declared as the systolic peak. The particular threshold of 85% was used in order to avoid recognizing an anacronic notch as the systolic peak.

First a global search for the dicrotic notch, from the systolic peak to 280 msec thereafter, identifies potential notch points. The global search starts with a pointer placed at the beginning of the search range. The global search involves weighting a group of 11 consecutive data samples, centered about the pointer. A summation of the weighted samples is calculated and the pointer is advanced until the end of the search range is reached. The sample location of the pointer which has the maximum sum is declared the potential dicrotic notch. A second a more localized search involving weighting a group of 3 consecutive data samples, within 34 msec about the potential notch point found with the global search, resolves the actual dicrotic notch. This process is repeated until the end of the search range is reached. The summation performed in the local search produces a second difference. The sample point with the maximum second difference is the dicrotic notch.

This particular algorithm works well in noisy environments but does not locate the dicrotic notch on arrhythmic beats or low pressure beats following higher amplitude beats due to the amplitude threshold governing the systolic peak detection. The algorithm has relatively good noise performance since it evaluates the first difference with a global operator (reducing higher frequency noise content).

3.4.3 Jundanian Algorithm

Jundanian et al [183] devised a slope analysis method to detect systolic peak and the "diastolic value" from arterial blood pressure waveforms. The diastolic value is determined by sliding a 40 msec slope bar along the pressure waveform where the derivative of the arterial pressure is negative, as outlined in figure 3.12. Results of testing this algorithm on the MGH database reveal that the diastolic value detection sometimes locates the dicrotic notch or locates end diastole or both. Due to the ambiguity of the definition of the "diastolic value", this algorithm tends to have a higher false positive rate, especially with noisy signals. This is a consequence of taking "diastolic value" to mean the dicrotic notch location and when the algorithm locates end diastole, it is considered as a false positive notch determination. However, the algorithm can track most low pressure beats (PVCs and arrhythmias) as well as adjacent higher pressure beats.

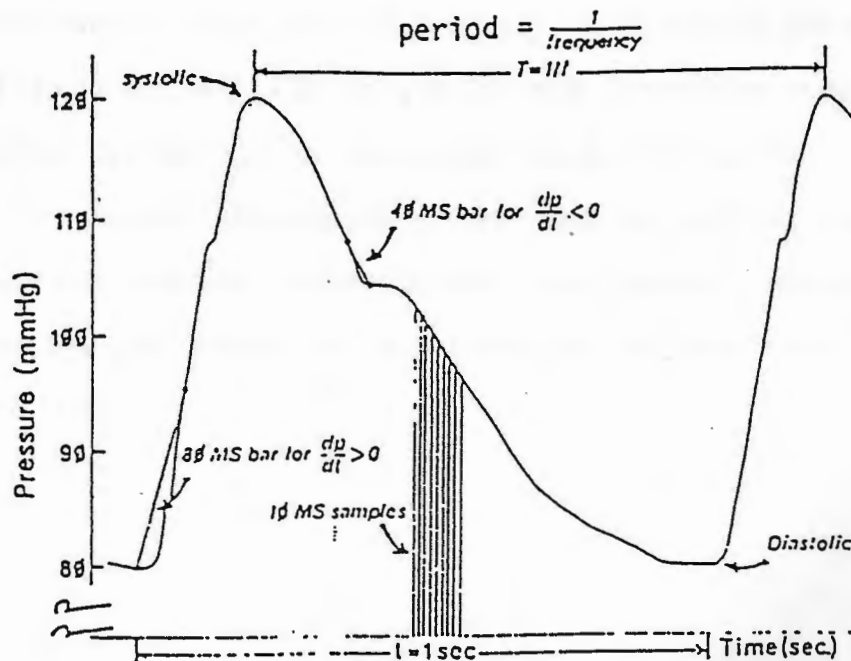


Figure 3.12 Dicrotic notch detection algorithm by Jundanian et al [183] displaying arterial pressure signal superimposed with proposed 40 msec slope bar detection method.

3.4.4 Martino Algorithm

A real time (80 msec) algorithm for detecting dicrotic notch and systolic upstroke developed by Martino and Risso [184] uses a first order digital (or analog) filter scheme with a cut-off frequency at 1.2 Hz (reprogrammed with a lowpass Butterworth filter design). The algorithm then identifies the intersections between the original and filtered (delayed) signals. The original pressure signal rises above the filtered signal during upstroke and falls below the filtered signal just prior to the dicrotic notch. Figure 3.13a shows the raw and filtered arterial pressure waveforms along with a step indicating systolic upstroke when the raw signal is greater in magnitude than the filtered signal. The upstroke determination is used to set a search window for the location of the dicrotic notch since the blood pressure signal falls below the filtered signal just prior to the notch. The detection of dicrotic notch is performed using the step waveform using four consecutive positive slopes in the first derivative, dP/dt . Figure 3.13b shows arterial blood pressure, pulse annotations indicating systolic upstroke and dicrotic notch, ECG and initial points of the QRS complex for three different heart rhythms. The tall pulses indicate upstroke and the short pulses indicate the locations of the dicrotic notches. This algorithm, although able to resolve most low amplitude beats (PVCs), it was typically early in locating the dicrotic notch in each cycle due to the generalization of four consecutive positive slopes and therefore incurred false positive and false negative rates above 25%.

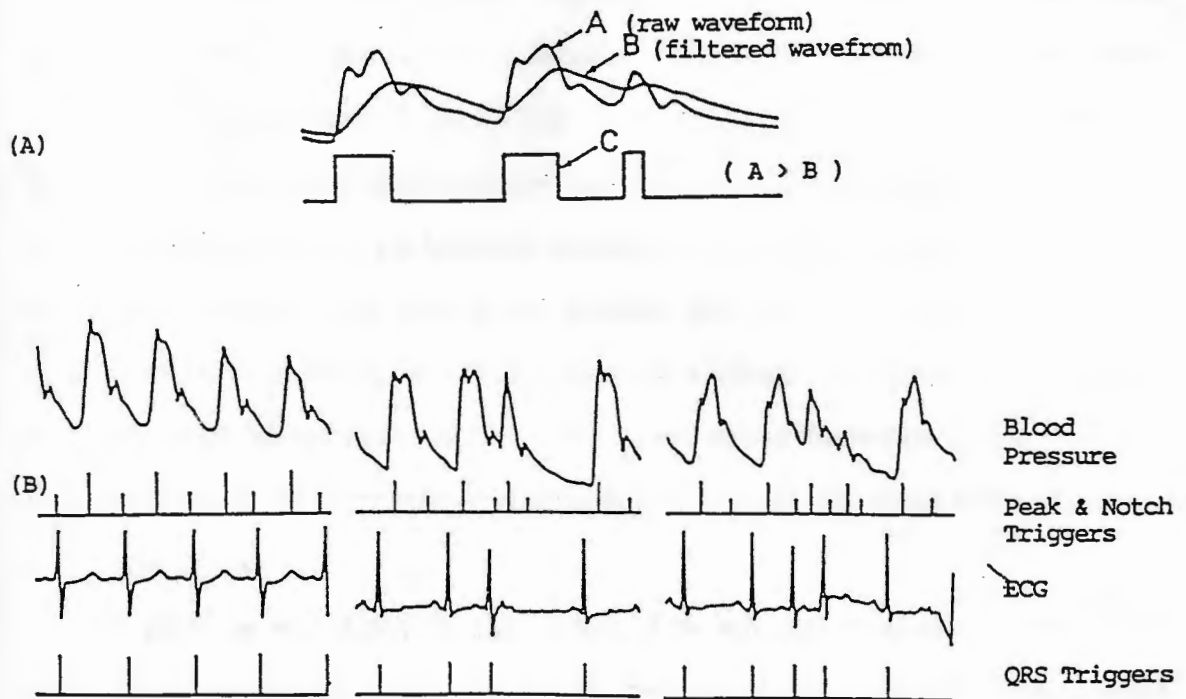


Figure 3.13 Dicrotic notch detection algorithm by Martino et al (a) Comparison of original and filtered waveforms; (b) blood pressure and ECG signals with estimated locations of systolic peaks and dicrotic notches [184].

3.4.5 Kinias Algorithm

Kinias et al [185] developed a bent point selection method to analyze a digitized blood pressure waveform filtered such that high frequency components (such as the dicrotic notch) are retained. The algorithm proceeds to detect the dicrotic notch based on an iterative bent point selection which identifies critical points where the curve changes in direction or concavity. The algorithm finds curvature zones, changes in the direction of the pressure derivative identified by an iterative "chord" approach, which uses successive chords with different lengths which slide along the pressure waveform, as shown in figure 3.14. When the difference of two successive chord lengths suggests a change in direction of the waveform, the length of the chord is reduced until the end of the iterative algorithm is reached. The final points obtained through this iterative procedure are referred to as bent points, or points indicating a change in curvature. Through a systematic and defined series of bent point combinations (upstroke, downstroke and inflection points), the bent point corresponding to the dicrotic notch for each cardiac cycle is determined.

The algorithm was shown by the authors to be accurate to within 11 msec in the placement of the dicrotic notch, but has not been as successful on the reprogrammed version tested on the MGH database files. The bent points were not technically on the maxima or minima and therefore the bent points corresponding to the dicrotic notch were offset from the actual notch area (the degree of offset is dependent on the chord length). Thus, the algorithm suffer high false positive and false negative rates. One author, H. A. Fozzard, was contacted to obtain the bent point selection algorithm code. However, the code which was written and optimized for a PDP-11 computer system was no longer available.

The BIOSPEAD program developed by Oppenheim et al [188] utilizes a combination of the bent point selection algorithm developed by Kinias and the negative spike of the

first derivative of aortic pressure to locate dicrotic notch in real time in noisy environments. The program employs parallel processing with variable filtering of the arterial pressure waveform to perform contour analysis using the first and second derivatives of the arterial pressure for extracting the location of systole, diastole and the dicrotic notch. The hybrid combination of the detection algorithms proved more reliable than either the Kinias or derivative algorithms alone.

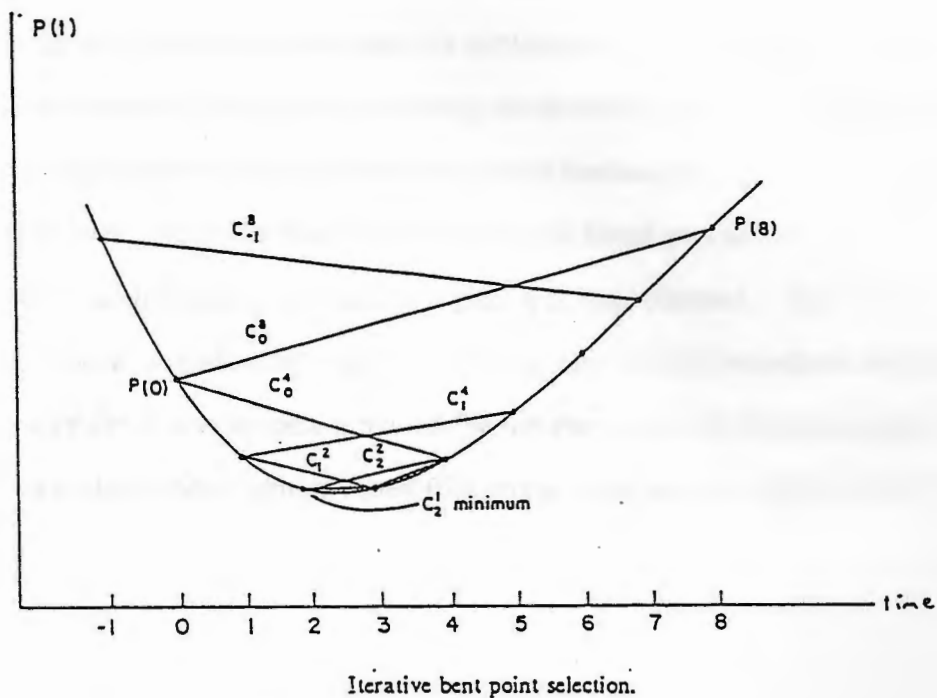


Figure 3.14 Dicrotic notch detection algorithm by Kinias et al displaying the dicrotic notch portion of an arterial pressure signal superimposed with proposed minima 'bent point' selection detection method [185].

3.4.6 Elghazzawi Algorithm

Elghazzawi et al [175] have developed a program to locate end diastole and the systolic peak. Within a period of time after the recognition of the ECG R wave, end diastole is declared as the last minimum in this time window by identifying the maximum amplitude of a negative to positive slope change for a given cardiac cycle. The peak systolic pressure is then identified as the last maximum in a defined time interval after the ECG R wave. The minima and maxima are determined from the slope of the arterial pressure waveform. This slope characterization of the critical points in the pressure waveform has been expanded to also locate the dicrotic notch.

The dicrotic notch algorithm was not published by Elghazzawi, but has been inferred from their method of signal analysis using the derivative of the pressure signal with the use of an appropriate search window within each cardiac cycle. In general, the algorithm performed well, except for the cases in which the blood pressure signal contained noise within the search window or when the signal was very damped. The R wave detection algorithm worked moderately well for relatively normal ECG waveform recordings. The locations of the R waves were provided for the dicrotic notch detection algorithm when the R wave detection algorithm failed (for proper comparison with the DyWT detection results).

Chapter 4

Simulations

4.1 Introduction

The methodology for generating a waveform test set and validating the performance of the DyWT based dicrotic notch detection algorithm and the five additional algorithms reprogrammed from the literature is demonstrated. All detection algorithms were tested on 3 test groups of MGH database files. The files were selected as an illustrative group of waveforms representative of a range of clinical and physiological conditions, including respiratory variations, ventricular tachycardias, catheter artifacts and other noise factors as well as on some noise free waveforms with normal sinus rhythms. The three test sets were generated to validate the detection algorithms and provide converging results indicative of algorithm performance. Performance criteria for determining the accuracy of the detection algorithms is defined and evaluated.

4.2 MGH Database of Clinical Recordings

The Massachusetts General Hospital (MGH) Database [22] contains 250 patient files each with roughly 1 hour worth of data, contained on a total of 10 CDROMs (25 patient files per CDROM). Selected epochs of each file numbered 1 to 200, illustrative of the file's physiological content, were stored on the UNIX mainframe at URI in Matlab format in the directory /bob3/mghdb. Due to limited computer storage space, only a

portion of each file was stored on the UNIX system, (there exists a tape backup which contains the entire archived data sets for CDROMs 1-6, all stored with a sample rate of 360 Hz). Files 1 to 50 were stored with a sample rate of 180 Hz; whereas files 51 to 200 were stored at 360 Hz, all with 12 bit accuracy.

Each patient file contains 8 channels of physiological data. Each patient file contains data for four physiological signals in column vector form as outlined in table 4.1:

Table 4.1

Column Vector Designation for the Physiological Signals in each MGH File

Column 1:	Data sample number counter starting at 1
Column 2 :	ECG trace (millivolts)
Column 3:	Arterial blood pressure (mmHg)
Column 4:	Central venous pressure (mmHg)

The files chosen for each of the three test sets for evaluating dicrotic notch algorithm performance are listed in tables 4.2 a, b and c, respectively according to the file number provided by the MGH database guide [22]. The three test sets were compiled to represent a range of different clinical conditions from nearly normal to irregular pathologies recorded from various points along the arterial system. The three test sets were compiled as: (A) 30 files, averaging 9 cardiac cycles per file (duplicate file numbers listed in table 4.21, indexed with lower case letters pertain to different time epochs of the same database file having slightly different waveshapes); (B) 50 files, with an average of 23 cardiac cycles per file, (includes all files in test set A, but with a larger number of cardiac cycles); and (C) 71 patient files averaging 22 cycles per file (includes all files in test sets A and B). Pressure recordings with circulatory assistance, although available in the database, were not included in the test sets due to the augmentation of

the arterial pressure waveform around the area of the dicrotic notch. Tables 4.2d lists the MGH filenames of all three test sets combined, according to their physiological description given in the MGH database patient guide [22] and by there observable waveform pattern.

Table 4.2 a

**List of 30 MGH Database Files used to Test Performance of Dicrotic Notch
Detection Algorithms (Test Set A)**

file003	file009	file021	file032	file089	file126a
file004	file010	file022	file033	file113b	file126b
file005	file015	file023	file034	file120a	file128
file007	file019	file027	file036	file120b	file136
file008	file020	file031	file046	file121	file137

Table 4.2 b

**List of 50 MGH Database Files used to Test Performance of Dicrotic Notch
Detection Algorithms (Test Set B)**

file001	file015	file035	file090	file121
file003	file016	file037	file091	file127
file005	file019	file039	file095	file130
file007	file020	file069	file101	file132
file009	file021	file076	file102	file139
file010	file023	file077	file108	file140
file011	file027	file082	file112	file141
file012	file029	file084	file113	file145
file013	file031	file088	file115	file146
file014	file034	file089	file117	file147

Table 4.2 c

List of 21 Additional MGH Database Files used to Test Performance of Dicrotic Notch Detection Algorithms (Test Set C)

file001	file023	file078	file115
file003	file027	file082	file116
file004	file029	file084	file117
file005	file030	file085	file120
file007	file031	file088	file121
file008	file032	file089	file126
file009	file033	file090	file127
file010	file034	file091	file130
file011	file035	file094	file132
file012	file036	file095	file137
file013	file037	file100	file138
file014	file039	file101	file139
file015	file046	file102	file140
file016	file060	file103	file141
file019	file069	file104	file145
file020	file071	file108	file146
file021	file076	file112	file147
file022	file077	file113	file149

Table 4.2d

**List of MGH Database Files used to Test Performance of Dicrotic Notch Detection
Algorithms (Test Sets A, B and C) According to Waveform Pathology**

Waveform Description	File Number Identification
Atrial fibrillation/flutter	019, 023, 069, 120, 126, 130, 139, 141, 145-147, 149
Axillary	032, 095, 104, 132
Baseline wander	001, 020, 094, 095, 100, 145
Brachial artery	086
Bradycardia	001, 034
Damped pressure	003, 020, 009, 013, 039, 084, 085, 088, 137, 146
Femoral artery	021, 084, 089
Hypertension	035, 085
Hypotension	108
Irregular pressures	021, 082, 090, 126, 140
Motion variation	005, 027, 039, 077, 078, 082, 089, 102, 108, 117, 112, 140
Noisy pressure signal	013, 039, 060, 076, 082, 084, 089, 108, 113
Normal sinus rhythm	007, 016, 029, 033, 034, 035, 036, 069, 091, 101, 104, 127, 130, 136, 138
Pedal	030
Pulsus paradoxus	003, 004, 009, 011, 019, 108, 141
Respiratory variation	008, 011, 012, 071, 077, 102
Tachycardia	003, 005, 009, 010, 020, 022, 027, 031, 046, 076, 077, 082, 085, 091, 100, 103, 108, 115, 116, 117, 121, 128, 136, 137

4.3 Performance Criteria

The original portions of the blood pressure waveforms, (which have been applied to the DyWT and each of the previously published dicrotic notch detection algorithms), were examined by Dr. W. Ohley, who annotated the dicrotic notch locations. Annotations were made on the original MGH file BP waveforms, prior to algorithm simulations.

The algorithm test results have been normalized in that each algorithm was evaluated for the same group of cardiac cycles for each patient file. The detection algorithms were considered to have successful detection of the dicrotic notch if they came within ± 33 msec of the actual dicrotic notch. The ± 33 msec range of acceptability for the dicrotic notch estimation (± 6 data samples for files with a sample frequency of 180 Hz, and ± 12 samples for files with a sample frequency of 360 Hz) was chosen since the dicrotic notch is represented in the majority of pressure waveforms as a curve or inflection. The minimum of the curve, or the initial change in curvature representing the start of aortic valve closure are possible correct solutions to estimating the dicrotic notch location. Therefore, a fair assessment for all of the algorithms tested, (the DyWT based algorithm and five others from the literature) was achieved with the ± 33 msec error range. Also, the error in the annotation is estimated to be ± 1 data samples, due to the system of notch location through the use of Matlab programming for user input. The dicrotic notch locations were actually recorded in terms of sample numbers which are easily converted to the time of occurrence, as shown in equation (4.1).

$$\text{time (seconds)} = \left(\frac{\text{sample number}}{\text{sample rate (Hz)}} \right) \quad (4.1)$$

The results were recorded in terms of true positives (TP), false positives (FP) and false negatives (FN). A computer spreadsheet algorithm [65] was designed for

determining the number of TP, FP and FN by comparing the results of the sample number locations of the detected dicrotic notches to the sample numbers of the annotations and for computing each algorithm's statistical performance. Statistical performance measured the percentage of sensitivity, positive productivity, false positive rate and false negative rate based on the TP, FP and FN. The equations used for these statistical indicators are shown in equations (4.2) to (4.5). TP (true positive) indicates that the algorithm correctly identified a dicrotic notch event; FP (false positive) indicates that a dicrotic notch event was estimated in a wrong location; and FN (false negative) indicates that a dicrotic notch event was not detected. Optimum performance would be signified by 100% sensitivity, 100% positive productivity, and 0% false positive and false negative rates.

$$\text{Sensitivity} = \frac{TP}{\# \text{ cardiac cycles}} * 100 (\%) \quad (4.2)$$

$$\text{Positive Productivity} = \frac{TP}{(TP + FP)} * 100 (\%) \quad (4.3)$$

$$\text{FP Rate} = \frac{FP}{\# \text{ cardiac cycles}} * 100 (\%) \quad (4.4)$$

$$\text{FN Rate} = \frac{FN}{\# \text{ cardiac cycles}} * 100 (\%) \quad (4.5)$$

4.4 Illustrative Examples of DyWT Dicrotic Notch Detection

This section presents the results of the performance of the DyWT based dicrotic notch detection algorithm for several problematic waveform types. For each example, the portion of the MGH blood pressure waveform is shown along with the corresponding DyWT decompositions for the three dyadic scales used in determining the temporal locations of the dicrotic notches. The annotated locations of the dicrotic notches, in the pressure versus time graph for each illustrated MGH file, is indicated by dotted vertical lines extending from the time axis to the upper graph boundary. The detected locations of the dicrotic notches are identified by solid vertical lines extending from the time axis to the upper graph boundary.

Also provided for each example is the graphical description of the application of the dicrotic notch detection results in determining the QS2 systolic time interval. The QS2 value calculated from the detected dicrotic notch is superimposed on the plot of the QS2 value derived from the regression equations given in equation (1.3), rewritten in equation (4.6). The QS2 value is calculated as the time between the detected R wave to the dicrotic notch. The regression equation results have been plotted using the HR (R to R interval) generated by the DyWT program. There is approximately a 20 msec difference between the QS2 derived from the regression equation and that evaluated using the algorithm's estimated dicrotic notch location. This difference is due to the fact that the QS2 calculated by regression equation is the duration from the Q wave of the ECG to the predicted location of the dicrotic notch. Whereas, the duration between the R wave of the ECG and the estimated dicrotic notch location is less than the regression result by an amount equal to the time difference between the Q and R waves, which is approximately 20 msec in most of the cases presented.

$$QS 2 = -0.020 * HR + 0.522 \quad (4.6)$$

The illustrative examples of signal irregularities include: a damped pressure signal (MGH file 009); pulsus alternans (MGH file 019); a sensor baseline variation (MGH file 077); a continuously changing HR (MGH file 023); noisy signal (MGH file 060); and a signal with irregular notching with major inflections in the waveform in the same frequency band as the dicrotic notch (MGH file 021).

Damped Pressure Signal: MGH file 009

Figure 4.1 demonstrates the effectiveness of the DyWT based dicrotic notch detection algorithm to locate minor fluctuations in the blood pressure waveform. The pressure signal is shown in figure 4.1 a and the 3 scales of the DyWT are shown in figures 4.1 c-d. The radial artery blood pressure signal of MGH file 009 is extremely damped and contains a small level of noise, some of which is in the same frequency band as the actual dicrotic notch. The waveform also exhibits a decreasing level of peak systolic pressure. Figure 4.1a provides the entire range of cardiac cycles examined in the QS2 calculation; whereas figure 4.1 e-h show a focused view of several of the cardiac cycles. Figure 4.2 compares the calculation of QS2 using dicrotic notch information, to the regression equation calculation, based on HR.

The performance of each of the dicrotic notch detection algorithms is presented in table 4.3, based on 48 cardiac cycles.

Table 4.3
Performance of Detection Algorithms on a Damped Pressure Signal
(MGH file 009)

Algorithm	Sensitivity (%)	Positive Productivity (%)	False Positive Rate (%)	False Negative Rate (%)
Wavelet	100	100	0	0
Lee	96	100	0	4
Jundanian	6	3	221	94
Martino	100	100	0	0
Kinias	90	90	18	18
Elghazzawi	15	15	85	85

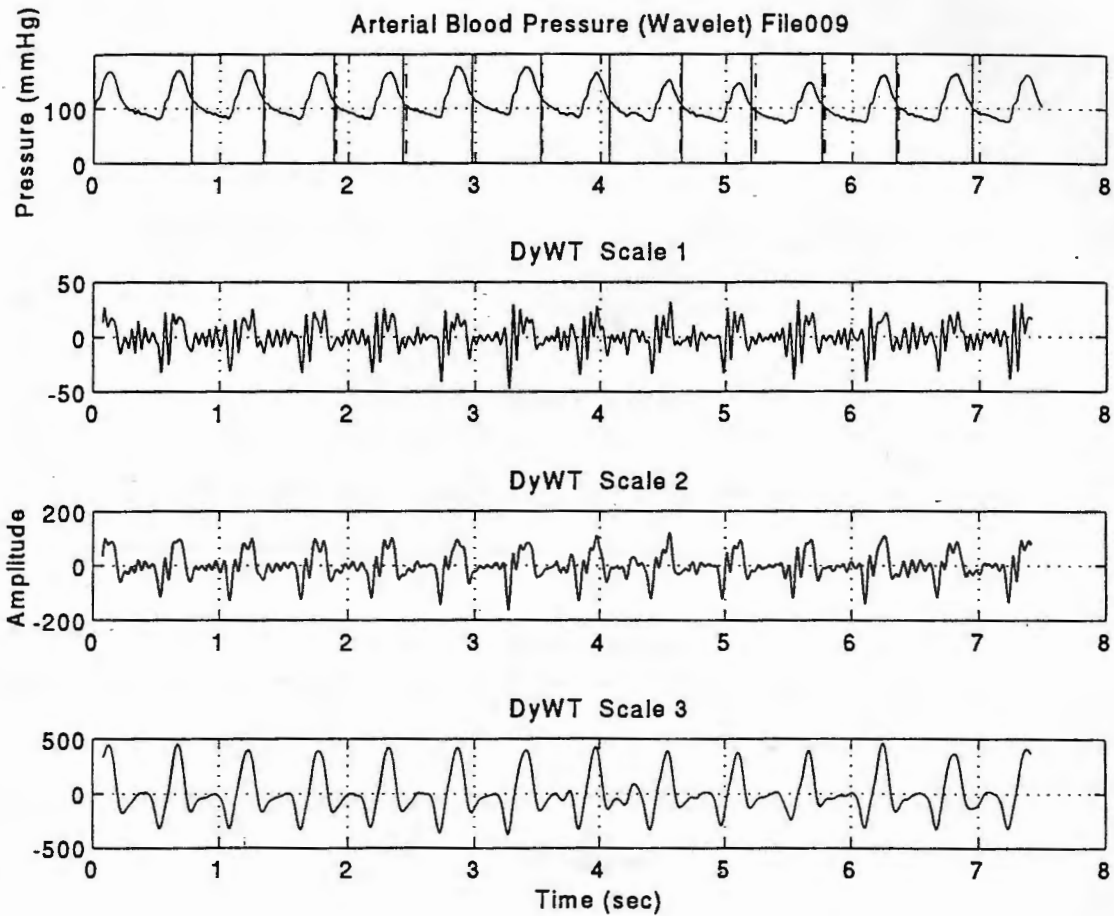


Figure 4.1 (a) MGH file 009 damped radial artery pressure signal; (b-d) DyWT decompositions for dyadic scales 1, 2 and 3, respectively. The dashed vertical lines indicate the annotated location of the dicrotic notch; whereas the solid vertical lines indicate the algorithm's estimation of the dicrotic notch locations.

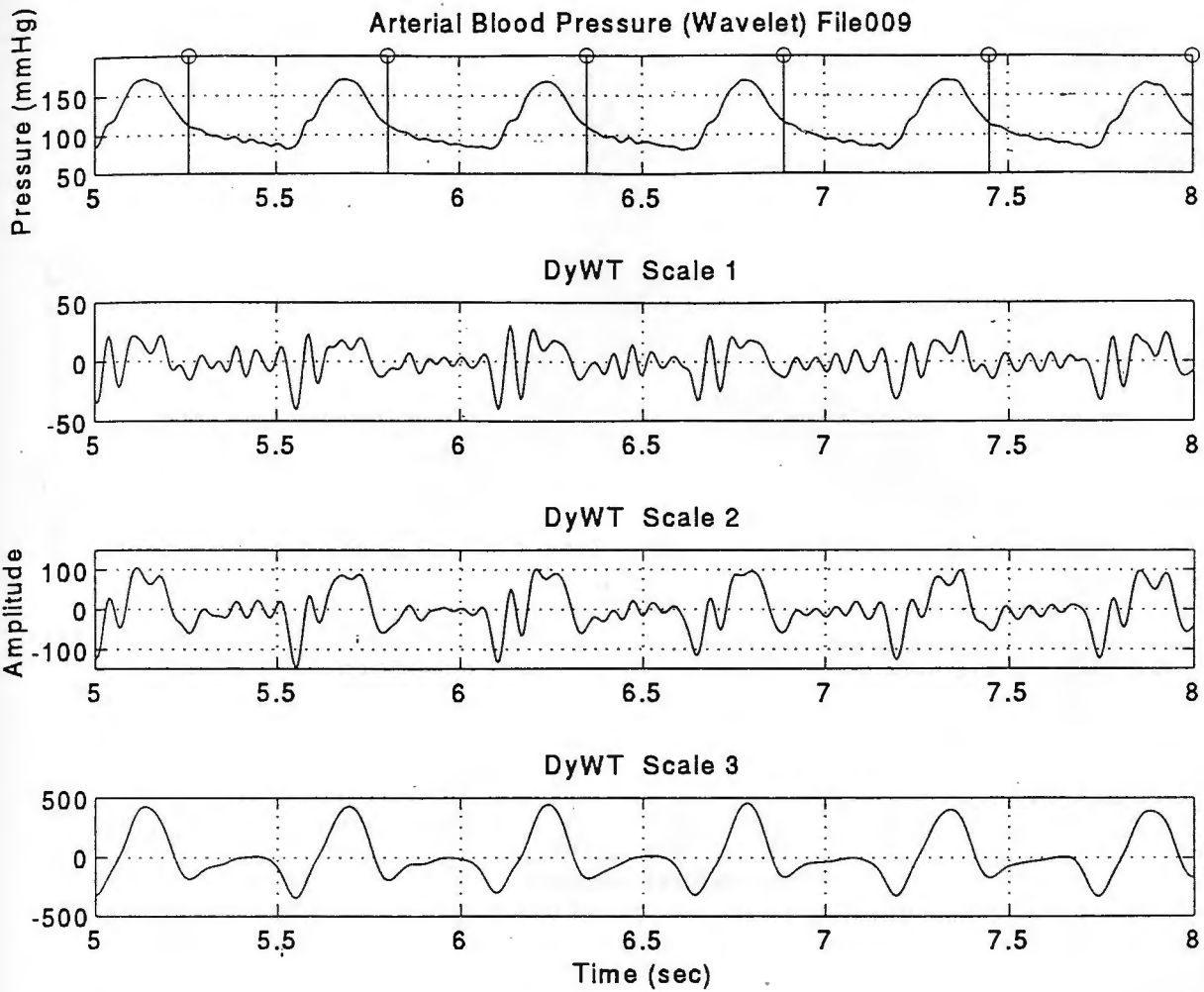


Figure 4.1 (e) Enlarged view of the MGH file 009 damped radial artery pressure signal; (f-h) DyWT decompositions for dyadic scales 1, 2 and 3, respectively. The dashed vertical lines indicate the annotated location of the dicrotic notch; whereas the solid vertical lines indicate the algorithm's estimation of the dicrotic notch locations.

QS2 Time Interval per Cardiac Cycle: File009.

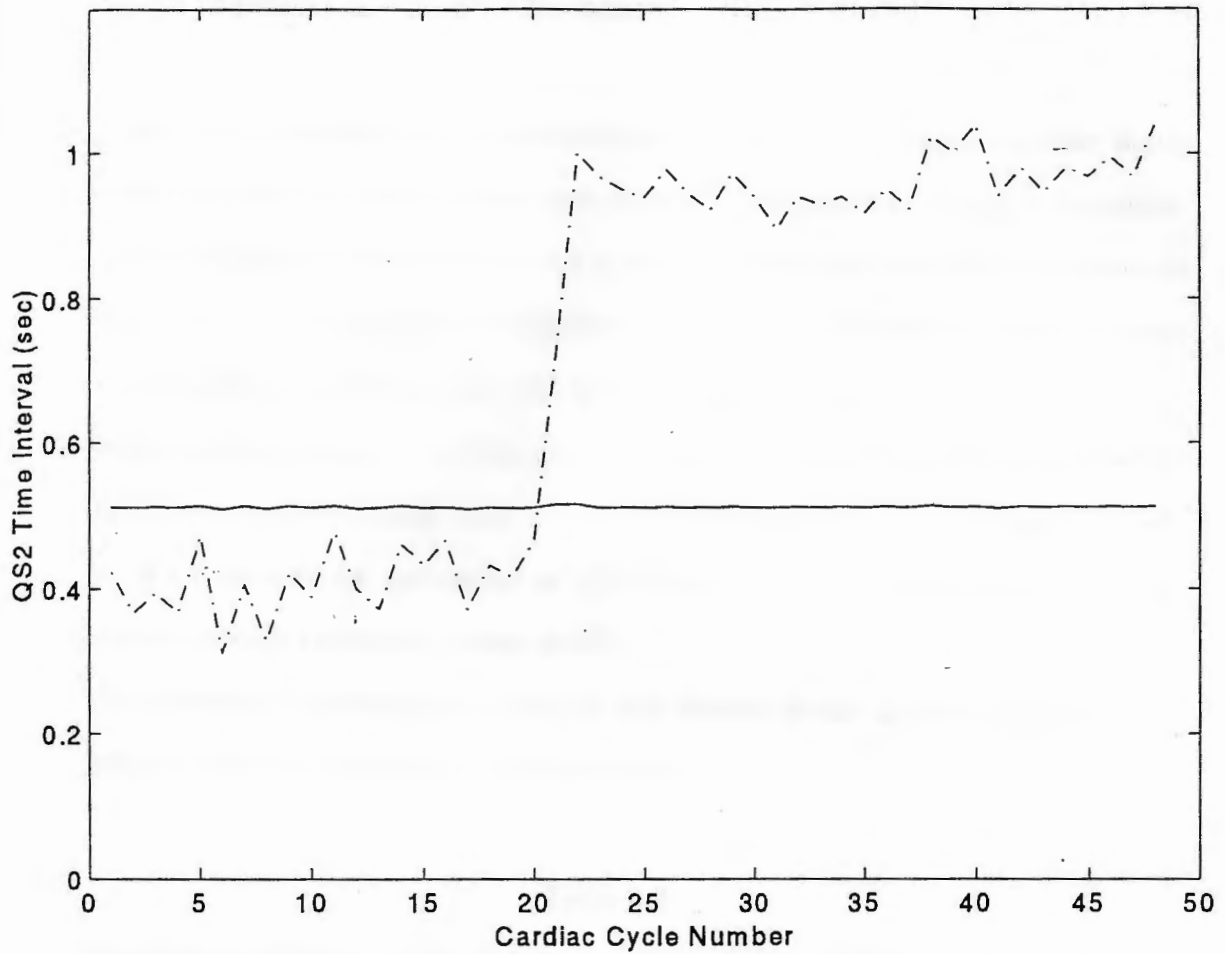


Figure 4.2 Comparison between the calculation of QS2 using the dicrotic notch information estimated by the detection algorithm, (dashed line), and using the regression equation based on HR (solid line), for MGH file 009.

Pressure Signal with Pulsus Alternans: MGH file 019

Figure 4.3 demonstrates the effectiveness of the DyWT based dicrotic notch detection algorithm to locate accommodate waveforms having peak amplitude variations. The pressure signal is shown in figure 4.3 a and the 3 scales of the DyWT are shown in figures 4.3 c-d. The radial artery blood pressure signal of MGH file 019 contains weak beats alternating with strong ones, but does not contain signal artifacts. Figure 4.3a provides the entire range of cardiac cycles examined in the QS2 calculation; whereas figure 4.3 e-h show a focused view of several of the cardiac cycles of figure 4.3 a-d. Figure 4.4 compares the calculation of QS2 using dicrotic notch information, to the regression equation calculation, based on HR.

The statistical performance of each of the dicrotic notch detection algorithms is presented in table 4.4, based on 35 cardiac cycles.

Table 4.4

Performance of Detection Algorithms on a Pressure Signal with Pulsus Alternans (MGH file 019)

Algorithm	Sensitivity (%)	Positive Productivity (%)	False Positive Rate (%)	False Negative Rate (%)
Wavelet	100	97	3	0
Lee	31	100	0	69
Jundanian	51	51	49	49
Martino	23	23	77	77
Kinias	29	29	71	71
Elghazzawi	83	88	11	17

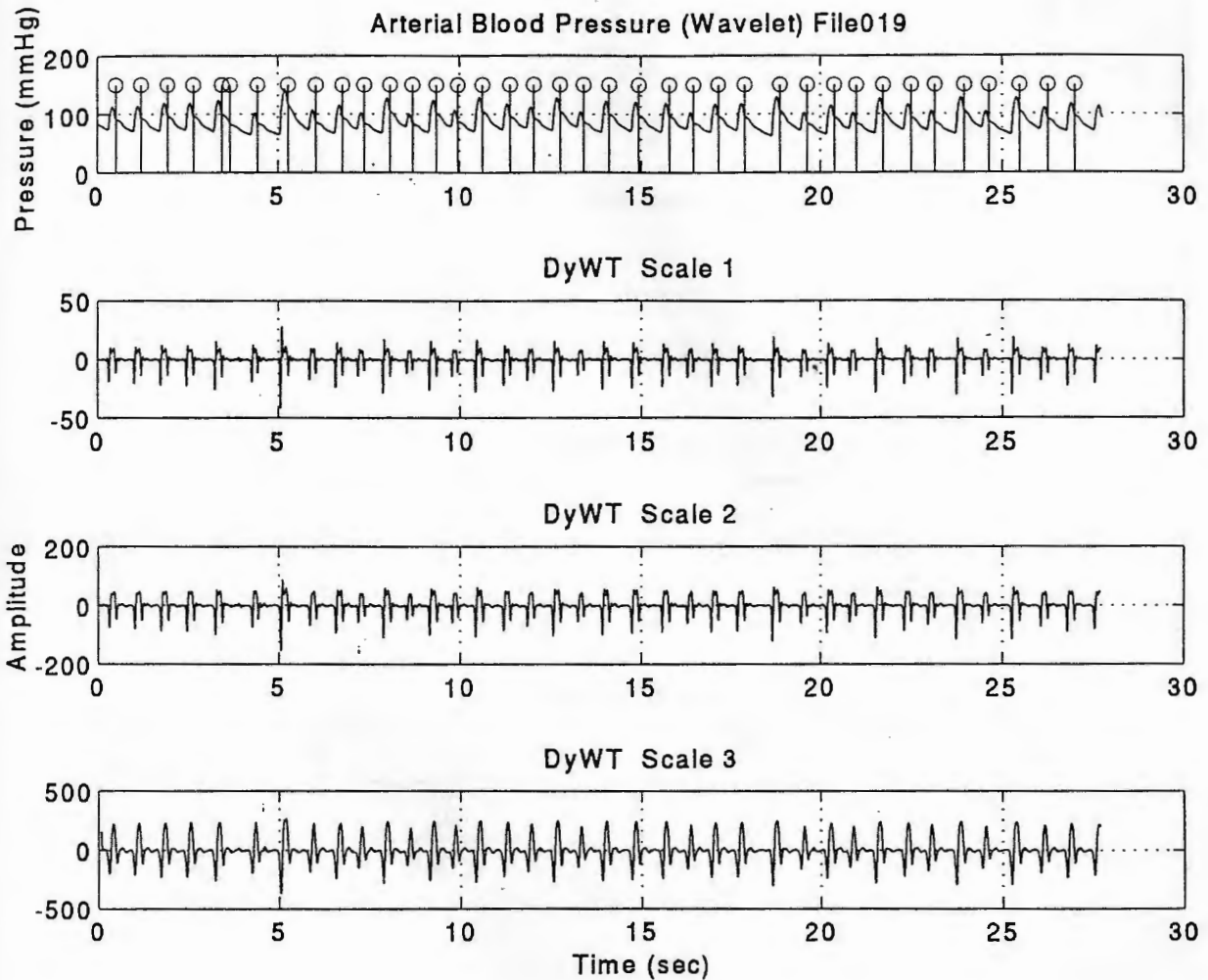


Figure 4.3 (a) MGH file 019 radial artery pressure signal containing pulsus alternans; (b-d) DyWT decompositions for dyadic scales 1, 2 and 3, respectively. The dashed vertical lines indicate the annotated location of the dicrotic notch; whereas the solid vertical lines indicate the algorithm's estimation of the dicrotic notch locations.

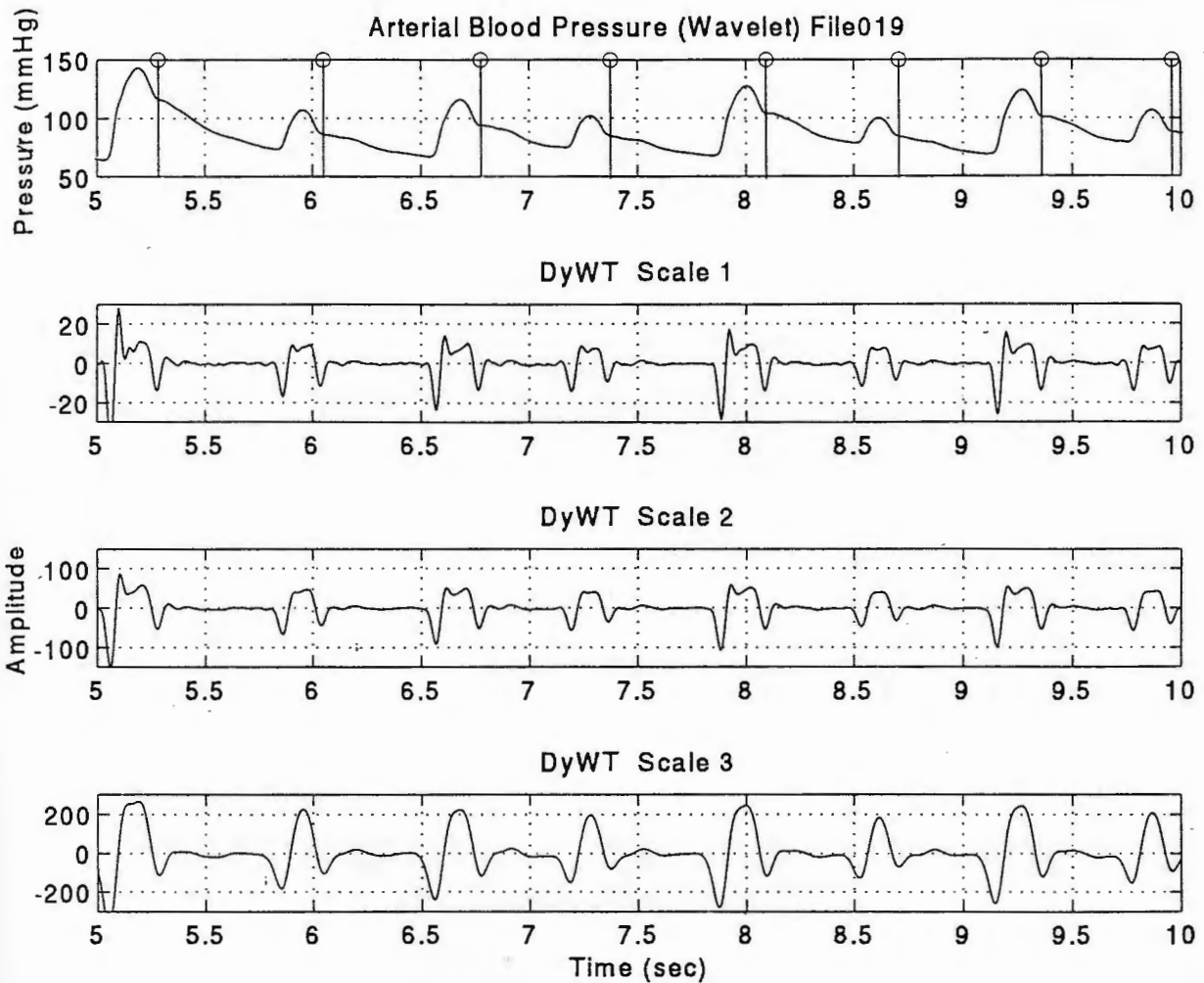


Figure 4.3 (e) Enlarged view of the MGH file 019 radial artery pressure signal containing pulsus alternans; (f-h) DyWT decompositions for dyadic scales 1, 2 and 3, respectively. The dashed vertical lines indicate the annotated location of the dicrotic notch; whereas the solid vertical lines indicate the algorithm's estimation of the dicrotic notch locations.

QS2 Time Interval per Cardiac Cycle: File019

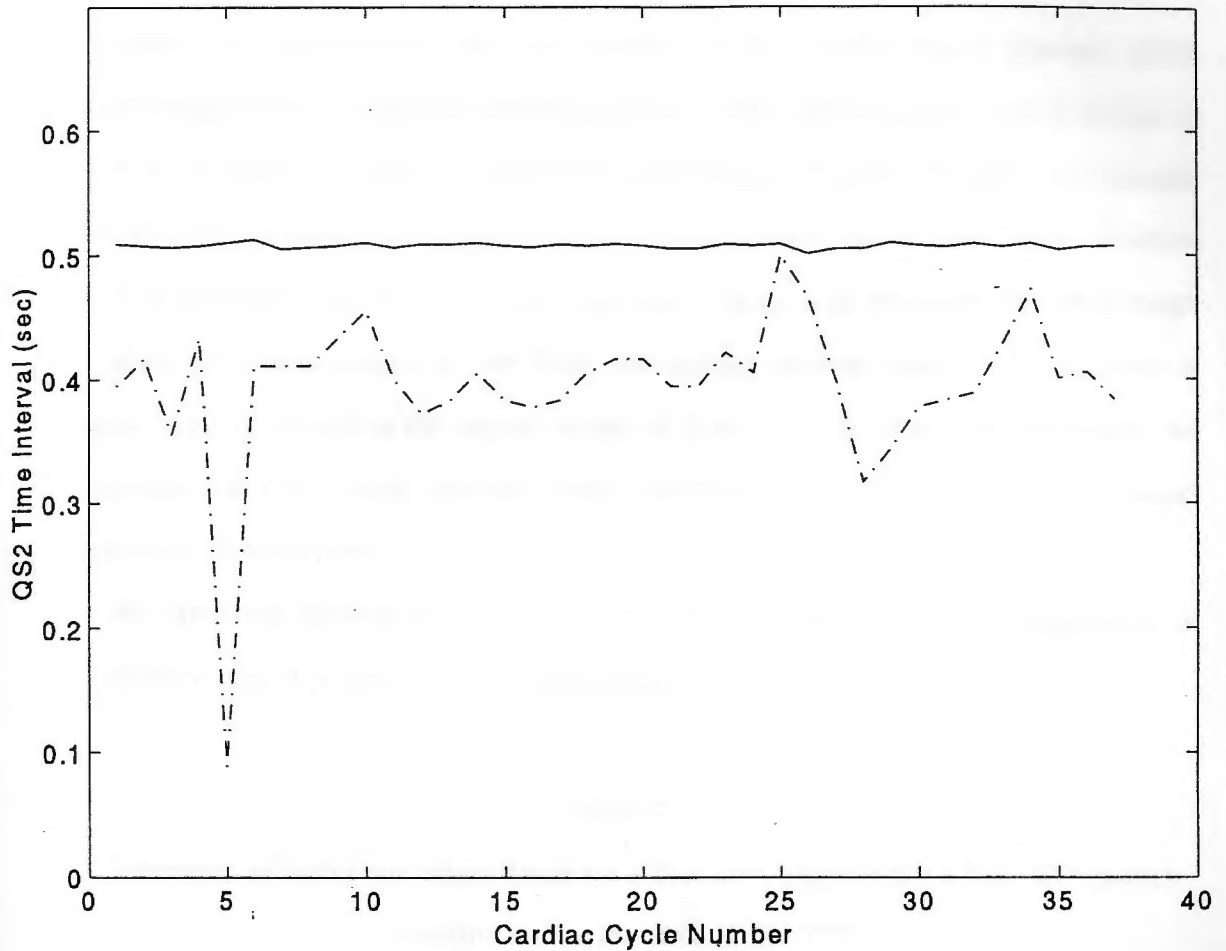


Figure 4.4 Comparison between the calculation of QS2 using the dicrotic notch information estimated by the detection algorithm, (dashed line), and using the regression equation based on HR (solid line), for MGH file 019.

Baseline Variation: MGH file 077

Figure 4.5 demonstrates the performance of the DyWT based dicrotic notch detection algorithm on a signal containing baseline drift. The pressure signal is shown in figure 4.5 a and the 3 scales of the DyWT are shown in figures 4.5 c-d. This example demonstrates the ability of the DyWT algorithm to resolve the dicrotic notch variation which modulated by a lower frequency variation. Figure 4.5a provides the entire range of cardiac cycles examined in the QS2 calculation; whereas figure 4.5 e-h show a focused view of several of the cardiac cycles of figure 4.5 a-d. Figure 4.6 compares the calculation of QS2 using dicrotic notch information, to the regression equation calculation, based on HR.

The statistical performance of each of the dicrotic notch detection algorithms is presented in table 4.5, based on 24 cardiac cycles.

Table 4.5

Performance of Detection Algorithms on a Pressure Signal with a Low Frequency Baseline Variation (MGH file 077)

Algorithm	Sensitivity (%)	Positive Productivity (%)	False Positive Rate (%)	False Negative Rate (%)
Wavelet	100	100	0	0
Lee	0	0	54	100
Jundanian	100	35	188	0
Martino	0	0	104	100
Kinias	4	10	38	96
Elghazzawi	100	100	0	0

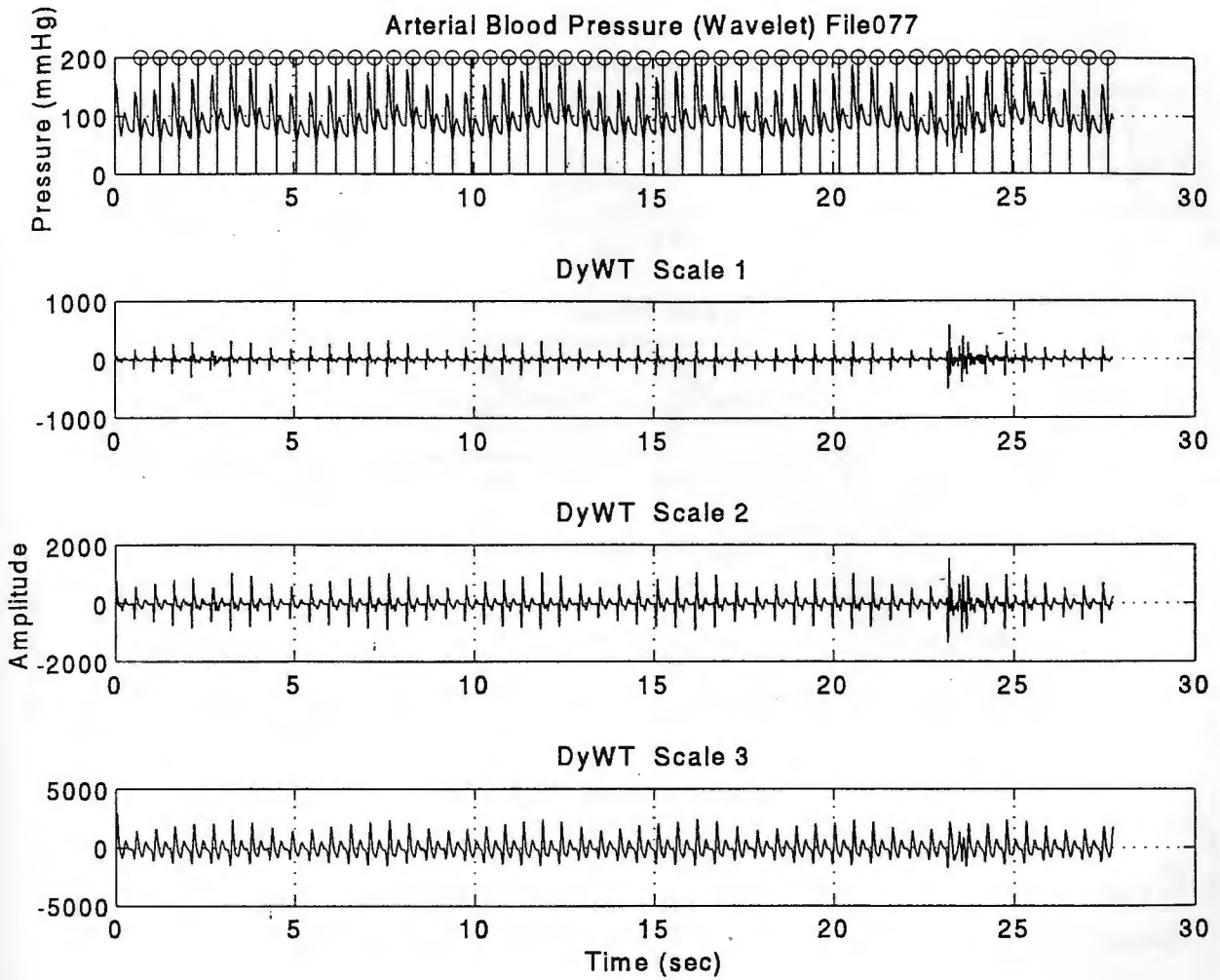


Figure 4.5 (a) MGH file 077 radial artery pressure signal containing a low frequency modulation; (b-d) DyWT decompositions for dyadic scales 1, 2 and 3, respectively. The dashed vertical lines indicate the annotated location of the dicrotic notch; whereas the solid vertical lines indicate the algorithm's estimation of the dicrotic notch locations.

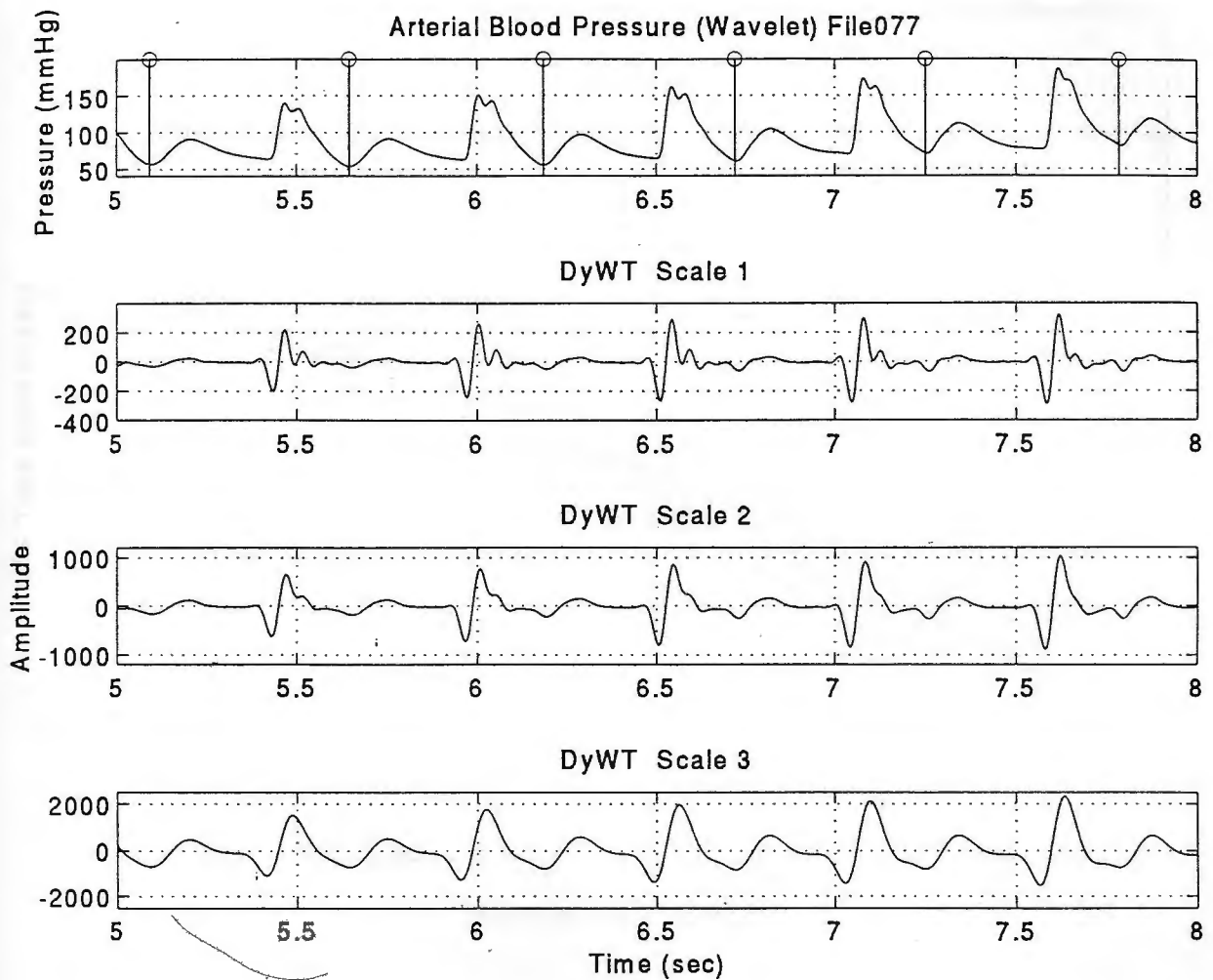


Figure 4.5 (e) Enlarged view of the MGH file 077 radial artery pressure signal containing a low frequency modulation; (f-h) DyWT decompositions for dyadic scales 1, 2 and 3, respectively. The dashed vertical lines indicate the annotated location of the dicotic notch; whereas the solid vertical lines indicate the algorithm's estimation of the dicotic notch locations.

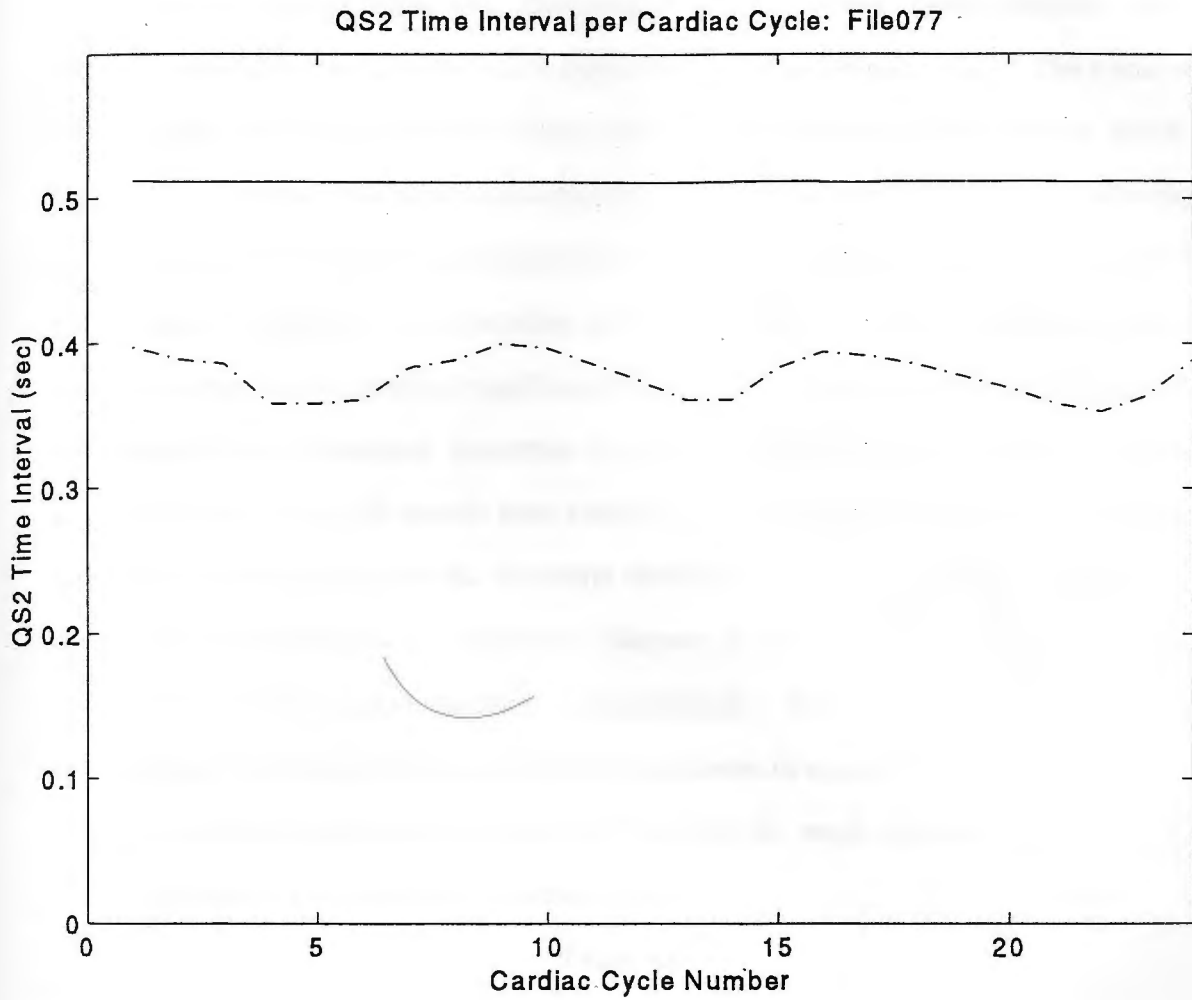


Figure 4.6 Comparison between the calculation of QS2 using the dicrotic notch information estimated by the detection algorithm, (dashed line), and using the regression equation based on HR (solid line), for a signal with a low frequency modulation, MGH file 077.

Pressure Signal with an Irregular Heart Rate: MGH file 023

Figure 4.7 demonstrates the effectiveness of the DyWT based dicrotic notch detection algorithm on a non stationary signal containing an irregular HR. The signal is non stationary but mostly free of noise with a slight inflection at the dicrotic notch. Figure 4.7a provides the entire range of cardiac cycles examined in the QS2 calculation; whereas figure 4.7 e-h show a focused view of several of the cardiac cycles of figure 4.7 a-d. Figure 4.8 compares the calculation of QS2 using dicrotic notch information, to the regression equation calculation, based on HR. Notice that the QS2 calculation based on the dicrotic notch detection algorithm results exhibits fluctuations between several cardiac cycles. The QS2 systolic time interval is decreasing as the heart rate increases. Since the detection algorithm has correctly identified each dicrotic notch in figure 4.7, the benefit of a background verification dicrotic notch location for determining the accuracy of the regression equation is appreciated. Such results would prompt a reevaluation of the regression equation offset parameter in equation (1.3).

The statistical performance of each of the dicrotic notch detection algorithms is presented in table 4.6, based on 11 cardiac cycles.

Table 4.6

Performance of Detection Algorithms on a Pressure Signal with an Irregular Heart Rate (MGH file 023)

Algorithm	Sensitivity (%)	Positive Productivity (%)	False Positive Rate (%)	False Negative Rate (%)
Wavelet	100	100	0	0
Lee	36	100	0	64
Jundanian	0	0	136	100
Martino	82	90	9	18
Kinias	73	73	27	27
Elghazzawi	9	9	91	91

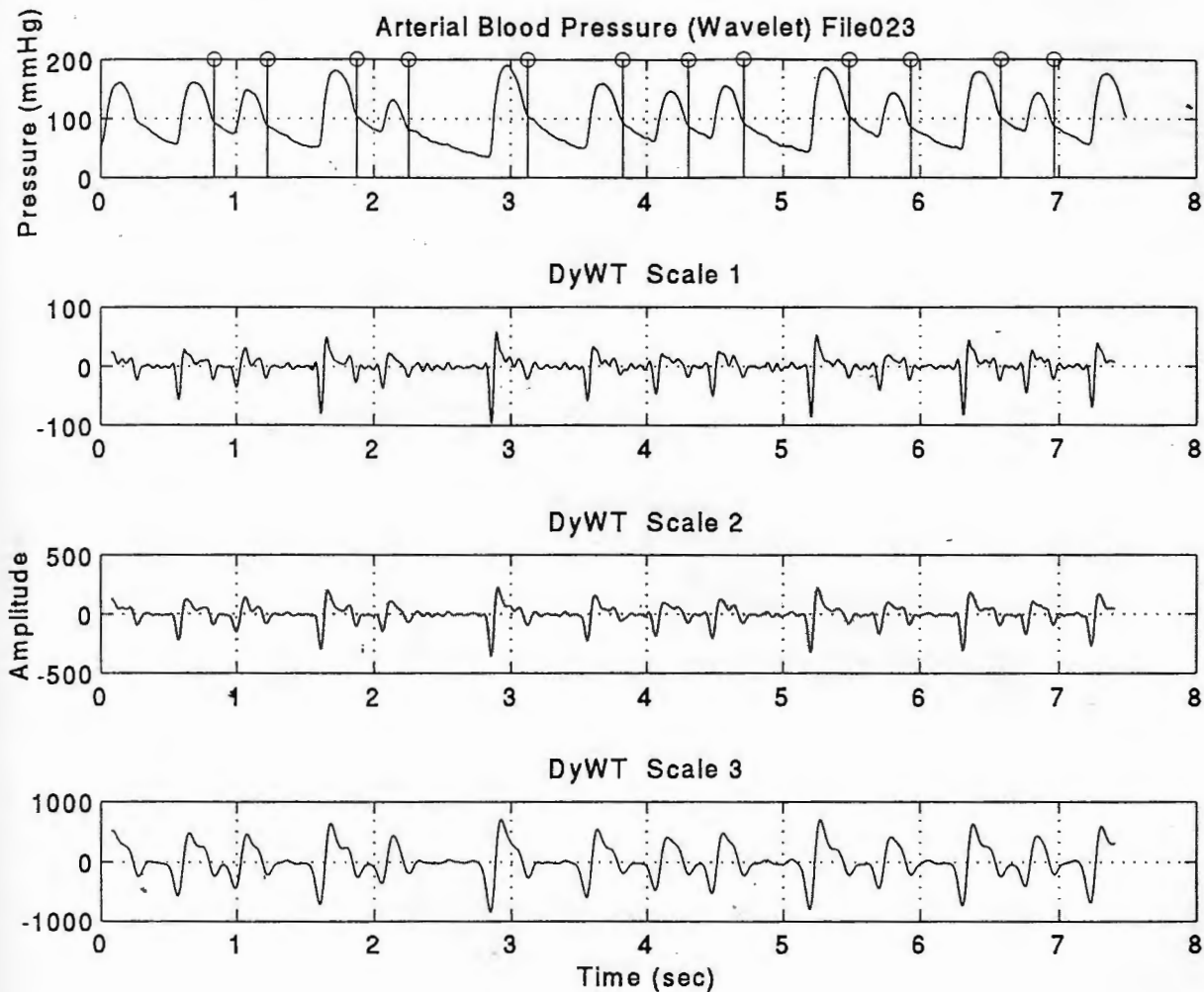


Figure 4.7 (a) MGH file 023 radial artery pressure signal exhibiting an irregular HR; (b-d) DyWT decompositions for dyadic scales 1, 2 and 3, respectively. The dashed vertical lines indicate the annotated location of the diastolic notch; whereas the solid vertical lines indicate the algorithm's estimation of the diastolic notch locations.

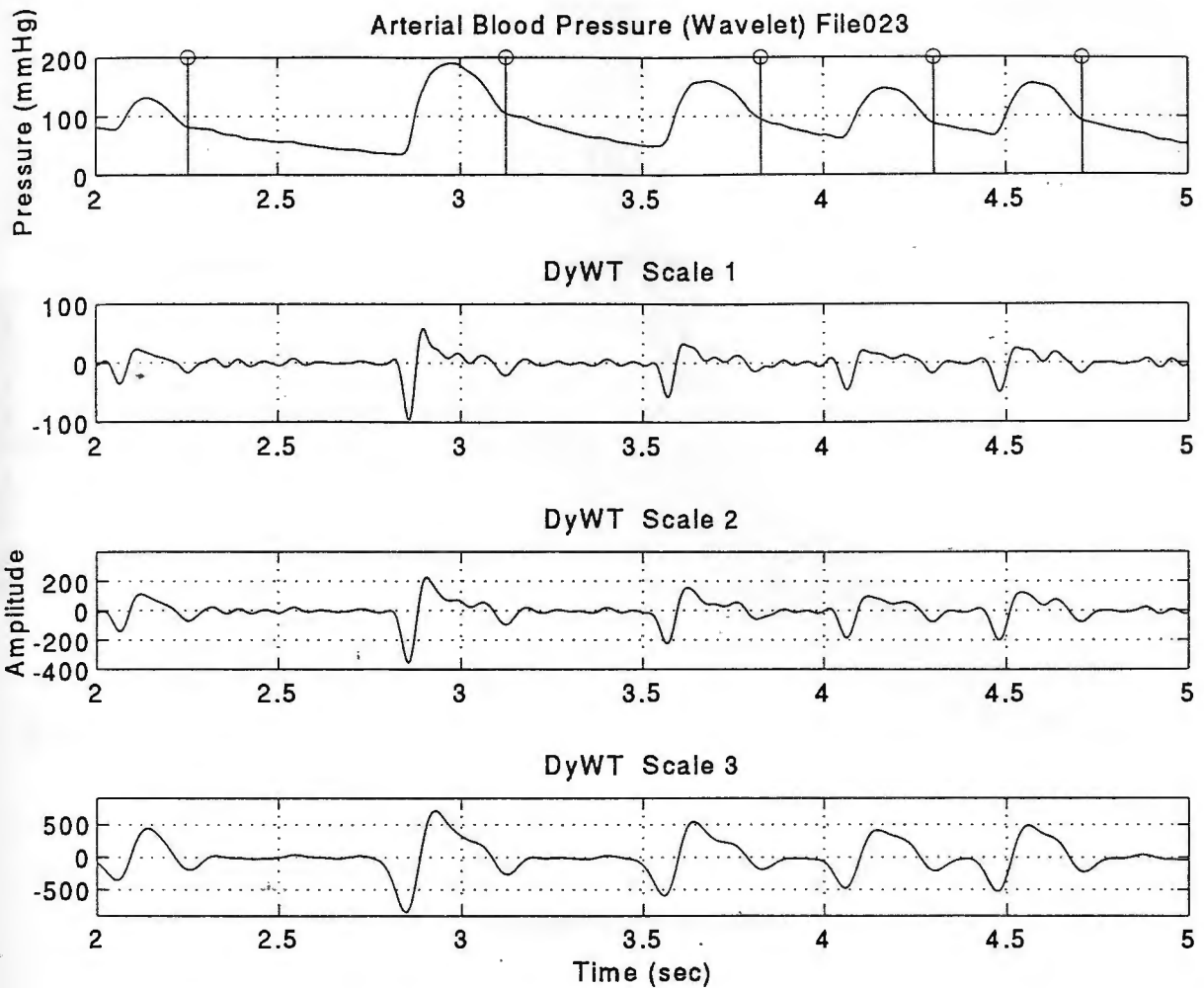


Figure 4.7 (e) Enlarged view of the MGH file 023 radial artery pressure signal exhibiting an irregular HR; (f-h) DyWT decompositions for dyadic scales 1, 2 and 3, respectively. The dashed vertical lines indicate the annotated location of the dicrotic notch; whereas the solid vertical lines indicate the algorithm's estimation of the dicrotic notch locations.

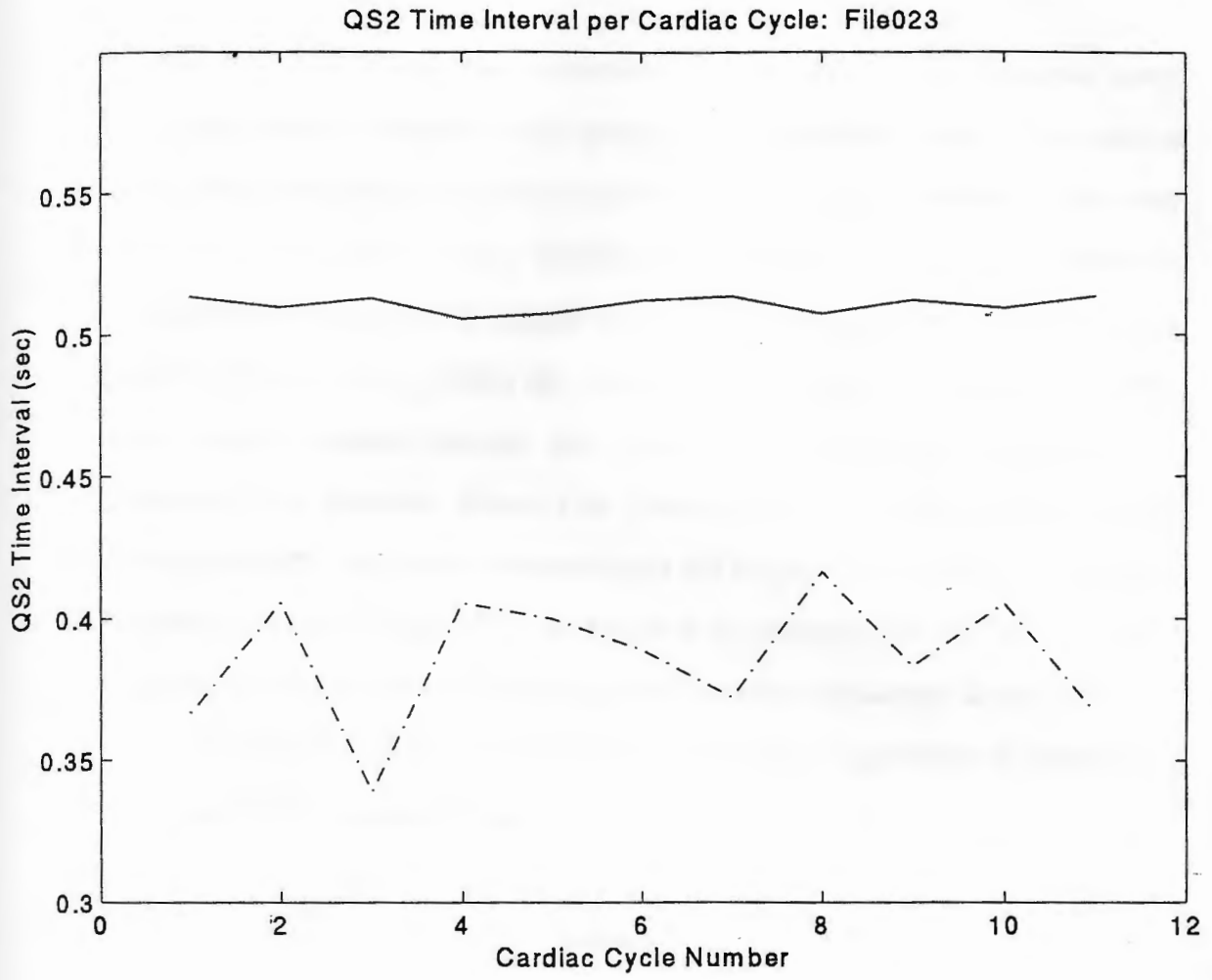


Figure 4.8 Comparison between the calculation of QS2 using the dicrotic notch information estimated by the detection algorithm, (dashed line), and using the regression equation based on HR (solid line), for a pressure signal exhibiting an irregular HR, MGH file 023. The dashed lines provide a more accurate estimation of the fluctuation in the QS2 systolic time interval, due to the changing heart rate.

Femoral Artery Pressure Signal with Noise: MGH file 060

Figure 4.9 demonstrates the performance of the DyWT based dicrotic notch detection algorithm on a femoral artery pressure signal containing noise. The noise is partially in the same frequency band as the dicrotic notch and is contained in the same temporal area as the dicrotic notch. This illustrates the ability of the DyWT algorithm to sift through noise whose spectral content does not correlate between the three scales of the DyWT. Noise content within the same frequency band as the dicrotic notch, however, would correlate between the scales of the DyWT and compromise the performance of the algorithm. Figure 4.9a provides the entire range of cardiac cycles examined in the QS2 calculation; whereas figure 4.9 e-h show a focused view of several of the cardiac cycles of figure 4.9 a-d. Figure 4.10 compares the calculation of QS2 using dicrotic notch information, to the regression equation calculation, based on HR.

The performance of each of the dicrotic notch detection algorithms is presented in table 4.7, based on 16 cardiac cycles.

Table 4.7
Performance of Detection Algorithms on a Pressure Signal Containing Noise
(MGH file 060)

Algorithm	Sensitivity (%)	Positive Productivity (%)	False Positive Rate (%)	False Negative Rate (%)
Wavelet	94	94	6	6
Lee	88	45	106	13
Jundanian	100	186	437	0
Martino	100	73	38	0
Kinias	44	54	38	56
Elghazzawi	6	6	94	94

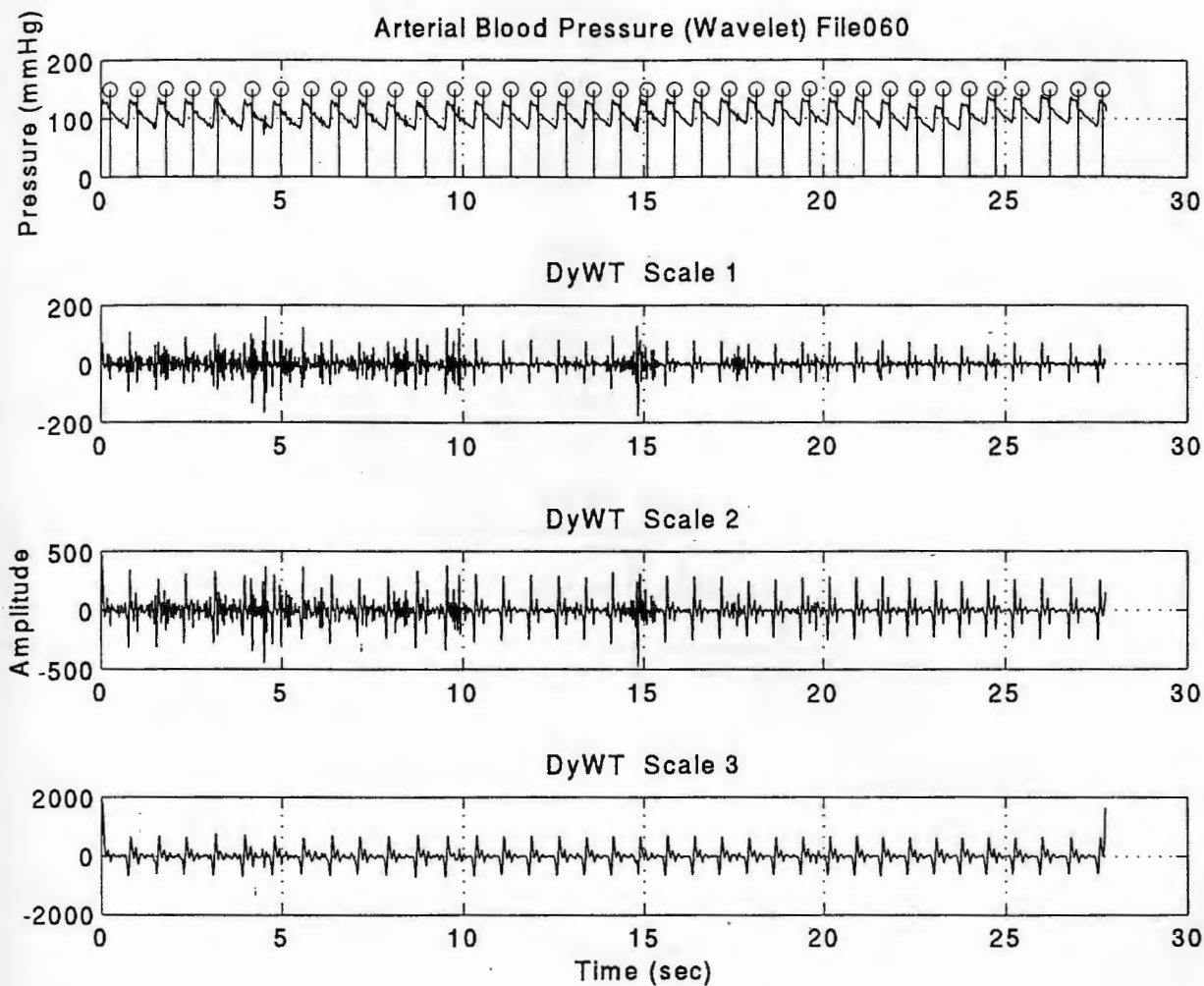


Figure 4.9 (a) MGH file 060 femoral artery pressure signal containing noise; (b-d) DyWT decompositions for dyadic scales 1, 2 and 3, respectively. The dashed vertical lines indicate the annotated location of the dicrotic notch; whereas the solid vertical lines indicate the algorithm's estimation of the dicrotic notch locations.

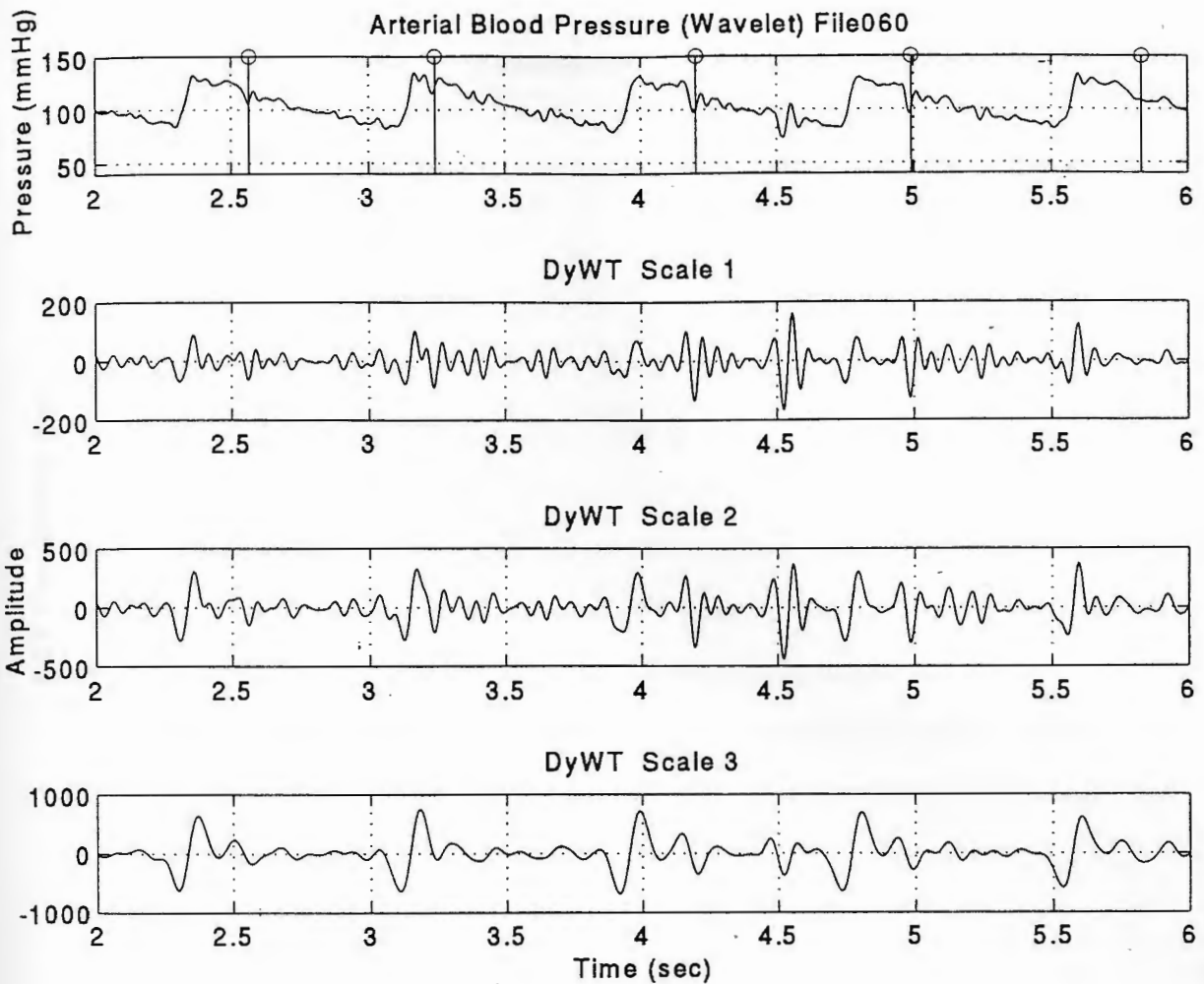


Figure 4.9 (e) Enlarged view of the MGH file 060 femoral artery pressure signal containing noise; (f-h) DyWT decompositions for dyadic scales 1, 2 and 3, respectively. The dashed vertical lines indicate the annotated location of the dicrotic notch; whereas the solid vertical lines indicate the algorithm's estimation of the dicrotic notch locations.

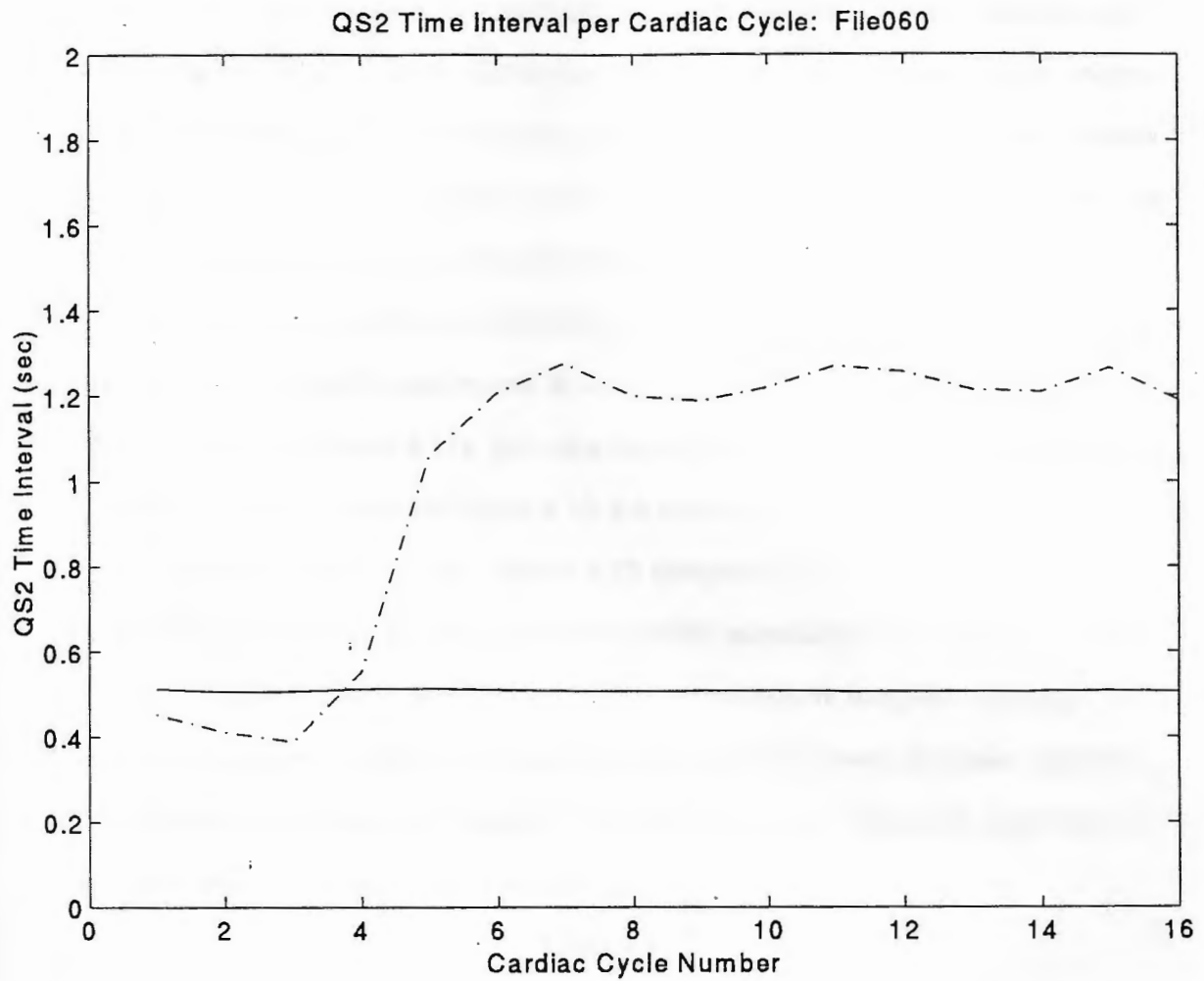


Figure 4.10 Comparison between the calculation of QS2 using the dicrotic notch information estimated by the detection algorithm, (dashed line), and using the regression equation based on HR (solid line), for a femoral artery pressure signal containing noise, MGH file 060.

Pressure Signal with a Notch Artifact: MGH file 021

Figure 4.11 demonstrates the performance of the DyWT based dicrotic notch detection algorithm on a signal containing artifacts that resemble the dicrotic notch. The signal is mostly free of random noise but contains a 'notch like' inflection between peak systole and the actual dicrotic notch. The artifact is possibly due to catheter motion. The example illustrates where the DyWT detection algorithm fails since it cannot distinguish non random oscillations from the true dicrotic notch contour. Notice that the artifact is not a random fluctuation and it occurs within the same frequency band as the actual dicrotic notch. Figure 4.11a provides the entire range of cardiac cycles examined in the QS2 calculation; whereas figure 4.11 e-h show a focused view of several of the cardiac cycles of figure 4.11 a-d. Figure 4.10 compares the calculation of QS2 using dicrotic notch information, to the regression equation calculation, based on HR. Similar results were obtained in MGH files 120 and 126 which also have irregular notching. This type of waveform presents the greatest problem to the DyWT based detection algorithm. The statistical performance of each of the dicrotic notch detection algorithms is presented in table 4.8, based on 11 cardiac cycles.

Table 4.8

**Performance of Detection Algorithms on a Pressure Signal with a Notch Artifact
(MGH file 021)**

Algorithm	Sensitivity (%)	Positive Productivity (%)	False Positive Rate (%)	False Negative Rate (%)
Wavelet	0	0	100	100
Lee	27	27	73	73
Jundanian	100	48	109	0
Martino	100	92	9	0
Kinias	0	0	73	100
Elghazzawi	0	0	100	100

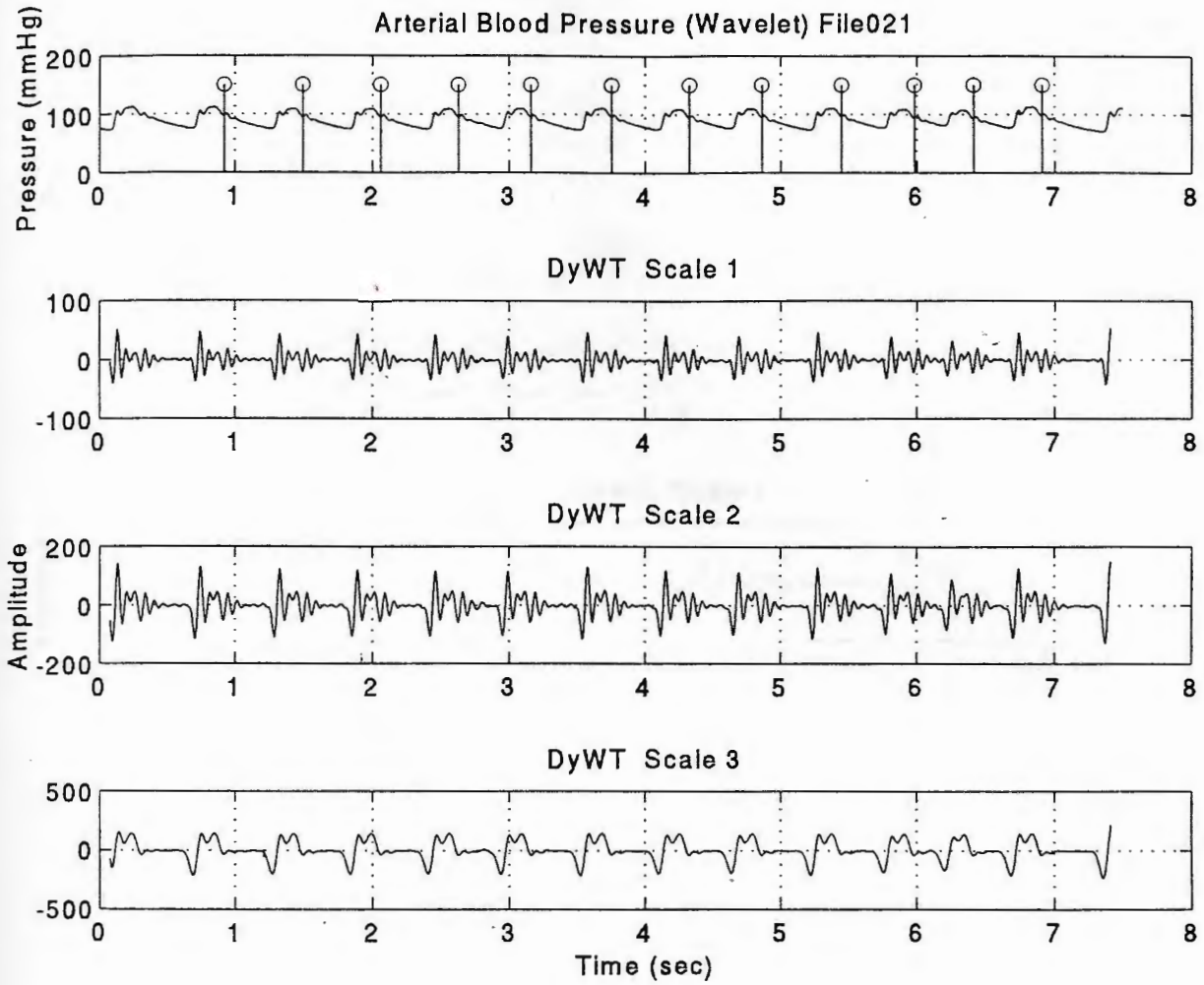


Figure 4.11 (a) MGH file 021 radial artery pressure signal containing a notch artifact; (b-d) DyWT decompositions for dyadic scales 1, 2 and 3, respectively. The dashed vertical lines indicate the annotated location of the dicrotic notch; whereas the solid vertical lines indicate the algorithm's estimation of the dicrotic notch locations.

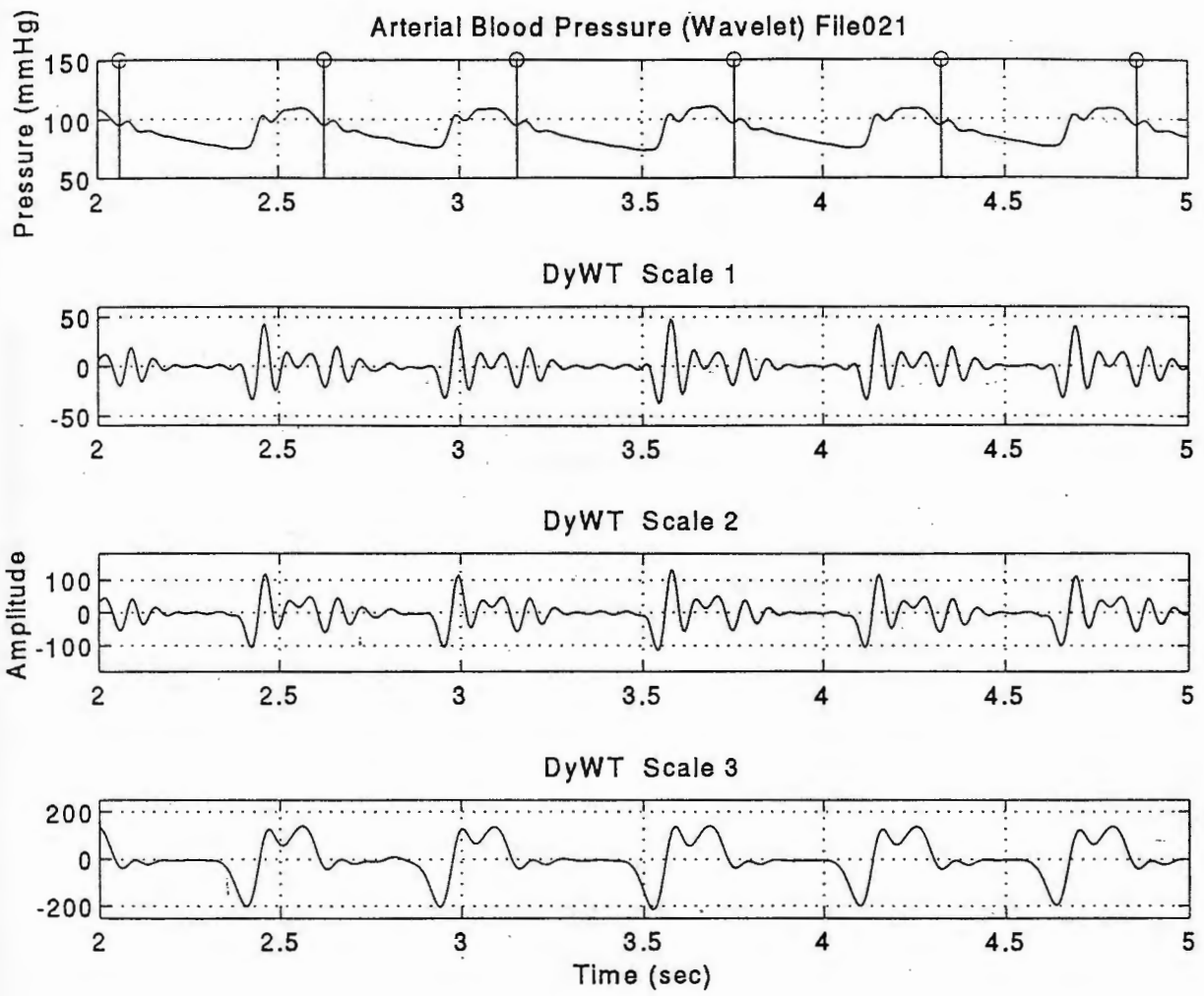


Figure 4.11 (e) Enlarged view of the MGH file 021 radial artery pressure signal containing a notch artifact; (f-h) DyWT decompositions for dyadic scales 1, 2 and 3, respectively. The dashed vertical lines indicate the annotated location of the dicrotic notch; whereas the solid vertical lines indicate the algorithm's estimation of the dicrotic notch locations.

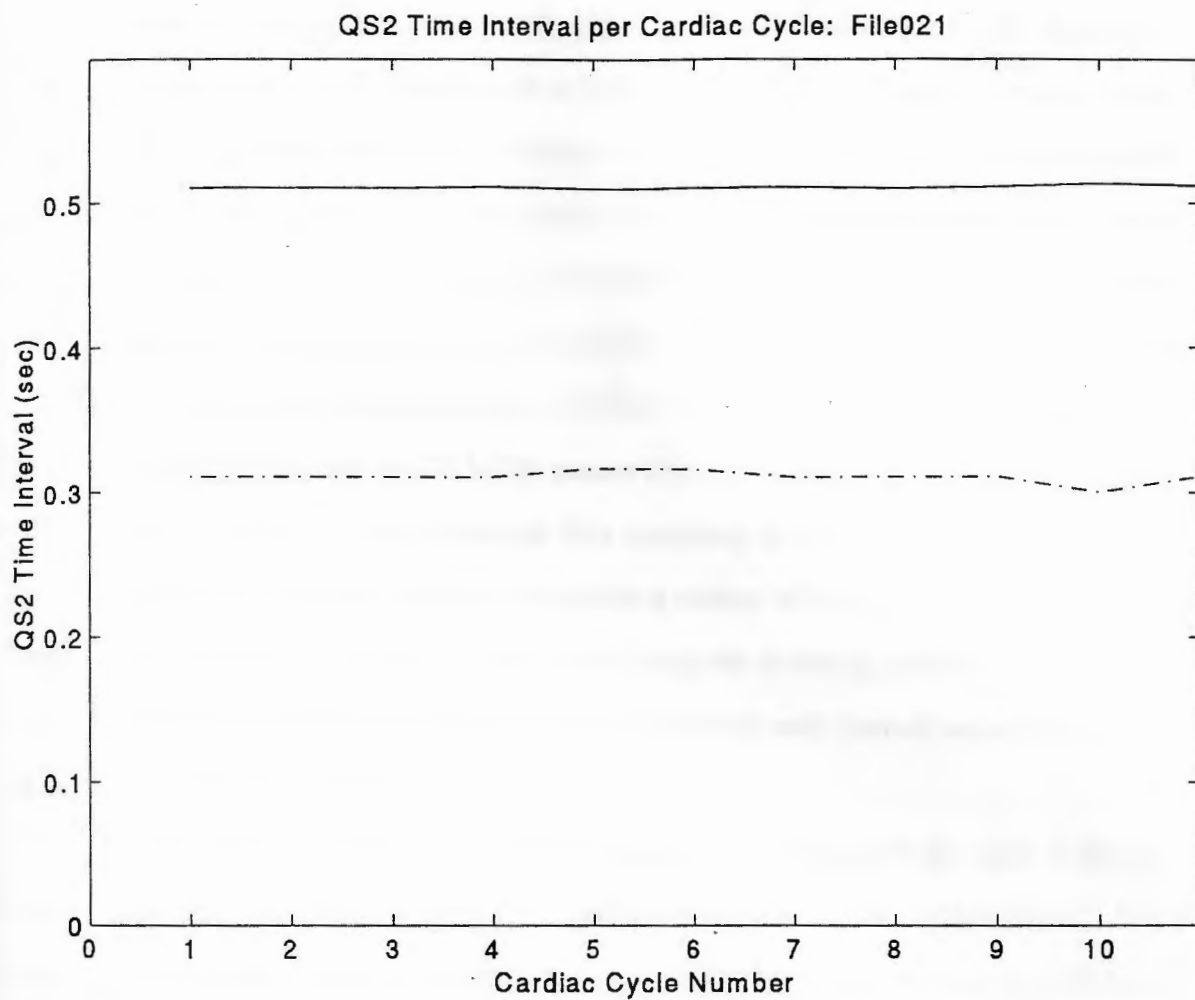


Figure 4.12 Comparison between the calculation of QS2 using the dicrotic notch information estimated by the detection algorithm, (dashed line), and using the regression equation based on HR (solid line), for a pressure signal containing a notch artifact, MGH file 021.

4.5 Statistical and Comparative Results of Simulation

A summary of the results of the dyadic wavelet dicrotic notch detection algorithm performance is presented. The 5 leading published algorithms, written by Lee et al [182], Jundanian et al [183], Martino et al [184], Kinias et al [185] and Elghazzawi et al [175] have been programmed and evaluated on the MGH database for comparison with the dyadic wavelet method. All algorithms including the dyadic wavelet method were tested on three test sets containing: (A) 30 MGH database files, with a total of 284 cardiac cycles, averaging 9 cardiac cycles per file; (B) 50 MGH patient files, with a total of 1301 cardiac cycles, which includes the files in set (A) but with an average of 26 cardiac cycles per file; and (C) 72 MGH patient files, with a total of 1647 cardiac cycles, (with an average of 23 cardiac cycles per file), including all of the same files (and cycles) as in set (B). The files were selected to contain a variety of clinical situations, including respiratory variations, ventricular tachycardias, irregular notching, catheter artifacts and other noise factors as well as on some classic waveforms with normal sinus rhythms (as previously outlined in table 4.3).

The results of notch detection results, in terms of TP, FP and FN for each of the six detection algorithms tested, is located in Appendix B, for each of the three test sets. The performance evaluation, indicating the accuracy of each of the six detection algorithms in terms of sensitivity, positive productivity, false positive rate and false negative rate, is provided in table 4.9 for the (A) 30 file, (B) 50 file, and (C) the 71 file test sets. The results in table 4.9 indicate that a stable or convergent representation of algorithm performance was achieved with test set B. Three algorithms [175,183,185] were stable to within $\pm 5\%$ of the statistics generated from the A to B test sets; whereas all algorithms maintained stable between test sets B and C to within $\pm 2\%$. Desirable algorithm performance is shown with high percentages of sensitivity and positive productivity, and low FN and FP rates. Depending upon the strengths and weaknesses

of each algorithm, additional test files improved or degraded the performance percentage value. Thus, a wide range of waveform types (normal to irregular pathologies), is necessary for algorithm validation. The proposed waveform test sets B and C represent valid subsets of the entire MGH database appropriate to determine the validity of blood pressure event detection algorithms, such as the dicrotic notch, based on the observed convergence of each of the four performance criteria for all six detection algorithms. A histogram showing the performance of each of the dicrotic notch detection algorithms, for test set B, is provided in figure 4.13.

The results have been normalized in that each algorithm was evaluated for the same group of cardiac cycles for each patient file. The graphical output results, of MGH database files illustrative of various clinical situations, for the DyWT based dicrotic notch detection algorithm and the 5 algorithms, implemented from the literature, are located in appendix B. The file identification for each of the waveforms provided in Appendix B is listed in table 4.10. The graphs presented in appendix B indicate the annotated locations of the dicrotic notches by dashed, vertical lines extending from the time axis to the upper graph boundary terminated in a circle. The detected locations of the dicrotic notches are identified by solid, vertical lines extending from the time axis to the upper graph boundary. Where the two lines overlap, there is a solid line terminated with a circle. The wavelet decomposition (DyWT results) for each of the three dyadic scales is also provided for each file. (Typically, the first and last cycles displayed in the graphical results in appendix B were not counted or evaluated for algorithm performance).

Comparative results of Dicrotic Notch Detection Algorithms

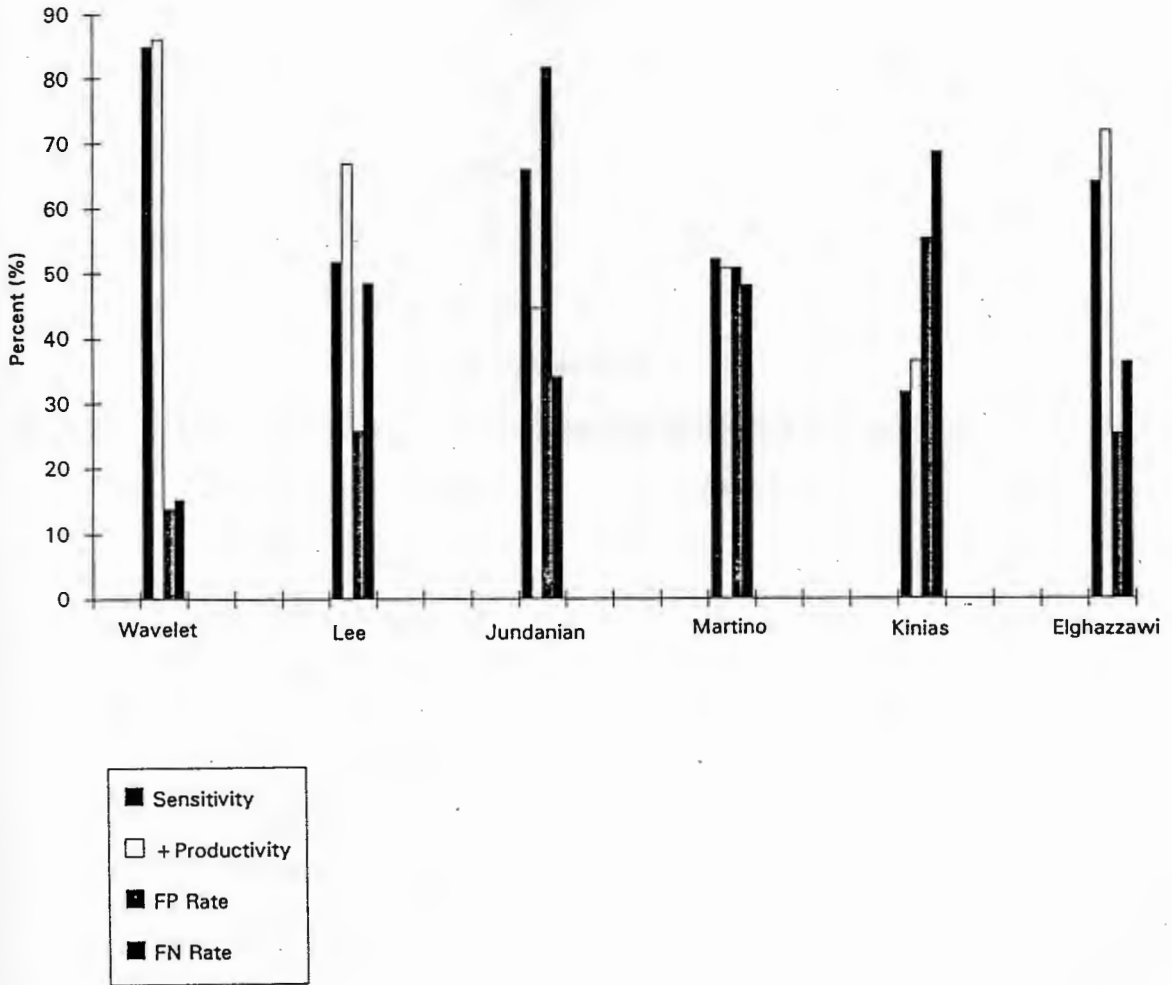


Figure 4.13 Histogram of the statistical results for all of the dicrotic notch detection algorithms.

Table 4.9

Simulation Performance Results for each of the Dicrotic Notch Detection Algorithms for

Test Sets (A) 30 files; (B) 50 files; (C) 72 files

Algorithm	Sensitivity (%)			Positive (%) Productivity			False Positive Rate (%)			False Negative Rate (%)		
	A	B	C	A	B	C	A	B	C	A	B	C
Wavelet	78	86	84	79	87	85	21	13	15	23	14	16
Lee	45	50	51	52	67	66	42	24	26	55	50	49
Jundanian	66	64	66	46	44	45	77	82	81	34	36	34
Martino	61	53	51	61	51	50	38	50	51	39	47	49
Kinias	29	33	31	36	37	36	50	56	56	71	67	69
Elghazzawi	67	63	64	68	70	72	31	26	25	33	37	36

Table 4.10

Illustrative MGH Patient Files Whose Detection Results are Contained in Appendix C

Fast heart rate (140 bpm)	003
Damped pressure signal	009
Pulsus Alternans	019
Varying heart rate	020
Irregular notching	021
Slow heart rate	034
Normal sinus rhythm, classic shape	036
Femoral pressure	089
Irregular notching	120a
Preventricular contraction	128

4.6 Observations

There are several observed cases where the DyWT based dicrotic notch detection algorithm was not effective.

- The R wave or systolic peak was not predetermined for a given cardiac cycle. Thus, there was no search window in that cardiac cycle for dicrotic notch detection. The search window spans from the time of the systolic peak in the BP signal to the time of the next R wave of the ECG signal.
- The R wave of the next cardiac cycle occurs before aortic valve closure of the current cardiac cycle (some pre-ventricular contractions), as shown in figure 4.14a, for MGH file120. This occurs due to the definition of the dicrotic notch search window which terminates at the R wave of the next cardiac cycle. If the search window definition is altered to include BP signal beyond the R wave of the next cardiac cycle, then the dicrotic notch is acknowledged as indicated in figure 4.14b, which was generated by eliminating the detected occurrence of the R wave for the next cardiac cycle.
- The pressure waveform contour has irregularities that resemble the dicrotic notch, in terms of its amplitude and spectral content, which are located in the search window between the systolic peak and the actual dicrotic notch. An example of this is shown in figure 4.15, for MGH file021.
- The dicrotic notch detection algorithm based on the DyWT has moderate success when the duration of the dicrotic notch is relatively long, as shown in figure 4.14a, for MGH file033. The DyWT algorithm tends to locate the start of valve closure, as does the algorithms presented by Lee [182], Martino [184] and Kinias [185] as shown in figure 4.14 b, d and e.

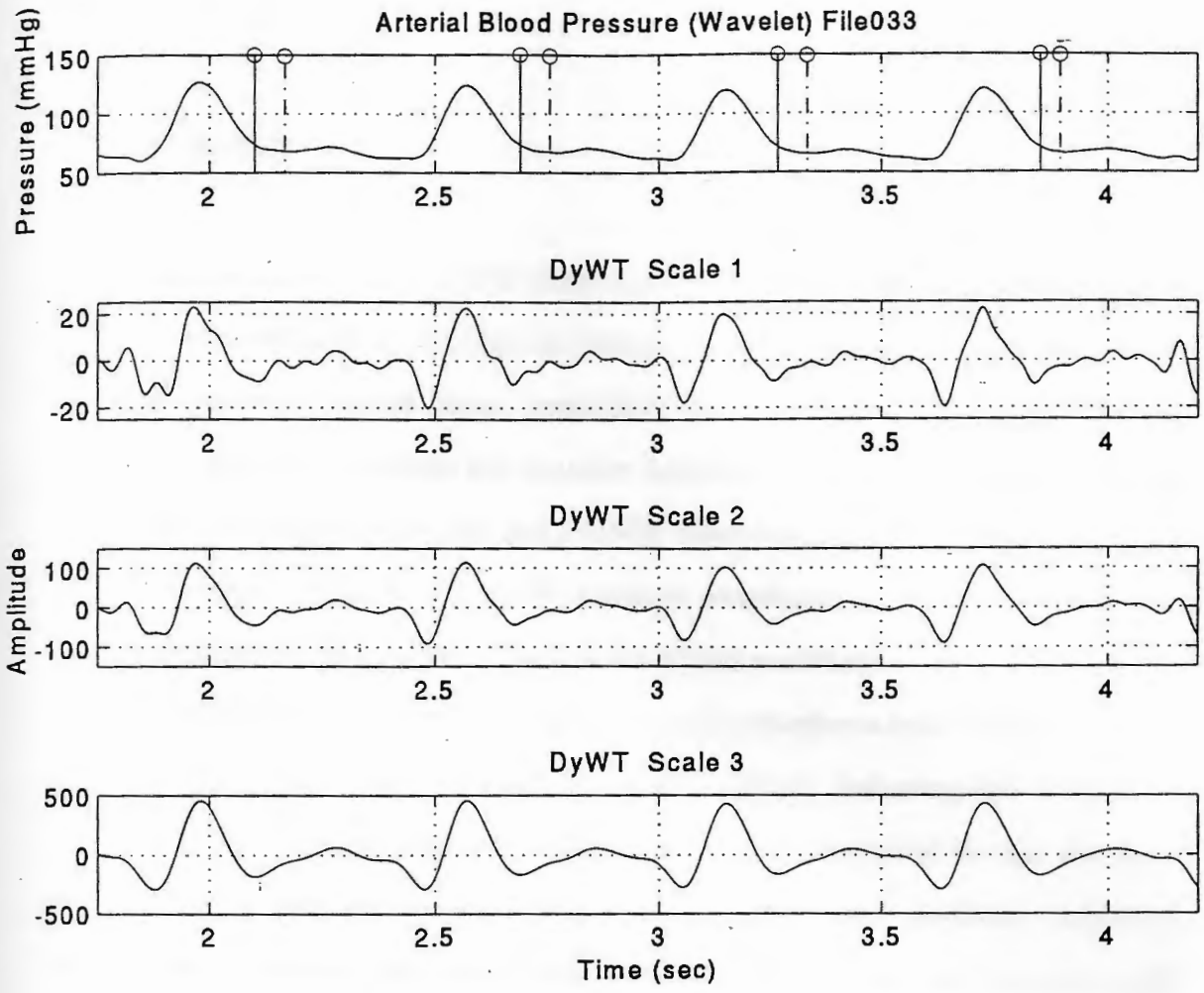


Figure 4.14 MGH file033 displaying dicotic notch detection results for a waveform with a notch of large radius of curvature. The dashed vertical lines indicate the annotated location of the dicotic notch; whereas the solid vertical lines indicate the algorithm's estimation of the dicotic notch locations.

Chapter 5

Conclusion

Reliable and consistent dicrotic notch detection of the arterial blood pressure signal has been accomplished by locating the consecutive minima and zero crossings of the pressure derivative across three consecutive dyadic scales of the dyadic wavelet transform using the Mexican Hat wavelet function. A computer program has been written and implemented on a PC and a UNIX based workstation using Matlab 4.2 and has been tested on 72 human blood pressure waveforms obtained from the MGH database encompassing a variety of clinical and patient conditions.

The dicrotic notch is observed in arterial pressure waveforms as a consequence of the closing of the aortic valve, after left ventricular ejection, indicating the start of the diastolic cycle. The detection of the dicrotic notch is non-trivial in that the blood pressure signal may be corrupted by noise, contain motion artifacts, respiratory modulation, change abruptly with arrhythmias or deviate from the classical arterial pressure wave shape, especially in sick patients. The dyadic wavelet transform method of dicrotic notch detection was devised to estimate the dicrotic notch location in arterial blood pressure signals for the various clinical situations.

The dyadic wavelet transform method of signal analysis inherently filters out band limited noise and low frequency variations by the comparison of the DyWT results across consecutive dyadic scales. Three consecutive dyadic scales of a Mexican Hat wavelet were generated and convolved with the arterial blood pressure signal to obtain the DyWT decomposition at these scales. The proposed dicrotic notch detection algorithm

locates minima which occur within a neighborhood of ± 33 msec across consecutive dyadic scales of the DyWT within a search window, defined from the systolic peak in the blood pressure signal to the R wave of the next cardiac cycle in the ECG signal. This algorithm is robust for signals which are noisy, contain irregular heart rhythms and those which exhibit erratic behavior. The dyadic wavelet transform based detection algorithm had only moderate success when the pressure waveform contained irregularities that resembled the dicrotic notch in terms of amplitude and frequency, located between the systolic peak and the actual dicrotic notch.

The dyadic wavelet transform method of detecting the dicrotic notch favorably compared and outperformed the five other leading detection algorithms found in the literature with respect to each of the four performance criteria: sensitivity (by 18%), positive productivity (by 13%), false positive rate (by 11%) and false negative rate (by 18%). The DyWT dicrotic notch detection algorithm has the highest sensitivity and positive productivity, and the lowest false positive and false negative rates, which are listed in table 5.1 for test set C (72 patient files), compared to the other leading detection algorithms.

Table 5.1

Performance Results of the DyWT Based Dicrotic Notch Detection Algorithm: Test Set C

Sensitivity	84 %
Positive Productivity	85 %
False Positive Rate	15 %
False Negative Rate	16 %

The original premise of the project was that the dicrotic notch detection algorithm was to be implemented as a background verification system for the accuracy of the

regression equation used to predict the temporal location of the dicrotic notch from previous R-wave information from the electrocardiogram. Thus, a real time algorithm was not a concern, but optimization of algorithm speed and accuracy was taken into consideration. Also, the R wave detection and search window criteria were designed such that simple modifications would allow implementation into the medical device environment for evaluating systolic time interval or analyzing prerecorded physiological data.

The QS2 systolic time interval calculated using the R wave to dicrotic notch duration favorably compared to the QS2 interval evaluated by the linear regression equation, based on the HR. The regression equations are considered valid indices under normal conditions. However, when heart rate changes, by roughly 10 bpm, then an adjustment in the regression prediction may be necessary. Thus, validation of the accuracy of the regression equation in the clinical environment, using a dicrotic notch detection scheme, is vital.

The algorithm can be adapted to detect the dicrotic notch when the ECG is not available by using the DyWT to locate the systolic upstroke transient between end diastole and the rise in left ventricle pressure. This point in the pressure waveform approximates the temporal location of the R wave. The detection of systolic upstroke is similar to the algorithm presented except relative maxima above a threshold would be compared across dyadic scales, (rather than the minima which are used for dicrotic notch detection). Noise on the pressure signal is commonly mechanical in nature, whereas electrical noise interferes more with the ECG. Thus, this algorithm is valid in circumstances where electrical noise may render the ECG signal unreadable such as during the use of electrosurgical units.

Appendix A

A.1 DyWT Based Dicrotic Notch Detection Matlab Program Code

```
% This program analyzes a BP and ECG signals and determines the temporal locations of
% the dicrotic notches in the BP waveform.
% The Mexican Hat wavelet function coefficients for 3 dyadic scales were precalculated.
% *****
% Calculate the DyWT using discrete convolution
d1=real(conv(BP,mexhat1));
d2=real(conv(BP,mexhat2));
d3=real(conv(BP,mexhat3));
% Truncated excess points from discrete convolution result relative to size of wavelet.
L=round(length(mexhat0)/2);
dywt1=d1(L:(round(length(d1)-L+1)));
dywt2=d2(L:(round(length(d2)-L+1)));
dywt3=d3(L:(round(length(d3)-L+1)));
% *****
% Program to find the R wave in the ECG using the Elghazzawi algorithm
% ECG R wave detection algorithm (to set search window for end diastole)
thresh=max(ecg)*0.60; % set 60% of global max threshold magnitude for R wave spike
% Locate sample # of threshold crossings
numups=0; % # of threshold upslope crossings found
numdowns=0; % # of threshold downslope crossings found
for i=1:nbp-1
    if ecg(i)<=thresh & ecg(i+1)>=thresh
        numups=numups+1;
        upslope(numups)=i; % ordered sample #s of upslopes found
```

```

end;
if ecg(i)>=thresh & ecg(i+1)<=thresh
    numdowns=numdowns+1;
    dnslope(numdowns)=i;    % ordered sample #s of downslopes found
end;
end;
% Find sample # of max in each section found above threshold (upslope to downslope).
if ((numups ~=0)&(numdowns ~=0)) % Need at least 1 threshold crossing pair
% If analysis waveform has the 1st upslope detected before a downslope:
if upslope(1)<dnslope(1)
    for i=1:numdowns
        [pks(i),offset(i)]=max(ecg(upslope(i):dnslope(i)));
        if i>length(offset); break; end
        rwave(i)=upslope(i)+(offset(i)-1);
    end
% If analysis waveform has the 1st downslope detected before an upslope:
elseif dnslope(1)<upslope(1)
    for i=1:numdowns-1
        [pks(i),offset(i)]=max(ecg(upslope(i):dnslope(i+1)));
        rwave(i)=upslope(i)+(offset(i)-1);    % sample # of maxima
    end
end
end
end    % end of analyzing threshold crossing pairs
% *****
% Calculate R to R interval (in time)
for i=1:(length(rwave)-1)

```

```

RR(i)=(rwave(i+1)-rwave(i))/rate;      % R to R wave time interval in seconds
HR(i)=1/RR(i)*60;                      % heart rate (bpm)
end;
%*****
% Find DN using DyWT of a BP signal, Mexican Hat wavelet and R wave information
% Locate minima <0 of DYWT(scale) and compare to minima of DYWT(scale+1)
% Minima are retained if they occur within +/-50 msec across consecutive dyadic scales.
range=round(0.05*rate);    % range for comparing minima (+/-50 msec)
dyadic=3;    % the total # of dyadic scales to be evaluated in the wavelet transform
for scale=1:dyadic
totalmin=0;    % initialize # of possible notch locations for all cardiac cycles in this scale
% Distinguish which wavelet transform scale result is to be processed.
if scale==1;    DYWT=dywt1;
elseif scale==2;    DYWT=dywt2;
elseif scale==3;    DYWT=dywt3;
end
% Locate zero crossings in the DYWT between consecutive R wave sample locations;
% then find a minimum between consecutive zero crossings.
% Set search window boundaries of cardiac cycle (start and stop)
for cycle=1:length(rwave)
miss(cycle)=0;    % # of cardiac cycles which did not have a notch detected
numups(cycle)=0;    % # of upslopes counted for this cardiac cycle.
if cycle==length(rwave)    % generate sample pts of search window for zero crossings
stop(cycle)=length(BP);
[PSP,offset]=max(BP(rwave(cycle):stop(cycle)));    % find PSP for window start
else stop(cycle)=rwave(cycle+1);

```

```

[PSP,offset]=max(BP(rwave(cycle):rwave(cycle+1)));
end
start(cycle)=rwave(cycle)+offset; % start of search window relative to R to R interval
% Initialize variables for minima search
numneg=0; % # of negative going (+ to -) zero crossings of DYWT found
numpos=0; % # of positive going (- to +) zero crossings of DYWT found
nummin=0; % # of minima in consecutive scales
% Locate zero crossings occurring within this cardiac cycle of the DYWT
for n=start(cycle):(stop(cycle)-1)
% Locate all zero crossings of the DYWT from negative slope (+ to -) in search window
if (DYWT(n)>=0 & DYWT(n+1)<=0)
    numneg=numneg+1;
    negnulls(numneg)=n+1; % ordered sample #s of zero crossings
end
% Locate all zero crossings of the DYWT(scale) from positive slope (- to +)
if (DYWT(n)<=0 & DYWT(n+1) >=0)
    numpos=numpos+1;
    posnulls(numpos)=n+1; % ordered sample #s of zero crossings
end
end % for start:stop loop
% Find sample # of the min in each section between zero crossings: (+ to -) and (- to +)
% Sample # of min search must start at downslope (+ to -) and end at an upslope (- to +).
if numneg ~= 0 % Need at least 1 (+ to -) zero crossing
    for i=1:numneg
        if negnulls(i)<stop(cycle)
            dwnslope(i)=negnulls(i);% sample # of start of min search window

```



```

end
if numpos ~= 0
    for k=1:numpos
        if posnulls(k)>negnulls(i)
            upslope(i)=posnulls(k);    % sample # of end of min search window
            numups(cycle)=numups(cycle)+1;
            break    % break out of for k=1:numpos loop
        end
    end
    if numups(cycle)==0
        upslope(i)=stop(cycle);
    end
    else upslope(i)=stop(cycle);    % no upslope detected so use last data point in cycle
    end    % end if numpos ~= 0
end    % end for i=1:numneg
else miss(cycle)=miss(cycle)+1;    % if no zero crossings; goto next cycle
end    % end if numneg~=0 loop (have arrays dwnslope & upslope for this cycle)
% Find minimum points between each dwnslope and upslope pair for this cardiac cycle
if miss(cycle)==0
    % First, determine # of valid zero crossing pairs available for a minimum search
    if length(dwnslope)<=length(upslope)
        crosses=length(dwnslope);
    else crosses=length(upslope);
    end
    for i=1:crosses
        [pks(i),offset(i)]=min(DYWT(dwnslope(i):upslope(i)));

```

```

    minima(i)=dwnslope(i)+(offset(i)-1);
end
% Accumulate minimas in each cycle for this dyadic scale as possible notch locations
for i=1:length(minima)
    finalmin(scale,totalmin+i)=minima(i);
end
totalmin=totalmin+length(minima); % update # of possible notch locations for this scale
end % end for miss(cycle)==0. Goto next cardiac cycle.
% clear for variable use in next cardiac cycle. Retain 'finalmin'(scale,i)
clear pks offset negnulls posnulls minima dwnslope upslope
end % end for cycle=1:length(rwave). Do next cycle for this scale DYWT
end % end for scale 1:dyadic. Do next scale
%*****
% All potential sample locations ('finalmin(scale,:)') for the dicrotic notch have been
% determined for each cardiac cycle in each dyadic scale.
% Compare 'finalmin' bewteen dyadic scales to locate the dicrotic notch.
for scale=1:dyadic
% Initialize matrix from which to compare final minima across dyadic scales
if scale==1
    compmin(1,:)=finalmin(1,:); % initialize finalmin array for scale comparison
end
if scale >= 2 % if calculated 2 consecutive dyadic scales then compare for peaks
% Locate minima of DyWT within +/- 50 msec across consecutive dyadic scales
for i=1:length(compmin(scale-1,:))
    if compmin(scale-1,i) ~= 0
        for n=1:length(finalmin(scale,:))

```


A.2 Lee Algorithm

```
% This program for dicrotic notch detection [52].
% Apply 4th order 10 Hz cutoff LP Butterworth filter to BP
cutoff=10/(rate/2);      % filter parameter for cutoff freq = 10 Hz.
[b,c]=butter(4,cutoff);  % generate Butterworth filter coefficients
BPfilt=filter(b,c,BP);   % signal has no phase delay
BPderiv=diff(BPfilt);    % Calculate the first derivative of the BP waveform
% Find where deriv goes from - to + (for finding end diastole)
numfoot=0;               % # of end diastoles found
for i=1:(length(BPderiv)-1)
    if BPderiv(i)<=0 & BPderiv(i+1)>=0
        numfoot=numfoot+1;
        foot(numfoot)=i;
    end;
end;
% Set threshold used to find systolic peak
thresh=max(BPfilt)*0.85; % threshold = 85% of global max of filtered data samples
% Find systolic peak by taking the max BP above a threshold following each foot
numsys=1;
for i=1:numfoot
    n=foot(i)+1;
    if BPderiv(n)>0      % initialize systolic peak value
        maxima(numsys)=BP(n);
    end
    if i==numfoot      % set endpoint for sample range for + deriv tracking
```



```

        endfoot(i)=(nbp-1);
    else endfoot(i)=foot(i+1);
end
for n=(foot(i)+1):endfoot(i)    % track + derivative between detected 'foot' locations
    if BPderiv(n)>0
        if BP(n)>=maxima(numsyst)
            maxima(numsyst)=BP(n);
        end
    elseif BPderiv(n)<0
        break    % break from maxima search loop
    end
end
% Determine if maxima are above threshold
if maxima(numsyst)>=thresh
    systole(numsyst)=n;    % array of systolic peak sample #s
    numsyst=numsyst+1;
end
end;    % end for 'foot' loop
% redefine foot array as those feet immediately preceding the detected systolic peaks
% Define the global search windows to find the possible dicrotic notch points
start1=round(0.034*rate);    % start search for notch 34 ms after PSP (global search)
end1=round(0.280*rate);    % end search for notch 280 ms after PSP (global search)
for i=1:length(systole)
    winstart1(i)=systole(i)+start1;
    if winstart1(i)>nbp-start1
        winstart1(i)=nbp-start1;    % ran out of data.:no samples in search window
    end
end

```

```

    end;
end;
for i=1:(length(systole)-1)
    winend1(i)=systole(i)+end1;
    if winend1(i)>systole(i+1)
        winend1(i)=systole(i+1);
    elseif winend1(i)>(nbp-start1)
        winend1(i)=nbp-start1; % ran out of data::too few samples in search window
    end;
end;
winend1(length(systole))=nbp-start1; % end of search window for last cardiac cycle

% Global search to find dicrotic notch (uses weighted sum of 11 samples in time window)
for i=1:length(winstart1)
    for n=winstart1(i):winend1(i); % search window for global search
        weight1(i,n)=BPfilt(n-5)+BPfilt(n-3)+BPfilt(n-1)-
            6*BPfilt(n+1)+BPfilt(n+2)+BPfilt(n+4)+BPfilt(n+6);
    end;
    [globe(i),notch1(i)]=max(weight1(i,:));
end;
% Set window durations for local search for the dicrotic notch
for i=1:length(notch1)
    winstart2(i)=notch1(i)-5;
    if winstart2(i)<=0
        winstart2(i)=2;
    end;
end;

```

```

winend2(i)=notch1(i)+5;
if winend2(i)>length(BPfilt)-2
    winend2(i)=length(BPfilt)-2;
end;
end;
% Local search to find the dicrotic notch (use weighted sum of 3 sample pts in window)
for i=1:length(winstart2)
    for n=winstart2(i):winend2(i);    % search window for global search
        weight2(i,n)=BPfilt(n-1)-2*BPfilt(n+1)+BPfilt(n+2);
    end;
    [globe(i),notch(i)]=max(weight2(i,:));
end;
% END OF PROGRAM

```

A.3 Jundanian Algorithm

```
% Systolic peak and diastolic value (end diastole) detection algorithms based on [53]
% Sliding slope bars method
% 80 msec slope bar = 14.4 samples [14 samples = 77.78 ms] (with sample rate = 180 Hz)
% 40 msec slope bar = 7.2 samples [7 samples = 38.89 ms] (with sample rate = 180 Hz)
%
%           SYSTOLIC PEAK DETECTOR
% test 80 ms slope bar condition (find slope between 2 pts: (i and i+14 points)
% criteria: ((i+14) - i)/80 ms >= 16 mmHg/80 ms (0.2)
% is approx: ((i+14) - i)/77.78 >= 15.56 mmHg/77.78 ms (0.20005)
% then find next minimum (slope changes from + to -)
numsys=1;
i=1;
while i<=(nbp-14)
    if (BP(i+14)-BP(i)) >= 15.56
        i=i+14;
        maxima(numsys)=BP(i-1);
        stop=0;
        while stop==0;
            if BP(i)>=maxima(numsys)
                maxima(numsys)=BP(i);
                i=i+1;
                if i>=length(BP)
                    stop=1;
                end;
            else systole(numsys)=i;
```

```

        numsys=numsys+1;
        i=i+1;
        stop=1;
    end;
end;          % end while: search for maximum point
else i=i+1;
end;
end;
%          DIASTOLIC VALUE DETECTOR
% test 40 ms slope bar condition (find slope between 2 pts: (i and i+7 points)
% criteria: ((i+7) - i)/40 ms <= -5 mmHg/40 ms (-0.125)
% is approx: ((i+7) - i)/38.89 <= -4.861 mmHg/38.89 ms (-0.12499)
% then find next minimum (slope changes from - to +)
numnotch=1;
i=1;
while i<=(nbp-7)
    if (BP(i+7)-BP(i)) <= -4.861
        i=i+7;
        minima(numnotch)=BP(i-1);
        stop=0;
        while stop==0
            if BP(i)<=minima(numnotch)
                minima(numnotch)=BP(i);
                i=i+1;
                if i==nbp
                    stop=1;

```



```
end;
else notch(numnotch)=i;
numnotch=numnotch+1;
i=i+1;
stop=1;
end;
end;
else i=i+1;
end;
end;
```

A.4 Martino Algorithm

```
% This program locates the dirotic notch using the algorithm presented in [54].
% Apply 2nd order 1.2 Hz cutoff LP Butterworth filter to BP
cutoff=1.2/(rate/2);          % filter parameter for cutoff freq = 1.2 Hz.
[b,c]=butter(2,cutoff);      % generate Butterworth filter coeffs
BPfilt=filter(b,c,BP);       % signal has no phase delay
% Compare original data with filtered (shifted) version
compare=0;                    % initialization
for i=1:nbp
    t(i)=i*(1/rate) - (1/rate);
    if BP(i) > BPfilt(i)
        compare(i)=100;
    elseif BP(i) < BPfilt(i)
        compare(i)=0;
    end;
end;
% Determine sample # of upstrokes (when 'compare' goes from 0 to 1)
% and the sample # of downstrokes (when 'compare' goes from 1 to 0)
numups=0;
numdowns=0;
for i=1:(nbp-1)
    if compare(i)==0 & compare(i+1)>0
        numups=numups+1;
        upstroke(numups)=i+1;
    end;
```

```

    if compare(i)>0 & compare(i+1)==0
        numdowns=numdowns+1;
        dnstroke(numdowns)=i+1;
    end;
end;
% Organize upstrokes with corresponding downstrokes
numdowns=0;
for i=1:length(upstroke)
    for n=1:length(dnstroke)
        if upstroke(i)<dnstroke(n)
            numdowns=numdowns+1;
            downstroke(numdowns)=dnstroke(n);
            break
        end;
    end;
end;
end;
% Calculate the first difference of the filtered blood pressure waveform
BPderiv=diff(BPfilt);
% Generate search window for the dicrotic notch
window=0.200*rate;          % dicrotic notch search window duration (in sample #s)
% find notch location in time window (200 msec after each dnstroke) using derivative
numnotch=0;
for i=1:length(downstroke)
    counter=0;
    for n=downstroke(i):min((downstroke(i)+window),length(BPderiv))
        if BPderiv(n)>0

```

```
    counter=counter+1;
end;
if counter==4
    numnotch=numnotch+1;
    notch(numnotch)=n;
    break
elseif BPderiv(n)<0
    counter=0;
end;
end;
end;
% END OF PROGRAM
```

A.5 Kinias Algorithm

```
% This program locates the dicrotic notch using the algorithm presented by [55].
P=BP; % Blood pressure data
scale=3; % exponent for chord length
n=2^scale; % initial length of slope analysis chord (need a power of 2)
thresh=10; % Threshold of blood pressure = 10 mmHg
numpoint=0; % initialize # of bent points found
for k=1:(nbp-n) % do until all data points are exhausted (STEP 1)
    delP(k)=P(k+n)-P(k); % n-difference at time k
% Compare the magnitude of delP to the threshold to define the class of the n-difference
    if (delP(k)>0 & (abs(delP(k))>thresh)) % class = + (designated by 1)
        class(k)=1;
    elseif (delP(k)>0 & (abs(delP(k))<thresh)) % class = +0 (designated by 10)
        class(k)=10;
    elseif (delP(k)<0 & (abs(delP(k))>thresh)) % class = - (designated by -1)
        class(k)=-1;
    elseif (delP(k)<0 & (abs(delP(k))<thresh)) % class = -0 (designated by -10)
        class(k)=-10;
    end;
end; % end for k=1:(nbp-n)
for k=2:length(class) % (STEP 2)
% test to see if class of delP(k-1) compared to class of delP(k) suggests a change of
direction (Table 1)
    if class(k-1)==1 & abs(class(k))==10
        action(k)=2; % class H2
    elseif class(k-1)==-1 & class(k)==10
```



```

        action(k)=-2; % class L2
elseif class(k-1) ~= 1 & class(k)==1
        action(k)=-1; % class L1
elseif class(k-1)==-1 & class(k)==-10
        action(k)=-2; % class L2 % changed from table 1 ( L1 to L2 class)
elseif class(k-1) ~= -1 & class(k)==-1
        action(k)=1; % class H1
else
        action(k)=0; % "no class" designation
end;
end; % end for k=2:length(class)
k=2; % initialize start of class comparison time
while k<=(length(delP)-1) % can analyze only available n differences -1
if action(k) ~= 0 % a change in direction has occurred else do next k = k+1
% Start bent point selection process (STEP 3)
start=k; % initialize interval for bent point search
finish=k+n; % set search time interval k to k+n
stop=0;
while stop==0 % bent point found if stop=1
j=n/2; % length of sub chord in interval (k to k+n)
if ((delP(start)>0 & delP(start+1)<0) | (delP(start)<0 & delP(start+1)>0))
if j==1 % change of sign occurs. Redefine search time interval
        numpoint=numpoint+1;
        bentpt(numpoint,1)=start+1;
        bentclass(numpoint)=action(k);
        stop=1;
else

```

```

        start=start+1;
        finish=start+1+j;
    end;
else numpoint=numpoint+1;    % no sign change. Take sample # of 1st point in
interval as the bent point
    bentpt(numpoint,1)=start;
    bentclass(numpoint)=action(k);
    stop=1;
end;
end;                                % end while stop = 0 search for bent point
end;                                % end if action ~=0 loop
k=k+1;                              % obtain next sample of data to analyze
end;                                % end while k<=(length(delP)-1)
% End of the search for bent points
% Start search for characteristics of the BP (end diastole, systolic peak and dicrotic notch)
% Generate u,(upstrokes) i (inflections) and d (downstroke) pts from bentpt array (Step 4)
numd=0;                              % initialize # of 'd's found
numi=0;                              % initialize # of 'i's found
numu=0;                              % initialize # of 'u's found
for m=2:length(bentpt(:,1))
    if bentclass(m-1)==1 & bentclass(m)<0
        numd=numd+1;
        bentpt(m,2)=-1;              % bentpt class = 'd' (downstroke)
        delvd(numd,1)=bentpt(m,1); % include sample # identification with delvd code
        delvd(numd,2)=P(bentpt((m-1),1))-P(bentpt((m),1)); % 'voltage' diff of 2 bent pts
        alphad(numd,1)=bentpt((m-1),1); % bentpt sample # of 1st pt in 'd' ID
    end
end

```

```

    alphad(numd,2)=bentpt(m,1); % bentpt sample # of 2nd pt used in 'd' identification
elseif bentclass(m-1)==-1 & bentclass(m)>0
    numu=numu+1;
    bentpt(m,2)=1; % bentpt class = 'u' (upstroke)
    delvu(numu,1)=bentpt(m,1);
    delvu(numu,2)=P(bentpt((m-1),1))-P(bentpt(m,1)); % 'voltage' diff of 2 bent pts
    alphau(numu,1)=bentpt((m-1),1); % bentpt sample # of 1st pt in 'u' ID
    alphau(numu,2)=bentpt(m,1); % bentpt sample # of 2nd point used in 'u' ID
elseif abs(bentclass(m-1))==2 & abs(bentclass(m))==1
    numi=numi+1;
    bentpt(m,2)=10; % bentpt class = 'i' (inflection point)
    delvi(numi,1)=bentpt(m,1);
    delvi(numi,2)=P(bentpt((m-1),1))-P(bentpt(m,1)); % 'voltage' diff of the 2 bent pts
    alphai(numi,1)=bentpt((m-1),1); % bentpt sample # of 1st point used in 'i' ID
    alphai(numi,2)=bentpt(m,1); % bentpt sample # of 2nd point used in 'i' ID
end;
end;
% Analyze array of 'u's and generate array of accepted 'u's according to p.215.
% Determine (for all 2 second zones) the acceptable 'u's
numsamp=rate*2; % rate (Hz) * 2 sec = # of samples in 2 seconds
numzones=round(nbp/numsamp); % # of available 2 sec zones in BP data
totalu=0; % initialize total # of accepted 'u's

for zone=1:numzones
    samples=numsamp*zone; % cumulative # of samples to the end of this zone
    numu=0; % initialize # of selected 'u' s in zone

```

```

clear uindex orderP zoneu zoneP acceptu % clear previous zone information
if zone==1
% Step 5: Start of monitoring the first zone & test for acceptable ratios.
% Truncate data for initial 2 sec interval 'starting zone'. Test zone for good ratios of 'u's
% pairs. The last 'u' in this zone is used to define 'u' ratios for subsequent 2 sec zones.
% Up to 8 'u's (in zone) w/the largest delv are arranged in order of magnitude.
for i=1:length(alphau) % find all 'u' s in zone
    if (alphau(i,2) ~=0 & alphau(i,2)<=samples) % 'u' is w/in zone
        numu=numu+1; % # of 'u' in this zone
        zoneu(numu)=alphau(i,2);
        zoneP(numu)=P(alphau(i,2)); % pressure at 'u' location in this zone
    end;
    if numu>8 % only want to analyze a max of 8 'u' in zone
        break; % break out of for loop if have > 8 'u's
    end;
end;
[orderP,uindex]=sort(zoneP); % pressure and original index of 'u' pts in this zone
% The ratios of of the delv's of the ordered 'u' are computed (step 5.2):
if length(uindex)>1
for i=2:length(uindex)
    ratio=delvu(uindex(i-1),2)/delvu(uindex(i),2);
    if ratio>2 % 'u's between uindex(i) and length(uindex) are rejected as 'u'
        uindex=uindex(1:(i-1)); % resize uindex eliminating rejected 'u's
        reject=1; % flag indicating 'u' rejection has occurred
        break; % no need to check rest of 'u's in zone
    end;
end;

```

```

end;
end; % end if length(uindex)>1
elseif zone>1
    for i=(totalu+1):length(alphau) % find all 'u' s in zone
        if (alphau(i,2)>u0(zone-1) & (alphau(i,2)<=samples)) % 'u' is w/in zone
            numu=numu+1; % # of 'u' in this zone
            zoneu(numu)=alphau(i,2);
            zoneP(numu)=P(alphau(i,2)); % pressure (mmHg) at 'u' location in this zone
        end;
        if numu>8 % only want to analyze a max of 8 'u' in zone
            break; % break out of for loop if have > 8 'u's
        end;
    end;
    [orderP,uindex]=sort(zoneP); % pressure & original index of 'u' points in this zone
    % The ratios of of the delv's of the ordered 'u' are computed (step 5.2):
    if length(uindex)>1
        for i=2:length(uindex)
            ratio=delvu((totalu+uindex(i-1)),2)/delvu((totalu+uindex(i)),2);
            % 'u's between uindex(i) and length(uindex) are rejected as 'u'
            if (delvu(totalu,2)>=(2*delvu(uindex(1),2)) & ratio>2)
                uindex=uindex(1:(i-1)); % resize uindex eliminating rejected 'u's
                reject=1; % flag indicating 'u' rejection has occurred
                break; % no need to check rest of 'u's in zone
            end;
        end;
    end;
end; % end if length(uindex)>1

```



```

end;                % end if zone==1
% Reorder 'u's (with appropriate 'u's removed)
orderindex=sort(uindex);
for i=1:length(uindex)
    acceptu(i)=alphau(totalu+orderindex(i),2);    % sample location of accepted 'u's
    finalu(totalu+i)=acceptu(i);                % final array of accepted 'u's
end;
totalu=totalu+length(acceptu);    % accumulated total # of 'u's accepted thus far
% The last entry in acceptu is the 'u' to compare the next zone 'u's
u0(zone)=acceptu(length(acceptu));
end;                % for zone = 1:numzones
% Define cardiac "cycle" relative to accepted upstrokes ('u's). Start every cycle on 'u'
thresh2=0.5;        % threshold for 'u's to define cycle
for i=1:length(finalu)
    for m=1:length(alphau)    % find matching delvu entry for finalu entry
        if alphau(m,2)==finalu(i)    % found correct index for finalu entry
            if abs(delvu(m,2))>thresh2
                cycle(i)=finalu(i);    % cycle starts at upstroke 'u'
            end;
        end;
    end;
end;
end;
end;
% Determine if proper character strings occur = dicrotic notch (diu, did, di or du) (step 6)
c=1;                % cardiac cycle # to start (in zone)
while c<=length(cycle)
    numnotch1=0;    % reset # of dicrotic notches found per cycle

```

```

for i=2:(length(bentpt)-1)           % look at bentpts in selected area of interest (cycle)
    if c==length(cycle)              % organize end of cycle window for notch search
        cyclend=nbp;
    else cyclend=cycle(c+1);
    end;
    if (bentpt(i,1)>=cycle(c) & bentpt(i,1)<cyclend)
        if (bentpt((i-1),2)==-1 & bentpt(i,2)==10 & bentpt((i+1),2)==1) % string= 'diu'
            numnotch1=numnotch1+1;
            notch1(c,numnotch1)=bentpt((i-1),1);           % alphas(:,1) or alphas(:,2)
        elseif (bentpt((i-1),2)==-1&bentpt(i,2)==10 & bentpt((i+1),2)==1) % string= did
            numnotch1=numnotch1+1;
            notch1(c,numnotch1)=bentpt((i-1),1);
        elseif (bentpt((i-1),2)==-1 & bentpt(i,2)==10) % string = 'di'
            numnotch1=numnotch1+1;
            notch1(c,numnotch1)=bentpt((i-1),1);
        elseif (bentpt((i-1),2)==-1 & bentpt(i,2)==1)
            numnotch1=numnotch1+1;
            notch1(c,numnotch1)=bentpt((i-1),1);
        end;
    end;
end;
end;
c=c+1;           % do next cycle
end;           % end while c < length(cycle)-1
% If more than 1 did, diu etc sequence has appeared in a cycle, select the notch bentpt
with % the largest slope curvature (step 7)
for row=1:length(notch1(:,1))% for all rows in notch1 (# of cycles)

```

```

notch2=find(notch1(row,:)); % determine # of nonzero elements in notch1 (per cycle)
if length(notch2)>1      % if there are > 1 possible notches in this cycle
    for col=1:length(notch1(row,:))
        for i=1:length(bentpt);% find bentpt index for notch1 to calc slopes & curvature
            if notch1(row,col)==bentpt(i,1)
                slope1=(delP(bentpt(i,1))-delP(bentpt((i+1),1)))/(bentpt(i,1)-
                                                                    bentpt((i+1),1));
                slope2=(delP(bentpt((i+1),1))-
                        delP(bentpt((i+2),1)))/(bentpt((i+1),1)-bentpt((i+2),1));
                curve(col)=abs(slope1*slope2);    % calc curvature of character string
                break;                            % found slopes for this notch string
            end;
        end;
        % find curvature for next notch1 string in this cycle
    end;
    [maxcurve,maxindex]=max(curve); % which notch1 col has > curvature (in row)
    notch3(row)=notch1(row,maxindex); % notch pt is notch1 with > curve in cycle
    else notch3(row)=notch1(row,1); % if only 1 string found then notch1 is the notch pt
end; % end notch selection for this cycle
end; % end of notch array determination

% Eliminate zeros in notch3 array to achieve array of valid dicrotic notch sample locations
index=find(notch3); % find indices of nnzero array elements
numnotch=length(index); % # of valid notches (# of nonzero elements)
for i=1:numnotch
    notch(i)=notch3(index(i));
end;

```

A.6 Elghazzawi Algorithm

```
% This program locates the dicrotic notch using the algorithm presented by [51]
% ECG R wave detection algorithm (to set search window for end diastole)
% R-wave = max of section above threshold (80% of global maximum)
thresh=max(ecg)*0.70;           % set threshold magnitude for R wave spike
for i=1:nbp
    height(i)=thresh;
end;
% Locate sample # of threshold crossings
numups=0;                       % # of threshold upslope crossings found
numdowns=0;                     % # of threshold downslope crossings found
for i=1:nbp-1
    if ecg(i)<=thresh & ecg(i+1)>=thresh
        numups=numups+1;
        upslope(numups)=i;      % ordered sample #s of upslopes found
    end;
    if ecg(i)>=thresh & ecg(i+1)<=thresh
        numdowns=numdowns+1;
        dnslope(numdowns)=i;    % ordered sample #s of downslopes found
    end;
end;
% Find sample # of maximum in each section found above threshold
% Sample # of max search must start at upslope and end at downslope threshold crossing
if ((numups ~=0)&(numdowns ~=0)) % Need at least 1 threshold crossing pair
```

```

% If analysis waveform has the 1st upslope detected before a downslope:
if upslope(1)<dnslope(1)
    for i=1:numdowns
        [pks(i),offset(i)]=max(ecg(upslope(i):dnslope(i)));
        rwave(i)=upslope(i)+(offset(i)-1);
    end;
% If analysis waveform has the 1st downslope detected before an upslope:
elseif dnslope(1)<upslope(1)
    for i=1:numdowns-1
        [pks(i),offset(i)]=max(ecg(upslope(i):dnslope(i+1)));
        rwave(i)=upslope(i)+(offset(i)-1);           % sample # of maxima
    end;
end;
end;
end;                                     % end of analyzing threshold crossing pairs
% Calculate R to R interval (in time)
for i=1:(length(rwave)-1)
    RR(i)=(rwave(i+1)-rwave(i))/rate;           % R to R wave time interval in seconds
    HR(i)=1/RR(i)*60;                          % heart rate (bpm)
    rr(i)=rwave(i+1)-rwave(i);                % R to R time interval in samples
end;
% Calculate the 1st derivative of the BP waveform
BPderiv1=diff(BP);
% Locate PSP and ED by locating the maximum and minimum of the BP waveform
% using zero crossings and change in slope direction of the derivative of the BP (dP/dt).
% Find where BPderiv1 goes from + to - (for finding systolic peaks)
numpeak1=0;                                   % # of end diastoles found

```



```

    end;

end;

%          SYSTOLIC PEAK DETECTION
% Locate last maximum in time window after Rwave::systolic peak detection
systole(i)=rwave(i)+round(rr(i)*0.25);    % initialization
for n=(rwave(i)+round(rr(i)*0.25)):(rwave(i)+round(rr(i)*0.60))
    for m=1:length(posneg1)
        if posneg1(m)==n
            if BP(n)>=BP(systole(i))
                systole(i)=n;
            end;
        end;
    end;
end;

end;

end;

end;

end;

end;

% end loop for rr cycles (finding all end diastoles and systolic peaks)
for i=1:(length(rr)-1)    % find dicrotic notches in all cycles
%          DICROTIC NOTCH DETECTION
% Dicrotic notch detection using - to + slope change and search window principles
% Locate 1st - to + slope change between (systole + 10%rr) to (systole + 70% of rr)
m=1;
n=systole(i)+round(rr(i)*0.10);    % search window starts at 10% of rr after notch
stop=0;
while stop==0
    if negpos1(m)==n
        notch(i)=n;
        stop=1;
    end;
end;

```

```

for i=1:(length(BPderiv1)-1)
    if BPderiv1(i)>=0 & BPderiv1(i+1)<=0
        numpeak1=numpeak1+1;
        posneg1(numpeak1)=i;
    end;
end;
% Find where BPderiv1 goes from - to + (for finding end diastoles and dicrotic notches)
numfoot1=0; % # of end diastoles found
for i=1:(length(BPderiv1)-1)
    if BPderiv1(i)<=0 & BPderiv1(i+1)>=0
        numfoot1=numfoot1+1;
        negpos1(numfoot1)=i;
    end;
end;
%
%           END DIASTOLE DETECTION
% Locate last min in time window after Rwave by identifying the max amplitude sample #
% of a - to + slope change within the appropriate time search window for each rr interval
for i=1:length(rr)
    diastole(i)=rwave(i); % initialization of possible end diastole sample locations
    for n=rwave(i):(rwave(i)+round(rr(i)*0.25)) %window=25% R-R intervals (in samples)
        for m=1:length(negpos1)
            if negpos1(m)==n
                if BP(n)<=BP(diastole(i))
                    diastole(i)=n;
                end;
            end;
        end;
    end;
end;

```

APPENDIX B

Tabular Performance Results of the Dicrotic Notch Detection Algorithms for each of the test sets (A) 30 files; (B) 50 files; (C) 72 files.

Filename	#Cycles	Wavelet			Lee			Jundanian			Martino			Kinias			Elghazzawi		
		TP	FP	FN	TP	FP	FN	TP	FP	FN	TP	FP	FN	TP	FP	FN	TP	FP	FN
FILE003	13	13	0	0	11	2	2	1	12	12	7	6	6	4	5	9	2	11	11
FILE004	7	7	0	0	6	0	1	4	9	3	7	0	0	7	0	0	6	1	1
FILE005	11	11	0	0	0	9	11	4	7	7	0	11	11	0	11	11	10	0	1
FILE007	9	9	0	0	8	1	1	9	5	0	9	0	0	9	0	0	9	0	0
FILE008	7	7	0	0	7	0	0	7	0	0	5	2	2	1	6	6	7	0	0
FILE009	11	11	0	0	9	0	2	1	23	10	11	0	0	11	0	0	2	10	9
FILE010	12	5	7	7	1	10	11	12	0	0	2	10	10	0	12	12	12	0	0
FILE015	9	9	0	0	8	1	1	9	0	0	8	1	1	1	8	8	9	0	0
FILE019	9	9	0	0	6	0	3	2	7	7	4	5	5	2	7	7	8	1	1
FILE020	12	11	1	1	6	4	6	0	11	12	10	2	2	8	4	4	0	11	12
FILE021	11	0	11	11	3	8	8	11	12	0	11	1	0	0	8	11	0	11	11
FILE022	9	9	0	0	8	0	1	5	9	4	1	8	8	3	1	6	5	4	4
FILE023	11	11	0	0	4	0	7	0	15	11	9	1	2	8	3	3	1	10	10
FILE027	8	8	0	0	5	0	3	7	1	1	7	0	1	2	6	6	8	0	0
FILE031	14	11	3	3	7	7	7	14	1	0	1	13	13	1	13	13	14	0	0
FILE032	9	9	0	0	6	0	3	9	8	0	9	0	0	6	3	3	9	0	0
FILE033	11	0	11	11	1	10	10	10	4	1	0	11	11	0	11	11	9	2	2
FILE034	5	5	0	0	1	4	4	5	4	0	5	0	0	2	3	3	5	0	0
FILE036	7	1	6	6	1	6	6	6	1	1	0	7	7	0	7	7	7	0	0
FILE046	12	9	0	3	1	0	11	6	8	6	4	5	8	7	3	5	7	4	5
FILE089	11	4	7	7	6	5	5	9	50	2	7	7	4	1	2	10	5	6	6
FILE113	9	9	0	0	9	0	0	8	1	1	7	2	2	0	0	9	8	0	1
FILE120a	8	4	3	4	0	5	8	8	6	0	6	2	2	2	4	6	6	3	2
FILE120b	7	7	0	0	2	7	5	7	7	0	7	0	0	5	2	2	6	1	1
FILE121	10	5	5	5	0	10	10	10	0	0	0	10	10	0	10	10	10	0	0
FILE126a	6	5	1	1	2	6	4	6	5	0	5	1	1	0	5	6	2	3	4
FILE126b	5	0	5	5	1	5	4	5	5	0	5	0	0	0	5	5	4	1	1
FILE128	10	10	0	0	0	6	10	10	0	0	8	1	2	1	3	9	10	0	0
FILE136	12	12	0	0	0	12	12	2	0	10	11	1	1	0	0	12	9	3	3
FILE137	9	9	0	0	9	0	0	1	8	8	7	2	2	0	0	9	1	7	8
Total	284	220	60	64	128	118	156	188	219	96	173	109	111	81	142	203	191	89	93
Sensitivity	%	77.5			45			66.2			61			29			67.3		
+Productivity	%	78.6			52			46.2			61			36			68.2		
FP Rate	%	21.1			42			77.1			38			50			31.3		
FN Rate	%	22.5			55			33.8			39			71			32.7		

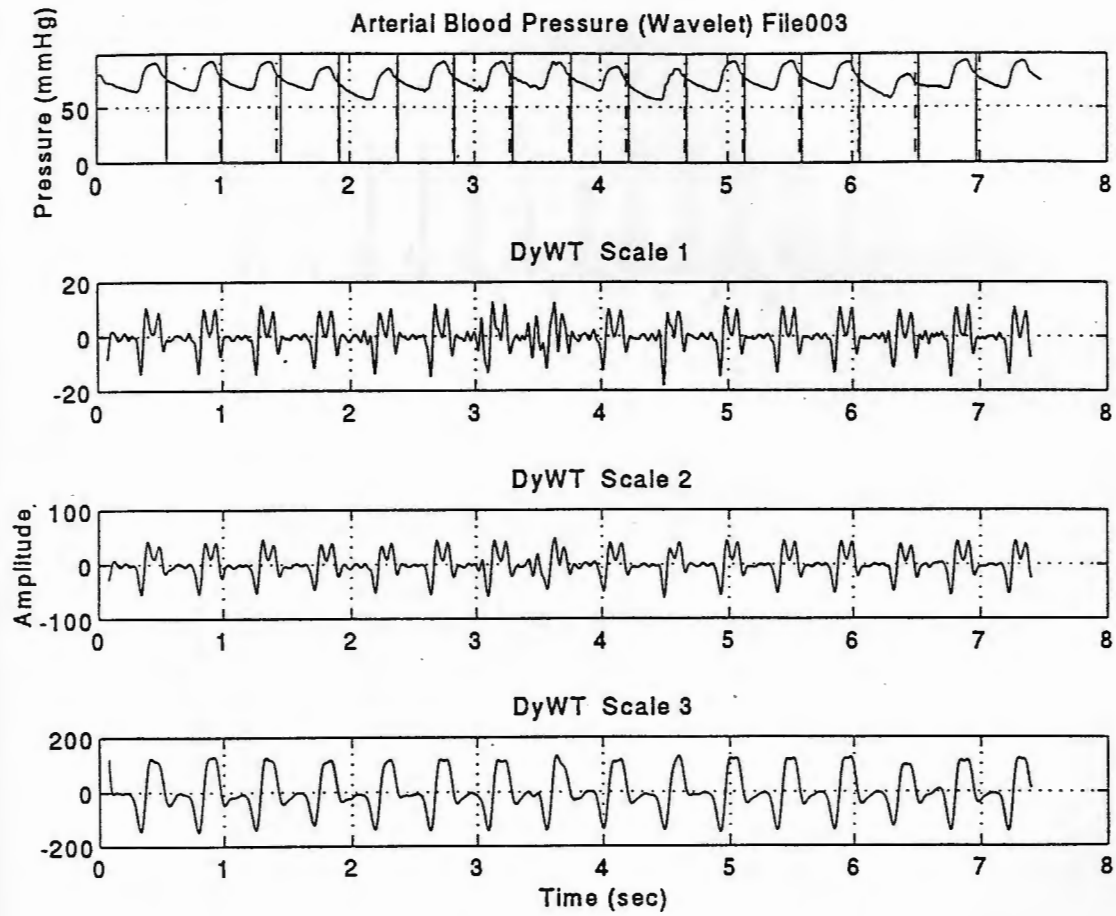
Filename	#Cycles	Wavelet			Lee			Jundanian			Martino			Kinias			Elghazzawi		
		TP	FP	FN	TP	FP	FN	TP	FP	FN	TP	FP	FN	TP	FP	FN	TP	FP	FN
FILE001	18	18	0	0	13	0	5	7	11	11	16	2	2	10	8	8	11	7	7
FILE003	58	54	4	4	46	11	12	4	56	54	32	26	26	20	24	38	9	47	49
FILE005	46	16	30	30	1	35	45	4	43	42	3	43	43	0	46	46	32	3	14
FILE007	41	41	0	0	26	1	15	41	15	0	41	0	0	40	1	1	41	0	0
FILE009	48	48	0	0	46	0	2	3	106	45	48	0	0	43	5	5	7	41	41
FILE010	12	5	7	7	1	10	11	12	0	0	2	10	10	0	12	12	12	0	0
FILE011	33	30	3	3	22	2	11	0	33	33	25	2	8	5	28	28	15	17	18
FILE012	49	47	2	2	35	3	14	38	13	11	11	38	38	3	46	46	36	5	13
FILE013	34	29	4	5	0	0	34	14	42	20	29	6	5	1	6	33	3	12	31
FILE014	43	38	1	5	17	4	26	43	31	0	40	3	3	32	11	11	39	0	4
FILE015	35	35	0	0	13	0	22	34	1	1	33	2	2	15	20	20	30	5	5
FILE016	23	16	7	7	5	17	18	23	0	0	3	20	20	0	23	23	23	0	0
FILE019	35	35	1	0	11	0	24	18	17	17	8	27	27	10	25	25	29	4	6
FILE020	47	23	24	24	12	21	35	0	47	47	6	41	41	44	3	3	0	33	47
FILE021	11	0	11	11	3	8	8	11	12	0	11	1	0	0	8	11	0	11	11
FILE023	11	11	0	0	4	0	7	0	15	11	9	1	2	8	3	3	1	10	10
FILE027	35	35	0	0	20	0	15	31	4	4	34	0	1	18	17	17	32	2	3
FILE029	41	41	0	0	40	0	1	41	41	0	25	15	16	33	8	8	39	1	2
FILE031	56	52	5	4	42	8	14	56	12	0	13	43	43	2	54	54	49	3	7
FILE034	25	25	0	0	16	9	9	25	24	0	25	0	0	5	20	20	25	0	0
FILE035	20	20	0	0	9	11	11	19	2	1	0	20	20	1	19	19	16	1	4
FILE037	30	28	2	2	23	2	7	30	0	0	2	28	28	0	30	30	9	4	21
FILE039	28	23	5	5	15	3	13	15	74	13	25	31	3	10	19	18	16	12	12
FILE069	22	1	21	21	0	9	22	4	18	18	0	22	22	0	22	22	3	2	19
FILE076	27	25	0	2	0	12	27	27	47	0	8	19	19	8	7	19	26	0	1
FILE077	24	24	0	0	0	13	24	24	45	0	0	25	24	1	9	23	24	0	0
FILE082	22	22	0	0	7	9	15	22	13	0	14	10	8	11	6	11	17	5	5
FILE084	23	22	0	1	23	0	0	11	56	12	23	0	0	0	22	23	2	15	21
FILE088	14	14	0	0	11	0	3	5	32	9	14	1	0	8	6	6	7	7	7
FILE089	11	4	7	7	6	5	5	9	50	2	7	7	4	1	2	10	5	6	6
FILE090	15	15	0	0	15	15	0	15	16	0	15	0	0	15	0	0	13	2	2
FILE091	21	21	0	0	0	21	21	21	0	0	0	21	21	0	21	21	21	0	0
FILE095	25	25	0	0	16	7	9	25	25	0	25	10	0	19	13	6	25	0	0
FILE101	14	1	12	13	0	14	14	4	10	10	0	14	14	0	14	14	7	3	7
FILE102	13	11	2	2	11	2	2	11	8	2	0	14	13	0	9	13	5	4	8
FILE108	22	19	0	3	11	0	11	15	7	7	18	7	4	11	9	11	2	11	20
FILE112	17	17	0	0	17	0	0	17	0	0	8	9	9	3	14	14	17	0	0
FILE113	18	17	1	1	17	1	1	18	5	0	18	1	0	0	2	18	12	2	6
FILE115	23	22	0	1	0	23	23	23	1	0	0	23	23	1	22	22	22	0	1
FILE117	24	23	1	1	15	0	9	24	0	0	0	24	24	0	22	24	15	9	9
FILE121	10	5	5	5	0	10	10	10	0	0	0	10	10	0	10	10	10	0	0
FILE127	13	13	0	0	13	0	0	10	6	3	0	13	13	4	9	9	13	0	0
FILE130	13	13	0	0	13	0	0	1	12	12	13	0	0	0	12	13	13	0	0
FILE132	26	26	0	0	16	0	10	2	41	24	25	0	1	14	12	12	2	22	24
FILE139	21	21	0	0	13	0	8	8	17	13	13	8	8	12	9	9	15	6	6
FILE140	21	18	1	3	4	3	17	13	17	8	6	16	15	2	16	19	14	4	7
FILE141	17	10	7	7	8	1	9	16	0	1	0	16	17	0	16	17	15	1	2
FILE145	23	23	0	0	13	0	10	8	16	15	14	9	9	0	13	23	16	7	7
FILE146	19	15	4	4	1	18	18	0	20	19	3	16	16	0	1	19	3	16	16
FILE147	24	24	0	0	0	7	24	24	1	0	22	0	2	22	1	2	19	3	5
Total	1301	1121	167	180	650	315	651	836	1062	465	687	654	614	432	735	869	817	343	484
Sensitivity	%	86.2			50			64.3			53			33			62.8		
+Productivity	%	87			67			44			51			37			70.4		
FP Rate	%	12.8			24			81.6			50			56			26.4		
FN Rate	%	13.8			50			35.7			47			67			37.2		

Filename	#Cycles	Wavelet			Lee			Jundanian			Martino			Kinias			Elghazzawi		
		TP	FP	FN	TP	FP	FN	TP	FP	FN	TP	FP	FN	TP	FP	FN	TP	FP	FN
FILE001	18	18	0	0	13	0	5	7	11	11	16	2	2	10	8	8	11	7	7
FILE003	58	54	4	4	46	11	12	4	56	54	32	26	26	20	24	38	9	47	49
FILE004	31	31	0	0	31	1	0	16	33	15	31	0	0	31	0	0	30	1	1
FILE005	46	16	30	30	1	35	45	4	43	42	3	43	43	0	46	46	32	3	14
FILE007	41	41	0	0	26	1	15	41	15	0	41	0	0	40	1	1	41	0	0
FILE008	7	7	0	0	7	0	0	7	0	0	5	2	2	1	6	6	7	0	0
FILE009	48	48	0	0	46	0	2	3	106	45	48	0	0	43	5	5	7	41	41
FILE010	12	5	7	7	1	10	11	12	0	0	2	10	10	0	12	12	12	0	0
FILE011	33	30	3	3	22	2	11	0	33	33	25	2	8	5	28	28	15	17	18
FILE012	49	47	2	2	35	3	14	38	13	11	11	38	38	3	46	46	36	5	13
FILE013	34	29	4	5	0	0	34	14	42	20	29	6	5	1	6	33	3	12	31
FILE014	43	38	1	5	17	4	26	43	31	0	40	3	3	32	11	11	39	0	4
FILE015	35	35	0	0	13	0	22	34	1	1	33	2	2	15	20	20	30	5	5
FILE016	23	16	7	7	5	17	18	23	0	0	3	20	20	0	23	23	23	0	0
FILE019	35	35	1	0	11	0	24	18	17	17	8	27	27	10	25	25	29	4	6
FILE020	47	23	24	24	12	21	35	0	47	47	6	41	41	44	3	3	0	33	47
FILE021	11	0	11	11	3	8	8	11	12	0	11	1	0	0	8	11	0	11	11
FILE022	9	9	0	0	8	0	1	5	9	4	1	8	8	3	1	6	5	4	4
FILE023	11	11	0	0	4	0	7	0	15	11	9	1	2	8	3	3	1	10	10
FILE027	35	35	0	0	20	0	15	31	4	4	34	0	1	18	17	17	32	2	3
FILE029	41	41	0	0	40	0	1	41	41	0	25	15	16	33	8	8	39	1	2
FILE030	20	0	14	20	0	9	20	10	10	10	0	20	20	0	20	20	18	2	2
FILE031	56	52	5	4	42	8	14	56	12	0	13	43	43	2	54	54	49	3	7
FILE032	9	9	0	0	6	0	3	9	8	0	9	0	0	6	3	3	9	0	0
FILE033	11	0	11	11	1	10	10	10	4	1	0	11	11	0	11	11	9	2	2
FILE034	25	25	0	0	16	9	9	25	24	0	25	0	0	5	20	20	25	0	0
FILE035	20	20	0	0	9	11	11	19	2	1	0	20	20	1	19	19	16	1	4
FILE036	7	1	6	6	1	6	6	6	1	1	0	7	7	0	7	7	7	0	0
FILE037	30	28	2	2	23	2	7	30	0	0	2	28	28	0	30	30	9	4	21
FILE039	28	23	5	5	15	3	13	15	74	13	25	31	3	10	19	18	16	12	12
FILE046	12	9	0	3	1	0	11	6	8	6	4	5	8	7	3	5	7	4	5
FILE060	16	15	1	1	14	17	2	16	70	0	16	6	0	7	6	9	1	15	15
FILE069	22	1	21	21	0	9	22	4	18	18	0	22	22	0	22	22	3	2	19
FILE071	14	13	1	1	8	1	6	5	11	9	1	13	13	0	12	14	0	6	14
FILE076	27	25	0	2	0	12	27	27	47	0	8	19	19	8	7	19	26	0	1
FILE077	24	24	0	0	0	13	24	24	45	0	0	25	24	1	9	23	24	0	0
FILE078	20	7	13	13	0	12	20	0	19	20	0	20	20	0	19	20	2	9	18
FILE082	22	22	0	0	7	9	15	22	13	0	14	10	8	11	6	11	17	5	5
FILE084	23	22	0	1	23	0	0	11	56	12	23	0	0	0	22	23	2	15	21
FILE085	29	29	0	0	21	8	8	29	29	0	8	21	21	25	4	4	26	0	3
FILE088	14	14	0	0	11	0	3	5	32	9	14	1	0	8	6	6	7	7	7
FILE089	11	4	7	7	6	5	5	9	50	2	7	7	4	1	2	10	5	6	6
FILE090	15	15	0	0	15	15	0	15	16	0	15	0	0	15	0	0	13	2	2
FILE091	21	21	0	0	0	21	21	21	0	0	0	21	21	0	21	21	21	0	0
FILE094	18	18	0	0	18	0	0	17	5	1	3	15	15	0	1	18	17	1	1
FILE095	25	25	0	0	16	7	9	25	25	0	25	10	0	19	13	6	25	0	0
FILE100	22	0	17	22	0	22	22	21	1	1	0	22	22	0	22	22	22	0	0
FILE101	14	1	12	13	0	14	14	4	10	10	0	14	14	0	14	14	7	3	7
FILE102	13	11	2	2	11	2	2	11	8	2	0	14	13	0	9	13	5	4	8
FILE103	14	14	0	0	5	0	9	10	4	4	13	1	1	0	13	14	13	0	1
FILE104	18	17	0	1	14	4	4	15	18	3	16	2	2	0	3	18	12	2	6
FILE108	22	19	0	3	11	0	11	15	7	7	18	7	4	11	9	11	2	11	20
FILE112	17	17	0	0	17	0	0	17	0	0	8	9	9	3	14	14	17	0	0
FILE113	18	17	1	1	17	1	1	18	5	0	18	1	0	0	2	18	12	2	6
FILE115	23	22	0	1	0	23	23	23	1	0	0	23	23	1	22	22	22	0	1
FILE116	16	16	0	0	16	0	0	16	0	0	6	10	10	0	13	16	14	0	2
FILE117	24	23	1	1	15	0	9	24	0	0	0	24	24	0	22	24	15	9	9
FILE120	15	9	6	6	0	12	15	15	13	0	15	0	0	2	11	13	9	3	6
FILE121	10	5	5	5	0	10	10	10	0	0	0	10	10	0	10	10	10	0	0

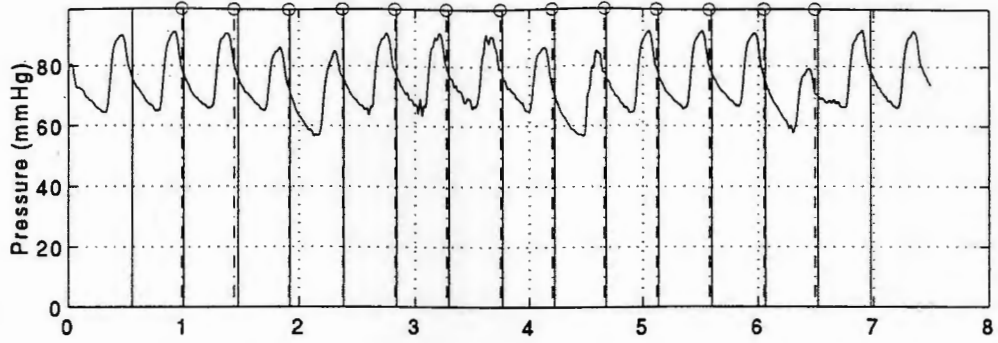
FILE126	12	11	1	1	3	10	9	12	10	0	12	0	0	0	10	12	4	7	8
FILE127	13	13	0	0	13	0	0	10	6	3	0	13	13	4	9	9	13	0	0
FILE130	13	13	0	0	13	0	0	1	12	12	13	0	0	0	12	13	13	0	0
FILE132	26	26	0	0	16	0	10	2	41	24	25	0	1	14	12	12	2	22	24
FILE137	17	16	1	1	10	0	7	0	17	17	7	10	10	0	0	17	0	11	17
FILE138	13	12	1	1	12	1	1	13	0	0	0	13	13	0	2	13	13	0	0
FILE139	21	21	0	0	13	0	8	8	17	13	13	8	8	12	9	9	15	6	6
FILE140	21	18	1	3	4	3	17	13	17	8	6	16	15	2	16	19	14	4	7
FILE141	17	10	7	7	8	1	9	16	0	1	0	16	17	0	16	17	15	1	2
FILE145	23	23	0	0	13	0	10	8	16	15	14	9	9	0	13	23	16	7	7
FILE146	19	15	4	4	1	18	18	0	20	19	3	16	16	0	1	19	3	16	16
FILE147	24	24	0	0	0	7	24	24	1	0	22	0	2	22	1	2	19	3	5
FILE149	16	16	0	0	14	0	2	8	7	8	12	4	4	1	15	15	14	2	2
Total	1647	1380	239	267	840	428	807	1082	1339	565	846	844	801	515	917	1132	1056	412	591
Sensitivity	%	83.8			51			65.7			51			31			64.1		
+Productivity	%	85.2			66			44.7			50			36			71.9		
FP Rate	%	14.5			26			81.3			51			56			25		
FN Rate	%	16.2			49			34.3			49			69			35.9		

Appendix C

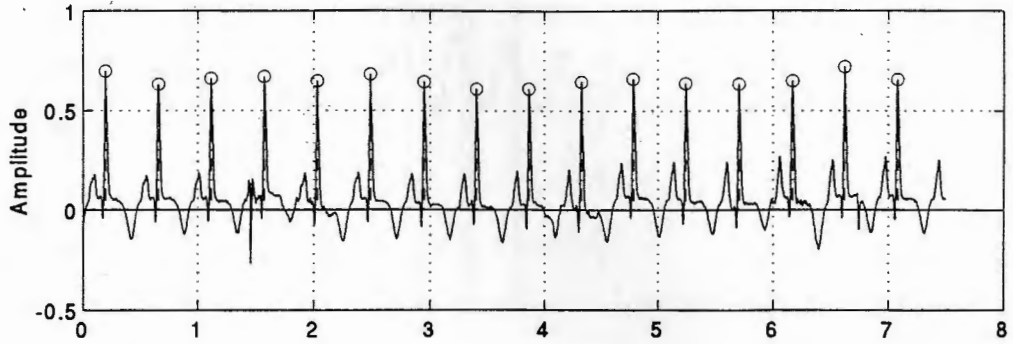
Graphical Results of Detection Algorithm Performance



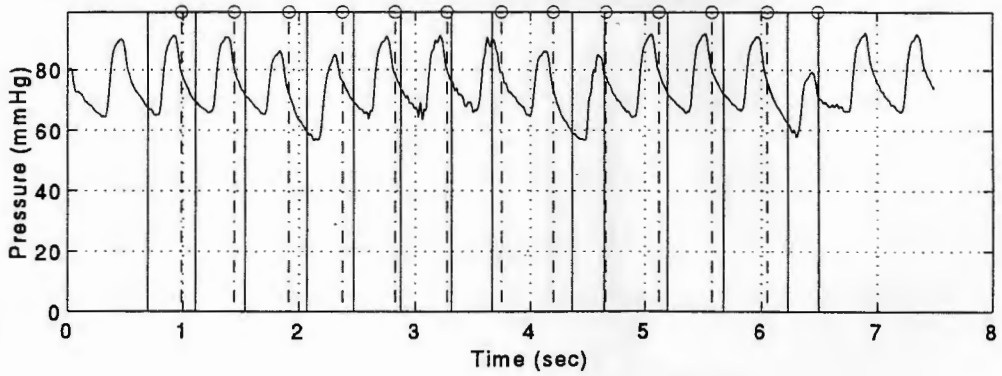
Arterial Blood Pressure (Wavelet) File003



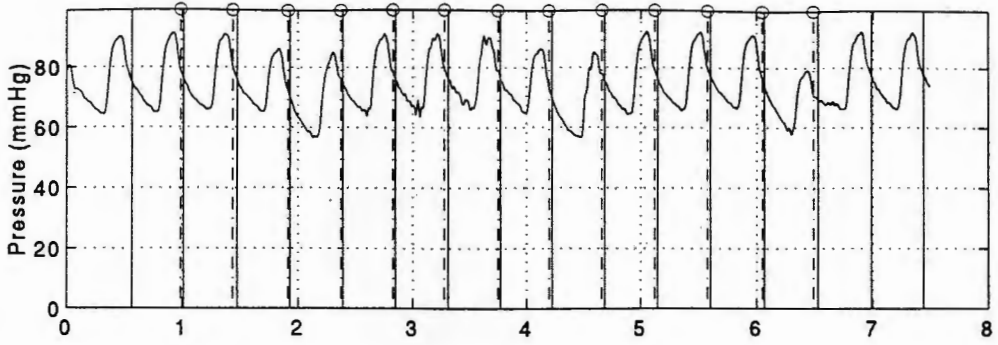
Electrocardiogram (ECG R waves) File003



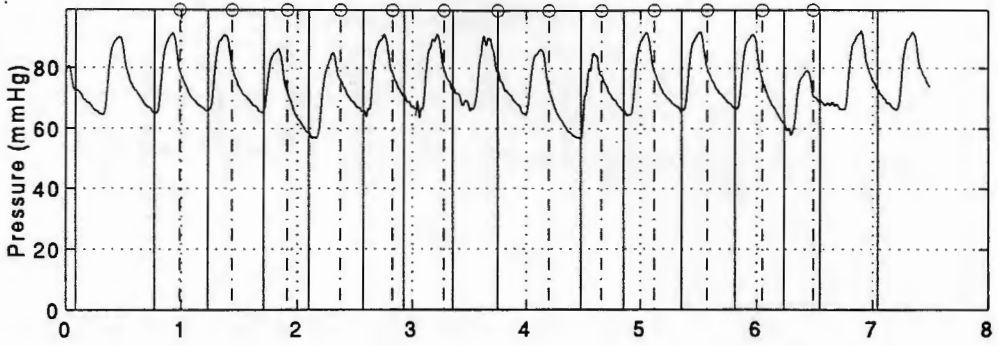
Arterial Blood Pressure (Eighazzawi) File003



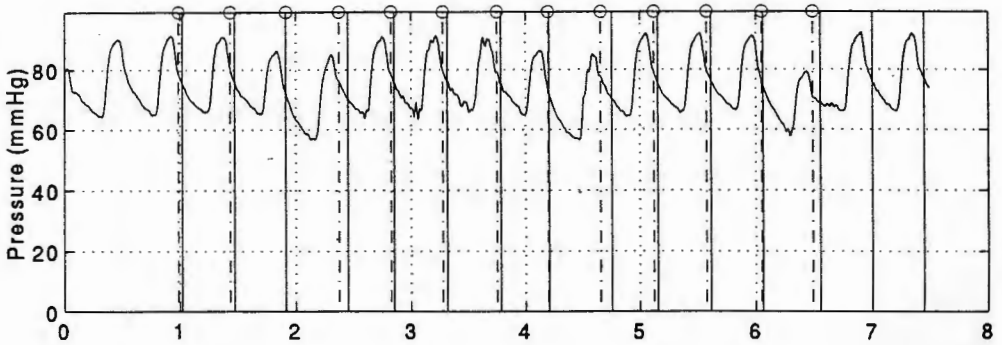
Arterial Blood Pressure (Lee) File003



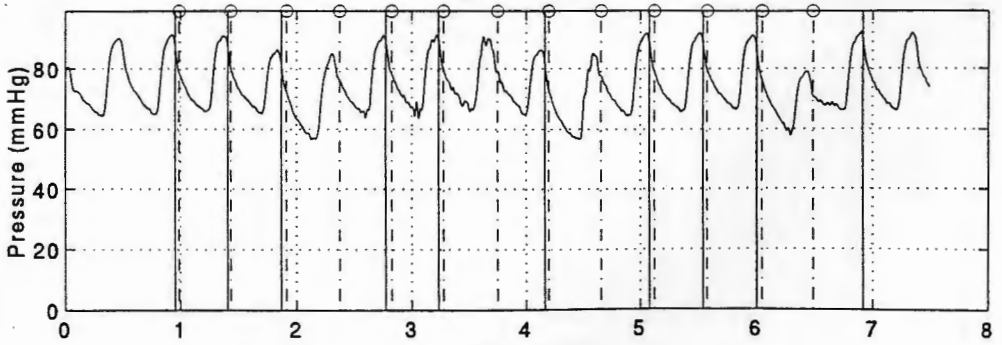
Arterial Blood Pressure (Jundanian) File003

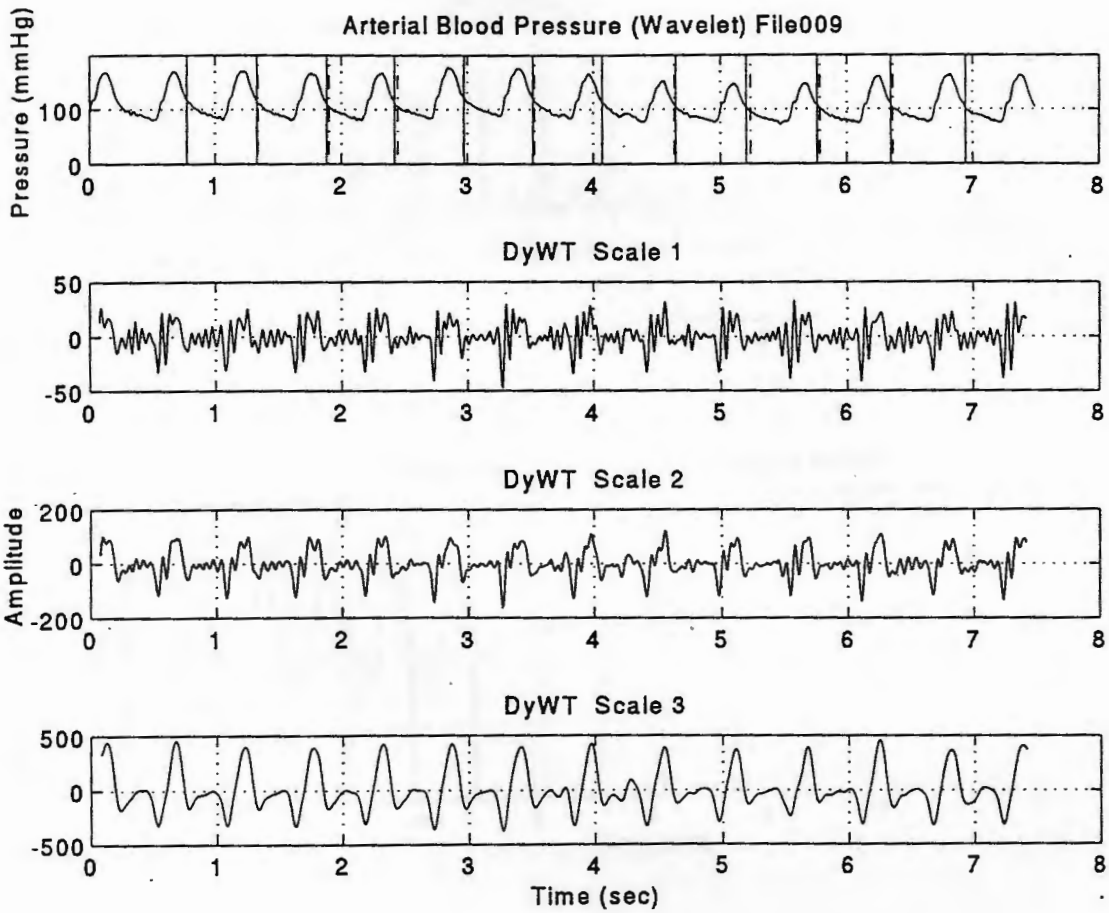


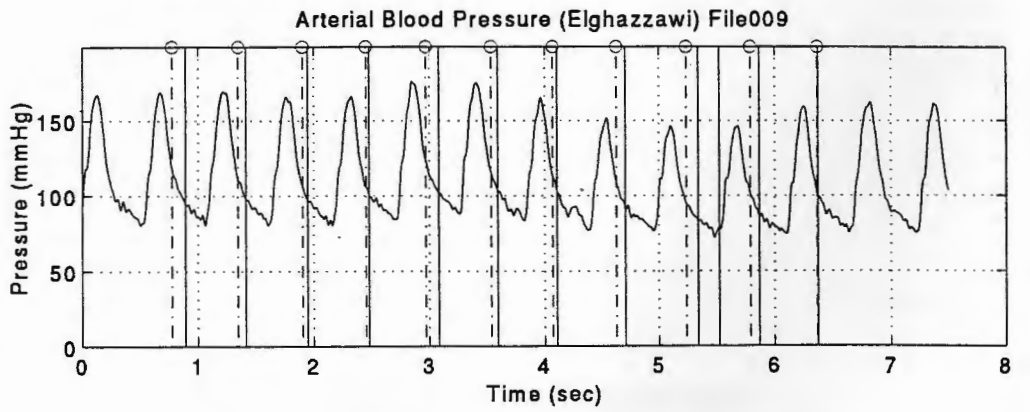
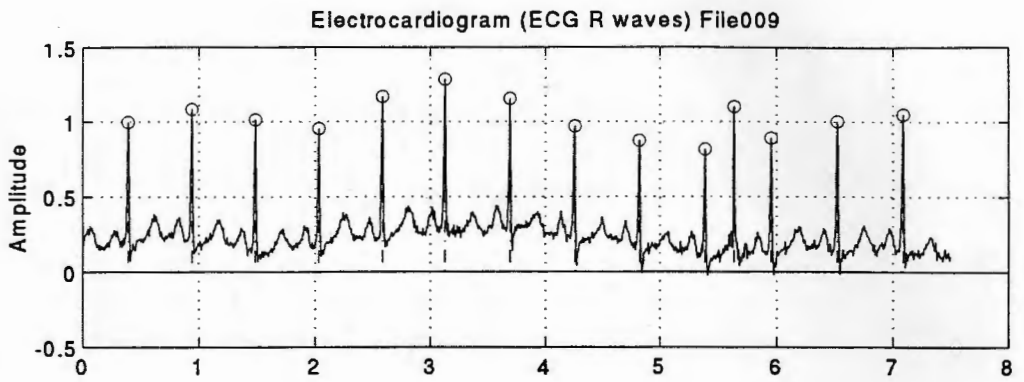
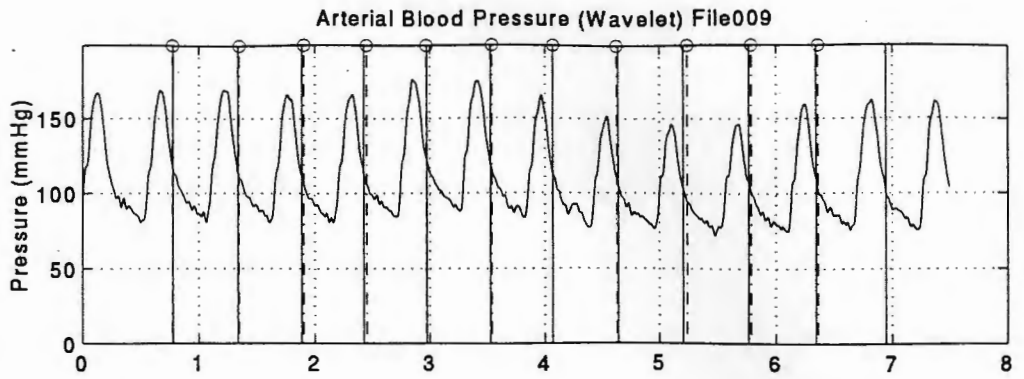
Arterial Blood Pressure (Martino) File003



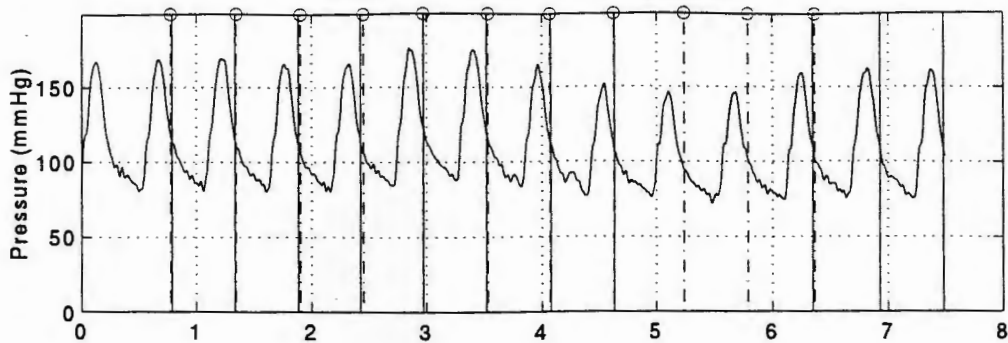
Arterial Blood Pressure (Kinias) File003



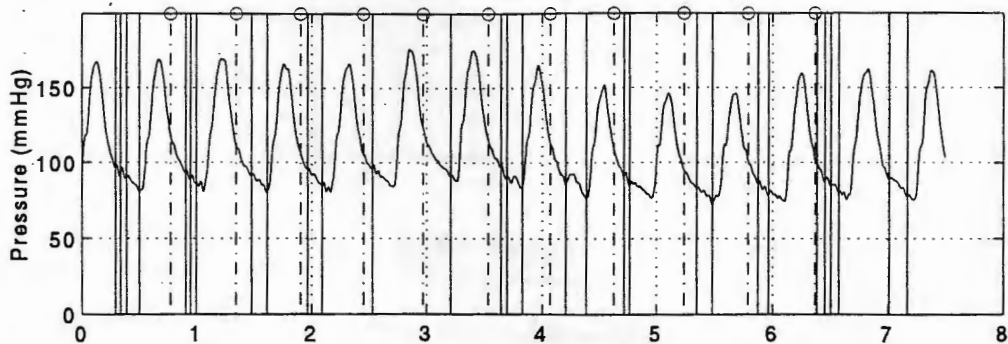




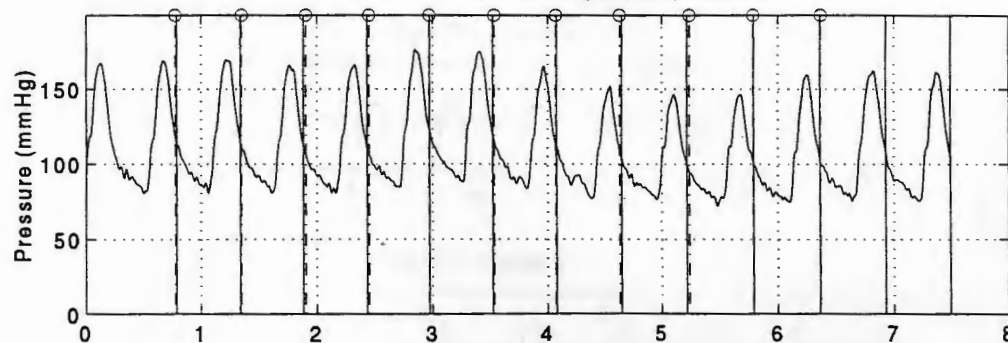
Arterial Blood Pressure (Lee) File009



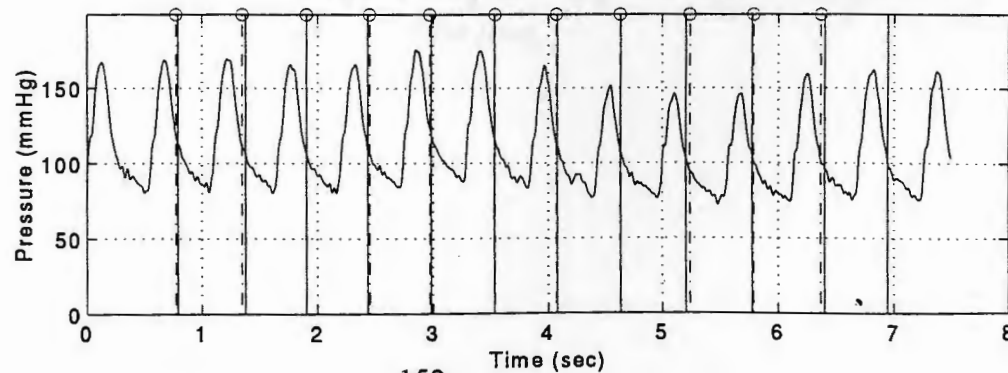
Arterial Blood Pressure (Jundanian) File009

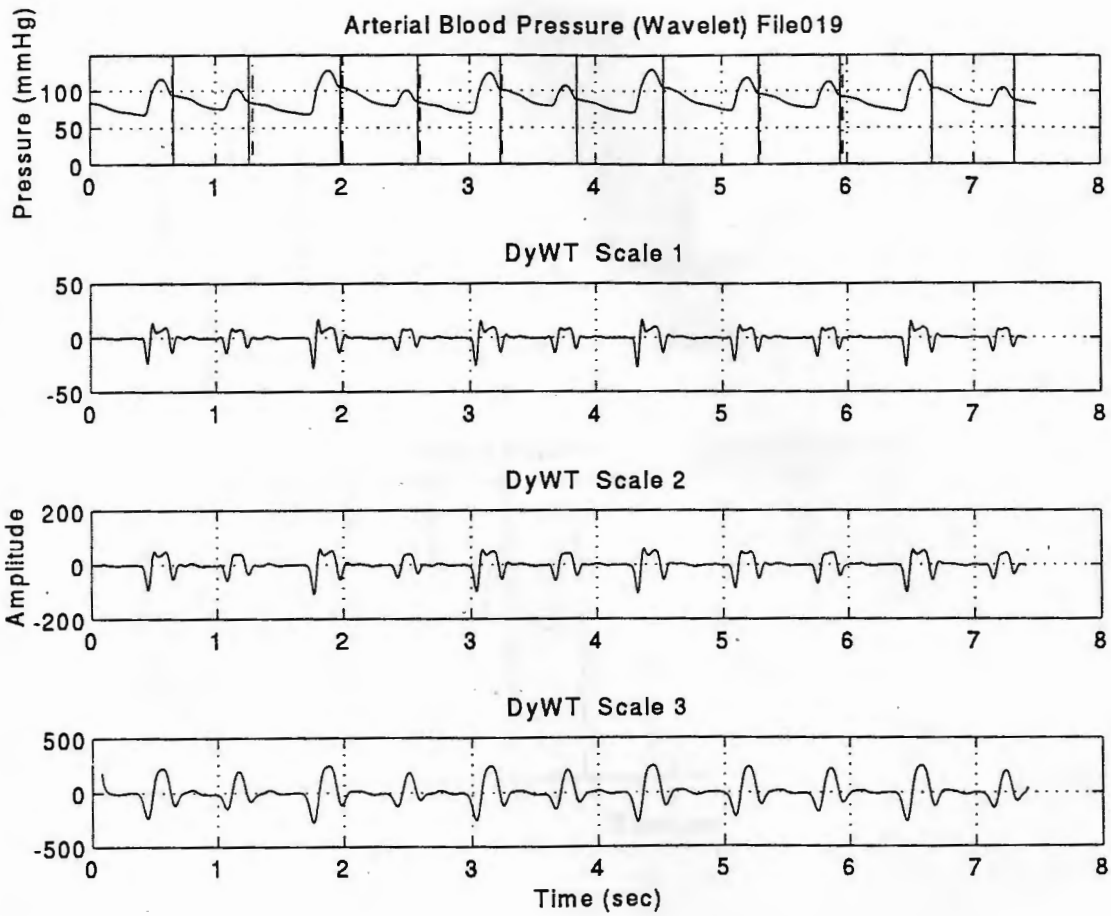


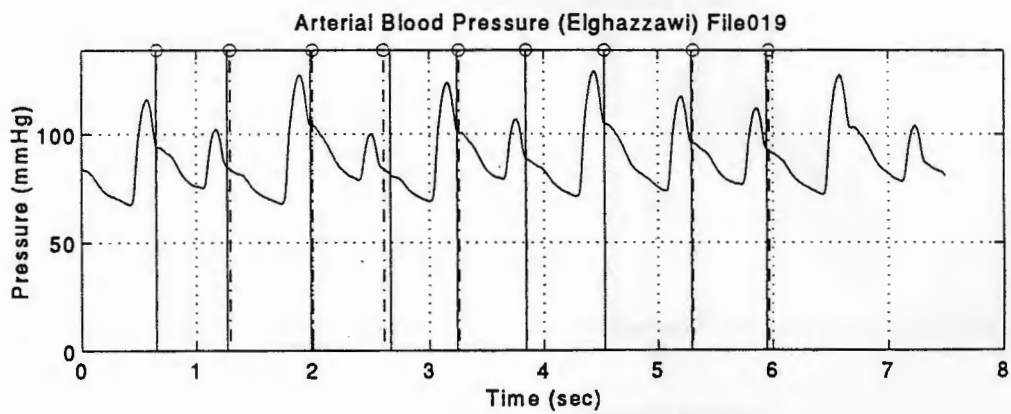
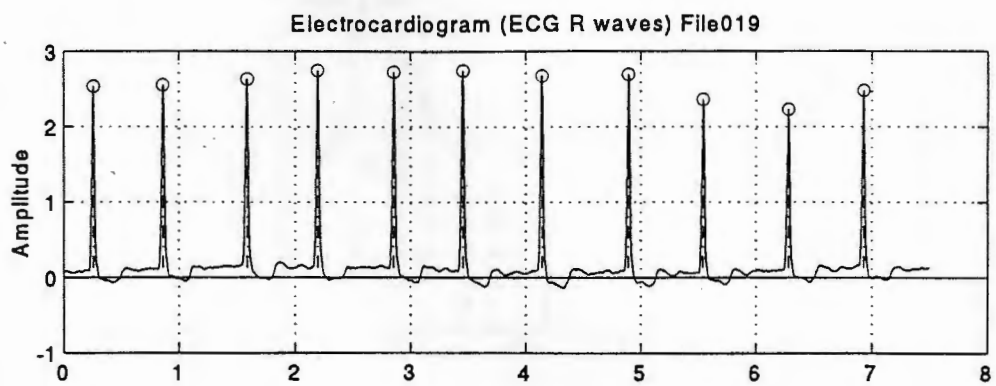
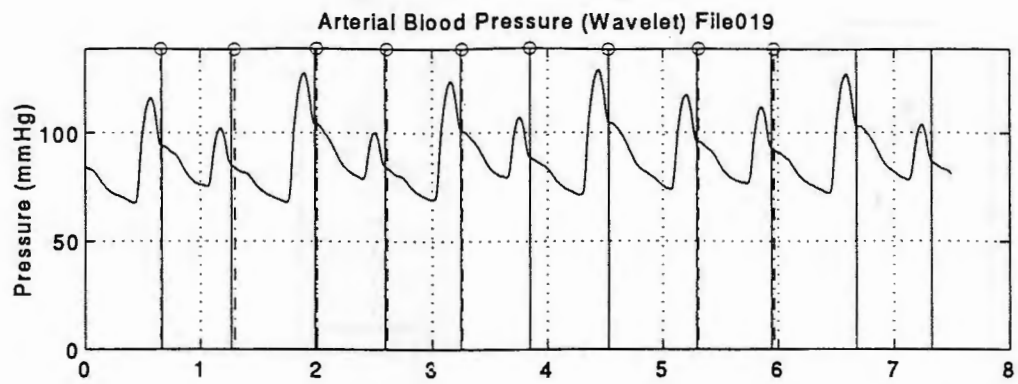
Arterial Blood Pressure (Martino) File009



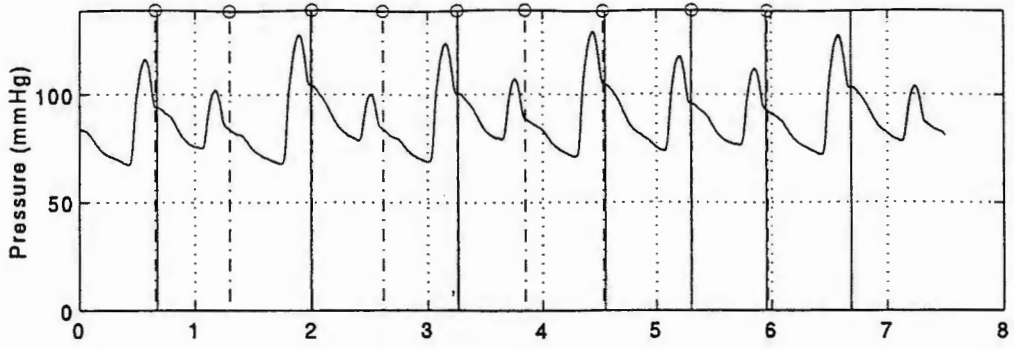
Arterial Blood Pressure (Kinias) File009



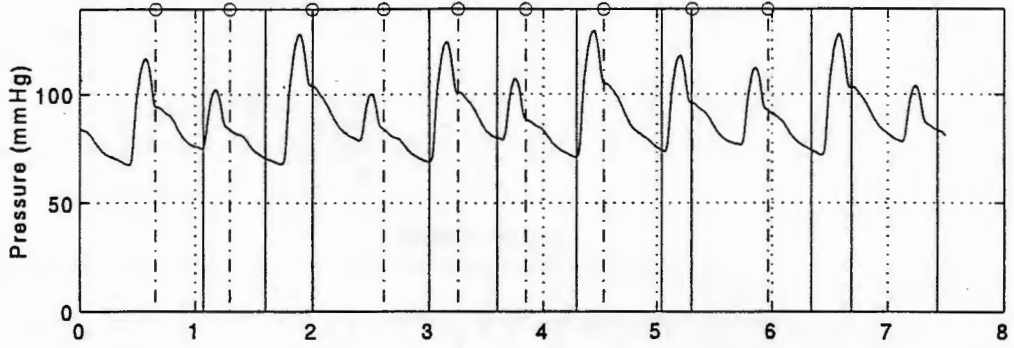




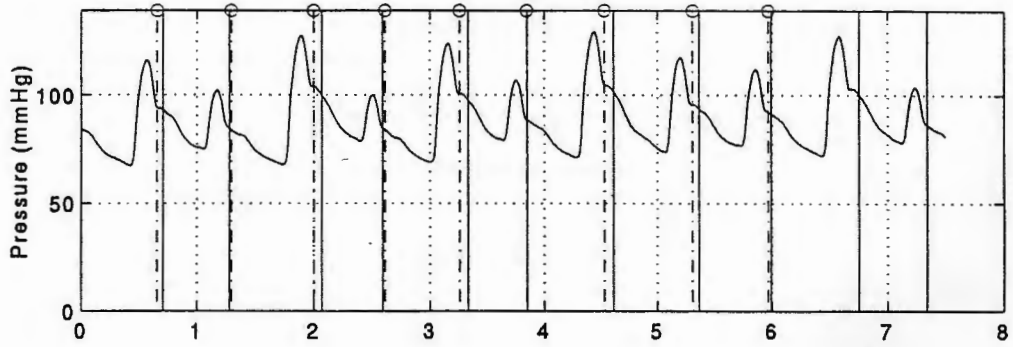
Arterial Blood Pressure (Lee) File019



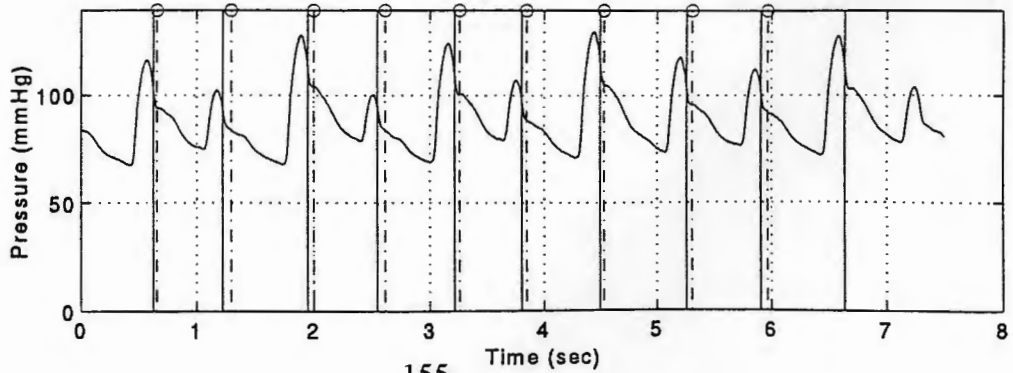
Arterial Blood Pressure (Jundanian) File019

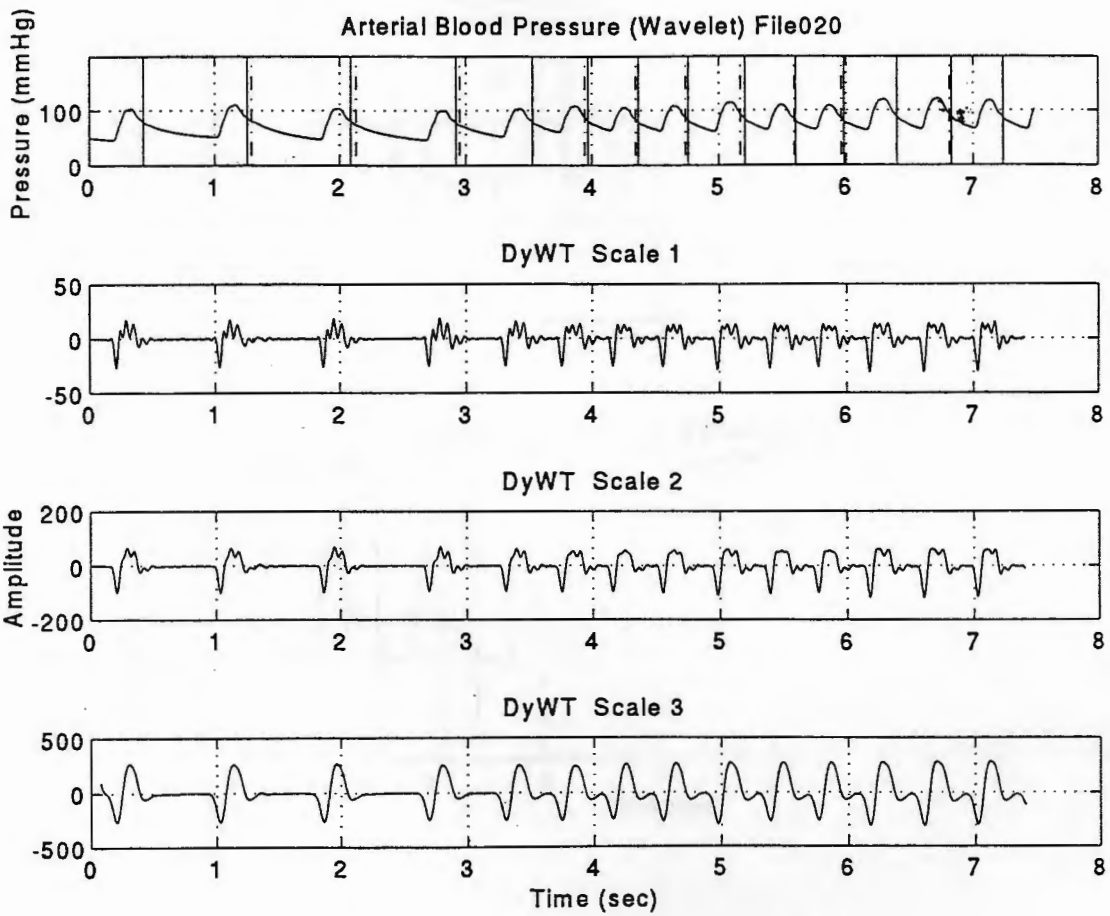


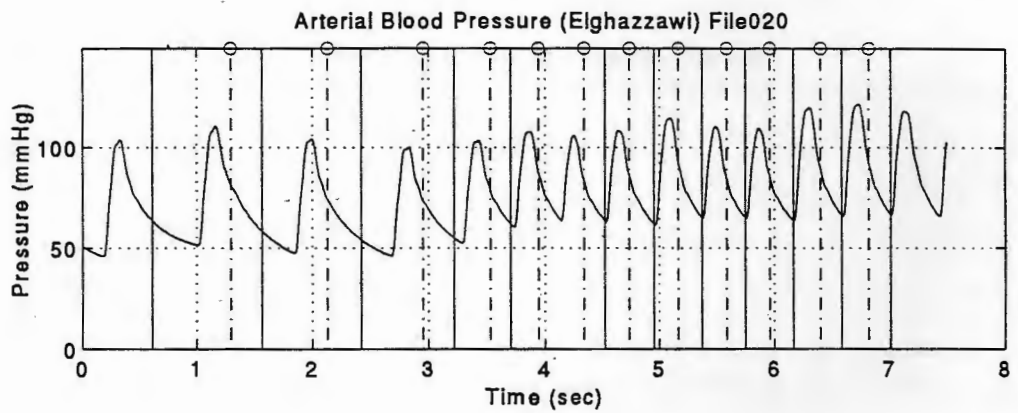
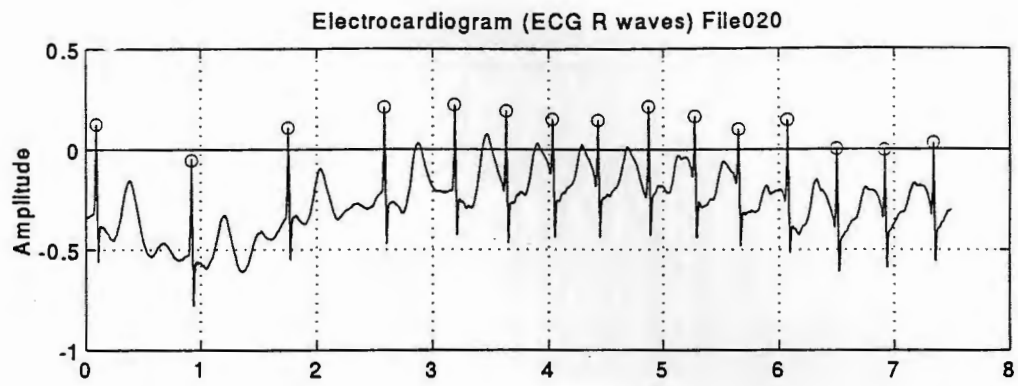
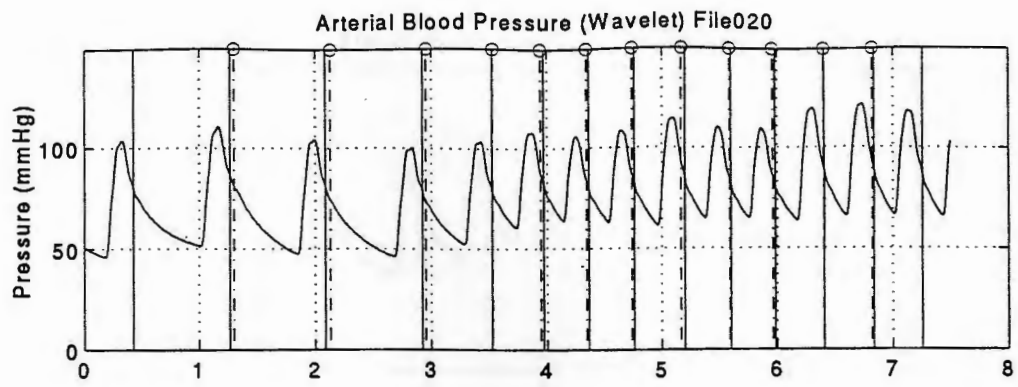
Arterial Blood Pressure (Martino) File019



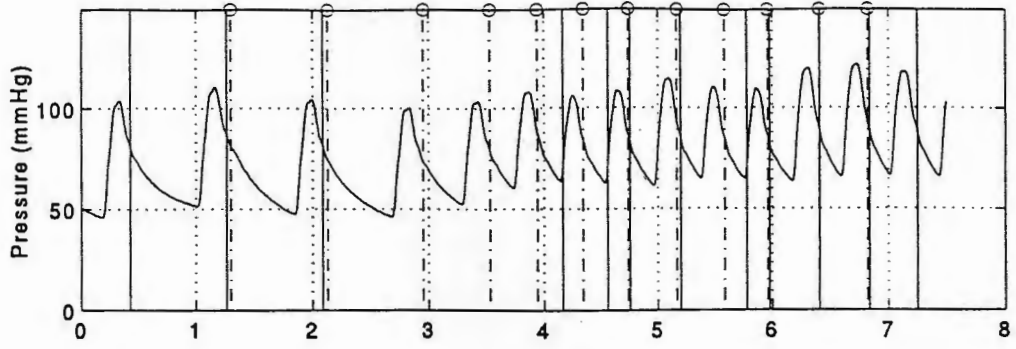
Arterial Blood Pressure (Kinias) File019



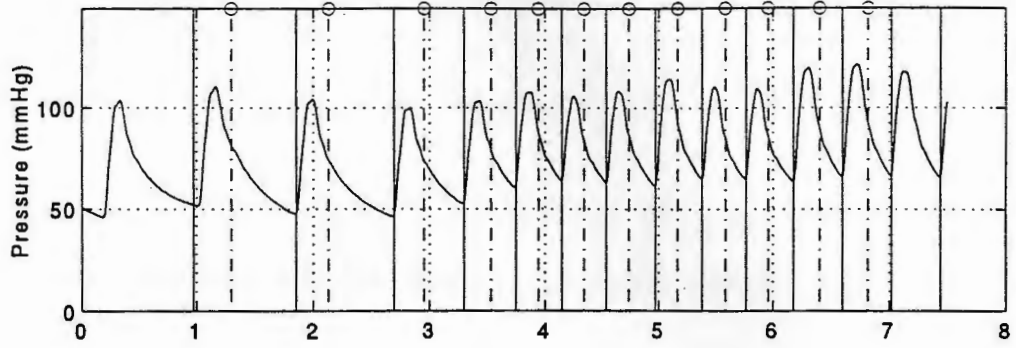




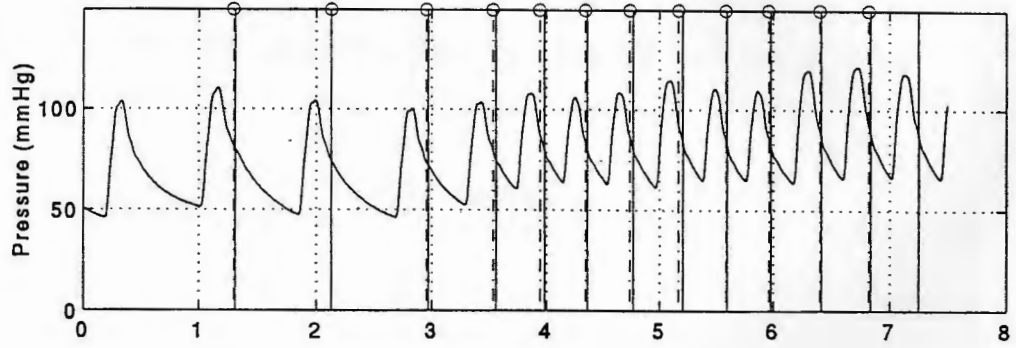
Arterial Blood Pressure (Lee) File020



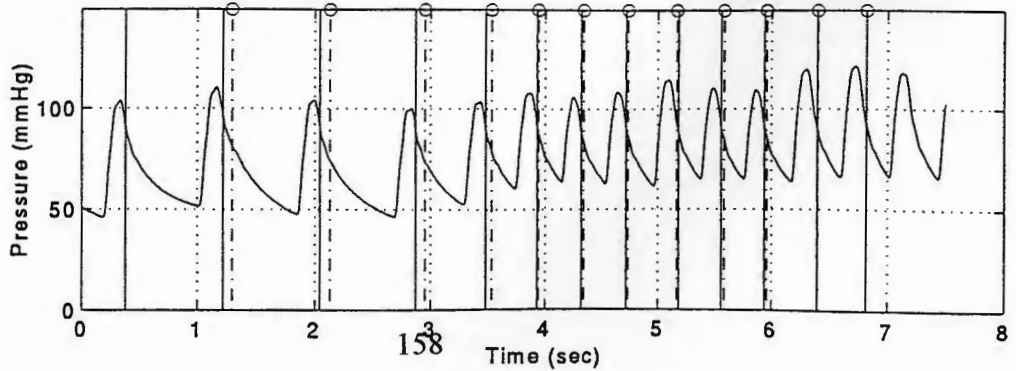
Arterial Blood Pressure (Jundanian) File020

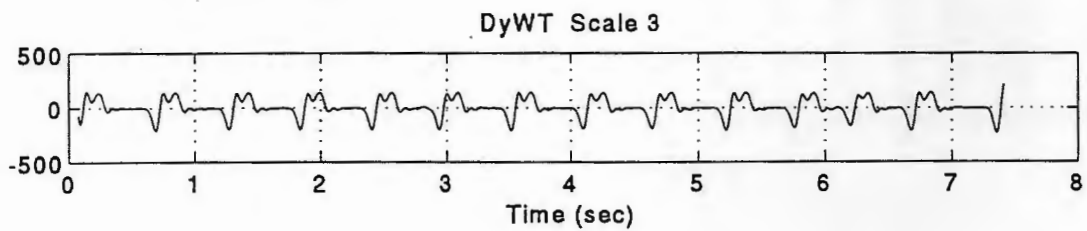
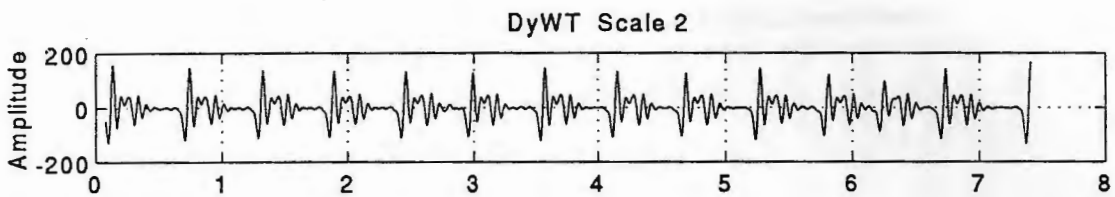
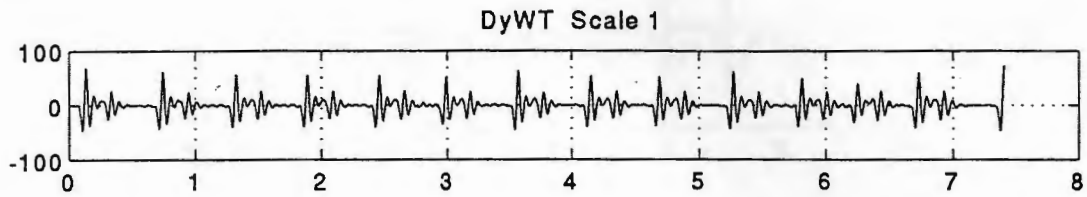
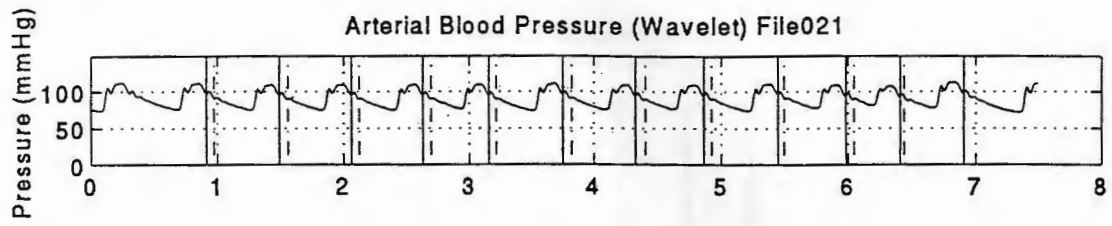


Arterial Blood Pressure (Martino) File020

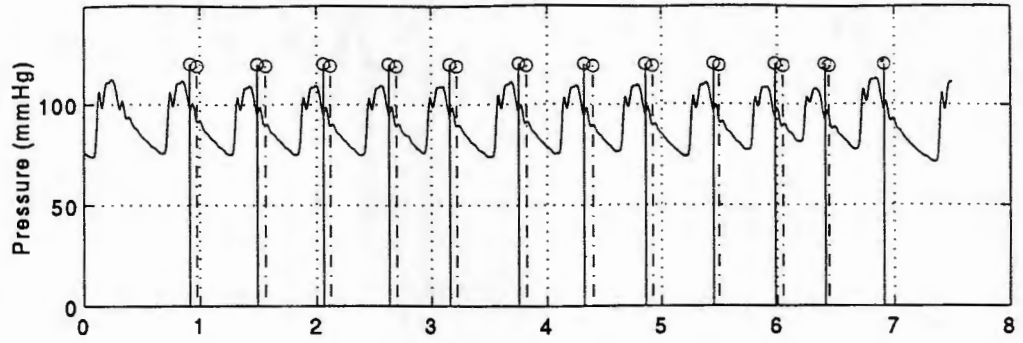


Arterial Blood Pressure (Kinias) File020

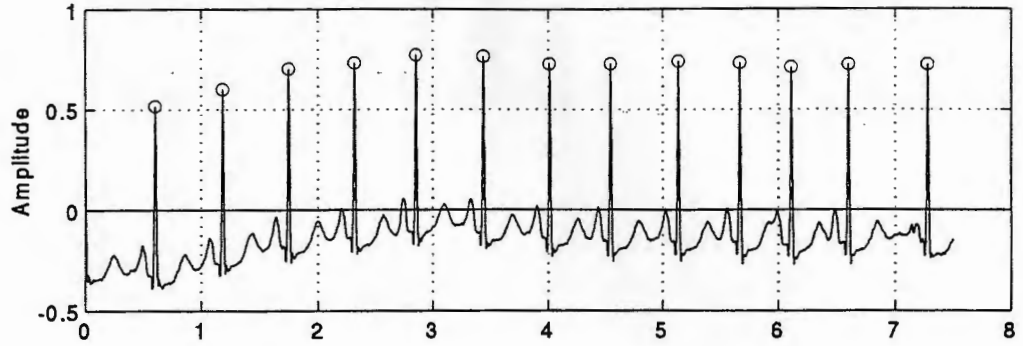




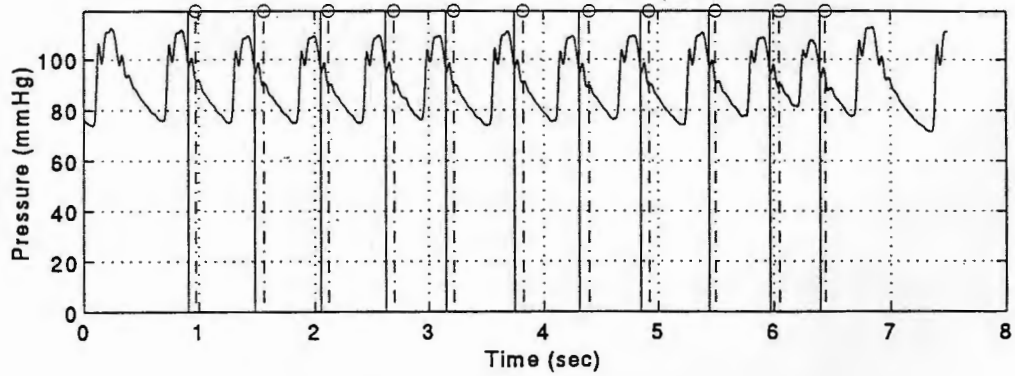
Arterial Blood Pressure (Wavelet) File021



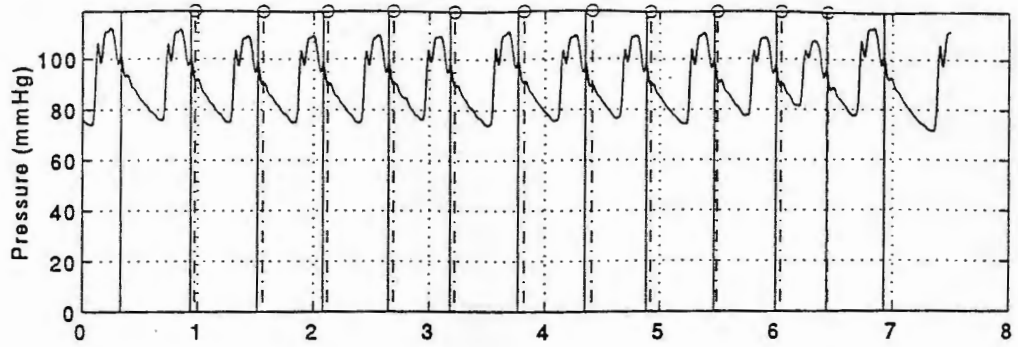
Electrocardiogram (ECG R waves) File021



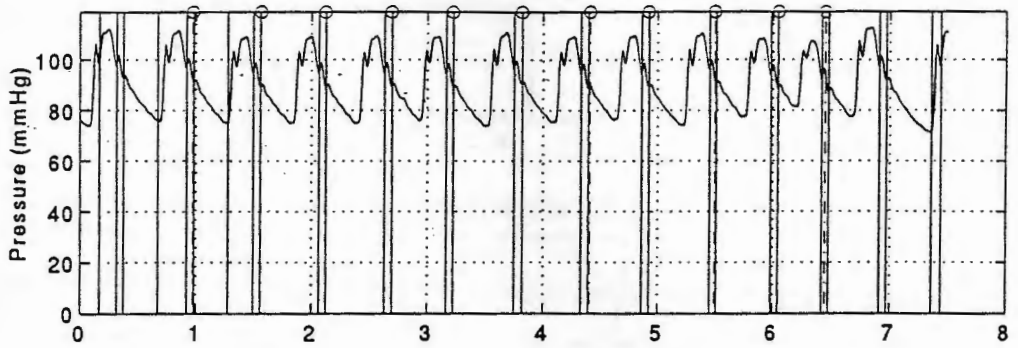
Arterial Blood Pressure (Elghazzawi) File021



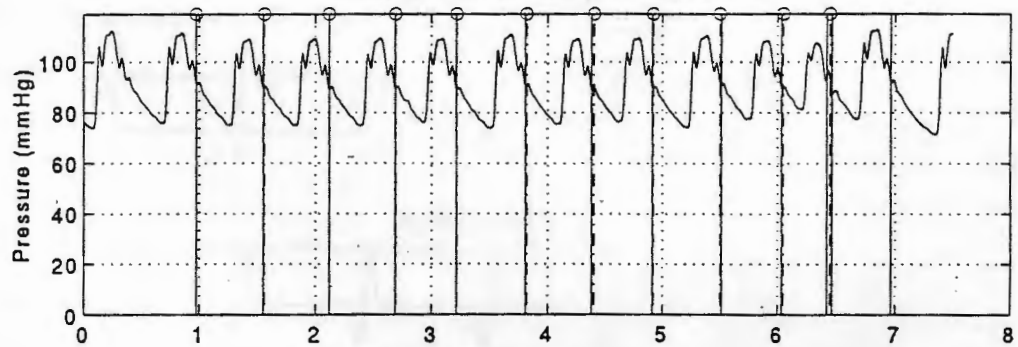
Arterial Blood Pressure (Lee) File021



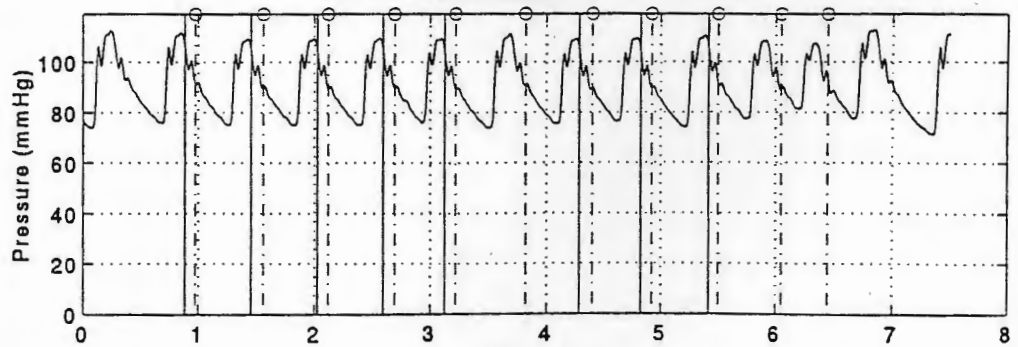
Arterial Blood Pressure (Jundanian) File021

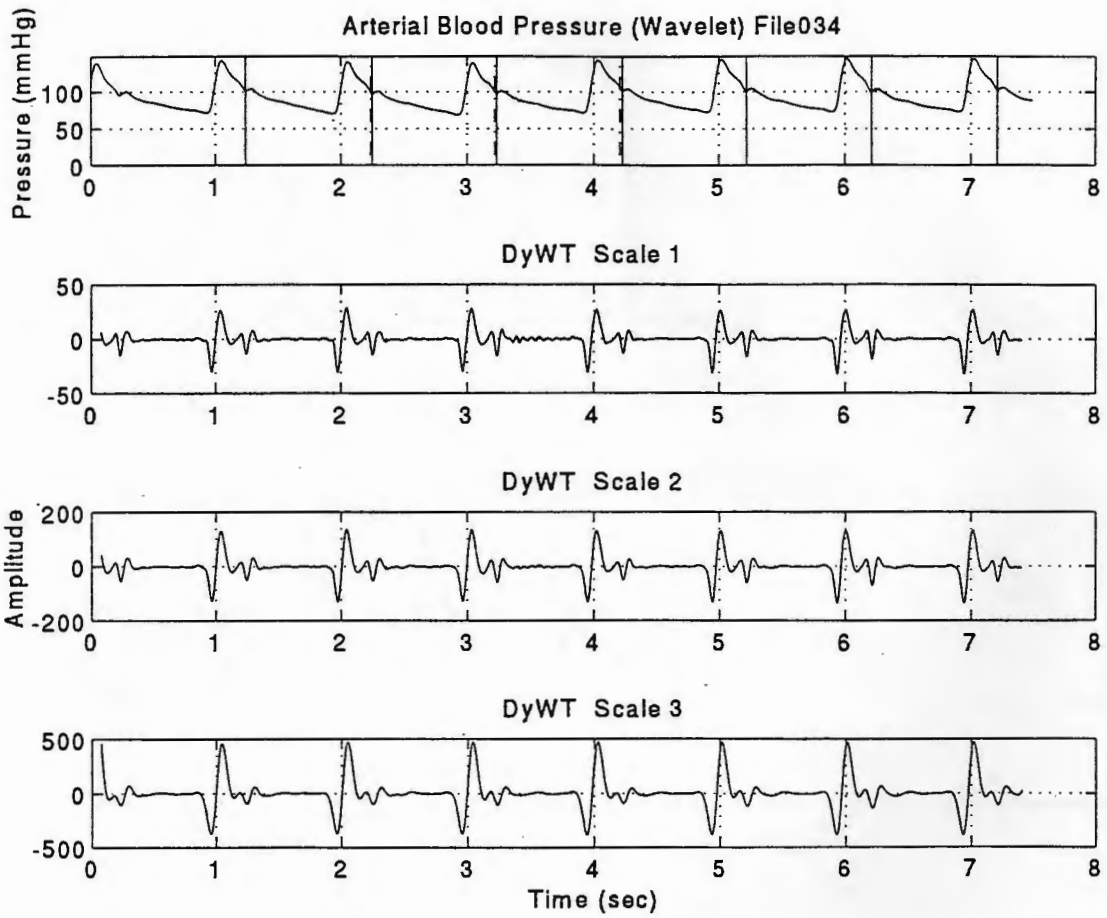


Arterial Blood Pressure (Martino) File021

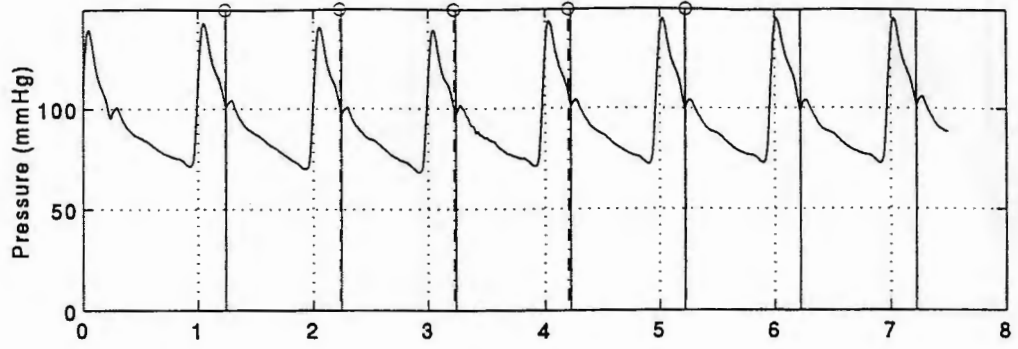


Arterial Blood Pressure (Kinias) File021

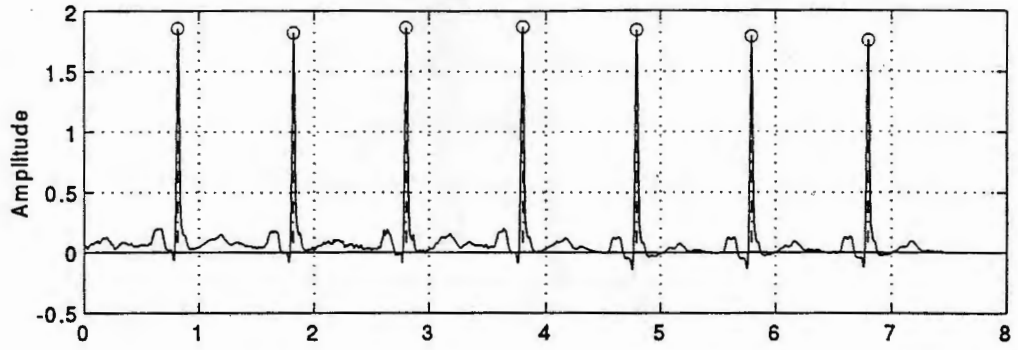




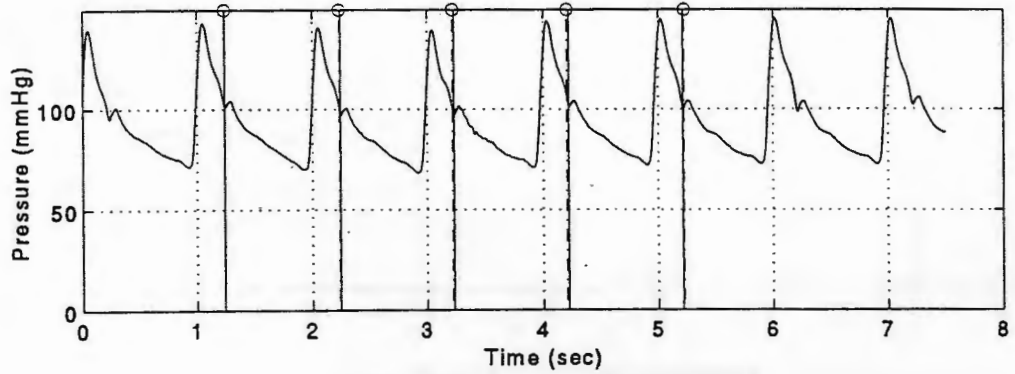
Arterial Blood Pressure (Wavelet) File034



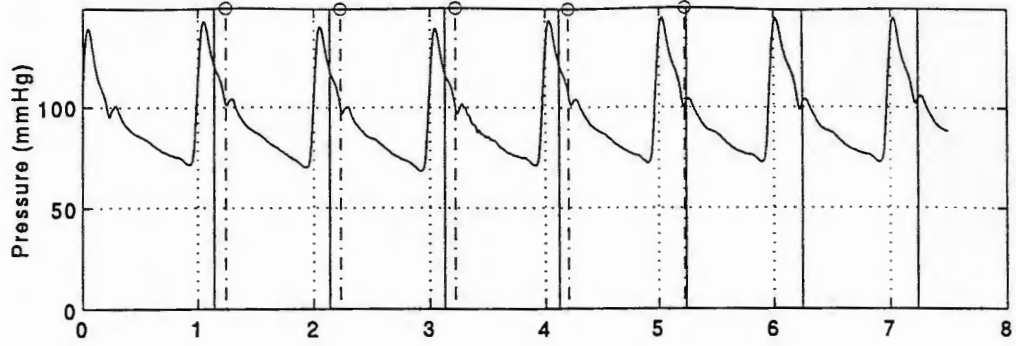
Electrocardiogram (ECG R waves) File034



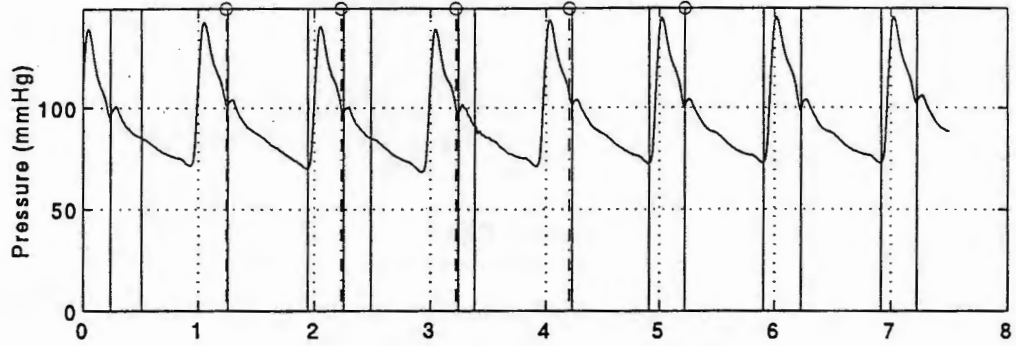
Arterial Blood Pressure (Elghazzawi) File034



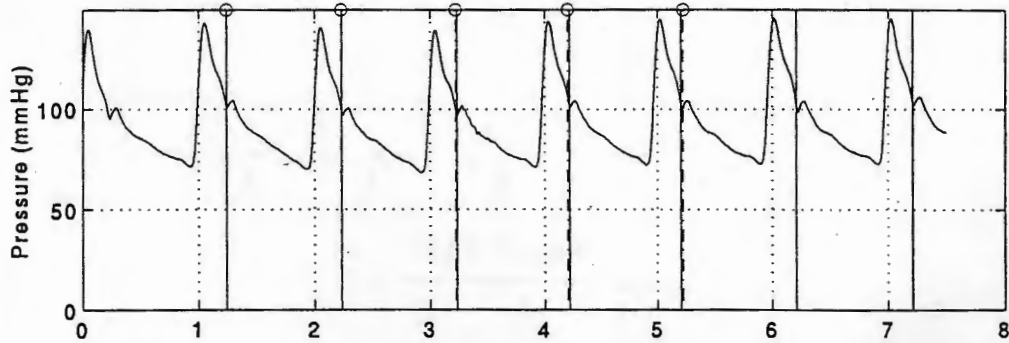
Arterial Blood Pressure (Lee) File034



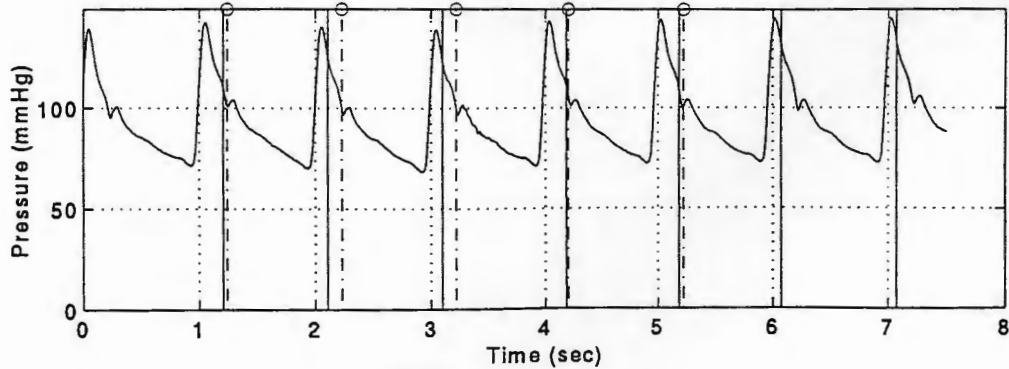
Arterial Blood Pressure (Jundanian) File034

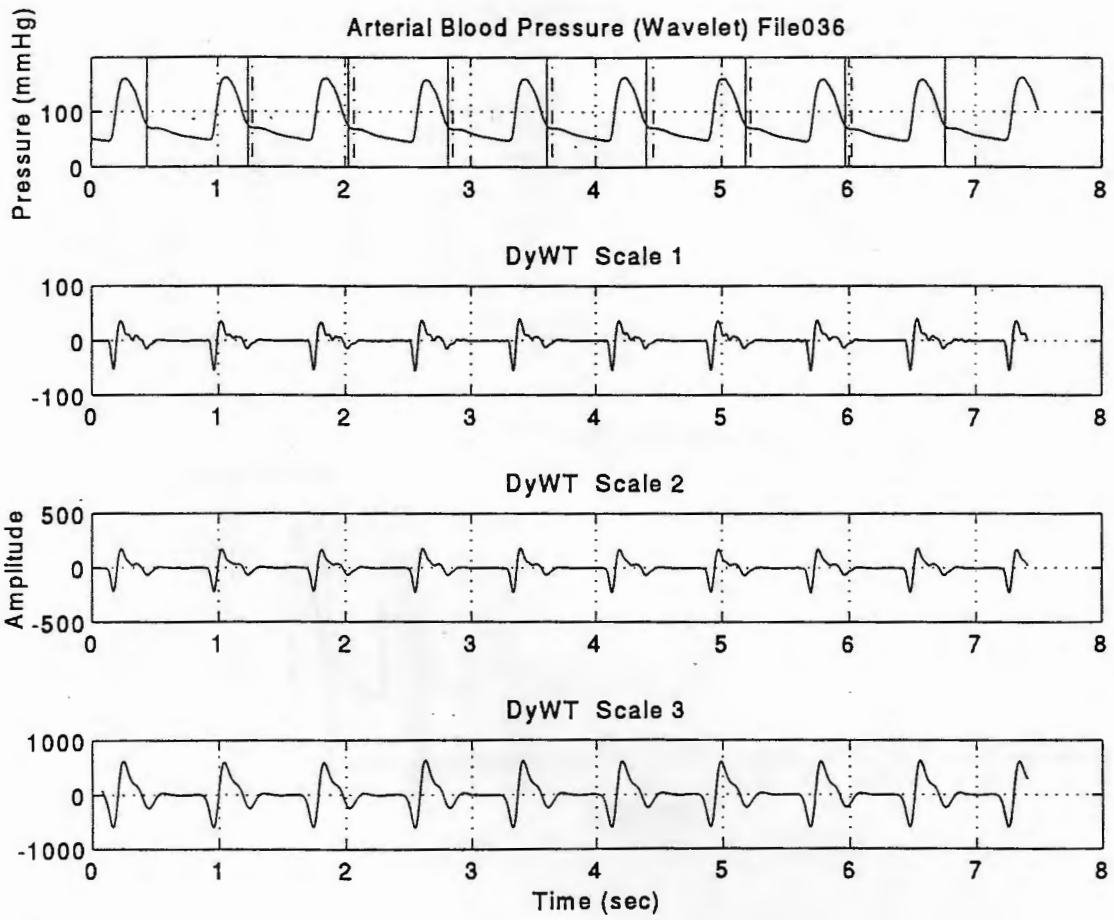


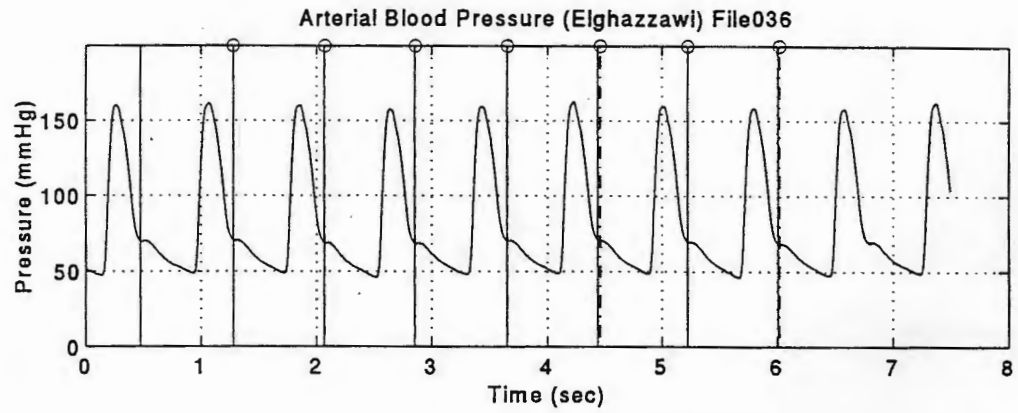
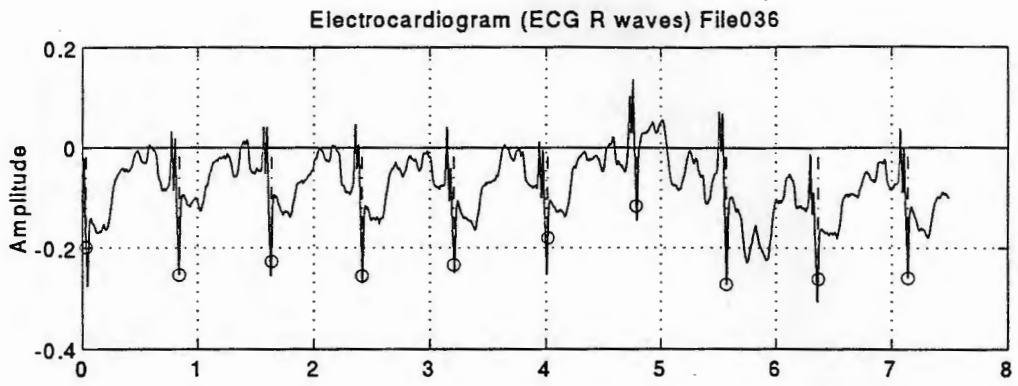
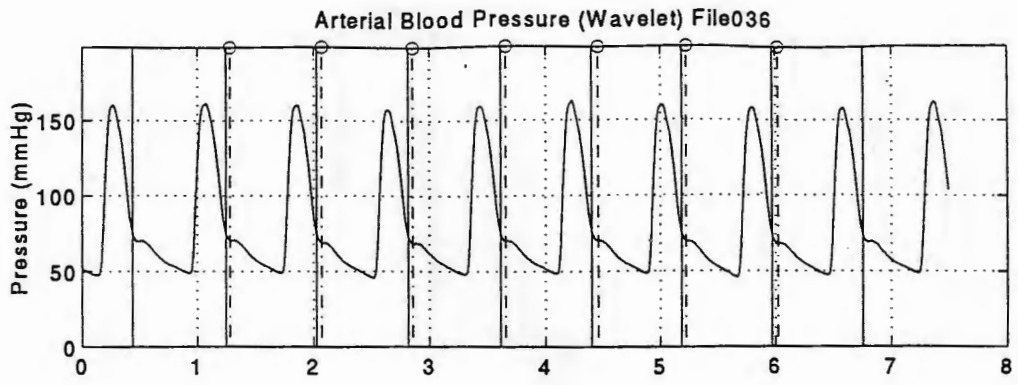
Arterial Blood Pressure (Martino) File034



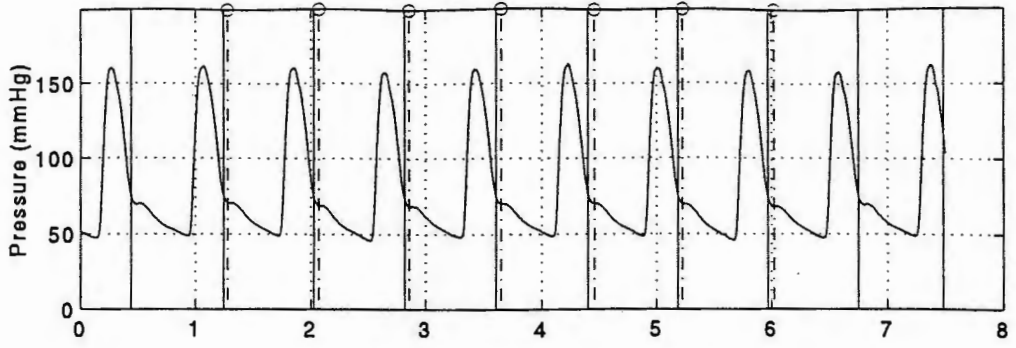
Arterial Blood Pressure (Kinias) File034



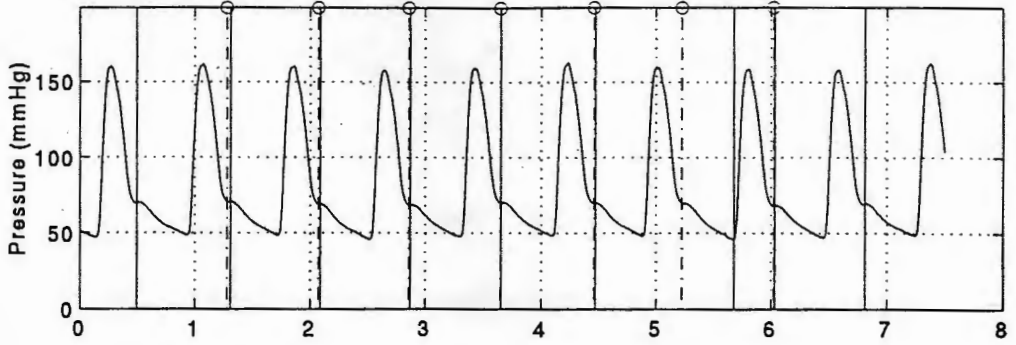




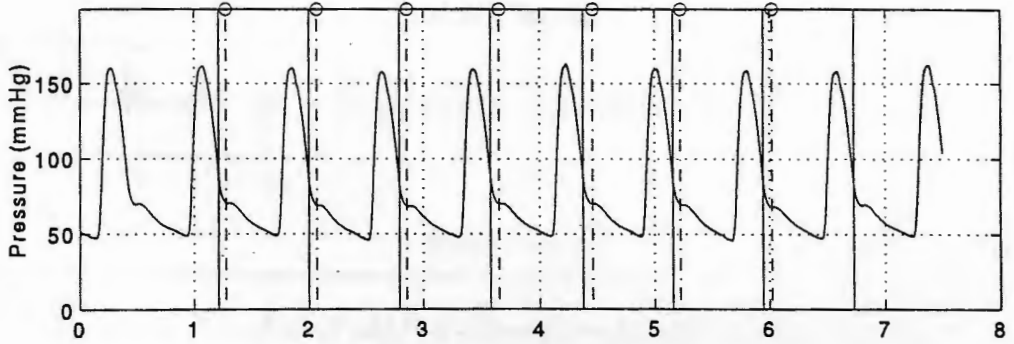
Arterial Blood Pressure (Lee) File036



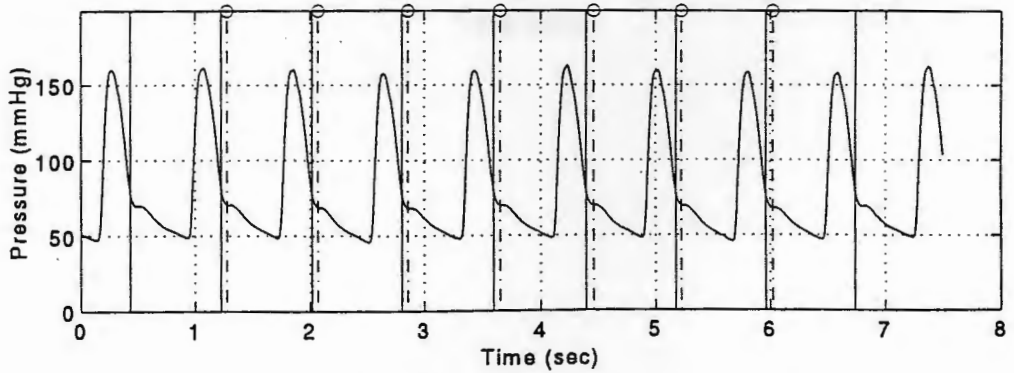
Arterial Blood Pressure (Jundanian) File036

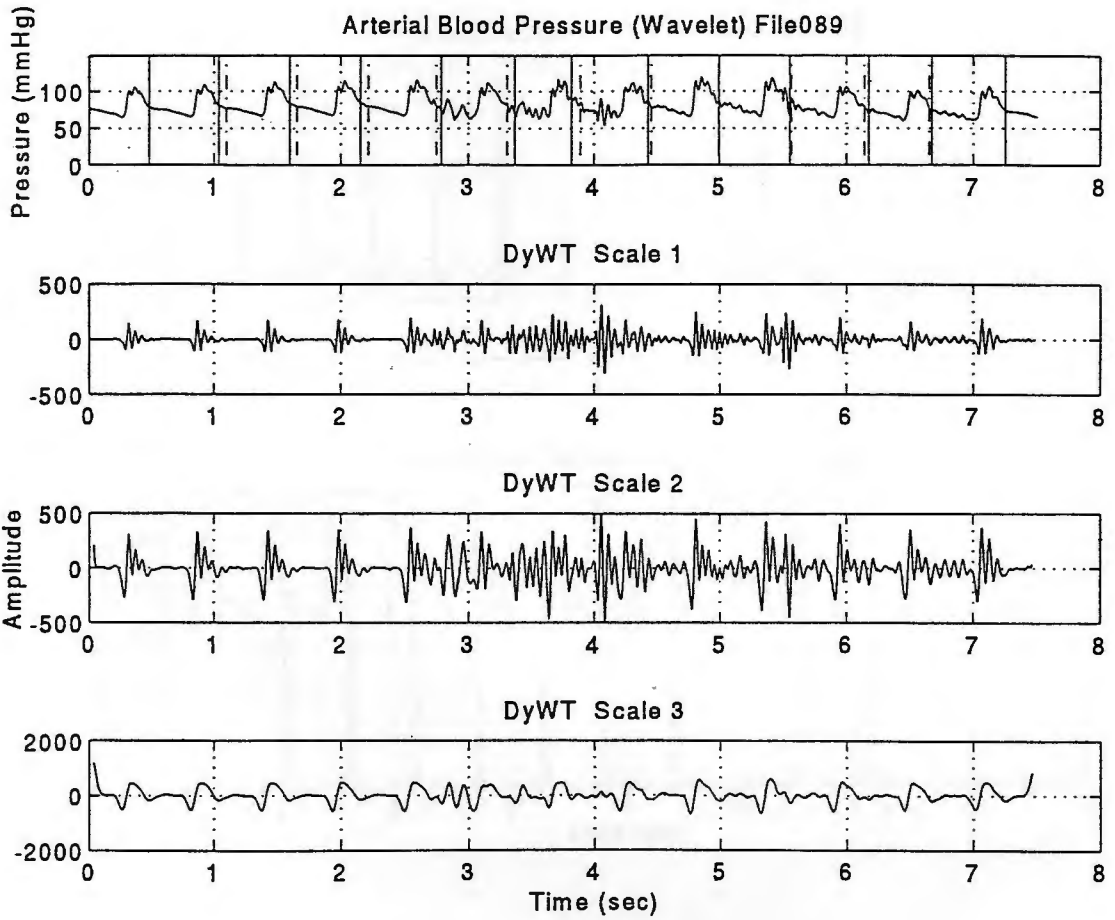


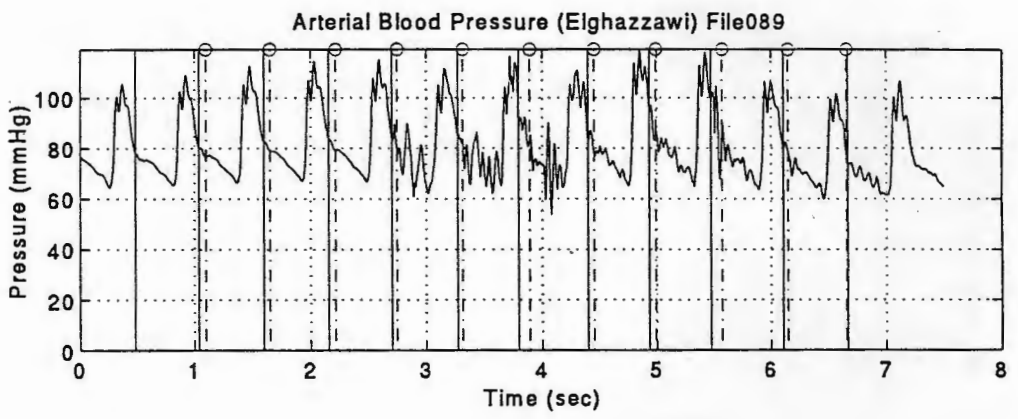
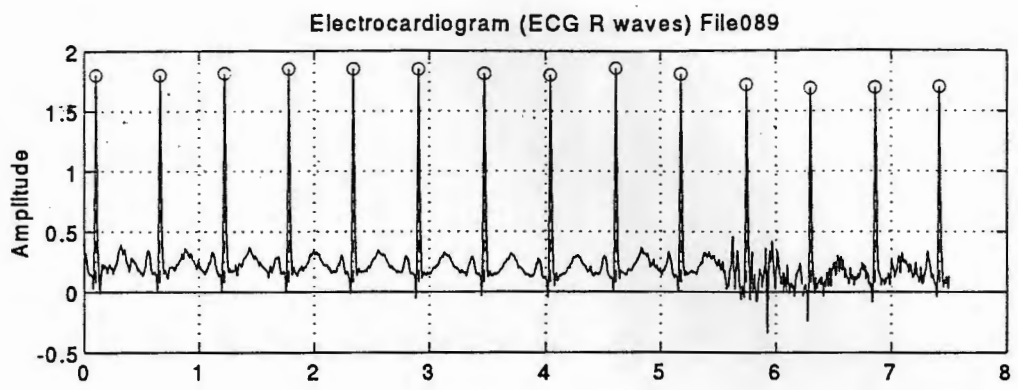
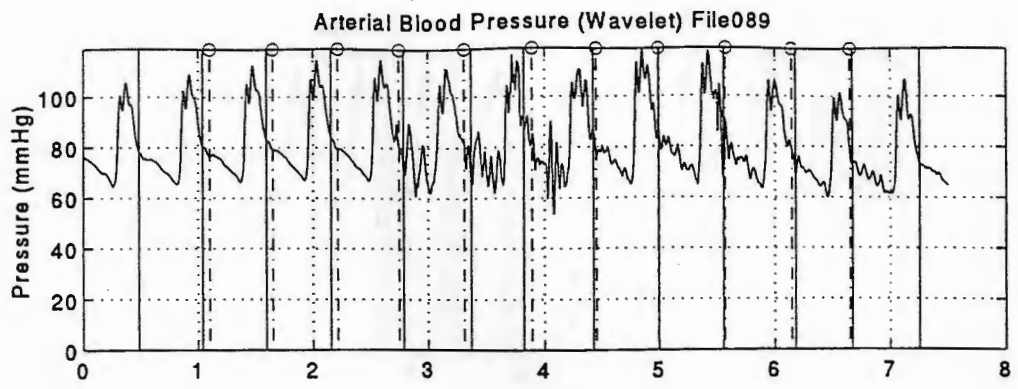
Arterial Blood Pressure (Martino) File036



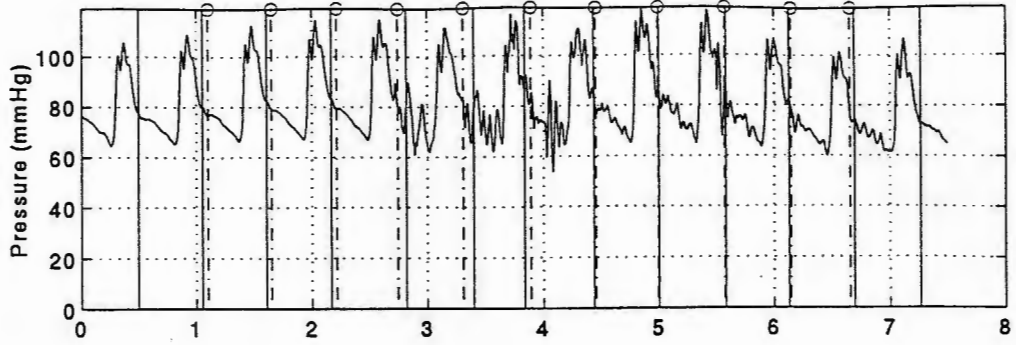
Arterial Blood Pressure (Kinias) File036



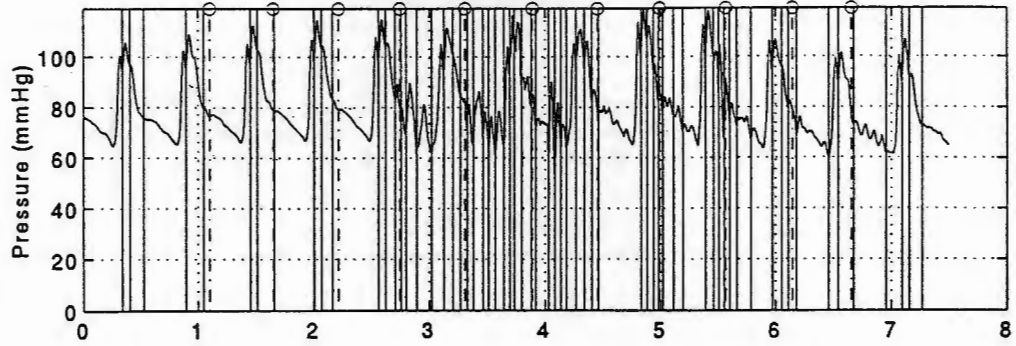




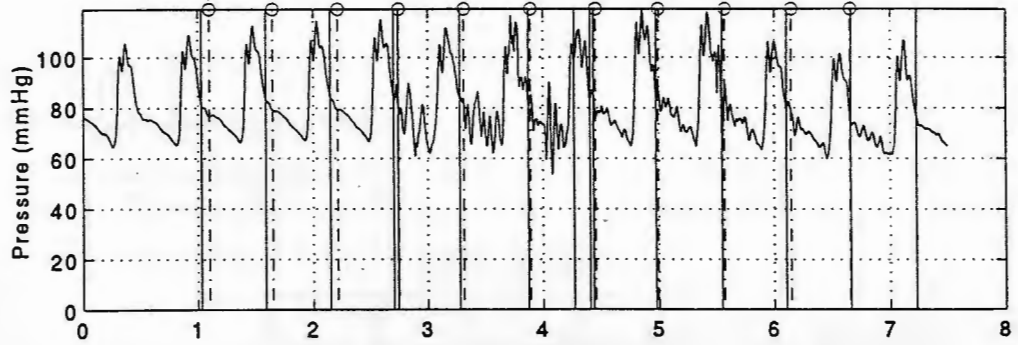
Arterial Blood Pressure (Lee) File089



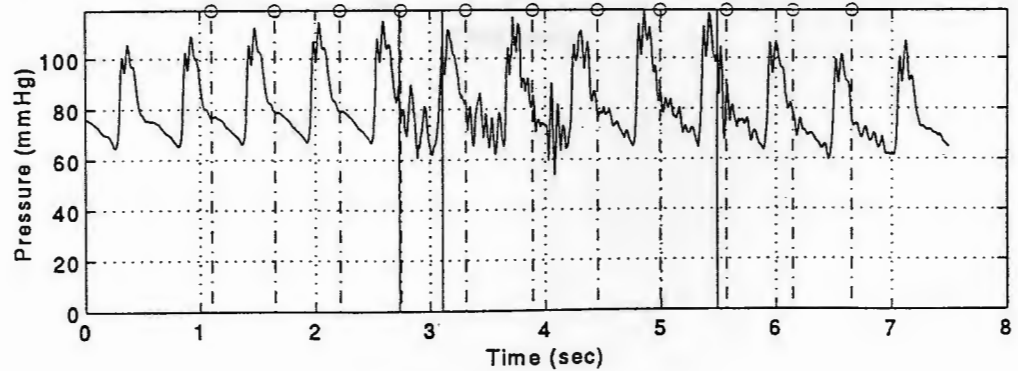
Arterial Blood Pressure (Jundanian) File089

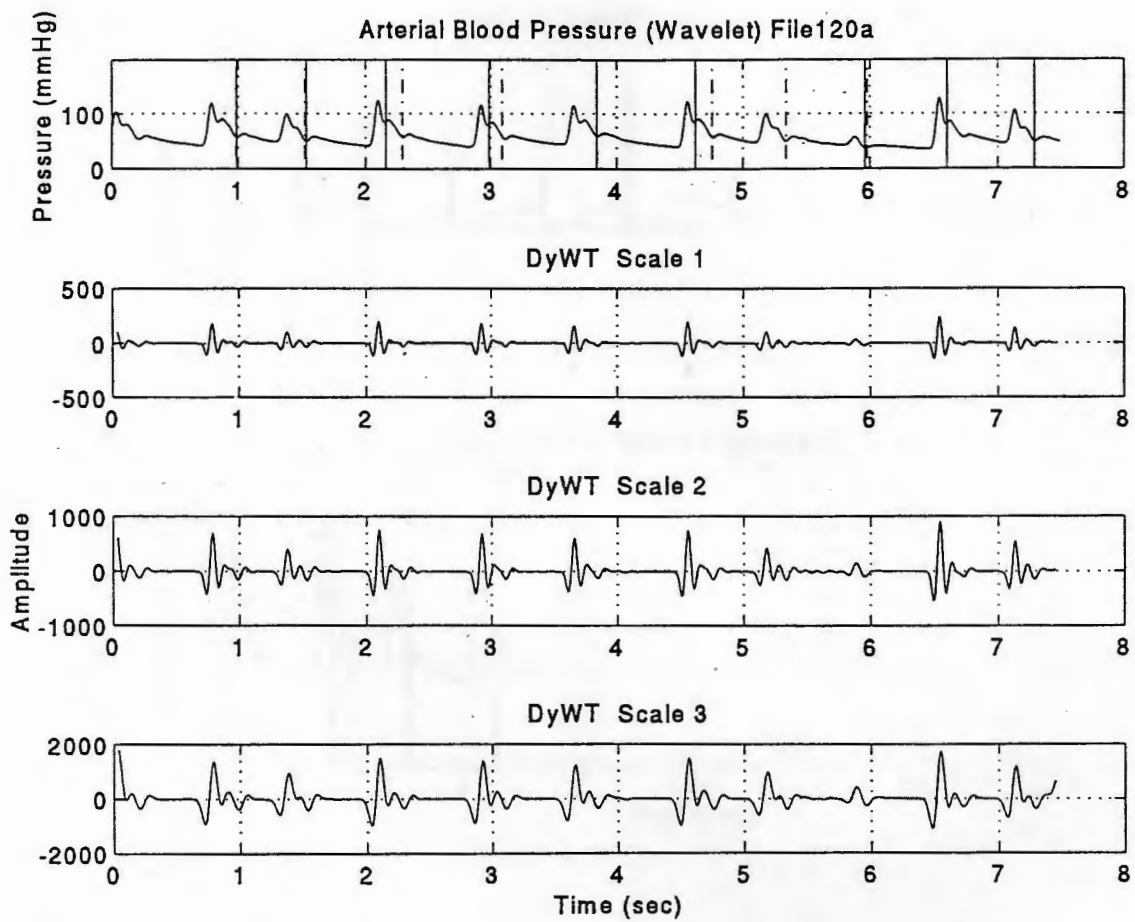


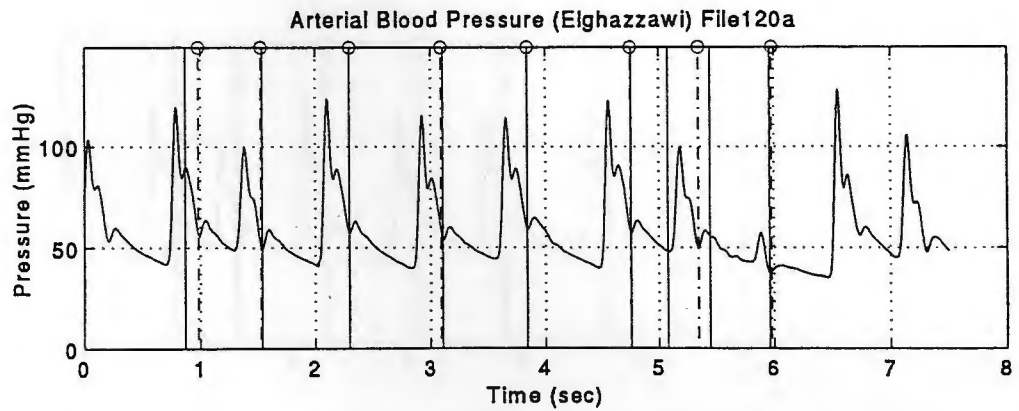
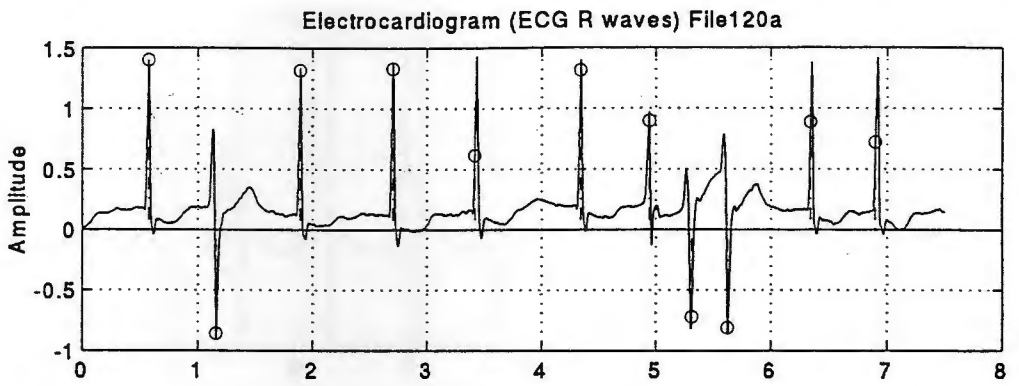
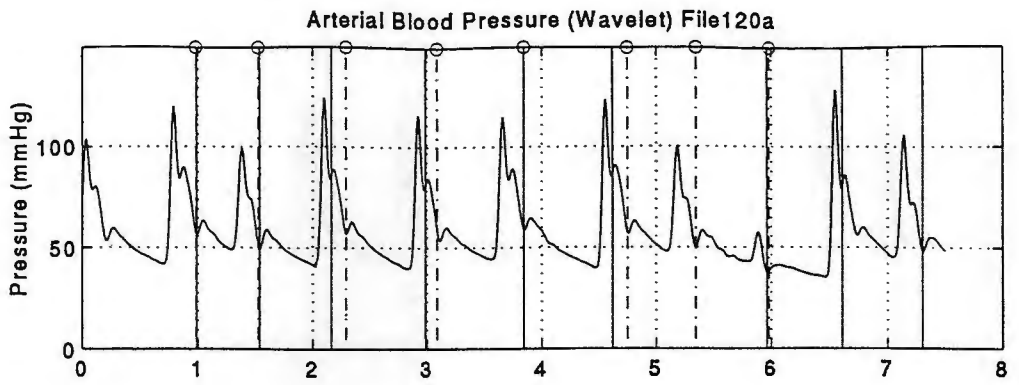
Arterial Blood Pressure (Martino) File089



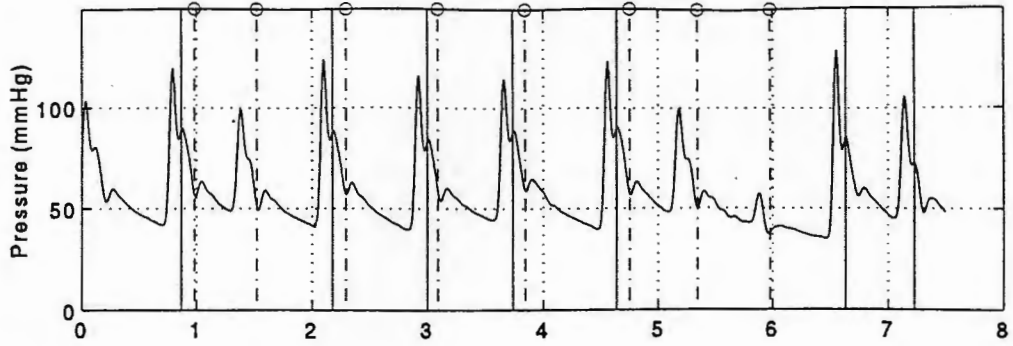
Arterial Blood Pressure (Kinias) File089



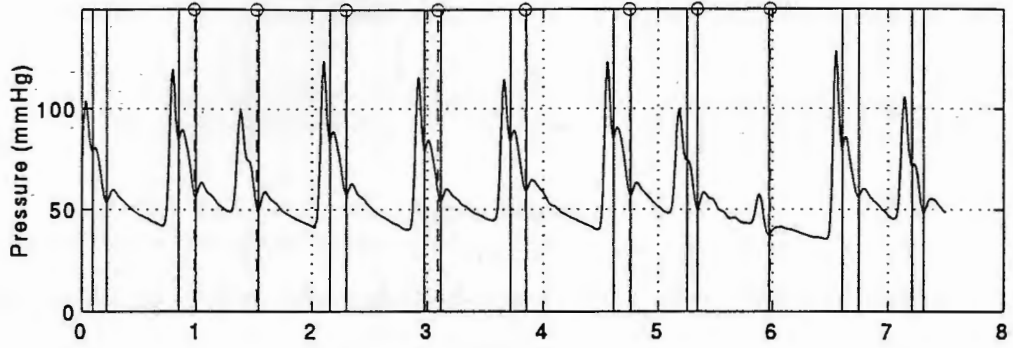




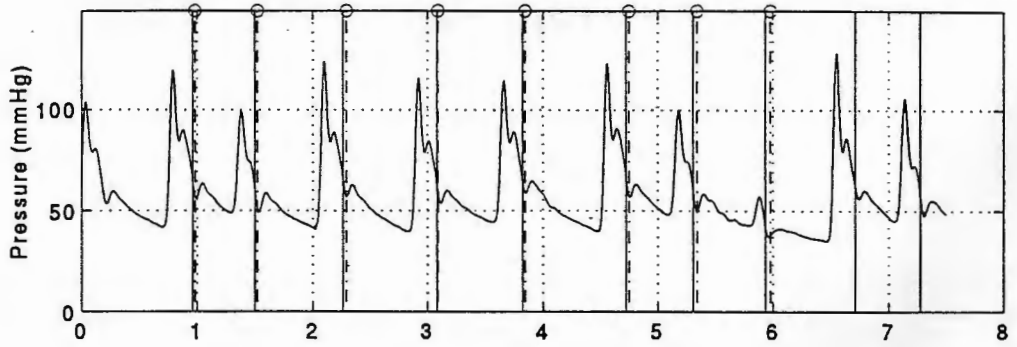
Arterial Blood Pressure (Lee) File120a



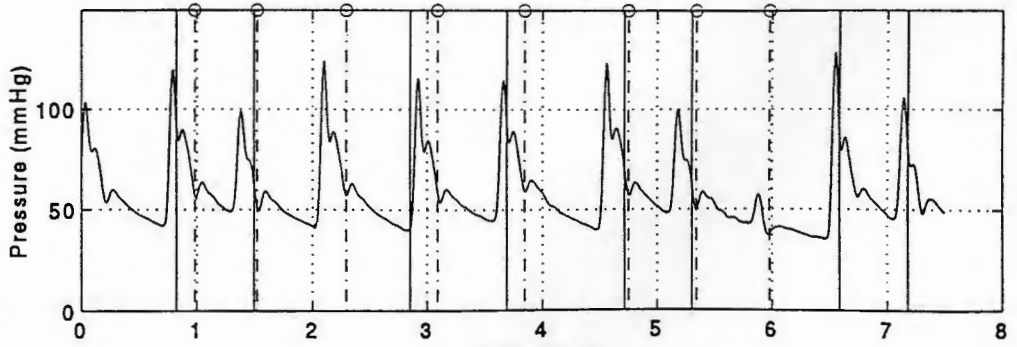
Arterial Blood Pressure (Jundanian) File120a



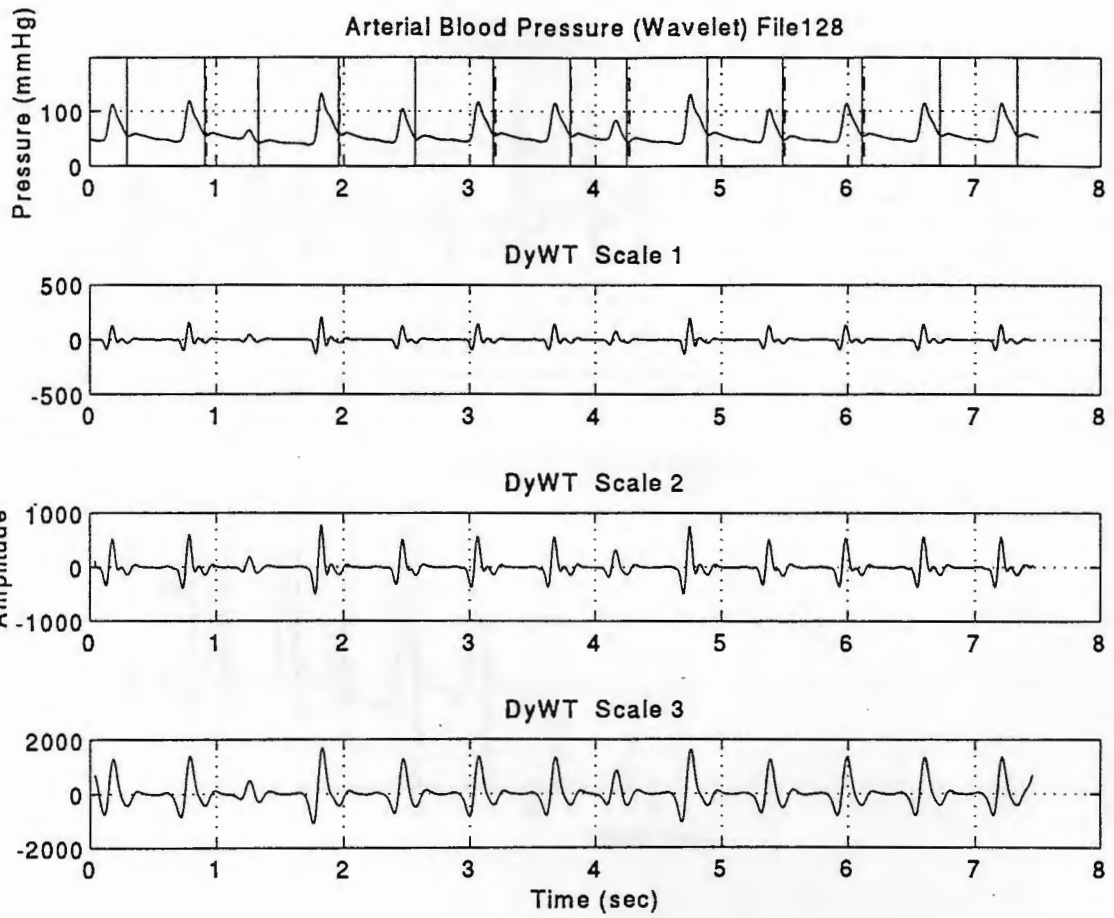
Arterial Blood Pressure (Martino) File120a

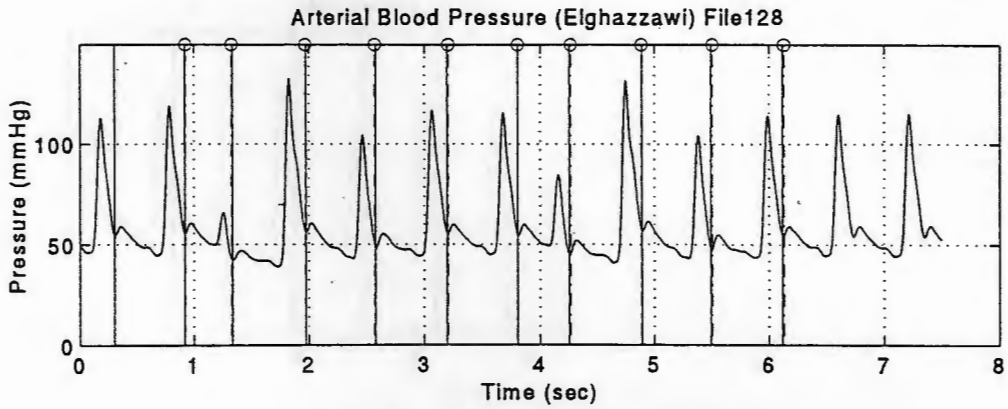
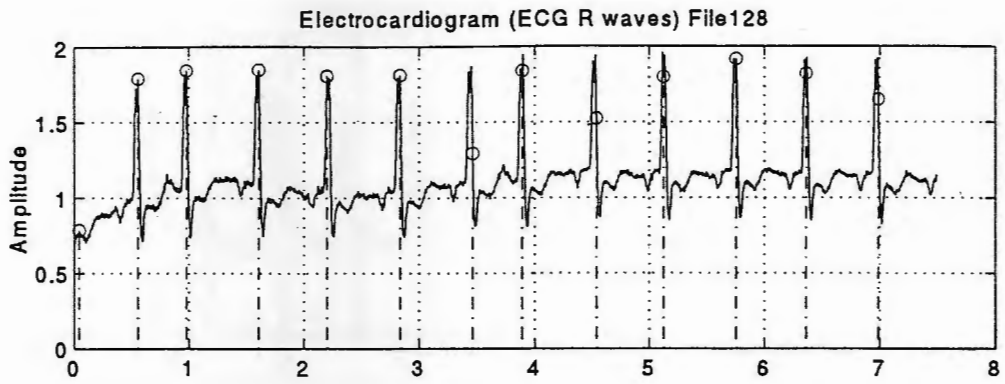
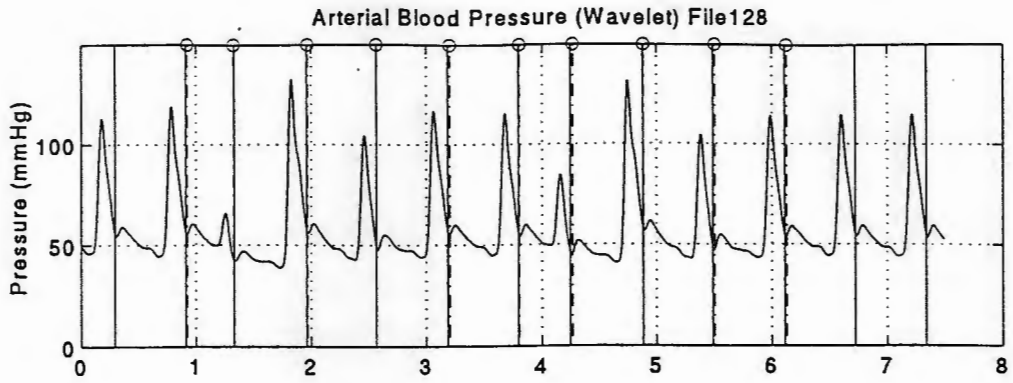


Arterial Blood Pressure (Kinias) File120a



Time (sec)

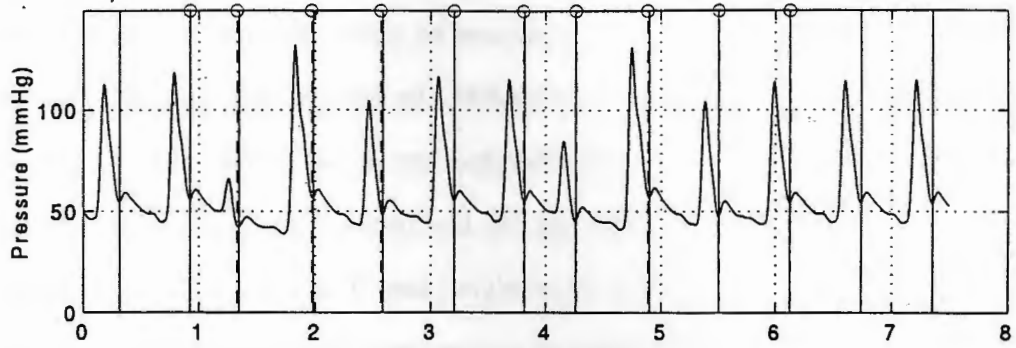




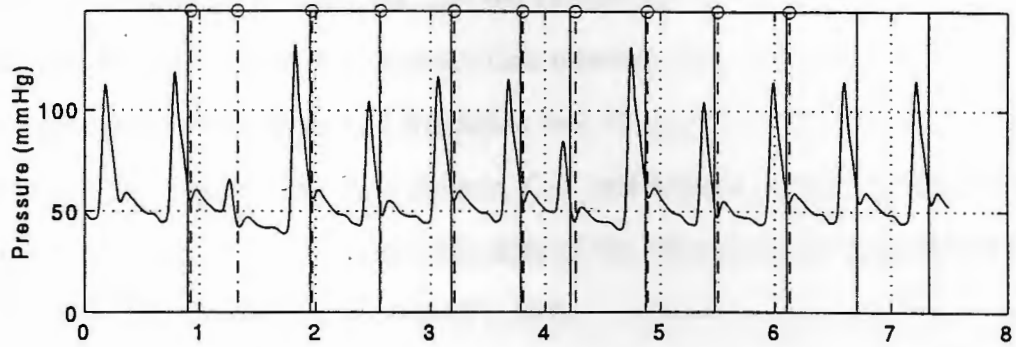
Arterial Blood Pressure (Lee) File128



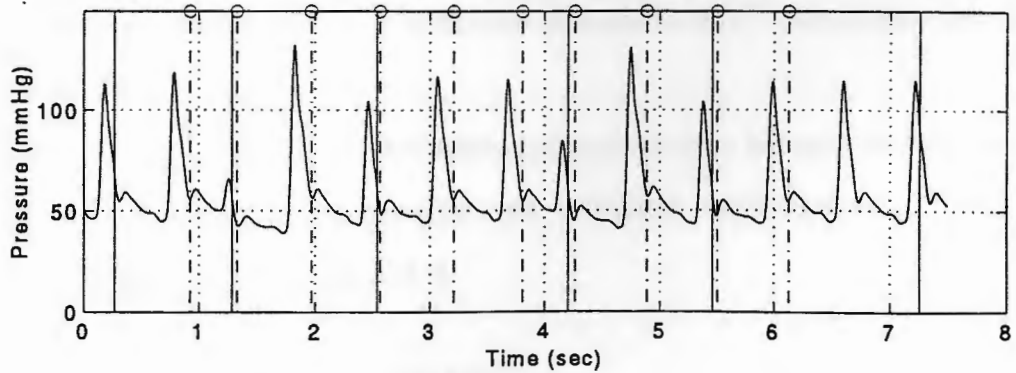
Arterial Blood Pressure (Jundanian) File128



Arterial Blood Pressure (Martino) File128



Arterial Blood Pressure (Kinias) File128



References

- [1] Lewis, R. P., Rittgers, S. E., Forester, W. F., and Boudoulad, H., "A critical review of the systolic time intervals," *Circulation*, vol. 56, pp.146-158, Feb 1977.
- [2] Lewis, R. P., Boudoulas, H., Welch, T. G. and Forester, W. F., "Usefulness of systolic time intervals in coronary artery disease," *American Journal of Cardiology*, vol. 37, pp. 787-796, 1976.
- [3] Lewis, R. P., "Diagnostic value of systolic time intervals in man," *Diagnostic Methods in Cardiology*, Fowler ed., Philadelphia, FA Davis, pp. 245-264, 1975.
- [4] Weissler, A. M., Harris, W. S. and Schoenfeld, C. D., "Systolic time intervals in heart failure in man," *Circulation*, vol. 37, pp. 149-159, Feb 1968.
- [5] Weissler, A. M., Lewis, R. P. and Leighton, R. F., "The systolic time intervals as a measure of left ventricular performance in man," *Progress in Cardiology*, Yu PN ed., Goodwin JF, Philadelphia, Lea and Febiger, pp. 155-183, 1972.
- [6] Hamosh, P. and Cohn, J. N., "Systolic time intervals and left ventricular function in acute myocardial infarction," *Circulation*, vol. 45, pp. 375-381, 1972.
- [7] Ahmed, S. S., Levinson, G. E., Schwartz, C. J. and Ettinger, P. O., "Systolic time intervals as measures of the contractile state of the left ventricular myocardium in man," *Circulation*, vol. 46, pp. 559-571, 1972.
- [8] Martin, C. E., and Shaver, J. A., "Direct correlation of external systolic time intervals with internal indices of ventricular function in man," *Circulation*, vol. 44, pp. 419, 1971.
- [9] Khullar, S. and Lewis, R. P., "Usefulness of systolic time intervals in differential diagnosis of constrictive pericarditis and restrictive cardiomyopathy," *British Heart Journal*, vol. 38, pp. 43, 1976.

- [10] Stack, R. S. and Lee, C. C., "Left ventricular performance in coronary artery disease evaluated with systolic time intervals and echocardiography," *American Journal of Cardiology*, vol. 37, pp. 331, 1976.
- [11] Kantrowitz, A: Origins of intraaortic balloon pumping. *Annals of Thoracic Surgery*, vol. 50, pp. 672-4, 1990.
- [12] Weber, K. T. and Janicki, J.S., "Intraaortic balloon counterpulsation," *Annals of Thoracic Surgery*, vol. 17, pp. 602-636, June 1974.
- [13] Kantrowitz, A., "Mechanical support to the failing heart," *Transactionscript-Assisted Circulation Colloquim at Bad Neuenahr*, Germany, pp. 78-95, 1967.
- [14] Kim, C., *Computer Simulation of the Intra Aortic Balloon Pump: A Timing Control Algorithm in the Presence of Arrhythmia*, PhD Thesis, University of Rhode Island, Electrical Engineering, May 1994.
- [15] Kantrowitz, A., Freed, P. S., Tacai, H. and Sukuki, A., *Electrocardiographic Measurement Method for Controlling an Intra-aortic Balloon Pump*, U. S. Patent # 4809681, March 1989.
- [16] Kern, M. J., Aguirre, F. V. and Tatineni, S., "Enhanced coronary blood flow velocity during intraaortic balloon counterpulsation in critically ill patients," *Journal of the American College of Cardiology*, vol. 21, pp. 359-68, Feb 1993.
- [17] Kantrowitz, A., Freed, P. S. and Cardona, R. R., "Initial clinical trial of a closed loop, fully automatic intra-aortic balloon pump," *ASAIO Transactions*, vol. 38, pp. M617-21, March 1992.
- [18] Fuchs, R. M., Brin, K. P., and Brinker, J. A., "Augmentation of regional coronary blood flow by intraaortic balloon counterpulsation in patients with unstable angina," *Circulation*, vol.68, pp.117, 1983.

- [19] Tyson, G. S., Davis, J. W. and Rankin, J.S., "Improved performance of the intra-aortic balloon pump in man," *Proceedings of the 42nd Fund Surg Prob, 72nd Annual Clinical Congress*, pp. 214-216, 1986.
- [20] Weber, K. T., Janicki, J.S. and Walker, A. A., "Intra-aortic balloon pumping: an analysis of several variables affecting balloon performance," *Transactions of ASAIO*, vol. 18, pp. 486-492, 1972.
- [21] Barnea, O., Moore, T. W., Dubin, S. E. and Jaron, D., "Cardiac energy considerations during intraaortic balloon pumping," *IEEE Transactions on Biomedical Engineering*, vol. 37, pp.170-181, Feb 1990.
- [22] *Massachusetts General Hospital MGH/MF Waveform Database, and Patient Guide*, Massachusetts Institute of Technology, 1992.
- [23] Hong, L., "Multiresolution filtering using wavelet transform," *IEEE Transactions on Aerospace and Electronic Systems*, vol. 29, pp.1244, April 1993.
- [24] Akansu, A. N., and Haddad, R. A., *Multiresolution Signal Decomposition, Transforms, Subbands and Wavelets*. Academic Press, San Diego, 1992.
- [25] Simoncelli, E. P., "Shiftable mult-scale transforms. *IEEE Transactions on Information Theory, Special Issue on Wavelet Transforms and Multiresolution Signal Analysis*, vol. 38, pp. 587-607, 1992.
- [26] Mallat, S., "Multifrequency channel decompositions of images and wavelet models," *IEEE Transactions on Acoustic, Speech and Signal Processing*, vol. 37, pp. 2091-2110, Dec 1989.
- [27] Mallat, S., "Multiresolution approximation and wavelet orthonormal bases of L_2 ," *Transactions of the American Mathematical Society*, vol. 315, pp. 69-87, Jan 1989.

- [28] Mallat, S., "A theory for multiresolution signal decomposition: the wavelet representation," *IEEE Transactions on Pattern Analysis and Machine Intelligence*, vol.11, pp. 674-693, July 1989.
- [29] Mallat, S., "Review of multifrequency channel decompositions of images and wavelet models," *IEEE Transactions on Acoustics, Speech and Signal Processing*, 1989.
- [30] Rioul, O. and Vetterli, M., "Wavelets and signal processing," *IEEE Signal Processing Magazine*, pp. 14-38, Oct 1991.
- [31] Daubechies, I., "The wavelet transform, time-frequency localization and signal analysis," *IEEE Transactions on Information Theory*, vol. 36, pp. 961-1005, May 1990.
- [32] Mallat, S., *IEEE Transactions Information Theory*, March, 1992.
- [33] Mallat, S. and Zhong, S., "Characterization of signals from multiscale edges," *IEEE Pattern Analysis and Machine Intelligence*, vol. 14, pp. 710-732, July 1992.
- [34] Zhong, S. and Mallat, S., "Compact image representation from multiscale edges," *Proceedings of the 3rd International Conference on Computer Vision*, Dec, 1990.
- [35] Mallat, S. and Zhong, S., "Complete signal representation with multiscale edges," Technical Report 91-16, New York University, vol. 1, pp. 76, 1989.
- [36] Guyton, A. C., *Human Physiology and Mechanics of Disease*. 4th ed., W.B. Saunders Company, Philadelphia, PA, 1987.
- [37] Schlant, R. C., *The Heart*. Hurst, J. W. and Logue, R. B., ed., second edition, McGraw-Hill, NY, 1970.
- [38] Noble, M. I. M., *The Cardiac Cycle*, Blackwell Scientific Publications, St. Louis, MO, 1979.
- [39] Spencer, F. C., "A critique of emergency and urgent operations for complications of coronary artery disease," *Circulation*, vol. 79, supplement I, pp. I-160-2, 1989.

- [40] Subramanian, V. A., Goldstein, J. E. and Sos, T. A., "Preliminary clinical experience with percutaneous intraaortic balloon pumping," *Circulation*, vol. 62, supplement I, pp. I-123-9, 1980.
- [41] Hedenmark, J., Ahn, H. and Nystrom, S. O., "Intra-aortic balloon counterpulsation with special reference to determinants of survival," *Scandinavian Journal of Thoracic and Cardiovascular Surgery*, vol. 23, pp. 57-62, 1989.
- [42] Smith, D. and Craige, E., "Influence of the aortic component of the second heart sound on left ventricular maximal negative dP/dt in the dog," *American Journal of Cardiology*, vol. 55, pp. 205-9, January 1985.
- [43] Nandagopal, D. and Mazaumdar, J., "Spectral analysis of second heart sound in normal children by selective linear prediction coding," *Medical and Biological Engineering & Computers*, vol. 22, pp. 229-239, March 1984.
- [44] Iwata, A., Ishii, N. and Suzumura, N. "Algorithm for detecting the first and the second heart sounds by spectral tracking," *Medical and Biological Engineering & Computers*, vol. 18, pp. 19-26, 1980.
- [45] Campbell, G. and Roberts, R., "Spectral estimation of cardiovascular sounds," *Biomedical Science Instrumentation*, vol. 14, pp.27-31, 1978.
- [46] Heckman, J. L., Stewart, G. H. and Lynch, P. R., "Frequency analysis approach to the origin of the first and second heart sounds," *American Heart Journal*, vol. 104, pp. 1309-1318, 1982.
- [47] Smith, D., Ozawa, Y. and Craige, E., "Chest wall velocity and the second heart sound. An improved sensor of S2 splitting," *Circulation*, vol. 67, pp. 1304-1311, June 1983.
- [48] Durand, L. G., Langlois, Y. E. and Lanthier, T., "Contribution of left ventricular vibrations to the spectrum of aortic valve closure sound," *Annual International*

- Conference of the IEEE Engineering in Medicine and Biology Society*, vol. 12, pp. 567-568, Feb 1990.
- [49] Yoganathan, A. P. and Gupta, R., "Use of the fast Fourier transform in the frequency analysis of the second heart sound in normal man," *Medical and Biological Engineering*, pp.455-459, July 1976.
- [50] Frome, E. L. and Frederickson, E. L., "Digital spectrum analysis of the first and second heart sounds," *Computers and Biomedical Research*, vol. 7 pp. 421-431, 1974.
- [51] Papoulis, A: *Signal Analysis*. McGraw-Hill, New York, 1977.
- [52] Oppenheim, A., Willsky, A. and Young, I., *Signals and Systems*. Prentice Hall, New Jersey, 1983.
- [53] Oppenheim, A. and Schaffer, R. W., *Discrete-Time Signal Processing*. Prentice Hall, New Jersey, 1989.
- [54] Allen, J. B., "Application of short-time Fourier transform to speech processing and spectral analysis," *Proceedings of the International Conference on ASSP*, pp.1012-1-15, May 1982.
- [55] Allen, J. B., "Short-term spectral analysis, synthesis and modification by discrete Fourier transform," *IEEE Transactions on Acoustics, Speech and Signal Processing*, vol. 25, pp. 235-238, March 1977.
- [56] Allen, J. B. and Rabiner, L. R., "A unified approach to STFT analysis and synthesis," *Proceedings of the IEEE*, vol. 65, pp. 1558-1564, 1977.
- [57] Crochiere, R. E., "A weighted overlapp-add method of short-time Fourier analysis/synthesis," *IEEE Transactions on Acoustics, Speech and Signal Processing*, vol. 28, pp. 99-102, 1980.

- [58] Griffin, D. W. and Lim, J. S., "Signal estimation from modified short-time Fourier transform," *Proceedings of the International Conference on ASSP*, pp.804-807, 1983.
- [59] Duhamel, P., Flandrin, P. and Nishitani, T., "Wavelets and signal processing," *IEEE Transactions on Signal Processing*, vol. 41, pp. 3213, Dec 1993.
- [60] Meyer, Y., *Ondelettes et Operateurs*. Hermann, New York, 1990.
- [61] Meyer, Y., *Wavelets: Algorithms & Applications*. SIAM, Philadelphia, PA, 1993.
- [62] Vetterli, M. and Herley, C., "Wavelets and filter banks: theory and design," *IEEE Transactions on Signal Processing*, vol. 40, Sept 1992.
- [63] Daubechies, I., "Ten lectures on wavelets," *CBMS-NSF Series Applied Mathematics, SIAM*, 1991.
- [64] Chui, C. K., *An Introduction to Wavelets*. Academic Press, Boston, MA, 1992.
- [65] Chui, C. K., *Wavelets: A Tutorial in Theory and Applications*. Academic Press, Boston, MA, 1992.
- [66] Young, R., *Wavelet Theory and Its Applications*. Klower Academic Publishers, Boston, MA, 1993.
- [67] Freeman, M. O., "Wavelets: signal representations with important advantages," *Optics & Photonics News*, vol. 4, pp. 8-14, Aug 1993.
- [68] Kaiser, G., *A Friendly Guide to Wavelets*. Birkhauser Boston, 1994.
- [69] Heil, C, and Walnut, D., "Continuous and discrete wavelet transforms," *SIAM Review* vol. 31, pp. 628-666, April 1989.
- [70] Zayed, A., "Wavelet transform of periodic generalized functions," *Journal of Mathematical Analysis and Application*, vol. 183, pp. 391, March 1994.
- [71] Starck, J. and Bijaoui, A., "Filtering and deconvolution by the wavelet transform," *Signal Processing*, vol. 35, pp. 195, March 1994.

- [72] Lhegu, B., *The Intra-aortic Balloon Pump (IABP)*. Rapport de Stage, Universite d'Orleans - DESS Systemes Temps Reel, Signaux et Images, at University of Rhode Island, 1993.
- [73] Khamlach, R., *Wavelet Transform Analysis for Dicrotic Notch Detection*. Rapport de Stage, Universite d'Orleans - DESS Systemes Temps Reel, Signaux et Images, at University of Rhode Island, 1994.
- [74] Jackson, L. B. and Wood, S., "Linear prediction in cascade form," *IEEE Transactions on Acoustics, Speech and Signal Processing*, vol. 26, pp. 518-528, June 1978.
- [75] Harris, F. J., "On the use of windows for harmonic analysis with the discrete Fourier transform," *Proceedings of the IEEE*, vol. 66, pp. 51-83, 1978.
- [76] Afonso, V. X. and Tompkins, W. J., "Detecting ventricular fibrillation: selecting the appropriate time-frequency analysis tool for the application," *IEEE Engineering in Medicine and Biology Society Magazine* vol. 14, pp.152-159, Feb 1995.
- [77] Hlawatsch, F. and Boudreaux-Bartels, G. F., "Linear and quadratic time-frequency signal representations," *IEEE Signal Processing Magazine*, pp.21-67, April 1992.
- [78] Loughlin, P. J., Pitton, J. W. and Atlas, L. E., "Bilinear time-frequency representations: new insights and properties," *IEEE Transactions on Signal Processing*, vol. 41, pp. 750-766, Feb 1993.
- [79] Grossmann, A. and Morlet, J., "Decomposition of Hardy functions into square integrable wavelets of constant shape," *SIAM Journal of Mathematical Analysis*, vol. 15, pp. 723-736, 1984.
- [80] Grossmann, A., "Wavelet transforms and edge detection," *Stochastic Processes in Physics and Engineering* (Abeverto, S., ed.), pp.149-157, 1988.

- [81] Kadambe, S., *The application of Time-Frequency and Time-Scale Representations in Speech Analysis*. PhD Thesis, University of Rhode Island, Electrical Engineering, 1990.
- [82] Murray, R., *Dyadic Wavelet Transform Based QRS Detector*. ScM Thesis, University of Rhode Island, Electrical Engineering, 1993.
- [83] Donoho, D. L. and Stark, P.B., "Uncertainty principles and signal recovery," *SIAM Journal on Applied Mathematics*, vol. 49, pp. 906, March 1989.
- [84] de Bruijn, N. G., *Uncertainty principles in Fourier analysis. Inequalities*, (Shisha, O. ed.), pp.57-71, Academic Press, New York, 1967.
- [85] Gabor, D., "Theory of communication," *Journal of the IEE (London)*, vol. 93, pp. 429-457, 1946.
- [86] Franklin, P., "A set of continuous orthogonal functions," *Mathematics. Annals*, vol. 100, pp. 522-529, 1928.
- [87] Littlewood, J. and Paley, R., "Theorems on Fourier series and power series," *Proceedings of the London Mathematical Society*, vol. 42, pp. 52-89, 1937.
- [88] Calderon, A., "Intermediate spaces and interpolation, the complex method," *Studia Mathematica*, vol. 24, pp. 113-190, 1964.
- [89] Witkin, A., "Scale-space filtering," *Proceedings of the International Joint Conference on Artificial Intelligence*, 1983.
- [90] Grossmann, A., Kronland-Martinet, R. and Morlet, J., "Reading and understanding continuous wavelet transforms," *Proceedings of the International Conference on Wavelets, Time-Frequency Methods and Phase Space*, pp. 2-20, Dec 1987.
- [91] Daubechies, I., "Orthornormal bases of compactly supported wavelets," *Communications on Pure and Applied Mathematics*, vol.41. pp.909-990, July 1988.

- [92] Daubechies, I., "Orthonormal bases of compactly supported wavelets II: variations on a theme. *SIAM Journal on Mathematical Analysis*, vol. 24, pp. 499, Feb 1993.
- [93] Cohen, A. and Daubechies, I., "On the instability of arbitrary biorthogonal wavelet packets," *SIAM Journal on Mathematical Analysis*, vol. 24, pp. 1340, May 1993.
- [94] Cohen, A., Daubechies, I. and Feauveau, J. C., "Orthonormal bases of compactly supported wavelets," *Communications on Pure and Applied Mathematics*, vol. 45, pp. 485, May 1992.
- [95] Daubechies, I. and Cohen, A., "A stability criterion for biorthogonal wavelet bases and their related subband coding scheme," *Duke Mathematical Journal*, vol. 68, pp. 313, Feb 1992.
- [96] Cohen, A. and Daubechies, I., "Orthonormal bases of compactly supported wavelets II: better frequency resolution," *SIAM Journal on Mathematical Analysis*, vol. 24, pp. 520, Feb 1993.
- [97] Kadambe, S. and Boudreaux-Bartels G. F., "A pitch detector based on event detection using the dyadic wavelet transform," *Proceedings of the International Conference on Spoken Language Processing*, (Kobe, Japan), pp.469-472, 1990.
- [98] Kadambe, S. and Boudreaux-Bartels G. F., "Application of the wavelet transform for pitch detection of speech signals," *IEEE Transactions Information Theory*, vol. 38, pp. 917-924, March, 1992.
- [99] Kadambe, S. and Boudreaux-Bartels, G. F., "A comparison of a wavelet transform event detection pitch detector with classical pitch detector," *Proceedings of the 24th Annual Asilomar Conference on Signals, Systems and Computers*, (Pacific Grove, CA), 1990.

- [100] Kadambe, S. and Boudreaux-Bartels G. F. "A comparison of wavelet functions for pitch detection of speech signals," *Proceedings of the International Conference on ASSP*, (Toronto, CA), 1991.
- [101] Kronland-Martinet, R., "The wavelet transform for analysis, synthesis, and processing of speech and music sounds," *Computer Music Journal*, vol. 12, pp. 11-20, April 1988.
- [102] Kronland-Martinet, R., Morlet, J. and Grossmann, A., "Analysis of sound patterns through wavelet transforms," *Recognition and Artificial Intelligence*, vol.1, pp. 273-302, 1987.
- [103] Grossmann, A., Holschneider, M., Kronland-Martinet, R. and Morlet, J., *Detection of Abrupt Changes in Sound Signals with the Help of the Wavelet Transform*. Center de Physique Theorique, CNRS, Marseille, France, 1988.
- [104] Ginette, S., Grossmann, A. and Tchamitchian, P., "Use of wavelet transforms in the study of propagation of transient acoustic signals across a plane interface between two homogeneous media," *Proceedings of the International Conference on Wavelets, Time-Frequency Methods and Phase Space*. pp.139-146, 1987.
- [105] Wilson, R., Calway, A. D. and Pearson, E. R. S., "A generalized wavelet transform for Fourier analysis: The multiresolution Fourier transform and its application to image and audio signal analysis," *IEEE Transactions on Information Theory*, vol. 38, pp. 674, Feb 1992.
- [106] Senhadji, L. and Bellanger, J., "Wavelet analysis of ECG signals," *Annual International Conference IEEE Engineering in Medicine and Biology Society*, vol. 12, pp. 811-12, Feb 1990.
- [107] Tuteur, F. B., "Wavelet transformations in signal detection," *Proceedings of the International Conference on ASSP*, pp.1435-1438, 1988.

- [108] Crowe, J. A., Gibson, N. M. and Woolfson, M. S., "Wavelet transform as a potential tool for ECG analysis and compression," *Journal of Biomedical Engineering*, vol. 14, pp. 268, March 1992.
- [109] Meste, O., and Rix, H., "Detection of late potentials by means of wavelet transform," *Proceedings of the IEEE International Conference Engineering in Medicine and Biology*. pp.637-638, 1991.
- [110] Meste, O., Rix, H., Thakor, N. V., "Ventricular late potentials characterization in time-frequency domain by means of wavelet transform," *IEEE Transactions on Biomedical Engineering*, vol. 41, pp. 625, July 1994.
- [111] Thakor, N. V. and Xin-Rong, G., "Multiresolution wavelet analysis of evoked potentials," *IEEE Transactions on Biomedical Engineering*, vol. 40, pp. 1085-1094, Nov 1993.
- [112] Bertrand, O., Bohorquez, J. and Pernier, J., "Time-Frequency digital filtering based on an invertible wavelet transform: an application to evoked potentials," *IEEE Transactions on Biomedical Engineering*, vol. 41, pp. 77, Jan 1994.
- [113] Bartnik, E. A., Blinowska, K. J. and Durka, P. J., "Single evoked potential reconstruction by means of wavelet transform. *Biological Cybernetics*, vol. 67, pp. 175, Feb 1992.
- [114] Kalayci, T. and Ozdamar, O., "Wavelet processing for automated neural network detection of EEG spikes," *IEEE Engineering in Medicine and Biology Magazine* vol.14, pp. 160-166, Feb 1995.
- [115] Senhadji, L., Carrault, G., Bellanger, J. and Passariello, G., "Comparing wavelet transforms for recognizing cardiac patterns," *IEEE Engineering in Medicine and Biology Society Magazine*, vol. 14, pp. 167-173, Feb 1995.

- [116] Lim, L. M., Akay, M. and Daubenspeck, J. A., "Identifying respiratory-related evoked potentials," *IEEE Engineering in Medicine and Biology Society Magazine* vol. 14, pp. 174-178, Feb 1995.
- [117] Karrakchou, M., van den Branden Lambrecht, C. and Kunt, M., "Analyzing pulmonary capillary pressure: more accurate measurements using mutual wavelet packets for adaptive filtering," *IEEE Engineering in Medicine and Biology Society Magazine* vol. 14, pp. 179-185, Feb 1995.
- [118] Yomogida, K., "Detection of anomalous seismic phases by the wavelet transform," *Geophysical Journal International*, vol. 116, pp. 119, Jan 1994.
- [119] Larssonneur, J. L., Morlet, J., "Wavelets and seismic interpretation," *Proceedings of the International Conference on Wavelets, Time-Frequency Methods and Phase Space*, (Marseille, France), pp.126-131, Dec 1987.
- [120] Coupinot, G., Hecquet, J. and Auriere, M., "Photometric analysis of astronomical images by the wavelet transform," *Astronomy and Astrophysics*, vol.259, pp. 701, Feb 1992.
- [121] Bendjoya, P., Slezak, E. and Froeschle, C., "The wavelet transform: a new tool for asteroid family determination," *Astronomy and Astrophysics*, vol. 251, pp. 312, Jan 1991.
- [122] Slezak, E., Bijaou, A. and Mars, G., "Identification of structures from galaxy counts: use the wavelet transform," *Astronomy and Astrophysics*, vol. 227, pp. 301, Feb 1990.
- [123] Starck, J., Bijaoui, A. and Lopez, B., "Image reconstruction by the wavelet transform applied to aperture synthesis," *Astronomy and Astrophysics*, vol. 283, pp. 349, Jan 1994.
- [124] Wang, W., Jin, G. and Wu, M., "Image feature extraction with the optical Haar wavelet transform," *Optical Engineering*, vol. 34, pp. 1238, April 1995.

- [125] Wang, W., Jin, G. and Wu, M., "Joint wavelet-transform correlator for image feature extraction," *Applied Optics*, vol. 34, pp. 370, Feb 1995.
- [126] Lee, J., Sun, Y. and Chen, C., "Multiscale corner detection by using wavelet transform," *IEEE Transactions on Image Processing*, vol. 4, pp. 100, Jan 1995.
- [127] Yaou, M. and Chang, W., "Fast surface interpolation using multiresolution wavelet transform," *IEEE Transactions on Pattern Analysis and Machine Intelligence*, vol. 16, pp. 673, July 1994.
- [128] Clarke, L., Kallergi, M. and Silbiger, M., "Tree-structured non-linear filter and wavelet transform for microcalcification segmentation in digital mammography," *Cancer Letters*, vol. 77, part 2, pp. 173, Feb 1994.
- [129] Chang, T. and Kuo, C., "Texture analysis and classification with tree-structured wavelet transform," *IEEE Transactions on Image Processing*, vol. 2, pp. 429, April 1993.
- [130] Antoine, J., Carrette, P. and Murenzi, R., "Image analysis with two-dimensional continuous wavelet transform," *Signal Processing*, vol. 31, pp. 241, March 1993.
- [131] Djamdji, J. P., Bijaoui, A. and Maniere, R., "Geometrical registration of images: the multiresolution approach," *Photogrammetric Engineering and Remote Sensing*, vol. 59, pp. 645, May 1993.
- [132] Beltran del Rio, L., Gomez, A. and Jose-Yacaman, M., "Image processing in TEM using the wavelet transform," *Ultramicroscopy*, vol. 38, part 4, pp. 319, March 1991.
- [133] Huh, Y., Hwang, J. and Rao, K., "Block wavelet transform coding of images using classified vector quantization," *IEEE Transactions on Circuits and Systems*, vol. 5, pp. 63, Jan 1995.

- [134] Goh, K., Soraghan, J. and Durrani, T., "Wavelet transform based adaptive bit-plane run-length coding for still images," *Electronic Letters*, vol. 30, pp. 395, May 1994.
- [135] Goh, K., Soraghan, J. and Durrani, T., "New 3-D wavelet transform coding algorithm for image sequences," *Electronic Letters*, vol. 29, pp. 401, April 1993.
- [136] Ohta, M., Yano, M. and Nishitani, T., "Wavelet picture coding with transform coding approach," *IEICCE Transactions on Fundamentals of Electronic*, vol. 75, pp. 776, July 1992.
- [137] Lewis, A. and Knowles, G., "Image compression using the 2-D wavelet transform," *IEEE Transactions on Image Processing*, vol. 1, pp. 244, Feb 1992.
- [138] Antonini, M., Barlaud, M. and Mathieu, P., "Image coding using wavelet transform," *IEEE Transactions on Image Processing*, vol. 1, pp. 205, Feb 1992.
- [139] DeVore, R., Jawerth, B. and Lucier, B., "Image compression through wavelet transform coding," *IEEE Transactions on Information Theory*, vol. 38, part 2, pp. 719, Feb 1992.
- [140] Chang, D. C., Su, C. N. and Fu, I. J., "Interpretation of a dynamic radar cross-section using the wavelet transform," *International Journal of Electronics*, vol. 78, pp. 67, Jan 1995.
- [141] Ehara, N., Sasase, I. and Mori, S., "Weak radar signal detection based on wavelet transform," *Electronics and Communications in Japan*, Part 3. vol 77, pp. 105, Aug 1994.
- [142] Sanghadasa, M., Erbach, P. and Sung, C., "Wavelet transform applied to synthetic aperture radar - Optical implementation and adaptive techniques," *Optical Engineering*. vol. 33, pp. 2282, July 1994.

- [143] Rothwell, E., Chen, K. and Bebermeyer, R., "A radar target discrimination scheme using the discrete wavelet transform for reduced data storage," *IEEE Transactions on Antennas and Propagation*, vol. 42, pp. 1033, July 1994.
- [144] Frisch, M. and Messer, H., "The use of the wavelet transform in the detection of an unknown transient signal," *IEEE Transactions Information Theory*, vol. 38, pp. 892, Feb 1992.
- [145] Mallat, S., Hwang, W., "Singularity detection and processing with wavelets," *IEEE Transactions on Information Theory*, vol. 38, part 2, pp. 617, Feb 1992.
- [146] Del Marco, S. and Weiss, J., "M-band wavepacket-based transient signal detector using a translation -invariant wavelet transform," *Optical Engineering*, vol. 33, pp. 2175, July 1994.
- [147] Onsay, T. and Haddow, A., "Wavelet transform analysis of transient wave propagation in a dispersive medium," *Journal of the Acoustical Society of America*, vol. 95, pp. 1441, March 1994.
- [148] Permann, D. and Teitelbaum, H., "Wavelet fast Fourier transform (WFFT) analysis of a millivolt signal for a transient oscillating chemical reaction," *Journal of Physical Chemistry*, vol. 97 n. 49, pp. 12670, 1993.
- [149] Kikuchi, H., Nakashizuka, M. and Watanabe, H., "Fast wavelet transform and its application to detecting detonation," *IEICE Transactions on Fundamentals of Electronic*, vol. 75, pp. 980, Aug 1992.
- [150] Masry, E., "The wavelet transform of stochastic processes with stationary increments and its application to fractional Brownian motion," *IEEE Transactions on Information Theory*, vol. 39, pp. 260, Jan 1993.
- [151] Tewfik, A. H. and Kim, M., "Correlation structure of the discrete wavelet coefficient of fractional Brownian motion," *IEEE Transactions on Information Theory*, vol. 38, part 2, pp. 904, Feb 1992.

- [152] Flandrin, P., "Wavelet analysis and synthesis of fractional Brownian motion," *IEEE Transactions on Information Theory*, vol. 38, part 2, pp. 910, Feb 1992.
- [153] Vaienti, S., "A frostman-like theorem for the wavelet transform on fractal sets," *Nonlinearity*, vol. 4, pp. 1241, April 1991.
- [154] Pouligny, B., Gabriel, G. and Muzy, J., "Optical wavelet transform and local scaling properties of fractals," *Journal Applied Crystallography*, vol. 24, pp. 526, May 1991.
- [155] Argoul, F., Arneodo, A. and Elezgaray, J., "Wavelet transform of fractal aggregates. *Physics Letters: part A*, vol. 135, pp. 327, June/July 1989.
- [156] Arneodo, A., "Wavelet transform of multifractals," *Physical Review Letters*, vol. 61, n. 20, pp. 2281, 1988.
- [157] Wornell, G. and Oppenheim, A., "Wavelet based representations for fractal modeling," *NSF/CBMS Conference on Wavelets*, (Lowell, MA), June 1990.
- [158] Goswami, J., Chan, A. and Chui, C., "An application of fast integral wavelet transforms to waveguide mode identification," *IEEE Transactions on Microwave Theory and Technology*, vol. 43, pp. 655, March 1995.
- [159] Kim, H. and Ling, H., "On the application of fast wavelet transform to the integral-equation solution of electromagnetic scattering," *Microwave and Optical Technology Letters*, vol. 6, pp. 168, March 1993.
- [160] Liandrat, J. and Moret-Bailly, F., "The wavelet transform: some applications to fluid dynamics and turbulence," *European Journal Mechanics*, vol. 9, pp. 1, Jan 1990.
- [161] Lagoutte, D., Cerisier, J. and Plagnaud, J., "High-latitude ionospheric electrostatic turbulence studied by means of the wavelet transform," *Journal of Atmospheric and Terrestrial Physics*, vol. 54, pp.1283, Oct 1992.

- [162] Zubair, L. and Sreenivasan, D., "Wavelet analysis applied to turbulence," *NSF/CBMS Conference on Wavelets*, (Lowell, MA), June 1990.
- [163] Morlet, J., *Sampling Theory and Wave Propagation*. NATO Series I, Issues in Acoustic Signal/Image Processing and Recognition, (Chen, C. H., ed.) Springer-Verlag, Berlin, 1983.
- [164] Daubechies, I., Grossmann, A. and Meyer, Y., "Painless nonorthogonal expansions. *Journal of Mathematics and Physics*, vol. 27, pp. 1271-1283, 1986.
- [165] Abry, P. and Flandrin, P., "On the initialization of the discrete wavelet transform algorithm," *IEEE Signal Processing Letters*, vol. 1, pp. 32, Feb 1994.
- [166] Vishwanath, M., "The recursive pyramid algorithm for the discrete wavelet transform," *IEEE Transactions on Signal Processing*, vol. 42, pp. 673, March 1994.
- [167] Shensa, M. J., "The discrete wavelet transform: wedding the A Trous and Mallat algorithms," *IEEE Transactions on Signal Processing*, vol. 40, pp. 2464, Oct 1992.
- [168] Yaou, M., Chang, W., "M-Ary wavelet transform and formulation for perfect reconstruction in M-band filter bank," *IEEE Transactions on Signal Processing*, vol. 42, pp. 3508, Dec 1994.
- [169] Szu, H., Sheng, Y. and Chen, J., "Wavelet transform as a bank of the matched filters," *Applied Optics*, vol. 31, n. 17, pp. 3267, 1992.
- [170] Akansu, A. N., Haddad, R. A. and Caglar, H., "The bionomial QMF-wavelet transform for multiresolution signal decomposition," *IEEE Transactions on Signal Processing*, vol. 41, pp. 13, Jan 1993.
- [171] Vaidyanathan, P., "Quadrature mirror filter banks, M-band extensions and perfect reconstruction techniques," *IEEE ASSP Magazine*, vol. 4, pp. 4-20, 1987.

- [172] Akansu, A. N., "An efficient QMF-wavelet structure," *NSF/CBMS Conference on Wavelets*, (Lowell, MA), June 1990.
- [173] Unser, M., Aldroubi, A. and Schiff, S. J., "Fast implementation of the continuous wavelet transform with integer scales," *IEEE Transactions on Signal Processing*, vol. 42, pp. 3519, Dec 1994.
- [174] Boudreaux-Bartels, G. F., Private Discussion, 1994.
- [175] El-Ghazzawi, Z. F. and Welch, J. P., "Algorithm to identify components of arterial blood pressure signals during use of an intra-aortic balloon pump," *Journal of Clinical Monitoring*, vol. 9 pp. 297-308, 1993.
- [176] Tewfik, A. H., Sinha, D. and Jorgensen, P., "On the optimal choice of a wavelet for signal representation," *IEEE Transactions on Information Theory*, vol. 38, part 2, pp. 747, Feb 1992.
- [177] Zou, H., Tewfik, A. H., "Parameterization of compactly supported orthonormal wavelets," *IEEE Transactions on Signal Processing*, vol, 41, pp. 1428, March 1993.
- [178] Wang, S. H., Tewfik, A. H. and Zou, H., "Correction to "Parameterization of compactly supported orthonormal wavelets," *IEEE Transactions on Signal Processing*, vol. 42, pp. 208, Jan 1994.
- [179] Donoho, D. L. and Stark, P. B., "A note of rearrangements, spectral concentration, and the zero-order prolate spherical wavefunctions," *IEEE Transactions on Information Theory*, vol. 39, pp. 257, Jan 1993.
- [180] Abry, P. and Aldroubi, A., "Designing multiresolution analysis-type wavelets and their fast algorithm," (preprint), pp.1-50, 1994.
- [181] Wilson, E., *Transient Detection and Feature Extraction Using Neural Networks*. PhD Thesis, University of Rhode Island, Electrical Engineering, 1993.

- [182] Lee, J. Y. and Lin, J. C., "A microprocessor-based noninvasive arterial pulse wave analyzer," *IEEE Transactions on Biomedical Engineering*, vol. 32, pp. 451-455, June 1985.
- [183] Jundanian, R. H., Armitage, J. W. and Peura, R. A., "A microprocessor based rate-pressure product computer," *Proceedings of the 5th Annual Conference of IEEE Frontiers of Engineering and Computers in Health Care*, pp. 188-90, 1983.
- [184] Martino, R. L. and Risso, W. L., "An arterial blood pressure preprocessor using a combined analog and digital signal processing method," *Proceedings of the 7th IEEE Northeast Biomedical Conference*, pp.267-70, 1979.
- [185] Kinias, P., Fozzard, H. A. and Norusis, M. J., "A real time pressure algorithm," *Computers in Biology and Medicine*, vol. 11, pp. 211-20, April 1981.
- [186] Burattini, R., Fioretti, S. and Jetto, L., "A simple algorithm for defining the mean cardiac cycle of aortic flow and pressure during steady state," *Computers and Biomedical Research*, vol. 18, pp. 303-312, 1985.
- [187] Gebber, V. and Welch, J., *Circuit for Detecting Initial Systole and Dicrotic Notch*. U. S. Patent # 3850169, 1974.
- [188] Oppenheim, M. I., Factor, M. and Sittig, D. F., "BIO-SPEAD. A parallel computing environment to accelerate development of biological signal processing algorithms," *Computational Methods & Programming in Biomedicine*, vol. 37, pp. 137-47, 1992.

Bibliography

Abry, P. and Flandrin, P., "On the initialization of the discrete wavelet transform algorithm," *IEEE Signal Processing Letters*, vol. 1, pp. 32, Feb 1994.

Abry, P. and Aldroubi, A., "Designing multiresolution analysis-type wavelets and their fast algorithm," (preprint), pp.1-50, 1994.

Afonso, V. X. and Tompkins, W. J., "Detecting ventricular fibrillation: selecting the appropriate time-frequency analysis tool for the application," *IEEE Engineering in Medicine and Biology Society Magazine* vol. 14, pp.152-159, Feb 1995.

Ahmed, S. S., Levinson, G. E., Schwartz, C. J. and Ettinger, P. O., "Systolic time intervals as measures of the contractile state of the left ventricular myocardium in man," *Circulation*, vol. 46, pp. 559-571, 1972.

Akansu, A. N., and Haddad, R. A., *Multiresolution Signal Decomposition, Transforms, Subbands and Wavelets*. Academic Press, San Diego, 1992.

Akansu, A. N., Haddad, R. A. and Caglar, H., "The binomial QMF-wavelet transform for multiresolution signal decomposition," *IEEE Transactions on Signal Processing*, vol. 41, pp. 13, Jan 1993.

Akansu, A. N., "An efficient QMF-wavelet structure," *NSF/CBMS Conference on Wavelets*, (Lowell, MA), June 1990.

Allen, J. B., "Application of short-time Fourier transform to speech processing and spectral analysis," *Proceedings of the International Conference on ASSP*, pp.1012-1-15, May 1982.

Allen, J. B., "Short-term spectral analysis, synthesis and modification by discrete Fourier transform," *IEEE Transactions on Acoustics, Speech and Signal Processing*, vol. 25, pp. 235-238, March 1977.

- Allen, J. B. and Rabiner, L. R., "A unified approach to STFT analysis and synthesis," *Proceedings of the IEEE*, vol. 65, pp. 1558-1564, 1977.
- Antoine, J., Carrette, P. and Murenzi, R., "Image analysis with two-dimensional continuous wavelet transform," *Signal Processing*, vol. 31, pp. 241, March 1993.
- Antonini, M., Barlaud, M. and Mathieu, P., "Image coding using wavelet transform," *IEEE Transactions on Image Processing*, vol. 1, pp. 205, Feb 1992.
- Argoul, F., Arneodo, A. and Elezgaray, J., "Wavelet transform of fractal aggregates." *Physics Letters: part A*, vol. 135, pp. 327, June/July 1989.
- Arneodo, A., "Wavelet transform of multifractals," *Physical Review Letters*, vol. 61, n. 20, pp. 2281, 1988.
- Barnea, O., Moore, T. W., Dubin, S. E. and Jaron, D., "Cardiac energy considerations during intraaortic balloon pumping," *IEEE Transactions on Biomedical Engineering*, vol. 37, pp.170-181, Feb 1990.
- Bartnik, E. A., Blinowska, K. J. and Durka, P. J., "Single evoked potential reconstruction by means of wavelet transform." *Biological Cybernetics*, vol. 67, pp. 175, Feb 1992.
- Beltran del Rio, L., Gomez, A. and Jose-Yacamán, M., "Image processing in TEM using the wavelet transform," *Ultramicroscopy*, vol. 38, part 4, pp. 319, March 1991.
- Bendjoya, P., Slezak, E. and Froeschle, C., "The wavelet transform: a new tool for asteroid family determination," *Astronomy and Astrophysics*, vol. 251, pp. 312, Jan 1991.
- Bertrand, O., Bohorquez, J. and Pernier, J., "Time-Frequency digital filtering based on an invertible wavelet transform: an application to evoked potentials," *IEEE Transactions on Biomedical Engineering*, vol. 41, pp. 77, Jan 1994.
- Boudreaux-Bartels, G. F., Private Discussion, 1994.

- Burattini, R., Fioretti, S. and Jetto, L., "A simple algorithm for defining the mean cardiac cycle of aortic flow and pressure during steady state," *Computers and Biomedical Research*, vol. 18, pp. 303-312, 1985.
- Calderon, A., "Intermediate spaces and interpolation, the complex method," *Studia Mathematica*, vol. 24, pp. 113-190, 1964.
- Campbell, G. and Roberts, R., "Spectral estimation of cardiovascular sounds," *Biomedical Science Instrumentation*, vol. 14, pp.27-31, 1978.
- Chang, T. and Kuo, C., "Texture analysis and classification with tree-structured wavelet transform," *IEEE Transactions on Image Processing*, vol. 2, pp. 429, April 1993.
- Chang, D. C., Su, C. N. and Fu, I. J., "Interpretation of a dynamic radar cross-section using the wavelet transform," *International Journal of Electronics*, vol. 78, pp. 67, Jan 1995.
- Chui, C. K., *An Introduction to Wavelets*. Academic Press, Boston, MA, 1992.
- Chui, C. K., *Wavelets: A Tutorial in Theory and Applications*. Academic Press, Boston, MA, 1992.
- Clarke, L., Kallergi, M. and Silbiger, M., "Tree-structured non-linear filter and wavelet transform for microcalcification segmentation in digital mammography," *Cancer Letters*, vol. 77, part 2, pp. 173, Feb 1994.
- Cohen, A. and Daubechies, I., "On the instability of arbitrary biorthogonal wavelet packets," *SIAM Journal on Mathematical Analysis*, vol. 24, pp. 1340, May 1993.
- Cohen, A., Daubechies, I. and Feauveau, J. C., "Orthonormal bases of compactly supported wavelets," *Communications on Pure and Applied Mathematics*, vol. 45, pp. 485, May 1992.
- Cohen, A. and Daubechies, I., "Orthonormal bases of compactly supported wavelets II: better frequency resolution," *SIAM Journal on Mathematical Analysis*, vol. 24, pp. 520, Feb 1993.

- Coupinot, G., Hecquet, J. and Auriere, M., "Photometric analysis of astronomical images by the wavelet transform," *Astronomy and Astrophysics*, vol. 259, pp. 701, Feb 1992.
- Crochiere, R. E., "A weighted overlapp-add method of short-time Fourier analysis/synthesis," *IEEE Transactions on Acoustics, Speech and Signal Processing*, vol. 28, pp. 99-102, 1980.
- Crowe, J. A., Gibson, N. M. and Woolfson, M. S., "Wavelet transform as a potential tool for ECG analysis and compression," *Journal of Biomedical Engineering*, vol. 14, pp. 268, March 1992.
- Daubechies, I., "The wavelet transform, time-frequency localization and signal analysis," *IEEE Transactions on Information Theory*, vol. 36, pp. 961-1005, May 1990.
- Daubechies, I., "Ten lectures on wavelets," *CBMS-NSF Series Applied Mathematics, SIAM*, 1991.
- Daubechies, I., "Orthonormal bases of compactly supported wavelets," *Communications on Pure and Applied Mathematics*, vol.41. pp.909-990, July 1988.
- Daubechies, I., "Orthonormal bases of compactly supported wavelets II: variations on a theme. *SIAM Journal on Mathematical Analysis*, vol. 24, pp. 499, Feb 1993.
- Daubechies, I. and Cohen, A., "A stability criterion for biorthogonal wavelet bases and their related subband coding scheme," *Duke Mathematical Journal*, vol. 68, pp. 313, Feb 1992.
- Daubechies, I., Grossmann, A. and Meyer, Y., "Painless nonorthogonal expansions. *Journal of Mathematics and Physics*, vol. 27, pp. 1271-1283, 1986.
- de Bruijn, N. G., *Uncertainty principles in Fourier analysis. Inequalities*, (Shisha, O. ed.), pp.57-71, Academic Press, New York, 1967.

Del Marco, S. and Weiss, J., "M-band wavepacket-based transient signal detector using a translation -invariant wavelet transform," *Optical Engineering*, vol. 33, pp. 2175, July 1994.

DeVore, R., Jawerth, B. and Lucier, B., "Image compression through wavelet transform coding," *IEEE Transactions on Information Theory*, vol. 38, part 2, pp. 719, Feb 1992.

Djamdji, J. P., Bijaoui, A. and Maniere, R., "Geometrical registration of images: the multiresolution approach," *Photogrammetric Engineering and Remote Sensing*, vol. 59, pp. 645, May 1993.

Donoho, D. L. and Stark, P.B., "Uncertainty principles and signal recovery," *SIAM Journal on Applied Mathematics*, vol. 49, pp. 906, March 1989.

Donoho, D. L. and Stark, P. B., "A note of rearrangements, spectral concentration, and the zero-order prolate spherical wavefunctions," *IEEE Transactions on Information Theory*, vol. 39, pp. 257, Jan 1993.

Duhamel, P., Flandrin, P. and Nishitani, T., "Wavelets and signal processing," *IEEE Transactions on Signal Processing*, vol. 41, pp. 3213, Dec 1993.

Durand, L. G., Langlois, Y. E. and Lanthier, T., "Contribution of left ventricular vibrations to the spectrum of aortic valve closure sound," *Annual International Conference of the IEEE Engineering in Medicine and Biology Society*, vol. 12, pp. 567-568, Feb 1990.

Ehara, N., Sasase, I. and Mori, S., "Weak radar signal detection based on wavelet transform," *Electronics and Communications in Japan, Part 3*, vol 77, pp. 105, Aug 1994.

El-Ghazzawi, Z. F. and Welch, J. P., "Algorithm to identify components of arterial blood pressure signals during use of an intra-aortic balloon pump," *Journal of Clinical Monitoring*, vol. 9 pp. 297-308, 1993.

- Flandrin, P., "Wavelet analysis and synthesis of fractional Brownian motion," *IEEE Transactions on Information Theory*, vol. 38, part 2, pp. 910, Feb 1992.
- Franklin, P., "A set of continuous orthogonal functions," *Mathematics. Annals*, vol. 100, pp. 522-529, 1928.
- Freeman, M. O., "Wavelets: signal representations with important advantages," *Optics & Photonics News*, vol. 4, pp. 8-14, Aug 1993.
- Frisch, M. and Messer, H., "The use of the wavelet transform in the detection of an unknown transient signal," *IEEE Transactions Information Theory*, vol. 38, pp. 892, Feb 1992.
- Frome, E. L. and Frederickson, E. L., "Digital spectrum analysis of the first and second heart sounds," *Computers and Biomedical Research*, vol. 7 pp. 421-431, 1974.
- Fuchs, R. M., Brin, K. P., and Brinker, J. A., "Augmentation of regional coronary blood flow by intraaortic balloon counterpulsation in patients with unstable angina," *Circulation*, vol.68, pp.117, 1983.
- Gabor, D., "Theory of communication," *Journal of the IEE (London)*, vol. 93, pp. 429-457, 1946.
- Gebber, V. and Welch, J., *Circuit for Detecting Initial Systole and Dicrotic Notch*. U. S. Patent # 3850169, 1974.
- Ginette, S., Grossmann, A. and Tchamitchian, P., "Use of wavelet transforms in the study of propagation of transient acoustic signals across a plane interface between two homogeneous media," *Proceedings of the International Conference on Wavelets, Time-Frequency Methods and Phase Space*. pp.139-146, 1987.
- Goh, K., Soraghan, J. and Durrani, T., "Wavelet transform based adaptive bit-plane run-length coding for still images," *Electronic Letters*, vol. 30, pp. 395, May 1994.
- Goh, K., Soraghan, J. and Durrani, T., "New 3-D wavelet transform coding algorithm for image sequences," *Electronic Letters*, vol. 29, pp. 401, April 1993.

- Goswami, J., Chan, A. and Chui, C., "An application of fast integral wavelet transforms to waveguide mode identification," *IEEE Transactions on Microwave Theory and Technology*, vol. 43, pp. 655, March 1995.
- Griffin, D. W. and Lim, J. S., "Signal estimation from modified short-time Fourier transform," *Proceedings of the International Conference on ASSP*, pp.804-807, 1983.
- Grossmann, A. and Morlet, J., "Decomposition of Hardy functions into square integrable wavelets of constant shape," *SIAM Journal of Mathematical Analysis*, vol. 15, pp. 723-736, 1984.
- Grossmann, A., "Wavelet transforms and edge detection," *Stochastic Processes in Physics and Engineering* (Abeverto, S., ed.), pp.149-157, 1988.
- Grossmann, A., Holschneider, M., Kronland-Martinet, R. and Morlet, J., *Detection of Abrupt Changes in Sound Signals with the Help of the Wavelet Transform*. Center de Physique Theorique, CNRS, Marseille, France, 1988.
- Grossmann, A., Kronland-Martinet, R. and Morlet, J., "Reading and understanding continuous wavelet transforms," *Proceedings of the International Conference on Wavelets, Time-Frequency Methods and Phase Space*, pp. 2-20, Dec 1987.
- Guyton, A. C., *Human Physiology and Mechanics of Disease*. 4th ed., W.B. Saunders Company, Philadelphia, PA, 1987.
- Hamosh, P. and Cohn, J. N., "Systolic time intervals and left ventricular function in acute myocardial infarction," *Circulation*, vol. 45, pp. 375-381, 1972.
- Harris, F. J., "On the use of windows for harmonic analysis with the discrete Fourier transform," *Proceedings of the IEEE*, vol. 66, pp. 51-83, 1978.
- Heckman, J. L., Stewart, G. H. and Lynch, P. R., "Frequency analysis approach to the origin of the first and second heart sounds," *American Heart Journal*, vol. 104, pp. 1309-1318, 1982.

- Hedenmark, J., Ahn, H. and Nystrom, S. O., "Intra-aortic balloon counterpulsation with special reference to determinants of survival," *Scandinavian Journal of Thoracic and Cardiovascular Surgery*, vol. 23, pp. 57-62, 1989.
- Heil, C, and Walnut, D., "Continuous and discrete wavelet transforms," *SIAM Review* vol. 31, pp. 628-666, April 1989.
- Hlawatsch, F. and Boudreaux-Bartels, G. F., "Linear and quadratic time-frequency signal representations," *IEEE Signal Processing Magazine*, pp.21-67, April 1992.
- Hong. L., "Multiresolution filtering using wavelet transform," *IEEE Transactions on Aerospace and Electronic Systems*, vol. 29, pp.1244, April 1993.
- Huh, Y., Hwang, J. and Rao, K., "Block wavelet transform coding of images using classified vector quantization," *IEEE Transactions on Circuits and Systems*, vol. 5, pp. 63, Jan 1995.
- Iwata, A., Ishii, N. and Suzumura, N. "Algorithm for detecting the first and the second heart sounds by spectral tracking," *Medical and Biological Engineering & Computers*, vol. 18, pp. 19-26, 1980.
- Jackson, L. B. and Wood, S., "Linear prediction in cascade form," *IEEE Transactions on Acoustics, Speech and Signal Processing*, vol. 26, pp. 518-528, June 1978.
- Jundanian, R. H., Armitage, J. W. and Peura, R. A., "A microprocessor based rate-pressure product computer," *Proceedings of the 5th Annual Conference of IEEE Frontiers of Engineering and Computers in Health Care*, pp. 188-90, 1983.
- Kadambe, S., *The application of Time-Frequency and Time-Scale Representations in Speech Analysis*. PhD Thesis, University of Rhode Island, Electrical Engineering, 1990.
- Kadambe, S. and Boudreaux-Bartels G. F., "A pitch detector based on event detection using the dyadic wavelet transform," *Proceedings of the International Conference on Spoken Language Processing*, (Kobe, Japan), pp.469-472, 1990.

Kadambe, S. and Boudreaux-Bartels G. F., "Application of the wavelet transform for pitch detection of speech signals," *IEEE Transactions Information Theory*, vol. 38, pp. 917-924, March, 1992.

Kadambe, S. and Boudreaux-Bartels, G. F., "A comparison of a wavelet transform event detection pitch detector with classical pitch detector," *Proceedings of the 24th Annual Asilomar Conference on Signals, Systems and Computers*, (Pacific Grove, CA), 1990.

Kadambe, S. and Boudreaux-Bartels G. F. "A comparison of wavelet functions for pitch detection of speech signals," *Proceedings of the International Conference on ASSP*, (Toronto, CA), 1991.

Kaiser, G., *A Friendly Guide to Wavelets*. Birkhauser Boston, 1994.

Kalayci, T. and Ozdamar, O., "Wavelet processing for automated neural network detection of EEG spikes," *IEEE Engineering in Medicine and Biology Magazine* vol.14, pp. 160-166, Feb 1995.

Kantrowitz, A: Origins of intraaortic balloon pumping. *Annals of Thoracic Surgery*, vol. 50, pp. 672-4, 1990.

Kantrowitz, A., "Mechanical support to the failing heart," *Transactionscript-Assisted Circulation Colloquim at Bad Neuenahr*, Germany, pp. 78-95, 1967.

Kantrowitz, A., Freed, P. S., Tacai, H. and Sukuki, A., *Electrocardiographic Measurement Method for Controlling an Intra-aortic Balloon Pump*, U. S. Patent # 4809681, March 1989.

Kantrowitz, A., Freed, P. S. and Cardona, R. R., "Initial clinical trial of a closed loop, fully automatic intra-aortic balloon pump," *ASAIO Transactions*, vol. 38, pp. M617-21, March 1992.

Karrakchou, M., van den Branden Lambrecht, C. and Kunt, M., "Analyzing pulmonary capillary pressure: more accurate measurements using mutual wavelet packets for

- adaptive filtering," *IEEE Engineering in Medicine and Biology Society Magazine* vol. 14, pp. 179-185, Feb 1995.
- Kern, M. J., Aguirre, F. V. and Tatineni, S., "Enhanced coronary blood flow velocity during intraaortic balloon counterpulsation in critically ill patients," *Journal of the American College of Cardiology*, vol. 21, pp. 359-68, Feb 1993.
- Khamlach, R., *Wavelet Transform Analysis for Dicrotic Notch Detection*. Rapport de Stage, Universite d'Orleans - DESS Systemes Temps Reel, Signaux et Images, at University of Rhode Island, 1994.
- Khullar, S. and Lewis, R. P., "Usefulness of systolic time intervals in differential diagnosis of constrictive pericarditis and restrictive cardiomyopathy," *British Heart Journal*, vol. 38, pp. 43, 1976.
- Kikuchi, H., Nakashizuka, M. and Watanabe, H., "Fast wavelet transform and its application to detecting detonation," *IEICE Transactions on Fundamentals of Electronic*, vol. 75, pp. 980, Aug 1992.
- Kim, C., *Computer Simulation of the Intra Aortic Balloon Pump: A Timing Control Algorithm in the Presence of Arrhythmia*, PhD Thesis, University of Rhode Island, Electrical Engineering, May 1994.
- Kim, H. and Ling, H., "On the application of fast wavelet transform to the integral-equation solution of electromagnetic scattering," *Microwave and Optical Technology Letters*, vol. 6, pp. 168, March 1993.
- Kinias, P., Fozzard, H. A. and Norusis, M. J., "A real time pressure algorithm," *Computers in Biology and Medicine*, vol. 11, pp. 211-20, April 1981.
- Kronland-Martinet, R., "The wavelet transform for analysis, synthesis, and processing of speech and music sounds," *Computer Music Journal*, vol. 12, pp. 11-20, April 1988.

- Kronland-Martinet, R., Morlet, J. and Grossmann, A., "Analysis of sound patterns through wavelet transforms," *Recognition and Artificial Intelligence*, vol.1, pp. 273-302, 1987.
- Lagoutte, D., Cerisier, J. and Plagnaud, J., "High-latitude ionospheric electrostatic turbulence studied by means of the wavelet transform," *Journal of Atmospheric and Terrestrial Physics*, vol. 54, pp.1283, Oct 1992.
- Larsonneur, J. L., Morlet, J., "Wavelets and seismic interpretation," *Proceedings of the International Conference on Wavelets, Time-Frequency Methods and Phase Space*, (Marseille, France), pp.126-131, Dec 1987.
- Lee, J., Sun, Y. and Chen, C., "Multiscale corner detection by using wavelet transform," *IEEE Transactions on Image Processing*, vol. 4, pp. 100, Jan 1995.
- Lee, J. Y. and Lin, J. C., "A microprocessor-based noninvasive arterial pulse wave analyzer," *IEEE Transactions on Biomedical Engineering*, vol. 32, pp. 451-455, June 1985.
- Lewis, R. P., Rittgers, S. E., Forester, W. F., and Boudoulad, H., "A critical review of the systolic time intervals," *Circulation*, vol. 56, pp.146-158, Feb 1977.
- Lewis, R. P., Boudoulas, H., Welch, T. G. and Forester, W. F., "Usefulness of systolic time intervals in coronary artery disease," *American Journal of Cardiology*, vol. 37, pp. 787-796, 1976.
- Lewis, R. P., "Diagnostic value of systolic time intervals in man," *Diagnostic Methods in Cardiology*, Fowler ed., Philadelphia, FA Davis, pp. 245-264, 1975.
- Lewis, A. and Knowles, G., "Image compression using the 2-D wavelet transform," *IEEE Transactions on Image Processing*, vol. 1, pp. 244, Feb 1992.
- Lhegu, B., *The Intra-aortic Balloon Pump (IABP)*. Rapport de Stage, Universite d'Orleans - DESS Systemes Temps Reel, Signaux et Images, at University of Rhode Island, 1993.

- Liandrat, J. and Moret-Bailly, F., "The wavelet transform: some applications to fluid dynamics and turbulence," *European Journal Mechanics*, vol. 9, pp. 1, Jan 1990.
- Lim, L. M., Akay, M. and Daubenspeck, J. A., "Identifying respiratory-related evoked potentials," *IEEE Engineering in Medicine and Biology Society Magazine* vol. 14, pp. 174-178, Feb 1995.
- Littlewood, J. and Paley, R., "Theorems on Fourier series and power series," *Proceedings of the London Mathematical Society*, vol. 42, pp. 52-89, 1937.
- Loughlin, P. J., Pitton, J. W. and Atlas, L. E., "Bilinear time-frequency representations: new insights and properties," *IEEE Transactions on Signal Processing*, vol. 41, pp. 750-766, Feb 1993.
- Mallat, S., "Multifrequency channel decompositions of images and wavelet models," *IEEE Transactions on Acoustic, Speech and Signal Processing*, vol. 37, pp. 2091-2110, Dec 1989.
- Mallat, S., "Multiresolution approximation and wavelet orthonormal bases of L_2 ," *Transactions of the American Mathematical Society*, vol. 315, pp. 69-87, Jan 1989.
- Mallat, S., "A theory for multiresolution signal decomposition: the wavelet representation," *IEEE Transactions on Pattern Analysis and Machine Intelligence*, vol. 11, pp. 674-693, July 1989.
- Mallat, S., "Review of multifrequency channel decompositions of images and wavelet models," *IEEE Transactions on Acoustics, Speech and Signal Processing*, 1989.
- Mallat, S., *IEEE Transactions Information Theory*, March, 1992.
- Mallat, S. and Zhong, S., "Characterization of signals from multiscale edges," *IEEE Pattern Analysis and Machine Intelligence*, vol. 14, pp. 710-732, July 1992.
- Mallat, S. and Zhong, S., "Complete signal representation with multiscale edges," Technical Report 91-16, New York University, vol. 1, pp. 76, 1989.

- Mallat, S., Hwang, W., "Singularity detection and processing with wavelets," *IEEE Transactions on Information Theory*, vol. 38, part 2, pp. 617, Feb 1992.
- Martin, C. E., and Shaver, J. A., "Direct correlation of external systolic time intervals with internal indices of ventricular function in man," *Circulation*, vol. 44, pp. 419, 1971.
- Martino, R. L. and Risso, W. L., "An arterial blood pressure preprocessor using a combined analog and digital signal processing method," *Proceedings of the 7th IEEE Northeast Biomedical Conference*, pp.267-70, 1979.
- Masry, E., "The wavelet transform of stochastic processes with stationary increments and its application to fractional Brownian motion," *IEEE Transactions on Information Theory*, vol. 39, pp. 260, Jan 1993.
- Massachusetts General Hospital MGH/MF Waveform Database, and Patient Guide*, Massachusetts Institute of Technology, 1992.
- Meste, O., and Rix, H., "Detection of late potentials by means of wavelet transform," *Proceedings of the IEEE International Conference Engineering in Medicine and Biology*. pp.637-638, 1991.
- Meste, O., Rix, H., Thakor, N. V., "Ventricular late potentials characterization in time-frequency domain by means of wavelet transform," *IEEE Transactions on Biomedical Engineering*, vol. 41, pp. 625, July 1994.
- Meyer, Y., *Ondelettes et Operateurs*. Hermann, New York, 1990.
- Meyer, Y., *Wavelets: Algorithms & Applications*. SIAM, Philadelphia, PA, 1993.
- Morlet, J., *Sampling Theory and Wave Propagation*. NATO Series I, Issues in Acoustic Signal/Image Processing and Recognition, (Chen, C. H., ed.,) Springer-Verlag, Berlin, 1983.
- Murray, R., *Dyadic Wavelet Transform Based QRS Detector*. ScM Thesis, University of Rhode Island, Electrical Engineering, 1993.

- Nandagopal, D. and Mazaumdar, J., "Spectral analysis of second heart sound in normal children by selective linear prediction coding," *Medical and Biological Engineering & Computers*, vol. 22, pp. 229-239, March 1984.
- Noble, M. I. M., *The Cardiac Cycle*, Blackwell Scientific Publications, St. Louis, MO, 1979.
- Ohta, M., Yano, M. and Nishitani, T., "Wavelet picture coding with transform coding approach," *IEICCE Transactions on Fundamentals of Electronic*, vol. 75, pp. 776, July 1992.
- Onsay, T. and Haddow, A., "Wavelet transform analysis of transient wave propagation in a dispersive medium," *Journal of the Acoustical Society of America*, vol. 95, pp. 1441, March 1994.
- Oppenheim, A., Willsky, A. and Young, I., *Signals and Systems*. Prentice Hall, New Jersey, 1983.
- Oppenheim, A. and Schaffer, R. W., *Discrete-Time Signal Processing*. Prentice Hall, New Jersey, 1989.
- Oppenheim, M. I., Factor, M. and Sittig, D. F., "BIO-SPEAD. A parallel computing environment to accelerate development of biological signal processing algorithms," *Computational Methods & Programming in Biomedicine*, vol. 37, pp. 137-47, 1992.
- Papoulis, A: *Signal Analysis*. McGraw-Hill, New York, 1977.
- Permann, D. and Teitelbaum, H., "Wavelet fast Fourier transform (WFFT) analysis of a millivolt signal for a transient oscillating chemical reaction," *Journal of Physical Chemistry*, vol. 97 n. 49, pp. 12670, 1993.
- Poulligny, B., Gabriel, G. and Muzy, J., "Optical wavelet transform and local scaling properties of fractals," *Journal Applied Crystallography*, vol. 24, pp. 526, May 1991.
- Rioul, O. and Vetterli, M., "Wavelets and signal processing," *IEEE Signal Processing Magazine*, pp. 14-38, Oct 1991.

Rothwell, E., Chen, K. and Bebermeyer, R., "A radar target discrimination scheme using the discrete wavelet transform for reduced data storage," *IEEE Transactions on Antennas and Propagation*, vol. 42, pp. 1033, July 1994.

Sanghadasa, M., Erbach, P. and Sung, C., "Wavelet transform applied to synthetic aperture radar - Optical implementation and adaptive techniques," *Optical Engineering*, vol. 33, pp. 2282, July 1994.

Schlant, R. C., *The Heart*. Hurst, J. W. and Logue, R. B., ed., second edition, McGraw-Hill, NY, 1970.

Senhadji, L. and Bellanger, J., "Wavelet analysis of ECG signals," *Annual International Conference IEEE Engineering in Medicine and Biology Society*, vol. 12, pp. 811-12, Feb 1990.

Senhadji, L., Carrault, G., Bellanger, J. and Passariello, G., "Comparing wavelet transforms for recognizing cardiac patterns," *IEEE Engineering in Medicine and Biology Society Magazine*, vol. 14, pp. 167-173, Feb 1995.

Shensa, M. J., "The discrete wavelet transform: wedding the A Trous and Mallat algorithms," *IEEE Transactions on Signal Processing*, vol. 40, pp. 2464, Oct 1992.

Simoncelli, E. P., "Shiftable mult-scale transforms. *IEEE Transactions on Information Theory, Special Issue on Wavelet Transforms and Multiresolution Signal Analysis*, vol. 38, pp. 587-607, 1992.

Slezak, E., Bijaou, A. and Mars, G., "Identification of structures from galaxy counts: use the wavelet transform," *Astronomy and Astrophysics*, vol. 227, pp. 301, Feb 1990.

Smith, D. and Craige, E., "Influence of the aortic component of the second heart sound on left ventricular maximal negative dP/dt in the dog," *American Journal of Cardiology*, vol. 55, pp. 205-9, January 1985.

Smith, D., Ozawa, Y. and Craige, E., "Chest wall velocity and the second heart sound. An improved sensor of S2 splitting," *Circulation*, vol. 67, pp. 1304-1311, June 1983.

Spencer, F. C., "A critique of emergency and urgent operations for complications of coronary artery disease," *Circulation*, vol. 79, supplement I, pp. I-160-2, 1989.

Stack, R. S. and Lee, C. C., "Left ventricular performance in coronary artery disease evaluated with systolic time intervals and echocardiography," *American Journal of Cardiology*, vol. 37, pp. 331, 1976.

Starck, J. and Bijaoui, A., "Filtering and deconvolution by the wavelet transform," *Signal Processing*, vol. 35, pp. 195, March 1994.

Starck, J., Bijaoui, A. and Lopez, B., "Image reconstruction by the wavelet transform applied to aperture synthesis," *Astronomy and Astrophysics*, vol. 283, pp. 349, Jan 1994.

Subramanian, V. A., Goldstein, J. E. and Sos, T. A., "Preliminary clinical experience with percutaneous intraaortic ballon pumping," *Circulation*, vol. 62, supplement I, pp. I-123-9, 1980.

Szu, H., Sheng, Y. and Chen, J., "Wavelet transform as a bank of the matched filters," *Applied Optics*, vol. 31, n. 17, pp. 3267, 1992.

Tewfik, A. H. and Kim, M., "Correlation structure of the discrete wavelet coefficient of fractional Brownian motion," *IEEE Transactions on Information Theory*, vol. 38, part 2, pp. 904, Feb 1992.

Tewfik, A. H., Sinha, D. and Jorgensen, P., "On the optimal choice of a wavelet for signal representation," *IEEE Transactions on Information Theory*, vol. 38, part 2, pp. 747, Feb 1992.

Thakor, N. V. and Xin-Rong, G., "Multiresolution wavelet analysis of evoked potentials," *IEEE Transactions on Biomedical Engineering*, vol. 40, pp. 1085-1094, Nov 1993.

Tuteur, F. B., "Wavelet transformations in signal detection," *Proceedings of the International Conference on ASSP*, pp.1435-1438, 1988.

Tyson, G. S., Davis, J. W. and Rankin, J.S., "Improved performance of the intra-aortic balloon pump in man," *Proceedings of the 42nd Fund Surg Prob, 72nd Annual Clinical Congress*, pp. 214-216, 1986.

Unser, M., Aldroubi, A. and Schiff, S. J., "Fast implementation of the continuous wavelet transform with integer scales," *IEEE Transactions on Signal Processing*, vol. 42, pp. 3519, Dec 1994.

Vaidyanathan, P., "Quadrature mirror filter banks, M-band extensions and perfect reconstruction techniques," *IEEE ASSP Magazine*, vol. 4, pp. 4-20, 1987.

Vaianti, S., "A frostman-like theorem for the wavelet transform on fractal sets," *Nonlinearity*, vol. 4, pp. 1241, April 1991.

Vetterli, M. and Herley, C., "Wavelets and filter banks: theory and design," *IEEE Transactions on Signal Processing*, vol. 40, Sept 1992.

Vishwanath, M., "The recursive pyramid algorithm for the discrete wavelet transform," *IEEE Transactions on Signal Processing*, vol. 42, pp. 673, March 1994.

Wang, W., Jin, G. and Wu, M., "Image feature extraction with the optical Haar wavelet transform," *Optical Engineering*, vol. 34, pp. 1238, April 1995.

Wang, W., Jin, G. and Wu, M., "Joint wavelet-transform correlator for image feature extraction," *Applied Optics*, vol. 34, pp. 370, Feb 1995.

Wang, S. H., Tewfik, A. H. and Zou, H., "Correction to "Parameterization of compactly supported orthonormal wavelets," *IEEE Transactions on Signal Processing*, vol. 42, pp. 208, Jan 1994.

Weber, K. T. and Janicki, J.S., "Intraaortic balloon counterpulsation," *Annals of Thoracic Surgery*, vol. 17, pp. 602-636, June 1974.

Weber, K. T., Janicki, J.S. and Walker, A. A., "Intra-aortic balloon pumping: an analysis of several variables affecting balloon performance," *Transactions of ASAIO*, vol. 18, pp. 486-492, 1972.

Weissler, A. M., Harris, W. S. and Schoenfeld, C. D., "Systolic time intervals in heart failure in man," *Circulation*, vol. 37, pp. 149-159, Feb 1968.

Weissler, A. M., Lewis, R. P. and Leighton, R. F., "The systolic time intervals as a measure of left ventricular performance in man," *Progress in Cardiology*, Yu PN ed., Goodwin JF, Philadelphia, Lea and Febiger, pp. 155-183, 1972.

Wilson, R., Calway, A. D. and Pearson, E. R. S., "A generalized wavelet transform for Fourier analysis: The multiresolution Fourier transform and its application to image and audio signal analysis," *IEEE Transactions on Information Theory*, vol. 38, pp. 674, Feb 1992.

Wilson, E., *Transient Detection and Feature Extraction Using Neural Networks*. PhD Thesis, University of Rhode Island, Electrical Engineering, 1993.

Witkin, A., "Scale-space filtering," *Proceedings of the International Joint Conference on Artificial Intelligence*, 1983.

Wornell, G. and Oppenheim, A., "Wavelet based representations for fractal modeling," *NSF/CBMS Conference on Wavelets*, (Lowell, MA), June 1990.

Yaou, M. and Chang, W., "Fast surface interpolation using multiresolution wavelet transform," *IEEE Transactions on Pattern Analysis and Machine Intelligence*, vol. 16, pp. 673, July 1994.

Yaou, M., Chang, W., "M-Ary wavelet transform and formulation for perfect reconstruction in M-band filter bank," *IEEE Transactions on Signal Processing*, vol. 42, pp. 3508, Dec 1994.

Yoganathan, A. P. and Gupta, R., "Use of the fast Fourier transform in the frequency analysis of the second heart sound in normal man," *Medical and Biological Engineering*, pp.455-459, July 1976.

Yomogida, K., "Detection of anomalous seismic phases by the wavelet transform," *Geophysical Journal International*, vol. 116, pp. 119, Jan 1994.

Young, R., *Wavelet Theory and Its Applications*. Klower Academic Publishers, Boston, MA, 1993.

Zayed, A., "Wavelet transform of periodic generalized functions," *Journal of Mathematical Analysis and Application*, vol. 183, pp. 391, March 1994.

Zhong, S. and Mallat, S., "Compact image representation from multiscale edges," *Proceedings of the 3rd International Conference on Computer Vision*, Dec, 1990.

Zou, H., Tewfik, A. H., "Parameterization of compactly supported orthonormal wavelets," *IEEE Transactions on Signal Processing*, vol, 41, pp. 1428, March 1993.

Zubair, L. and Sreenivasan, D., "Wavelet analysis applied to turbulence," *NSF/CBMS Conference on Wavelets*, (Lowell, MA), June 1990.